Stress and recovery dynamics in Scots pine:
The impacts of heat and drought on carbon and water cycling

Zur Erlangung des akademischen Grades eines
DOKTORS DER NATURWISSENSCHAFTEN

von der KIT-Fakultät für
Bauingenieur-, Geo- und Umweltwissenschaften
des Karlsruher Instituts für Technologie (KIT)

genehmigte
DISSERTATION

von

M.Sc. Romy Rehschuh
aus Zittau

Tag der mündlichen Prüfung: 21.10.2021
Referentin: Dr. Nadine K. Rühr
Korreferentin: Prof. Dr. Almut Arneth
Korreferent: Prof. Dr. Bernhard Schuldt

Karlsruhe
Garmisch-Partenkirchen
(2021)

Acknowledgements

This PhD thesis could not have been completed without the outstanding support of certain institutions and persons to whom I would like to express my sincere gratitude.

Financial support is gratefully acknowledged from the German Research Foundation through its Emmy Noether Program (RU 1657/2-1) within the project “Forests out of balance: Impacts of extreme events on carbon and water cycling” and from the KIT Graduate School of the Centre for Climate and Environment (GRACE).

Allowing this project to take place, setting up contacts, introducing myself into experimental and fieldwork and teaching me about science is the result of Dr. Nadine Rühr. I would not have accomplished this project without your help and support, and I am deeply grateful for the always open atmosphere! My special thanks also go to Dr. Henrik Hartmann and Prof. Almut Arneth for co-supervising this thesis and supporting me with valuable scientific advice and for critical reviews of my work. Thank you both! Prof. Bernhard Schuldt is thanked for his willingness to perform a second opinion. Further, I would like to thank Dr. Allan Buras for introducing me into science and statistics during my masters and further joint scientific work.

I would deeply like to thank the Plant Ecophysiology group of the KIT, Institute of Meteorology and Climate Research in Garmisch-Partenkirchen, especially Benjamin Birami, Andreas Gast, Andrea Jakab, Daniel Nadal-Sala and Ines Bamberger for your teamwork, fellowship, reliability, honesty and friendship.

For assistance with experimental, laboratory and field work, I sincerely thank the staff of IMK-IFU, especially Andrea Jakab, Eliana Häfele, Stephanie Rehschuh, our “FÖJlers” Juliane Bachmann and Paula Hainz, and the workshop staff, especially Stefan Schmidt. Setting up experiments, searching for roots in tree chambers, wrapping trees for micro-CT measurements and milling samples for hours would not have been possible without you. At the same time, I would like to thank all colleagues for their support during measurements, laboratory work and for fruitful scientific discussions at the KIT, Institute for Photon Science and Synchrotron Radiation, especially Angelica Cecilia, at the University of Innsbruck, especially Birgit Dämon and Prof. Stefan Mayr, and at the University Ulm Prof. Steven Jansen. Further, I am grateful for the possibility to perform my research stay at the Swiss Federal Research Institute WSL, and would particularly like to thank Marco Lehmann, Loïc Schneider, Manuela Oettli and Prof. Arthur Gessler for their time, support and input. Thank you all for your great help!

I am very thankful to my friends and colleagues, especially Maximilian Kehl, Frederik De Roo, Andrea Jakab, Anne Schucknecht, Ines Bamberger, and Paula Hainz, as well as my sister Stephanie for supporting me and making this period during my PhD to a pleasant time. I really enjoyed the time with you during lunch and coffee breaks, during hiking and skiing in the mountains around Garmisch-Partenkirchen, swimming in the Eibsee and at game evenings!

Finally yet importantly, I would also like to express my profound gratitude to my family for the support during my studies, for the confidence, advice and suggestions during my PhD.

Die Wissenschaft hat über Jahrhunderte

unsere rationale Betrachtung des Waldes geschärft,

aber es braucht nur einen Augenblick,

um Leidenschaft für ihn auszulösen.

Alexander Skog

Table of contents

Summary

Stress and recovery dynamics in Scots pine: The impacts of heat and drought on carbon and water cycling

Forests play a key role in the Earth's water and carbon (C) cycles and provide numerous ecosystem services. However, forest functioning is increasingly affected by climate extremes. Often co-occurring drought spells and heat waves are projected to increase further in their intensity, frequency and duration within the 21st century. These circumstances have large implications for tree physiological processes and require a fast post-stress recovery potential if trees are not to suffer from stress damage. Scots pine (*Pinus sylvestris* L.) is one of the most abundant conifers globally, while its resilience to changing environmental conditions has been questioned in past years. Despite the important role of stress survival and resilience, we lack knowledge on associated physiological mechanisms affecting recovery pace and performance. Stress-induced functional impairment might persist if hydraulic and metabolic processes recovered only partially. Therefore, an improved understanding of the recovery of tree hydraulic functioning and C and nitrogen allocation is indispensable.

The present thesis aims to improve the understanding of the impacts of heat and drought on hydraulic processes and above- and belowground C allocation patterns in Scots pine during and post stress. The following research questions were addressed: (1) Is Scots pine able to refill drought-induced xylem embolism, and is leaf gas exchange recovery linked to hydraulic functioning? (2) What are the legacy effects of heat and hot drought on C allocation and how is it coupled with the plant N metabolism?, and (3) What are the impacts of heat and hot drought stress on C and water relations and associated stem diameter change during and post-stress?

To answer these questions, two separately designed greenhouse experiments were conducted. Environmental conditions were adjusted according to extreme climatic events in Franconia, Germany, where stress-induced Scots pine mortality has been observed. In the first experiment (first research question), *P. sylvestris* seedlings were drought-stressed for c. 1 month until a percent loss of stem hydraulic conductivity (PLC) of c. 50% was recorded, then re-watered and allowed a 4-week recovery period. Thereby, the dynamics of leaf gas exchange, nonstructural carbohydrates (NSC), and hydraulic properties were analyzed. To determine the degree of xylem embolism and refilling potential within a short-term (2 days) and long-term (4 weeks) recovery period, *in vivo* x-ray microtomography combined with intrusive techniques were applied, including measurements of hydraulic conductivity and dye staining. In the second experiment (research questions 2 and 3), a custom-built individual gas exchange chamber (n=18) system was used. This served to continuously measure shoot and root gas exchange, $\delta^{13}CO_2$ of respiration and stem diameter change in well-watered and drought-treated *P. sylvestris* seedlings during a daytime 20-day heatwave (max. 42°C) and a 3-week

recovery period. Hydraulic properties, leaf temperature, electrolyte leakage and maximum light adapted quantum yield of photosystem II (F'_v/F'_m) as indicators of stress severity and recovery capacity were assessed. Following stress release, a ^{15}N tracer was applied to the soil, followed by $^{13}CO_2$ canopy pulse-labeling (2 days post-stress) to trace the labels through plant compartments, respiration and the soil microbial biomass (SMB).

Results from the first experiment showed that drought causing a stem xylem water potential (Ψ_{Stem}) of -3.2 MPa and c. 50% PLC severely impaired hydraulic and metabolic functioning of Scots pine seedlings. Both x-ray microtomography and intrusive measurements demonstrated that embolized tracheids were not refilled and stem hydraulic conductivity did not recover within 4 weeks. These drought-induced damages caused a reduced water transport capacity, which was reflected in the incomplete recovery of leaf gas exchange to c. 50-60% of control values. Moreover, I could not find evidence for NSC reserves limiting hydraulic recovery as strong storage formation was observed post-drought. In the second experiment, the limited capacity of leaf cooling in drought-treated compared to well-watered seedlings under a heat wave due to reduced transpiration rates was highlighted. However, impacts on electrolyte leakage in leaf tissues were negligible, but F'_v/F'_m declined moderately under heat and strongly under drought-heat stress, indicating a photoprotective process. The heat treatment alone resulted in little functional impairment, enabling fast recovery of metabolic and hydraulic parameters. In contrast, the combination of heat and drought caused a decline of needle water potential (Ψ_{Needle}) to -2.7 MPa, resulting in metabolic dysfunction by suppressed photosynthesis and partial hydraulic impairment. These dynamics were also reflected in stem diameter shrinkage, indicating a large formation of tree water deficit. Legacy effects of drought-heat stress were observed in a delayed or incomplete recovery of leaf and stem hydraulic conductance, and shoot and root gas exchange. Considering C allocation dynamics shortly post-stress, I found seedlings recovering from heat stress to rapidly translocate recent C along the long-distance transport path, to root respiration (R_{root}; 7.1 h) and the SMB (3 days). Further, these seedlings strongly allocated ^{13}C to branch cellulose, indicating a compensatory response by secondary growth enhancement. Contrary, in previously drought-heat treated seedlings, ^{13}C accumulated in needles, while C translocation to R_{root} was delayed (13.8 h). Stress-induced meristem inactivation might have inhibited short-term growth, supported by reduced N uptake and aboveground allocation. Further, C was strongly allocated to starch (i.e. storage) post drought-heat, which might have occurred passively shortly post-stress due to reduced C transport to other organs, but actively later during the recovery period (7 days after stress release), when also growth appeared to be a strong C sink.

The findings of this thesis demonstrate that Scots pine is capable of surviving and partially recovering from extreme climatic events, while soil water availability was shown to be of high

importance in lowering heat stress impacts. The large limitations to leaf gas exchange recovery following water limitation result from hydraulic constraints such as persisting stem xylem embolism. Albeit delayed, the upregulation of stem growth during recovery from drought-heat stress might therefore suggest the importance of restoring hydraulic conductivity to enable improved C uptake. Further, I could demonstrate that C and N allocation dynamics early during recovery depend on stress impacts. The initially reduced above-belowground coupling following combined drought and heat stress indicates considerable functional impairment, particularly in phloem loading and transport, as well as meristem inactivation. Large investments into storage formation post-stress might serve as safety measure for upcoming stress periods. In summary, this thesis highlights that stress-induced impairment of important physiological processes in Scots pine seedlings can affect C and water cycling in the long-term. Such legacy effects could be important when addressing forest responses to increasing extreme events under climate change.

Zusammenfassung

Stress- und Erholungsdynamiken in der Waldkiefer: Die Auswirkungen von Hitze und Trockenheit auf den Kohlenstoff- und Wasserkreislauf

Wälder spielen eine zentrale Rolle im Wasser- und Kohlenstoffkreislauf der Erde und erbringen zahlreiche Ökosystemleistungen. Ihre Funktionen werden jedoch zunehmend durch den Klimawandel beeinträchtigt, der im 21. Jahrhundert durch oft gleichzeitig auftretende Dürreperioden und Hitzewellen gekennzeichnet sein wird, die an Dauer, Intensität und Frequenz bereits zunehmen. Diese Entwicklungen haben große Auswirkungen auf baumphysiologische Prozesse und erfordern ein schnelles Erholungspotenzial nach einem Stressereignis, vorausgesetzt die Bäume sind nicht den Stressschäden erlegen. Die Waldkiefer (*Pinus sylvestris* L.) ist eine der weltweit am häufigsten vorkommenden Nadelbaumarten. In den vergangenen Jahren wurde jedoch festgestellt, dass ihre Widerstandsfähigkeit gegenüber sich ändernden Umweltbedingungen begrenzt ist. Trotz der enormen Bedeutung der Resilienz gegenüber Stress sind die physiologischen Mechanismen, die die Erholungsgeschwindigkeit und Leistungsfähigkeit beeinflussen, noch unklar. Falls sich hydraulische und metabolische Prozesse nicht vollständig erholen sollten und die Bäume unfähig sind, geschädigtes Gewebe nachwachsen zu lassen, könnten Funktionsbeeinträchtigungen fortbestehen. Daher ist ein verbessertes Verständnis der Erholung der hydraulischen Funktionen von Bäumen und des Kohlenstoff- (C) und Stickstoff- (N) Kreislaufs unerlässlich.

Das Ziel der vorliegenden Arbeit war es, das Verständnis über die Auswirkungen von Hitze und Trockenheit auf hydraulische Prozesse sowie die ober- und unterirdischen C-Allokationsmuster in Kiefern während und nach dem Stress zu verbessern. Die folgenden Forschungsfragen wurden davon abgeleitet: (1) Sind Kiefern fähig, trockenheitsbedingte Stammembolien wieder aufzufüllen, und ist die Erholung des Blattgasaustausches mit der hydraulischen Funktion verbunden? (2) Welche Auswirkungen haben Hitze und heiße Trockenheit auf die C-Allokation nach dem Stress und wie ist diese mit dem pflanzlichen N-Stoffwechsel verbunden? und (3) Welche Einflüsse haben Hitze und heiße Trockenheit auf die Zusammenhänge des C- und Wasserkreislaufs und die damit verbundene Veränderung des Stammdurchmessers während und nach dem Stressereignis?

Um diese Fragen zu beantworten, wurden zwei separat angelegte Gewächshausexperimente durchgeführt. Die Umweltbedingungen wurden entsprechend extremer klimatischer Ereignisse in Franken, Deutschland, angepasst, wo in letzter Zeit vermehrt Kiefernsterben beobachtet wurde. Im ersten Experiment (1. Forschungsfrage) wurden Kiefernsämlinge ca. 1 Monat unter Trockenstress gesetzt, bis ein Verlust der hydraulischen Leitfähigkeit des Stammes von ca.

50% zu verzeichnen war. Daraufhin wurden die Sämlinge wiederbewässert und eine 4-wöchige Erholungsphase gewährt. Dabei wurden die Dynamiken des Blattgasaustausches, der Nicht-Strukturkohlenhydrate und hydraulischer Eigenschaften analysiert. Um den Grad der Xylem-Embolien und das Wiederauffüllungspotential innerhalb einer kurzfristigen (2 Tage) und langfristigen (4 Wochen) Erholungsphase zu bestimmen, wurden *in vivo* Röntgenmikrotomographie und konventionelle Techniken, einschließlich hydraulischer Leitfähigkeitsmessungen und Färbetechniken angewandt.

Im zweiten Experiment (Forschungsfrage 2 und 3) wurden speziell angefertigte individuelle Gasaustauschkammern (n=18) verwendet, die in Spross- und Wurzelkompartimente unterteilt waren. Diese dienten dazu, den kontinuierlichen Gasaustausch, $\delta^{13}CO_2$ der Atmung, und die Veränderung des Stammdurchmessers in gut bewässerten und trockenbehandelten *P. sylvestris* Sämlingen während einer 20-tägigen Hitzewelle (max. 42°C) und einer 2,5-wöchigen Erholungsphase zu bestimmen. Des Weiteren untersuchte ich hydraulische Eigenschaften, die Blatttemperatur, den Elektrolytaustritt aus den Blättern und die maximale Quantenausbeute des Photosystems II nach Lichtadaption (F'_v/F'_m) als Indikatoren für die Stressintensität und Erholungsfähigkeit. Mit der Wiederbewässerung wurde ^{15}N in den Boden eingebracht und 2 Tage darauf erfolgte eine $^{13}CO_2$-Pulsmarkierung, um die Marker durch die Pflanzenkompartimente (strukturell und nicht-strukturell), die Atmung und die mikrobielle Bodenbiomasse zu verfolgen.

Experiment 1 zeigte, dass ein trockenheitsinduziertes Stammwasserpotential von -3.2 MPa und ca. 50% Verlust der hydraulischen Leitfähigkeit des Stammes die hydraulischen und metabolischen Funktionen von Kiefernsämlingen signifikant beeinträchtigen. Sowohl Röntgenmikrotomographie als auch konventionelle Messungen zeigten, dass die luftgefüllten Tracheiden nicht wieder aufgefüllt wurden und sich die hydraulische Leitfähigkeit des Stammes innerhalb von 4 Wochen nicht erholte. Diese trockenheitsbedingten Schäden verursachten eine reduzierte Wassertransportkapazität, die sich in der unvollständigen Erholung des Blattgasaustausches auf ca. 50-60% der Kontrollwerte widerspiegelte. Außerdem fand ich keine Hinweise darauf, dass Nicht-Strukturkohlehydratreserven die hydraulische Erholung begrenzen könnten, da eine starke Speicherbildung nach dem Stress beobachtet wurde. Experiment 2 zeigte, dass trockenbehandelte Sämlinge eine reduzierte Kühlkapazität der Blätter im Vergleich zu gut bewässerten Sämlingen während einer Hitzewelle aufwiesen, was auf die reduzierten Transpirationsraten zurückzuführen ist. Die Auswirkungen auf den Elektrolytaustritt in Blattgeweben waren vernachlässigbar, jedoch nahm F'_v/F'_m unter Hitzestress mäßig und unter heißer Trockenheit stark ab, was auf einen lichtschützenden Prozess hinweist. Alleiniger Hitzestress führte zu einer geringen funktionellen Beeinträchtigung und ermöglichte eine schnelle Erholung metabolischer und hydraulischer

Parameter. Im Gegensatz dazu verursachte die Kombination von Hitze und Trockenheit einen Abfall des Wasserpotenzials auf -2,7 MPa, was zu einer metabolischen Dysfunktion aufgrund unterdrückter Photosynthese und teilweiser hydraulischer Beeinträchtigung führte. Diese Dynamik spiegelte sich auch in einer Reduzierung des Stammdurchmessers wider, was auf eine starke Ausbildung eines Wasserdefizits im Baum hinweist. Nach kombiniertem Hitze- und Trockenstress wurde eine verzögerte oder unvollständige Erholung der hydraulischen Leitfähigkeit von Blättern und Stämmen sowie des Spross- und Wurzelgasaustausches beobachtet. Bezüglich der C-Allokationsdynamiken kurz nach dem Stressereignis stellte ich fest, dass hitzegestresste Sämlinge den kürzlich aufgenommenen C rasch entlang des Langstreckentransportweges zur Wurzelatmung (7,1 h) und der mikrobiellen Bodenbiomasse (3 Tage) transportierten. Weiterhin investierten diese Sämlinge ^{13}C verstärkt in die Astzellulose, was auf eine Kompensationsmaßnahme durch verbessertes sekundäres Dickenwachstum hinweist. Im Gegensatz dazu akkumulierte bei trockenheits- und hitzebehandelten Sämlingen ^{13}C in den Nadeln, was sich im verzögerten C-Transport in die Wurzelatmung (13,8 h) widerspiegelte. Die kurzfristige Hemmung des Wachstums in diesen Sämlingen, unterstützt durch eine reduzierte N-Aufnahme und oberirdische Verteilung, könnte durch eine stressinduzierte Meristeminaktivierung hervorgerufen worden sein. Weiterhin wurde C nach der Trockenheit verstärkt in Stärke (d.h. in die Speicherung) investiert. Dabei nehme ich an, dass die Speicherbildung kurz nach dem Stress passiv stattfand, da der C-Transport zu anderen Organen reduziert war, währenddessen später in der Erholungsphase (ca. 7 Tage nach dem Stress) Stärke möglicherweise aktiv gebildet wurde als auch das Wachstum eine bedeutende C-Senke darstellte.

Mithilfe meiner Arbeit konnte gezeigt werden, dass die Kiefer in der Lage ist, extremen Klimaereignissen zu widerstehen und sich teilweise davon zu erholen, wobei das verfügbare Bodenwasser für die Verringerung der Auswirkungen von Hitzestress eine wichtige Rolle spielt. Der Blattgasaustauch erholte sich nach der Wasserlimitierung unvollständig, was auf hydraulische Einschränkungen zurückzuführen ist, wie z.B. verbleibende Embolien in Stämmen. Das - wenn auch verzögert - stark zunehmende Stammwachstum nach heißer Trockenheit könnte daher auf die enorme Bedeutung der Wiederherstellung der vollen hydraulischen Leitfähigkeit hinweisen, um eine verbesserte C-Aufnahme zu ermöglichen. Weiterhin zeige ich, dass die Dynamiken der C- und N- Verteilung kurz nach dem Stress von der Stressintensität abhängen. Das anfangs reduzierte Zusammenwirken der ober- und unterirdischen C-Verteilung nach kombiniertem Hitze- und Trockenstress deutet auf erhebliche funktionelle Beeinträchtigungen hin, v.a. bei der Phloembeladung und dem -transport sowie der Inaktivierung von Meristemen. Die Bildung von großen Speicherreserven in sich erholenden Kiefern könnte als Sicherheitsmaßnahme für nachfolgende Stressperioden gelten. Zusammenfassend zeigt diese Arbeit, dass stressbedingte Beeinträchtigungen wichtiger

physiologischer Prozesse in Kiefernsämlingen langfristig den Kohlenstoff- und Wasserhaushalt beeinflussen können. Solche Folgewirkungen könnten wichtig für die Vorhersage der Widerstandsfähigkeit von Wäldern gegenüber dem Klimawandel sein.

List of Publications

The content and structure of the included publications were retained in the form of the original publication or submission. 1. is included as chapter in the state after peer-review but before journal typesetting. 2. and 3. are presented in the state of submission to the journal/pre-print server.

1. **Rehschuh, R.**, Cecilia, A., Zuber, M., Faragó, T., Baumbach, T., Hartmann, H., Steven, J., Stefan, M. & Ruehr, N.K. (2020). Drought-induced xylem embolism limits the recovery of leaf gas exchange in Scots pine. *Plant Physiology*, 184(2), 852-864. https://doi.org/10.1104/pp.20.00407
2. **Rehschuh, R.,** Rehschuh, S., Gast, A., Jakab, A., Lehmann, M.M., Saurer, M., Gessler, A., & Ruehr, N.K. (in review). Tree allocation dynamics beyond heat and hot drought stress reveal changes in carbon storage, belowground translocation and growth. *New Phytologist*
3. **Rehschuh, R.** and Ruehr, N.K. (2021). Unrevealing water and carbon relations during and after heat and hot drought stress in *Pinus sylvestris*. bioRxiv 2021.06.29.450316. https://doi.org/10.1101/2021.06.29.450316

As the paper (or manuscripts in preparation for publication) involve the work of co-authors, I detail my contribution to 1.-3. are as follows:

1. I contributed to the conceptualization of the study, conducted the experiment, was involved in micro-CT measurements and performed all other physiological and hydraulic measurements, analyzed the data, and led the writing of the paper.
2. I contributed to the conceptualization of the study, conducted the experiment and extractions for isotopic mass spectrometry and nonstructural carbohydrate analyses, analyzed the data, and led the writing of the paper.
3. I contributed to the conceptualization of the study, conducted the experiment and performed measurements, analyzed the data, and led the writing of the paper.

During my PhD project, I had the chance to write or contribute as a co-author to the following publications. These papers were not included as separate chapters in this thesis, but were used for the interpretation of the results.

- **Rehschuh, R**., Mette, T., Menzel, A., & Buras, A. (2017). Soil properties affect the drought susceptibility of Norway spruce. *Dendrochronologia*, 45, 81-89.
- Gut, U., Árvai, M., Bijak, S., Camarero, J. J., Cedro, A., Cruz-García, R., Garamszegi, B., Hacket-Pain, A., Hevia, A., Huang, W., Isaac-Renton, M., Kaczka, R., Kazimirović, M.,

Kędziora, W., Kern, Z., Klisz, M., Kolář, T., Körner, M., Kuznetsova, V., Montwé, D., Petritan, A., Petritan, I., Plavcová, L., **Rehschuh, R.**, Rocha, E., Rybníček, M., Sánchez-Salguero, R., Schröder, J., Schwab, N., Stajić, B., Tomusiak, R., Wilmking, M., Sass-Klaassen, U. & Buras, A. (2019). No systematic effects of sampling direction on climate-growth relationships in a large-scale, multi-species tree-ring data set. *Dendrochronologia*, 57, 125624.

- Töchterle, P., Yang, F., Rehschuh, S., **Rehschuh, R.**, Ruehr, N.K., Rennenberg, H. & Dannenmann, M. (2020). Hydraulic water redistribution by Silver fir (*Abies alba* Mill.) occurring under severe soil drought. *Forests*, 11(2), 162

- Buras, A., **Rehschuh, R.**, Lange, J., Fonti., M., Fonti. P., Menzel, A., Gessler, A., von Arx, G., Treydte, K. & Rigling, A. (in preparation). Stable isotopes and xylem anatomy corroborate higher drought-susceptibility of Scots pine at the forest edge.

- Hikino, K., Danzberger, J., Riedel, V., **Rehschuh, R.**, Ruehr, N.K., Hesse, B.D., Lehmann, M.M., Buegger, F., Weikl, F., Pritsch K. & Grams, T.E.E. (submitted to *Global Change Biology*). High resilience of carbon transport in long-term drought stressed mature Norway spruce trees within two weeks after drought release.

- Nadal-Sala, D., Grote, R., Birami B., Knüver, T., **Rehschuh, R.**, Schwarz, S. & Ruehr, N.K. (submitted to *Frontiers in Plant Science*). Leaf shedding and non-stomatal limitations of photosynthesis improve hydraulic resistance of Scots pine saplings during severe drought stress.

Abbreviations

A_{net}	net assimilation
A_{SAT}	light-saturated photosynthesis
AICc	Akaike's information criterion corrected for small sample size
Air_{sample}	sample air
Air_{suppy}	supply air
BAI	basal area increment
C	carbon
^{13}C	natural, stable isotope of carbon
c_a	atmospheric CO_2 concentration
c_i	intercellular CO_2 concentration
CO_2	carbon dioxide
$[CO_2]$	carbon dioxide concentration
dH_2O	distilled and filtered water
DW	dry weight
E	transpiration
$F´_v/F´_m$	maximum light-adapted quantum yield of photosystem II
g_s	stomatal conductance
HLT	half-life time
H_2O	water
$[H_2O]$	H_2O concentration
HPLC	high-performance liquid chromatography
K_{Leaf}	leaf hydraulic conductance
k(M)Pa	kilo (mega) pascal
K_S	stem hydraulic conductivity
lme	linear-mixed effects model
micro-CT	x-ray microtomography
µ(m)mol	micro (mili) mole
MRT	mean residence time
N	nitrogen
n	sample count
^{15}N	natural, stable isotope of nitrogen
NSC	nonstructural carbohydrates
P_{12}	Ψ_{Xylem} at which 12% hydraulic conductivity is lost
P_{50}	Ψ_{Xylem} at which 50% hydraulic conductivity is lost
PAR	photosynthetic active radiation
PLA	percent loss of water-conducting area

PLC	percent loss of hydraulic conductivity
PPFD	photosynthetic photon flux density
ppm	parts per million
P. sylvestris	*Pinus sylvestris*
Ψ	water potential
Ψ_{Needle}	needle water potential
Ψ_{Xylem}	stem xylem water potential
R	carbon loss through respiration
RH	relative humidity (air)
RMSE	root-mean-square error
R_{root}	root respiration
R_{shoot}	shoot respiration
$R_{shoot\ night}$	shoot dark respiration
RWC_{Needle}	relative needle water content
SD	standard deviation
sdw	soil dry weight
SE	standard error
SMB	soil microbial biomass
SPEI	standardized precipitation evapotranspiration index
SWC	soil water content
TDN	total dissolved nitrogen
TE	treatment effect
Tukey's HSD	Tukey's honestly significant difference test
VOC	volatile organic compounds
VPD	vapor pressure deficit
VPDB	Vienna Pee Dee Belemnite
VWC	soil volumetric water content
WSC	water-soluble compounds
WUE_i	intrinsic water-use efficiency

1 General introduction

1.1 Forests are threatened by climate extremes

Forests cover about one third of the terrestrial land mass and are highly relevant for providing ecological, economic, social, and aesthetic ecosystem services (Millennium Ecosystem Assessment, 2005; FAO, 2020). They serve as habitat for a rich biological diversity and are important for matter cycling, such as water, carbon (C) and nutrient cycling (Bonan, 2008; Pan et al., 2011; Rennenberg and Dannenmann, 2015). Forests largely contribute to the atmospheric hydrological cycle via evapotranspiration, affecting cloud formation and precipitation (Bonan, 2008; Gupta et al., 2018; Sheil, 2018). Thereby, they enhance environmental surface cooling and promote water redistribution over terrestrial surfaces. Further, forests regulate climate by absorbing up to 1.2 GtC per year, equaling to approx. 20% of C emerging from anthropogenic sources (Liu et al., 2015; Friedlingstein et al., 2019). At a global scale, they represent important C sinks, sequestering c. 600 Gt of C, which is about 50% of all terrestrial C (Luyssaert et al., 2008; Pan et al., 2011; FAO, 2020). Thus, forests provide important climate feedbacks, however, these functions are negatively affected by climate change (IPCC, 2018), which may turn them into C sources (Bonan, 2008; Kurz et al., 2008; Bradshaw and Warkentin, 2015, Hubau et al. 2020). Additionally, biogeochemical processes of nutrient cycling are affected by a changing climate (Lukac et al., 2010; Dannenmann et al. 2016).

One main driver of climate change is the increase of the atmospheric carbon dioxide (CO_2) concentration by more than 100 parts per million (ppm) before the industrial era to c. 420 ppm in 2020 (Patra et al., 2005; Le Quéré et al., 2018; Dlugokencky and Tans, 2021), which is predicted to rise further due to anthropogenic activities. This increase in [CO_2] leads –together with an increase of other greenhouse gases as e.g. methane and nitrous oxide– to higher temperatures at the Earth surface (Morison and Lawlor, 1999). This in turn increases the occurrence of weather extremes (Meehl et al., 2000; Baker et al., 2018; Pidcock and McSweeney, 2021) such as heat waves and drought periods, which are projected to become more prolonged, severe and frequent within the 21st century, while being intermitted by heavy rain falls (Jacob et al., 2014; IPCC, 2018). Often heat and drought events occur simultaneously, resulting in hot droughts associated with high vapor pressure deficit (VPD; Hao et al., 2013; Stéfanon et al., 2014).

In recent decades, climatic stress on forests has increased substantially and threatened the productivity, vitality and survival of trees worldwide (Allen et al., 2010; Grossiord et al., 2020; McDowell et al., 2020). Heat waves combined with prolonged drought periods have been identified as a major cause (Allen et al., 2010; Anderegg et al., 2013a; Millar and Stephenson,

2015), with biotic factors such as pests and pathogens largely contributing to these effects (Allen et al., 2015; Wermelinger et al., 2008).

Therefore, climate change will force trees to withstand increasingly challenging conditions while maintaining live-sustaining physiological processes. The limited capacity of trees to rapidly adapt to changing conditions in the short-term is owed to their long life (Lindner et al., 2010). However, trees have developed various strategies to cope with a variety of stressors to avoid larger damage (Harfouche et al., 2014; Saijo and Loo, 2020). Following stress survival, stress-induced legacy effects might prevail, largely depending on stress severity (Yin and Bauerle, 2017; Ruehr et al., 2019). Frequently, plant responses to changing environmental and stress conditions will be delayed and involve chain processes, if full recovery is not reached. This has particularly been observed using dendrochronological analyses, while reduced stem growth rates were observed in subsequent years following a drought event (Anderegg et al., 2015b; Kannenberg et al., 2019a; Itter et al. 2019; DeSoto et al., 2020). Such growth reductions post-stress have been linked to a decrease of leaf area and/or C storage reserves during the stress event (Galiano et al., 2011; Anderegg et al., 2013b), as well as an impairment of the hydraulic system (Brodribb et al., 2010; Kannenberg et al., 2019b). Thereby, gymnosperms, including conifers, were found to exhibit larger legacy effects than angiosperms (Anderegg et al., 2015b). In existing vegetation models, however, the recovery of plant physiological processes post-drought is often considered to be rapid and complete (Anderegg et al., 2015b), which is not appropriate given the current state of research, especially with respect to long-lived plants such as trees. Further, modelling of forest responses to disturbances is currently challenged by the limited knowledge of C allocation fundamentals and the respective role of nonstructural carbohydrates (NSC) post-stress (Merganičová et al., 2019). This calls for an improved understanding of recovery processes and performance post-stress to be integrated into process-based models, which could then improve the predictability of future trends in tree survival, resilience and species distribution.

1.2 Drought impacts on Scots pine

Scots pine (*Pinus sylvestris* L.) is one of the dominant coniferous species worldwide. It grows from Siberia to Spain, and forms boreal to Mediterranean forests from the sea level up to 2600 m a.s.l. (Matías and Jump, 2012). Scots pine is one of the most studied species and has a large economic importance in forestry (Martínez-Vilalta et al., 2009; Krakau et al., 2013). It is considered a relatively drought tolerant species with an isohydric stomatal behavior, i.e. stomata close early under dry conditions (Martínez-Vilalta et al., 2004). However, extreme climate events in the past decades have resulted in reduced productivity and increased Scots pine mortality across Europe (Bigler et al., 2006; Buras et al., 2018; Etzold et al., 2019; Jaime

et al., 2019; Schuldt et al., 2020), including Franconia, Germany (Gößwein et al., 2017; Walentowski et al., 2017; Buras et al., 2018). For Franconian regions, where mortality events have been observed around 2015, the standardized precipitation evapotranspiration index (SPEI; i.e. a measure for water availability) revealed that the water availability was often below average since the 1990s, with exceptionally severe water deficits in the last decade (Fig. 1b-c, Buras et al. 2018). Climate-growth relationships for three affected forest stands (Heßdorf, Maisenlach, and Neustadt/Aisch) showed that these circumstances resulted in lower stem basal area increment (BAI) over the past 30 years in trees close to the south-facing forest edge

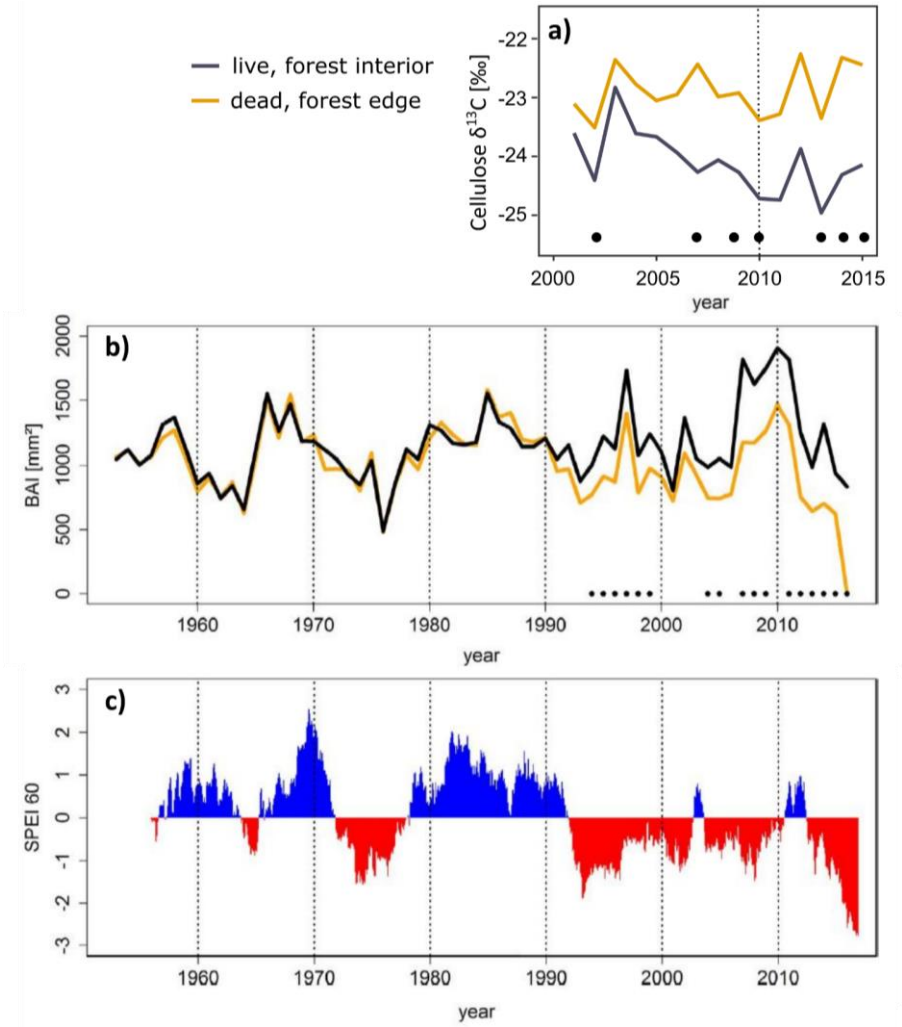

Fig 1: a) $\delta^{13}C$ in wood cellulose of Scots pine (n=5) for Maisenlach, Franconia, Germany, b) stem basal area increment (BAI) averaged for three Franconian Scots pine forest stands (Heßdorf, Maisenlach, and Neustadt/Aisch) as well as c) the standardized precipitation evapotranspiration index (SPEI). Shown are live trees in the forest interior (black lines) and dead trees at the forest edge (orange lines). Dots indicate significant differences between live and dead trees per year (paired Wilcoxon rank-sum test, P<0.05). The SPEI integrated over 60 months serves as a measure of long-term water availability. Blue bars represent water availability above average and red bars below average. Figure (b-c) adapted from Buras et al. (2018), cellulose $\delta^{13}C$ data from Buras et al. (in prep.).

that subsequently died, compared to surviving trees in the forest interior. Forest edges are often prone to higher sun light and wind exposure, higher soil and air temperatures, and VPD, and a lower water availability compared to the interior (Davies-Colley et al., 2000; Riutta et al., 2012). In general, tree performance does not only depend on weather and climate conditions, but also on soil characteristics, i.e. trees have been found to perform better in sites with a higher water holding capacity than in well drained soils during drought (Weber et al., 2007; Lévesque et al. 2013; Rehschuh et al., 2017). Higher $\delta^{13}C$ in wood cellulose of forest-edge compared to interior trees (Fig. 1a, investigated independently of the PhD thesis) supports the assumption of drought-induced stomatal control, resulting in discrimination against ^{13}C. Under optimal conditions, discrimination in C_3 plants and the dependence on the ratio of the intercellular to the ambient CO_2 concentration (c_i/c_a) has been well documented (Farquhar et al., 1982, 1989). Under drought conditions, inducing stomatal conductance (g_s) decline, lower discrimination against ^{13}C has been reported due to lower c_i (Olivas-García et al., 2000; Klein et al., 2005). Therefore, the strong drought events during the last 15 years affected particularly Scots pine at the forest edge, which apparently experienced NSC storage decline following reduced g_s, resulting in C depletion and subsequent tree death (Buras et al., 2018). This does not rule out hydraulic constraints, as C starvation can be associated with hydraulic failure, i.e. the inhibition of the water transport by damage to the vascular hydraulic system (Sevanto et al., 2014; Gentine et al., 2016; Adams et al., 2017; Li et al., 2020).

1.3 Water transport and the tree hydraulic system

According to the widely accepted cohesion-tension theory, water loss via transpiration (E) generates the driving force for water to be pulled within the xylem from the soil to leaves (Dixon and Joly, 1895; Angeles et al., 2004). This process is generated by the development of a gradient of water potential (Ψ), i.e. negative pressure, along the long-distance water transport path (Meinzer et al., 2001; Cruiziat et al., 2002), with water moving from higher to lower Ψ.

1.3.2 Drought and heat impacts on the tree hydraulic system

Nearly all transpirational water loss occurs through the stomata, while after stomatal closure in response to intense drought stress or high VPD, water is further lost by cuticular permeability (Riederer and Schreiber, 2001). In the short-term, E is controlled by stomatal opening, while in the long-term it is regulated by leaf area and biomass (Löf and Welander, 2000; Otieno et al., 2005). In contrast to the water-saving strategy under drought conditions, heat causes an increase in E under sufficient water supply, thus enabling effective leaf cooling, although g_s responses are not uniform (Urban et al., 2017b; De Kauwe et al., 2018; Drake et al., 2018). If drought and heat waves co-occur, however, drought-induced g_s decline will inevitably lead to

higher leaf temperatures (Scherrer et al., 2011; Birami et al., 2018; Drake et al., 2018), thus exacerbating plant physiological responses manifold (Rennenberg et al., 2006; Teskey et al., 2015). Soil water limitation and high evaporative demand cause a decrease in Ψ and affect the water transfer along the soil-tree-atmosphere continuum (Bréda et al., 2006; Urban et al., 2017b). Water under tension is in a metastable state and susceptible to cavitation and embolism. If Ψ reaches critical values, the continuous water column within the xylem can be disrupted, resulting in air bubbles entering into xylem conduits (=cavitation) and subsequent air spreading to adjacent conduits via pit membranes, thus blocking the water transport path (=embolism; Sperry and Tyree, 1988; Tyree and Sperry, 1989; Kaack et al., 2019). This leads to reduced hydraulic conductivity at the whole plant level and a subsequent reduction in water supply to leaves, resulting in reduced g_s to avoid further water loss (Meinzer, 2002; Martínez-Vilalta et al., 2004). Under prolonged and severe drought stress, embolism can accumulate rapidly, resulting in runaway embolism, and subsequently lead to irreversible hydraulic failure and tree desiccation (Tyree and Sperry, 1988; Sevanto et al., 2014; Martin-StPaul et al., 2017).

The xylem hydraulic safety characterizes the resistance of the xylem to embolism and the vulnerability of a tree to drought (Cruiziat et al., 2002; Mayr and Cochard, 2003). Hydraulic safety margins describe the difference between the minimum naturally occurring Ψ and a reference based on the xylem vulnerability curve such as P_{50}, i.e. the Ψ causing 50% loss of hydraulic conductivity in a plant organ (Meinzer and McCulloh, 2013). These safety margins have been shown to be wider in gymnosperms than in angiosperms (see Johnson et al., 2012), thus inhibiting or delaying stem xylem embolism. Susceptibility to embolism differs not only among species but also among organs within a species due to hydraulic segmentation, which means that embolism is often restricted to more dispensable organs (leaves, small branches or roots) than to indispensable organs such as the stem (Brodribb and Cochard, 2009; Bartlett et al., 2016; Bucci et al., 2016; Creek et al., 2018). Embolism formation in leaves has been shown to occur at more severe water limitation (Cochard et al., 2004; Brodribb and Cochard, 2009; Johnson et al., 2009; Skelton et al., 2017), while a decline in leaf hydraulic conductance (K_{Leaf}) was already observed at lower drought levels due to extra-xylary tissue shrinkage, cell collapse or the decline in aquaporin activity (Cochard et al., 2004; Scoffoni et al., 2014; Sack et al., 2016; Trifiló et al., 2016). In contrast, the effects of high temperatures on the response of hydraulic conductance under well-watered conditions were found to be lower (Way et al., 2013; McCulloh et al., 2016). In general, heat effects on the plant hydraulic system are less studied than drought effects, demonstrating an area of further research.

1.3.3 Hydraulic limitations post-stress

Following stress release, a subject of intense debates has been the question if trees are able to refill embolized conduits and which methods are suitable to test for this (Brodersen and McElrone, 2013; Cochard et al., 2015; Klein et al., 2018). Trees were found to recover their stem hydraulic system by different strategies: (1) The growth of new functional xylem in the long-term (Brodribb et al., 2010; Christensen-Dalsgaard and Tyree, 2014) or (2) refilling of embolized conduits on the short-term (Nardini et al., 2011; Klein et al., 2016). The refilling capacity of xylem embolism in some angiosperms, which has been reported to occur even on a daily basis (Salleo et al., 1996; Leng et al., 2013; Charrier et al., 2016; Gleason et al., 2017), is supported by the higher level of parenchyma cells in their xylem compared to gymnosperms (Johnson et al., 2012; Morris et al., 2016). The capacity for refilling also supports the lower safety margin compared to gymnosperms, which provides the advantage of keeping stomata open for a longer time despite the earlier onset of embolism formation, thus maintaining C uptake. Considering gymnosperms, reversal of winter embolism in spring has been reported repeatedly (McCulloh et al., 2011; Mayr et al., 2014). While some studies also suggest refilling to occur in gymnosperms after drought-induced embolism (Klein et al., 2016; Tomasella et al., 2017), the lack thereof is increasingly reported (Utsumi et al., 2003; Brodribb et al., 2010; Choat et al., 2015). Possible explanations for refiling are bubble dissolution under very low tensions or even positive pressures in the root or stem xylem, particularly occurring in spring (Sperry et al., 1987; Yang and Tyree, 1992; Brodersen and McElrone, 2013; Nardini et al., 2017), but also 'novel' refilling, i.e. when the xylem is still under tension, might exist (Hacke and Sperry, 2003; Ogasa et al., 2013; Nardini et al., 2017). Therefore, sugars or starch degradation in parenchyma cells may play a critical role by affecting the osmotic potential and thus enabling the flow of water into embolized conduits (Canny, 1998; Pickard, 2003; Salleo et al., 2009; Savi et al., 2016). However, the exact mechanisms behind embolism reversal still remain elusive, and controversies exist regarding novel embolism refilling since it seems impossible according to thermodynamic constraints (Yang and Tyree, 1992; Rockwell et al., 2014). Experimental artifacts during classic hydraulic measurements could create an illusion of refilling when xylem is still under tension (Wheeler et al., 2013; Venturas et al., 2017). Therefore, nondestructive methods such as magnetic resonance imaging (Holbrook et al., 2001; Bouda et al., 2019) or x-ray microtomography (Brodersen et al., 2010; Choat et al., 2015) are further evolving to visualize and measure the hydraulic status of the xylem, moreover to validate the results from indirect measurements. Therefore, the mechanisms for hydraulic recovery of Scots pine post-stress are going to receive further attention in this thesis.

1.4 Tree carbon and nitrogen cycling

Water loss by transpiration and the diffusion-driven process for CO_2 uptake via the leaf stomata are closely coupled processes. According to the Münch mechanism (Münch 1930), C is transported in forms of sugars along the long-distance transport path via sieve tubes of the phloem to sites of C demand (C sinks), e.g. regions of growth (Jensen et al. 2016). This process is driven by osmotic pressure differences in sugar concentration between C sources and sinks. If C is not used instantaneously, it is accumulated as NSC and lipids (Hoch et al., 2003; Hartmann and Trumbore, 2016; Galiano et al., 2017), while stored NSC have been known as important source for growth and energy.

Importantly, plant growth and productivity depend not only on water and C availability, but also largely rely on nutrient availability (Oren et al., 2001; Rennenberg et al., 2009; Fisher et al., 2012), particularly nitrogen (N), and phosphorus (P) in sites with high N deposition (Akselsson et al., 2008). N is an essential nutrient and available in soils in mineral and organic forms, as well as in the atmosphere as N_2, and is taken up via roots or leaves, respectively (Rennenberg and Dannenmann, 2015).

1.4.1 Drought and heat impacts on metabolic processes and C cycling

Considering stomatal behavior under water limitation, hydraulics and the carbon budget of trees are closely linked as C uptake decreases following a decline in g_s (McDowell et al., 2008; Mitchell et al., 2013; Sevanto et al., 2014). Stomatal closure most likely occurs after a threshold for embolism has been reached (Sperry, 2004), and hinders the fast desiccation and hydraulic dysfunction of plants, while limiting photosynthesis (Flexas and Medrano, 2002; Martínez-Vilalta and Garcia-Forner, 2017). Concurrently, the strong downregulation of metabolic processes causes the decrease of the content of ribulose 1,5-bisphosphate (RuBP), which has been found to be the main cause for restricted photosynthesis under severe drought stress (Flexas and Medrano, 2002).

The thermal optimum of photosynthesis is generally around 30 °C (Rennenberg et al., 2006; Blankenship, 2014). Temperatures significantly exceeding this optimum reduce photosynthesis by decreasing g_s (Ruehr et al., 2016; Birami et al., 2018), reducing enzymatic activity and impacting the thylakoid membrane (Feller et al., 1998; Schrader et al., 2004; Rennenberg et al., 2006). Photosystem II is highly temperature sensitive, particularly the enzyme Rubisco activase that reactivates Rubisco, wherefore high temperatures cause a reduction of the efficiency of electron transport (Berry and Bjorkman, 1980; Rennenberg et al., 2006). After reaching a threshold for leaf temperatures, membranes can get leaky, typically observed by electrolyte leakage (Saelim and Zwiazek, 2000; Correia et al., 2013; Escandón et al., 2016), while proteins have been found to denature and lose their function (Saxe et al.,

2001; Daniel et al., 2008). Further, characteristic responses to heat stress are the emission of volatile organic compounds (VOC) to prevent damage from reactive oxygen species, amongst others (Holopainen, 2004; Loreto and Schnitzler, 2010), while these processes largely depend on stress severity.

High air temperatures and/or water limitation could further stimulate C metabolic processes such as mitochondrial respiration and photorespiration, inducing a decrease in net C uptake rates (Atkin et al., 2000b; Weston and Bauerle, 2007). Photorespiration, in turn, serves to avoid the strong reduction of the photosynthetic electron transport chain and photoinhibition, which can protect the photosynthetic apparatus (Wingler et al., 2000). If respiration costs offset photosynthesis, net C uptake turns negative (Zhao et al., 2013; Birami et al., 2020), which might affect the C storage pools (see below). While respiration is vital for maintenance and growth processes (Atkin et al., 2000a), it is also affected by water limitation and heat stress (Jarvi and Burton, 2013; Gauthier et al., 2014; Birami et al., 2018, 2020; Gattmann et al., 2020). Decreases in shoot and root respiration have been documented in response to drought (Birami et al., 2018; Gattmann et al., 2020), while elevated temperatures typically result in increased respiration rates (Burton et al., 2002; Jarvi and Burton, 2013; Birami et al., 2020), but have been found to decline at higher temperatures (Jarvi and Burton, 2013; Birami et al., 2020). However, our knowledge particularly on the combined effects of heat and drought on respiratory processes still remains limited.

Under water limitation, NSC are responsible for water movement and retention by decreasing the osmotic potential to increase the resistance to lower water potentials (Bartlett et al., 2012; Sala et al., 2012). While the soluble fraction is predominantly important for osmotic adjustment, starch might also play an important role as osmotically active substance after depolymerization (Salleo et al., 2009). NSC storage pools, however, have been shown to decline when C uptake rates were reduced during stress (Bréda et al., 2006; McDowell, 2011). This might lead to metabolic imbalances and tremendously affect tree survival and post-stress recovery (Sevanto et al., 2014; Gentine et al., 2016).

1.4.2 Tree nutrition affected by climate change

N uptake by roots is most likely influenced by climate change due to shifted precipitation patterns, resulting in drying-wetting cycles that may be amplified by heat waves. A limited number of studies have addressed the role of nutrients in tree response to drought stress (e.g. Fotelli et al., 2002; Geβler et al., 2004a; Schönbeck et al., 2020) and following stress release, information are scarce (Gessler et al., 2017). Low soil nutrient availability, induced by low soil water content, might impair the nutritional status of a plant, thus reducing its functioning, tissue

growth and resistance (Kreuzwieser and Gessler, 2010). This might also impact its survival negatively in combination with C starvation (Gessler et al., 2017).

Following rewetting of dry forest soil, inorganic nitrogen (NH_4^+ and NO_3^-) has been found to increase due to higher microbial activity (Birch, 1964; Xu and Luo, 2012). Therefore, if leaching remains low, the abundance of soil available N increases, while the capacity of trees to utilize these nutrients depends on their N uptake capacity. Firstly, N uptake is subjected to a functioning root system, which might be disrupted by increased root mortality or loss of functionality following severe stress (Gaul et al., 2008; Schönbeck et al., 2020). Additionally, the regulation of N uptake depends on the internal N status of a tree (Geβler et al., 2004b). A tree-internal cycling pool of amino compounds is operated as a bidirectional exchange between the xylem and phloem within the whole plant, i.e. along the long-distance transport path from roots to leaves and vice versa. If N is not used immediately at the site of uptake, it will be loaded into this N cycling pool (Rennenberg and Dannenmann, 2015), from which it is continuously used for growth, storage and other metabolic processes (Millard and Grelet, 2010). Before the dormant season e.g., N is stored in species-specific N storage pools, while leaf growth in spring strongly relies on this pool as N root uptake starts with delay (Millard and Grelet, 2010; Rennenberg and Dannenmann, 2015). Therefore, N can be stored, remobilized and transported within plant organs, while the actual demand for N is signaled to roots, important for adapting the nutrient uptake (Herschbach et al., 2012; Rennenberg and Dannenmann, 2015). Further, cytokinins (plant hormones) are involved in signaling the soil mineral N status to the shoot, thus adjusting growth to N availability (Geβler et al., 2004b).

Following drought periods, grassland species were found to increase their root N uptake with the time lag largely depending on the species, while root growth lagged behind in all the investigated species (Cui and Caldwell, 1997; Ivans et al., 2003). However, these processes still remain elusive in forest ecosystems, and depend largely on stress intensity and duration. Following severe stress resulting in tissue impairment, N is necessary to regrow lost or damaged tissues or organs such as leaves, stems or roots, e.g. to increase plant hydraulic conductance or leaf area to upregulate photosynthesis (Brodribb and Cochard, 2009; Hammond et al., 2019). However, if nutrients were limiting at a stand and nutrient loss occurred, stress-induced impacts might not be fully reversible (Gessler et al., 2017). Therefore, the capacity of the regeneration of root nutrient uptake and subsequent assimilation influences the recovery of physiological processes and tree long-term performance.

1.4.3 Post-stress recovery of C and N cycling analyzed using stable isotope labeling

When stress is released, water availability increases, associated with an upregulation of g_s and C uptake rates (Ruehr et al., 2016; Birami et al., 2018). If stress caused tissue impairment, C should preferentially be supplied to sinks that allow trees to fully recover their hydraulic and metabolic processes until the occurrence of a subsequent stress event, e.g. invest into the repair of the root or hydraulic system to increase the uptake and transport of limiting resources (Freschet et al., 2018; Trugman et al., 2018). C allocation refers to the partitioning of C between tissues, compounds, fluxes and the soil microbial biomass, and further involves its function in plant growth, development and survival. C allocation is complex and depends on nutrient demands, while it is controlled by biogeochemical, physiological and ecological restrictions (Hartmann et al., 2018a). Therefore, C allocation is driven by source strength -depending on C supply via assimilation or C remobilized from resources- and sink strength, i.e. C demand in sinks such as metabolism, growth or storage (Klein and Hoch, 2015; Hartmann et al., 2015, 2018). C supply to sinks, however, may be limited by the reduced capacity of transporting new assimilates to demanding pools due to a damaged phloem (Sevanto, 2014, 2018). Concurrently, N uptake might be limited post-stress due to reduced root biomass. To elucidate legacy effects on plant physiological processes such as C and N cycling, stable isotope labeling techniques are powerful tools (Millard and Grelet, 2010; Epron et al., 2012). They allow to trace recently assimilated C or N through the plant, while the pace and quantity of the label allocated to competing pools or fluxes can be determined in a specific time frame (Kuzyakov and Gavrichkova, 2010; Hartmann and Trumbore, 2016). Most importantly, trees are not disturbed by this approach. $^{13}CO_2$ pulse-labeling is performed by exposing trees for a short time span (c. 1 - 4 h) to an atmosphere containing CO_2 that has an isotopically different signature than normal (Epron et al., 2012). Measurements at high temporal resolution of the CO_2 concentration and isotopic signature of respiratory effluxes provide the most accurate estimates of the time lags between the labeling onset and appearance of the label in respiration, while discontinuous measurements might underestimate the pace of label appearance in respiration (e.g. Pumpanen et al., 2009).

^{15}N tracer studies are generally performed by applying a solution containing mineral ^{15}N to the soil with watering or fertilization (Pellicer et al., 2000; Schönbeck et al., 2020), while avoiding overfertilization to ensure an undisturbed system. Further, the uptake of organic N (e.g. amino acids or proteins) has been investigated, and found to significantly contribute to plant nutrition (Öhlund and Näsholm, 2004; Dannenmann et al., 2009; Näsholm et al., 2009; Simon et al., 2011). To estimate uptake capabilities, enriched amino acids are added to soil solutions, in

which soil-cleared roots are immersed and analyzed after a specific time frame (Gessler et al., 1998).

In regard of seasonal and climate change related changes in C and N cycling, ^{15}N and ^{13}C labeling approaches have been used predominantly to determine changes in allocation patterns during the stress event itself. During drought, ^{13}C (e.g. Ruehr et al., 2009; Zang et al., 2014; Hagedorn et al., 2016) and ^{15}N labeling (Aaltonen et al., 2016; Dannenmann et al., 2016) has been applied more frequently, but also under elevated temperatures (^{13}C: Blessing et al., 2015; Drake et al., 2019 and ^{15}N: Giri et al., 2017). Further, several studies exist, which have investigated C allocation after drought release (Zang et al., 2014; Hagedorn et al., 2016; Galiano et al., 2017; Joseph et al., 2020), while recovery patterns following heat stress remain largely unexplored. Additionally, results post-drought indicate contradictory responses in temperate tree species, i.e. upregulated C allocation to the belowground (Hagedorn et al., 2016; Joseph et al., 2020) versus C remaining particularly in aboveground organs (Zang et al., 2014; Galiano et al., 2017). Therefore, in respect of the importance of C and N assimilated after stress release, the investigation of their role in regaining functionality will be one of the focal points of the present thesis.

1.5 Objectives of the thesis

This thesis is embedded within the research scope of the Emmy Noether project “Forests out of balance”, which investigates the impacts of extreme climatic events on carbon and water cycling in Scots pine (*Pinus sylvestris* L.). The present thesis aims at improving the understanding of the effects of heat and drought on tree hydraulics and above- and belowground C allocation patterns in Scots pine during and post stress.

In detail, the research objectives of my thesis are to (see also Fig. 2):

(1) Investigate drought-induced xylem embolism formation and potential refilling post-stress using classical hydraulic techniques and x-ray microtomography (micro-CT), and examine the coupling with leaf gas exchange and the carbon metabolism.

(2) Determine legacy effects of heat and hot drought on C allocation to plant tissues and compounds, respiration and the soil microbial biomass, and identify the coordination with the plant N metabolism.

(3) Evaluate the impacts of heat and hot drought stress on C and water relations and associated stem diameter variations during and post-stress.

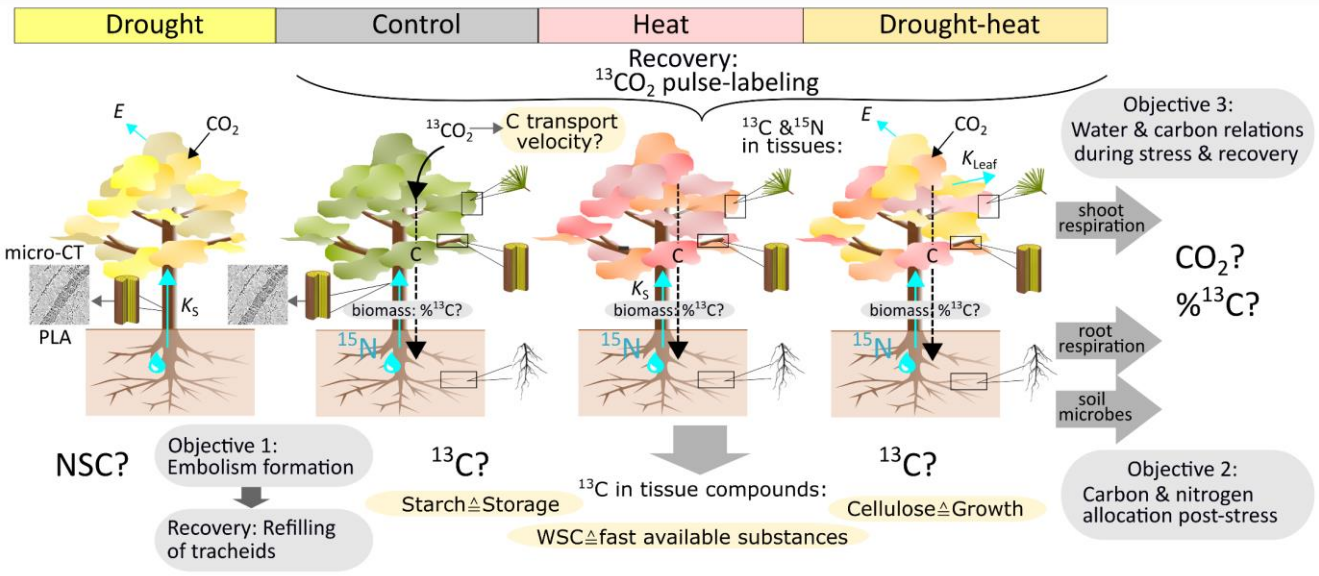

Fig. 2: Graphical representation of the objectives of the thesis. Shown are the analyzed stress and recovery treatments, while in the two experiments conducted, a control treatments was used for comparison both times. Carbon, water and nitrogen fluxes are indicated exemplarily. Micro-CT= x-ray microtomography, PLA = percent loss of water-conducting area, NSC = nonstructural carbohydrates, *E* = transpiration, K_s = stem hydraulic conductivity, K_{Leaf} = leaf hydraulic conductance, WSC = water-soluble compounds.

1.6 Approach

To address these objectives, I conducted two separately designed experiments under controlled conditions in a glasshouse facility at the Institute of Meteorology and Climate Research in Garmisch-Partenkirchen (KIT-IMK/IFU), Germany (708 m a.s.l., 47°28932.999N, 11°3944.299E). The objectives were chosen to elucidate the effects of the expected increase in the intensity of climate change, and therefore, environmental conditions adjusted as realistic as possible. For this, I analyzed climate data of extreme climatic years (2003, 2015) from a meteorological station of the German Meteorological Service in Weißenburg-Emetzheim, Franconia, Bavaria (435 m a.s.l., N49° 1′ 38,28″ E10° 58′ 55,2″). In this region, Scots pine forest die-back has been reported recently (Gößwein et al., 2017; Walentowski et al., 2017; Buras et al., 2018). Environmental conditions in the experiments were adjusted accordingly, and control conditions based on 30-year-averages, i.e. on averages of August 1986-2016.

Objective 1 was investigated in Experiment 1 (2017):

Seedlings were drought stressed for c. 1 month by withholding irrigation until a predetermined drought level was reached. We aimed at a stem xylem water potential (Ψ_{Xylem}) causing 40-50% percent loss of hydraulic conductivity (PLC), i.e. triggering severe stress, but preventing mortality (Brodribb and Cochard, 2009). For the visualization of stem xylem embolism in intact

plants, seedlings were transferred to the IMAGING beamline at the KARA Synchrotron of the Institute for Photon Science and Synchrotron Radiation, KIT, Eggenstein-Leopoldshafen, Germany. We performed micro-CT on drought stressed seedlings, as well as during recovery, i.e. shortly (2 days) and 4 weeks after re-watering. Measurements were complemented by classical hydraulic, leaf gas exchange and NSC measurements.

Objective 2 and 3 were analyzed in Experiment 2 (2018):

To tackle these research objectives, we used a custom-build tree gas exchange chamber system, allowing us to continuously measure shoot and root gas exchange (water (H_2O) and CO_2), $\delta^{13}CO_2$ of respiration and stem diameter variations. Seedlings were subjected to a 20-day heatwave, while daytime air temperature was progressively increased to max. 42°C, either under well-watered or water-limiting conditions. We measured NSC, various hydraulic characteristics and parameters serving as indicators for stress severity and recovery capacity, including electrolyte leakage and F'_v/F'_m in leaves. Two days after stress release, we applied a canopy $^{13}CO_2$ pulse-label to identify the C transport velocity to root respiration and C allocation patterns within plant tissues and compounds, respiration and the soil microbial biomass during 2.5 weeks. Additionally, we used soil-applied ^{15}N to analyze N uptake and the within-tree N allocation post-stress in relation to the C metabolism. In this experiment, we were able to derive a whole-tree C balance.

Based on the objectives, the following hypotheses were addressed:

(1) Under combined drought and heat stress, the impacts on the hydraulic and metabolic processes and other processes regarding tree functional integrity are larger than under single stressors.
(2) Embolism formation in stem xylem of Scots pine is not fully reversible one month after drought stress, and must therefore be compensated by stem growth.
(3) Leaf gas exchange recovery is delayed following drought, heat or combined stress once embolism has developed in leaf or stem xylem.
(4) Translocation of recently assimilated C to the belowground is enhanced shortly post-heat, but delayed post drought-heat. Recent C will be strongly invested into repair and growth, if stress impairment occurs.
(5) N uptake and allocation are in sync with the tree C metabolism post-stress.

1.7 Structure of the thesis

The structure of the present thesis is organized as follows. Chapter 2 presents details on stem xylem embolism formation during drought and a potential refilling in Scots pine during a 1-month recovery period (objective 1). Chapter 3 addresses the legacy effects of heat and hot

drought on C and N allocation patterns by means of stable isotope labeling (objective 2). Chapter 4 evaluates the effects of heat and hot drought during and post-stress on C and water relations, and associated stem diameter change (objective 3). Chapter 5 answers the hypotheses and summarizes the main results of the thesis, while outlining the conclusions and implications for future research.

2 Drought-induced xylem embolism limits the recovery of leaf gas exchange in Scots pine

This chapter has been published as: Rehschuh, R. [1], Cecilia, A. [2], Zuber, M. [2], Faragó, T. [2], Baumbach, T. [2], Hartmann, H. [3], Steven, J. [4], Stefan, M. [5], and Ruehr, N. [1] (2020): Drought-induced xylem embolism limits the recovery of leaf gas exchange in Scots pine. *Plant Physiology*, 184(2), 852-864. doi: 10.1104/pp.20.00407.

[1] Karlsruhe Institute of Technology, KIT Campus Alpin, Institute of Meteorology and Climate Research- Atmospheric Environmental Research, Garmisch-Partenkirchen, Germany

[2] Karlsruhe Institute of Technology, Institute for Photon Science and Synchrotron Radiation, Eggenstein-Leopoldshafen, Germany

[3] Max Planck Institute for Biogeochemistry, Department of Biogeochemical Processes, Jena, Germany

[4] Ulm University, Institute of Systematic Botany and Ecology, Ulm, Germany

[5] University of Innsbruck, Institute of Botany, Innsbruck, Austria

Abstract

Climate change increases the occurrence of prolonged drought periods with large implications for forest functioning. Scots pine (*Pinus sylvestris* L.) is one of the most abundant conifers worldwide and evidence is rising that its resilience to severe drought is limited. However, we know little about its ability to recover from drought-induced embolism. To analyze post-drought hydraulic recovery, we investigated stress and recovery dynamics of leaf gas exchange, nonstructural carbohydrates (NSC), and hydraulic properties in 2.5-year-old Scots pine seedlings. We quantified the degree of xylem embolism by combining *in vivo* X-ray microtomography (micro-CT) with intrusive techniques including measurements of hydraulic conductivity and dye staining during drought progression, short-term (2 days), and long-term (4 weeks) recovery. Seedlings were grown under controlled conditions and irrigation was withheld until stomata closed and xylem water potential (Ψ_{Xylem}) declined to -3.2 MPa on average, causing a 46% loss of stem hydraulic conductivity (K_S). Following drought release, we found a gradual recovery of leaf gas exchange to 50–60% of control values. This partial recovery indicates hydraulic limitations due to drought-induced damage. Whereas Ψ_{Xylem} recovered close to control values within 2 days, both micro-CT and intrusive measurements revealed no recovery of K_S. Moreover, we did not find indications for NSC reserves limiting hydraulic recovery. Our findings demonstrate that Scots pine is able to survive severe drought and to partially recover, although we assume that xylem development during the next growing

season might compensate some of the hydraulic impairment. Such drought-induced legacy effects are important when considering vegetation responses to extreme events.

Keywords: climate change, drought, dye staining, percent loss of hydraulic conductivity (PLC), xylem embolism, X-ray microtomography (micro-CT)

2.1 Introduction

Forests play a key role in the earth system by maintaining hydrological cycles, storing carbon and providing various ecosystem services (Watson et al., 2018; Jonsson et al., 2019). However, with increasingly frequent occurrences of climate extremes and particularly drought events, these pivotal services of forests are at risk (Choat et al., 2012; Reichstein et al., 2013). Additionally, severe drought events can result in forest decline as has been observed worldwide (Allen et al., 2015; Adams et al., 2017; Buras et al., 2018; Hartmann et al., 2018b). Often trees do not die during the stress event, but may succumb weeks to years later, and gymnosperms were found to show larger drought legacy effects than angiosperms (Anderegg et al., 2015b; DeSoto et al., 2020). Stress-induced functional damage may persist by incomplete recovery of plant hydraulic and metabolic processes (Trugman et al., 2018; Ruehr et al., 2019), making trees vulnerable (McDowell, 2011) to pests and pathogen attacks (Allen et al., 2015; Rehschuh et al., 2017). Due to the important role of recovery in stress resilience and tree survival, the physiological mechanisms associated with drought recovery and carry-over effects require more attention.

The time necessary for complete recovery of physiological functioning is crucial for tree survival, because further stress events could affect trees even more strongly (Schwalm et al., 2017). In addition, the severity of stress is an important factor influencing recovery dynamics (Ruehr et al., 2019). Hence, we can assume that recovery is slow when drought stress impairs critical plant physiological processes, such as carbon uptake or water transport. Recent studies have revealed that the damage to the plant hydraulic system plays a critical role in impeding plant survival during drought (Anderegg et al., 2015a; Salmon et al., 2015; Adams et al., 2017; Choat et al., 2018), as well as affecting post-drought recovery (Choat et al., 2019; Ruehr et al., 2019), but it needs to be proven if hydraulic impairment is one of the main factors preventing or postponing full recovery of vital physiological processes in the long-term (Körner, 2019).

Drought periods limit tree water uptake and cause plants to close stomata to prevent excessive water loss from transpiration and thus critical water potentials (Meinzer, 2002; Martínez-Vilalta et al., 2004). If drought persists, trees will continue to dehydrate and the water potential declines. Below a critical threshold, large gas bubbles can be formed in the water conducting pathway of the xylem, and the resulting embolism may spread to neighboring water-filled

conduits via pit membranes (Sperry and Tyree, 1988; Tyree and Sperry, 1989; Kaack et al., 2019). Consequently, the hydraulic conductivity of embolized xylem tissue will be impaired, leading to reduced leaf water supply, and ultimately to stomatal limitation and reduction of carbon uptake (Nardini and Salleo, 2000; Nardini et al., 2017), thus affecting nonstructural carbohydrate (NSC) storage pools (McDowell, 2011).

There is clear evidence for seasonal and daily refilling of embolized conduits in some angiosperm species based on positive xylem pressure at the local or whole-plant level (Leng et al., 2012; Charrier et al., 2016; Gleason et al., 2017). A frequently cited assumption is that refilling is largely driven by active transport and osmotic exudation of inorganic ions, sugars, or larger organic molecules into embolized conduit lumina (Taiz et al., 2014; Nobel, 2020). Alternatively, osmotic agents (e.g. sugars, degraded starch) could be mainly concentrated in parenchyma cells that are directly connected to embolized conduits, resulting in increased turgor pressure in these parenchyma cells, and water flow by osmotic pressure (Canny, 1998; Pickard, 2003). Nevertheless, the exact mechanisms behind positive xylem pressure remain unknown. Although conifers, which have no vessels and low levels of parenchyma in their xylem tissue (Johnson et al., 2012; Morris et al., 2016), have also been reported to refill embolism (Laur and Hacke, 2014; Klein et al., 2016; Tomasella et al., 2017), a growing body of literature indicates a lack of refilling capability in most conifer species (Utsumi et al., 2003; Brodribb et al., 2010; Choat et al., 2015). Moreover, instead of developing the ability to generate positive xylem pressure, conifers may prevent embolism by early stomatal closure during drought, regain hydraulic conductivity by quickly growing new xylem during recovery (Brodribb et al., 2010; Hammond et al., 2019), or use another -yet unknown- refilling mechanism. *Picea abies*, for instance, shows severe levels of embolism by freeze-thaw cycles during winter, but refilling during spring, which could be associated with water uptake via needles and bark tissue (Mayr et al., 2014, 2020).

Observations of embolism could also be hampered by artifacts associated with hydraulic conductivity measurements, such as bubble formation by cutting of xylem under negative pressure, and artificial refilling of embolized conduits (Wheeler et al., 2013; De Baerdemaeker et al., 2019). For this reason, nonintrusive methods provide a welcoming alternative to visualize the hydraulic status of xylem conduits *in vivo*. Examples include the application of magnetic resonance imaging (Holbrook et al., 2001; Bouda et al., 2019) and X-ray microtomography (Brodersen et al., 2010; Choat et al., 2015, 2016, 2019; Nardini et al., 2017). Application of these high-tech methods has become increasingly popular in recent years, providing novel insights into the ability of plants to recover embolized conduits following release from drought.

In recent years, Scots pine (*Pinus sylvestris* L.), one of the most abundant conifer species worldwide, has exhibited increasing mortality rates in many regions of Europe (Rigling et al.,

2013; Salmon et al., 2015; Buras et al., 2018; Etzold et al., 2019). This is surprising because Scots pine is considered to be relatively drought tolerant based on its isohydric stomatal behavior causing stomata to close early during drought (Martínez-Vilalta et al., 2004). A likely explanation is that Scots pine -typically occurring on the driest sites in commercially used forests of Central Europe- may be pushed beyond its physiological limits by more frequent and more severe drought events during the last decades. In light of these recent developments, an improved physiological understanding of the ability of Scots pine to tolerate drought and to recover hydraulic and metabolic functioning post drought is urgently needed.

The interaction of the recovery of leaf gas exchange and xylem hydraulic functioning has rarely been analyzed over the long term (one month following drought release) using hydraulic intrusive and non-intrusive methods. In this study, we analyzed tree physiological questions while testing methodological agreements. To elucidate mechanisms governing post-drought recovery, we exposed 2.5-year-old Scots pine seedlings to a severe drought stress, which resulted in c. 50% loss of hydraulic conductivity (PLC), re-watered them, and followed their recovery trajectories for four weeks. We then assessed whether the hydraulic system can be repaired via xylem refilling in the short term (2 days after re-watering) and in the long term (4 weeks after re-watering). For this, we measured *in vivo* embolism spread using X-ray microtomography (micro-CT), as well as stem hydraulic conductivity (K_S) of stem segments using a pressure-flow method, and performed dye staining experiments. To relate hydraulic functioning to seedling carbon metabolism, we determined leaf gas exchange dynamics and NSC concentrations of needle, stem, and root tissues. We hypothesized a delayed recovery of leaf gas exchange due to an impaired hydraulic system by drought. In case of embolism reversal, we expected the degradation of starch into soluble sugars to lower the osmotic potential in embolized conduits, thus allowing for refilling. Furthermore, we expected agreement between the destructive and non-destructive methods used to test for hydraulic recovery.

2.2 Results

2.2.1 Responses of leaf gas exchange and Ψ_{Xylem} during drought and post-drought recovery

Leaf gas exchange in Scots pine seedlings was sensitive to drought and declined progressively with decreasing xylem water potential Ψ_{Xylem} (Tukey's honestly significant difference test [HSD], $P<0.001$; Fig. 1A-D), while leaf gas exchange in the seedlings of the control treatment showed little variation. Stomatal conductance (g_s) was almost zero about 28 days after the drought treatment was initiated when Ψ_{Xylem} declined below -2 MPa. Simultaneously, relative needle water content (RWC_{Needle}) decreased with drought progression to 66% (compared to a

RWC_{Needle} of 80% in control seedlings; Tukey's HSD, P<0.001; Fig. 1E) when Ψ_{Xylem} was as low as -3.2±0.2 MPa on the last day of the drought treatment (Fig. 1D). This relates to about

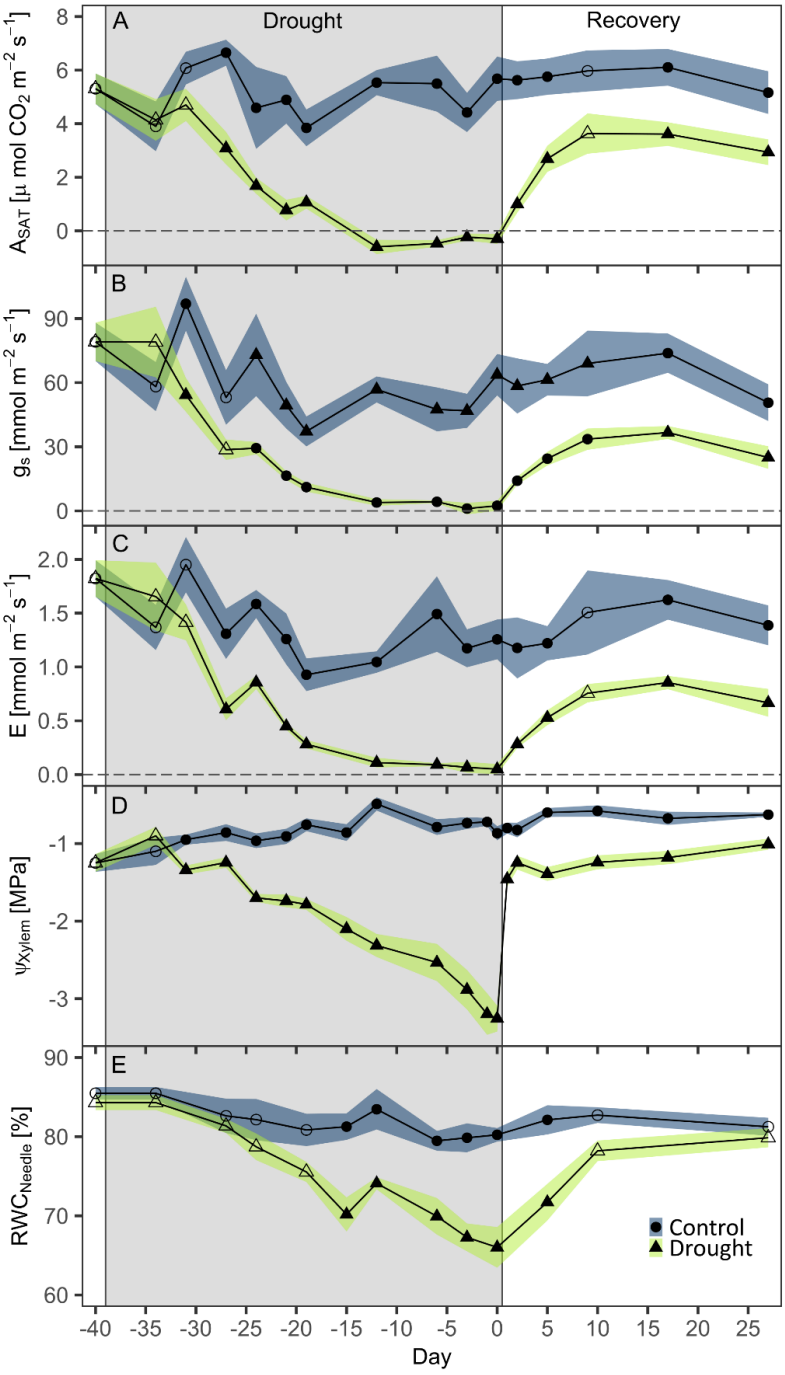

Fig. 1: Dynamics of leaf gas exchange and water relations during drought and recovery. Shown are light-saturated photosynthesis A_{SAT} (A), stomatal conductance g_s (B), transpiration E (C), xylem water potential Ψ_{Xylem} (D), and relative needle water content RWC_{Needle} (E) during drought (grey area) and recovery. Data are treatment averages and shaded areas are ±SE; n=6 control and n=10-12 drought-recovery seedlings. Filled symbols indicate significant differences between treatments (Wilcoxon rank-sum test). Seedlings were re-watered in the evening of day 0. From day 5 onwards, only those seedlings experiencing a slightly longer drought phase were measured.

50% PLC based on vulnerability curves (Supplemental Fig. S1). Despite this severe drought treatment, we did not observe browning or loss of needles.

After drought seedlings were re-watered (day 0), we observed an initial increase in leaf gas exchange, which subsided about 9 days later (Fig. 1A-C). After 27 days, light-saturated photosynthesis (A_{SAT}) had recovered to 57% of control values, while g_s and transpiration (E) reached about 50% (Tukey's HSD, P<0.001; see also Table 1). This resulted in intrinsic water-use efficiency (WUE_i) to increase by 19% in previously drought-treated seedlings.

In contrast to gas exchange rates, Ψ_{Xylem} recovered much faster and reached -1.25 MPa two days after re-watering. Throughout the following 25 days of recovery, the difference in Ψ_{Xylem} between the control and drought treatment remained relatively constant, and hence seedlings recovering from drought did not reach the Ψ_{Xylem} of control seedlings (Tukey's HSD, P<0.001). The recovery trajectory of RWC_{Needle} appeared to differ from Ψ_{Xylem} with a much slower increase, but reached control values at the end of the experiment.

Table 1: Treatment effect (TE) between control and drought seedlings at the end of the drought period and after the 27-day recovery period. Shown are gas exchange parameters A_{SAT}, g_s and E, as well as Ψ_{Xylem}, RWC_{Needle} and WUE_i (intrinsic water use efficiency). Values are treatment averages ±SE (n= 5-6 control and n= 10–12 drought-recovery seedlings).

Parameter	Treatment	End of stress	TE [%]	End of recovery period	TE [%]
A_{SAT}	Control	5.7±0.8	-	5.2±0.8	-
[µmol CO_2 m^{-2} s^{-1}]	Drought	-0.3±0.1	**-105.2**	3.0±0.5	**-43.1**
g_s	Control	63.7±9.7	-	50.6±8.6	-
[mmol m^{-2} s^{-1}]	Drought	2.4±2.4	**-96.2**	25.0±5.3	**-50.7**
E	Control	1.3±0.2	-	1.4±0.2	-
[mmol m^{-2} s^{-1}]	Drought	0.05±0.05	**-96.0**	0.67±0.1	**-51.9**
WUE_i	Control	94.9±15.6	-	103.7±4.2	-
[µmol mol^{-1}]	Drought	290.5±213.6	**206.1**	123.1±10.1	**18.7**
Ψ_{Xylem}	Control	-0.87±0.1	-	-0.63±0.03	-
[MPa]	Drought	-3.25±0.2	**-275.7**	-1.00±0.1	**-60.6**
RWC_{Needle}	Control	80.2±0.9	-	81.2±1.1	-
[%]	Drought	66.0±2.6	**-17.7**	79.9±1.2	**-1.7**

2.2.2 Dynamics of nonstructural carbohydrates

The drought-induced decrease in photosynthesis and Ψ_{Xylem} was mirrored by NSC dynamics, which showed a significant decline by 80-95% in starch concentrations of all tissues studied (Fig. 2C-D, Table 2). In contrast to starch, soluble sugar concentrations seemed to be unaffected by drought in needles and bark (Fig. 2A-B).

Table 2: Absolute values and treatment effect (TE) between control and drought-recovery seedlings for the soluble sugar and starch concentration at the end of the drought period and after a 27-day recovery period. Values are treatment averages ±SE; n=5-8 per tissue and treatment.

Parameter	Tissue	Treatment	End of stress	TE [%]	End of recovery period	TE [%]
Soluble sugars [mg/g]	Needle	Control	33.1±3.4		48.7 ±7.2	
		Drought	34.0±2.1	**2.6**	42.9±3.1	**-12.0**
	Bark	Control	28.6±3.3		52.3±7.2	
		Drought	28.9±4.3	**1.0**	41.0±2.3	**-21.5**
	Wood	Control	4.8±0.6		15.1±2.2	
		Drought	6.1±0.8	**26.9**	10.8±1.3	**-28.2**
	Roots	Control	22.0±2.3		36.3±2.2	
		Drought	18.2±5.0	**-17.0**	8.4±0.9	**-76.8**
Starch [mg/g]	Needle	Control	5.0±1.4		5.3±1.7	
		Drought	0.9±0.2	**-81.6**	15.7±3.1	**199.7**
	Bark	Control	15.8±1.3		20.1±8.3	
		Drought	0.8±0.4	**-95.0**	32.7±5.5	**63.0**
	Wood	Control	2.9±1.0		2.8±1.2	
		Drought	0.21±0.04	**-92.7**	2.4±0.7	**-13.5**
	Roots	Control	7.9±1.7		24.0±8.0	
		Drought	0.9±0.2	**-88.4**	11.5±2.0	**-52.1**

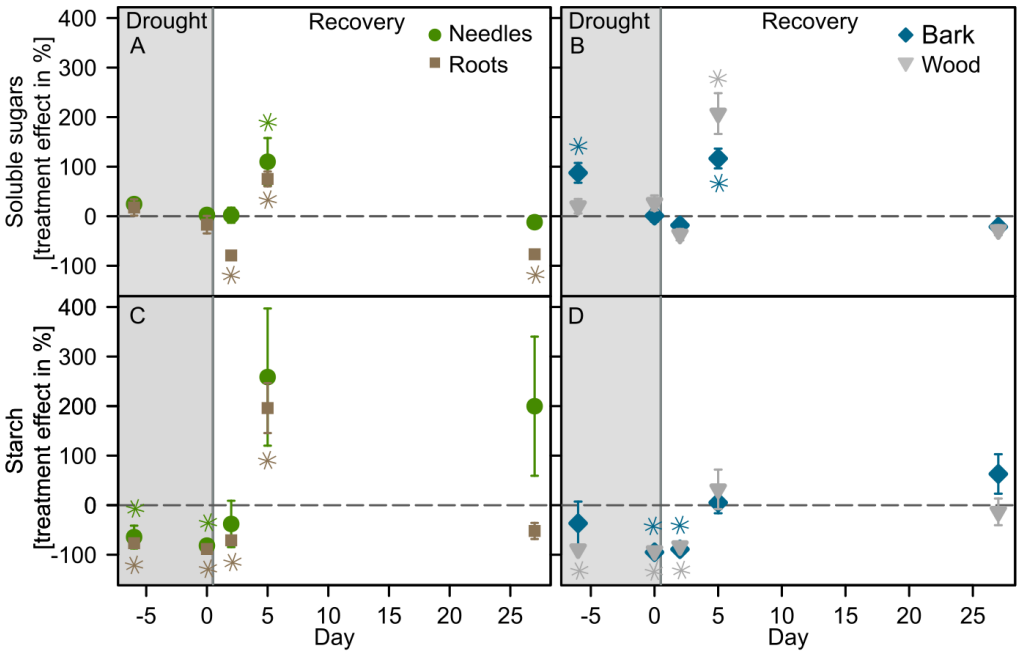

Fig. 2: NSC dynamics during drought and recovery. Tissue-specific soluble sugar (A and B) and starch (C and D) concentrations of the drought treatment are shown as treatment effects in percentage of control values ±SE (n= 5-8 per tissue and treatment). The dashed horizontal line indicates the mean of the control treatment. Asterisks indicate significant differences to the control treatment derived from the concentrations measured (Wilcoxon rank-sum test). The grey box represents the last week of the drought period; seedlings were re-watered in the evening of day 0.

Following re-watering, soluble sugars showed an initial decline in all tissues compared to the control, followed by a pronounced increase 5 days after re-watering. Simultaneously, we found the most pronounced increases of starch concentrations in needle and root tissues, which tripled compared to those of control seedlings (Fig. 2C). Interestingly, this increase in sugar and starch concentrations initially followed the recovery trajectory of photosynthesis (Fig. 1A), but vanished four weeks after re-watering (Fig. 2). One exception was a persistent high level of starch in needles and an accumulation in the bark compared to the control seedlings. Dynamics in starch concentrations seemed to be closely linked to Ψ_{Xylem} (Supplemental Fig. S3 F), likely due to a drought-related suppression of carbon uptake.

2.2.3 Hydraulic conductivity and xylem embolism

We tested the ability of *P. sylvestris* to refill embolized conduits using independent approaches: a) visual assessment of water- versus air-filled conduits *in vivo* using micro-CT, b) observation of conductive xylem area via dye staining, and c) measurements of stem hydraulic conductivity (K_S) using a pressure-flow technique.

Micro-CT images revealed that drought (average Ψ_{Xylem}=-3.2±0.2 MPa) resulted in c. 28±3% dysfunctional, air-filled xylem area (Fig. 3B, see also Supplemental Fig. S4 for additional micro-CT images), which manifested mainly in the latewood (on average c. 70% of embolized tracheid area). The embolized areas were most pronounced in tracheids of the first growth ring (near the pith) and in a distinct concentric ring of latewood tracheids in the 2nd year growth ring. Under progressive levels of drought, they also occurred in the earlywood of the 2nd year and in the most recently developed tracheids of early- and latewood. The xylem of control seedlings appeared generally functional with a small fraction of c. 4% non-conducting tracheids, of which c. 85% were present in the latewood. Embolized tracheids occurred mainly close to the pith and also in the 2nd-year latewood ring (Fig. 3A, Supplemental Fig. S4 A-C).

Following re-watering, when Ψ_{Xylem} had recovered to -1.25±0.08 MPa two days later (Fig. 1D), we re-measured two thirds of the previously analyzed drought-recovery seedlings. We could not detect indications of embolism reversal and the patterns of dysfunctional xylem area remained similar to the patterns observed before re-watering started (Fig. 3B-C, Supplemental Fig. S4). Four weeks after re-watering, we re-measured embolism on another set of drought-recovery seedlings (which had been stressed to a similar Ψ_{Xylem} of - 3.15±0.1 MPa). Once more, we did not detect any evidence of refilling of embolized xylem area (Fig. 3D, Supplemental Fig. S4 F,I,M), which was also reflected in calculated percent loss of water-conducting area (PLA; Fig. 4A). In addition, we found that the degree of embolism apparently had no effect on hydraulic recovery, because seedlings that were only stressed to their P_{12} values (i.e., Ψ_{Xylem} of - 1.5 to - 2.4 MPa), did not show signs of embolism reversal

(Supplemental Fig. S4 D-F). The results gained via micro-CT were further confirmed by dye staining, which indicated similar patterns of conducting versus non-conducting xylem areas, showing c. 4% non-conducting area in control seedlings compared to c. 26% non-conducting area in drought-stressed and recovering seedlings (Supplemental Fig. S5).

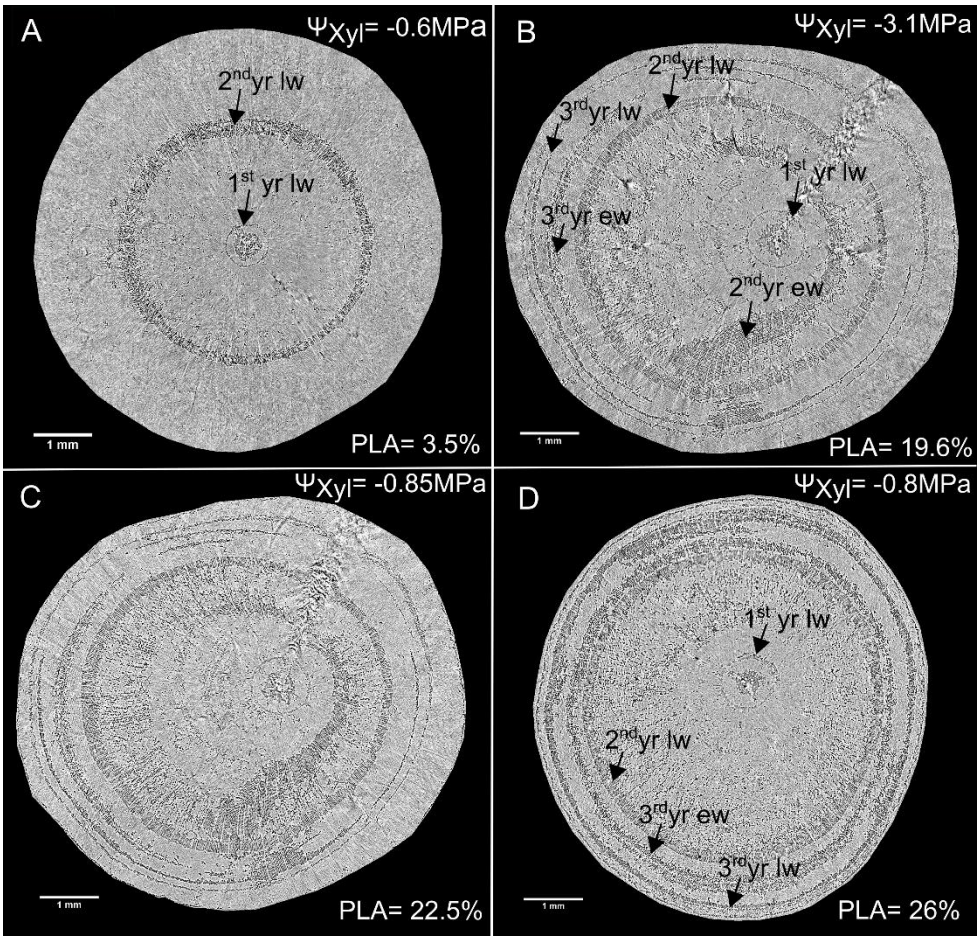

Fig. 3: Micro-CT images of Scots pine stems. Shown are examples of transverse slices of stem xylem of a control seedling (A), a drought-stressed seedling (B), the same one 2 d after re-watering (C), and another seedling that was stressed to -3 MPa but analyzed after 4 weeks of re-watering (D). Embolized tracheids appear black and water-filled tracheids in a light grey color. Xylem water potential (Ψ_{xyl}) before micro-CT measurements and percent loss of water-conducting area (PLA) is given. Main areas embolized in different growth rings are indicated by arrows (lw= latewood, ew= earlywood). Bars= 1 mm.

We further verified the agreement between micro-CT and the pressure-flow method on a subsample of seedlings previously measured at the synchrotron, and on seedlings that were not scanned. K_S declined significantly with drought progression by an average of 46% compared to control seedlings, and neither recovered within 2 days, nor within a longer period of 27 days (Fig. 4B).

In addition, we plotted loss of hydraulic conductivity estimated from pressure-flow analyses, and PLA calculated from micro-CT images vs. Ψ_{Xylem} at sample taking (Supplemental Fig. S1). Considering PLC from hydraulic measurements, we observed an overall good agreement with the vulnerability curve (VC) generated by the Cavitron. Regarding PLA, we found values to lie within the Cavitron vulnerability curve when observing Ψ_{Xylem} up to about -3 MPa. At Ψ_{Xylem} < -3MPa, however, the Cavitron curve showed an earlier increase in PLC at less negative Ψ_{Xylem} than PLA.

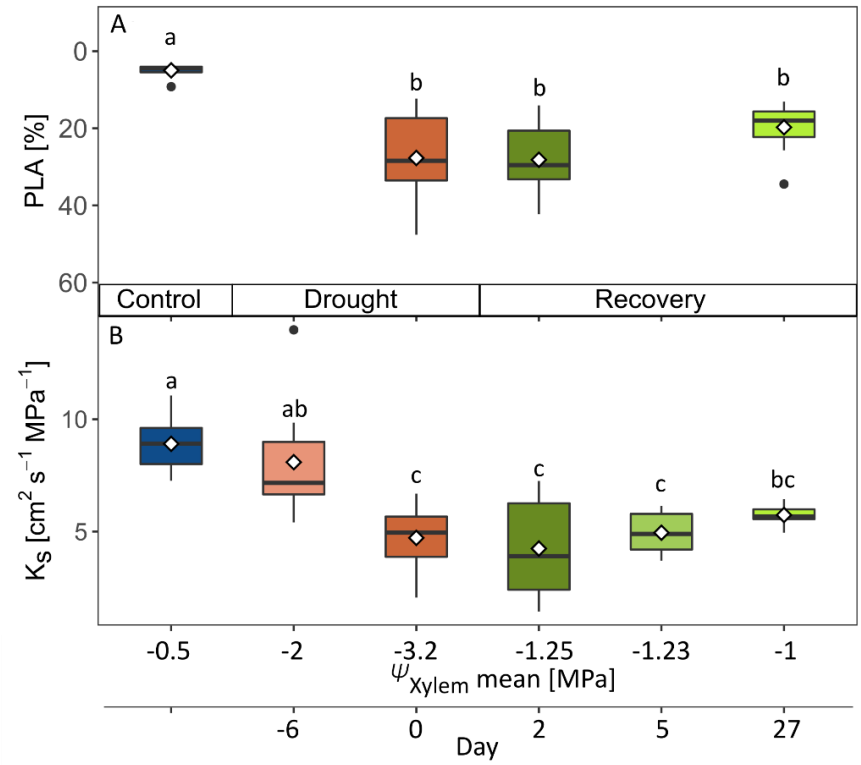

Fig. 4: Percent loss of water-conducting area (PLA) and stem hydraulic conductivity (K_S) during drought and recovery. Given are PLA from micro-CT images (A) and K_S from pressure-flow measurements (B) for control (blue), drought (reddish colors), and drought-recovery (greenish colors) seedlings (n=6-12). Diamonds depict the mean per treatment and time step. Small letters indicate significant differences between treatments (Kruskal-Wallis test & Bonferroni post hoc test).

In addition, linking NSC concentrations to the hydraulic parameters K_S, PLA or RWC_{Needle}, did not indicate a dependency (Supplemental Fig. S3).

2.2.4 Relationships of leaf gas exchange with Ψ_{Xylem} during drought and recovery

We found A_{SAT} (R^2 =0.68) and g_s (R^2 =0.63) to be closely related to Ψ_{Xylem} during drought, and stomatal closure was at -2.4±0.5 MPa close to P_{12} (Fig. 5), which corresponded approximately to the Ψ_{Xylem} when embolism started to form (Supplemental Fig. S1). A_{SAT} became negative, i.e. respiration exceeded assimilation rates, slightly earlier at a Ψ_{Xylem} of ca. -1.9 MPa.

The close relationships of A_{SAT} and g_s with Ψ_{Xylem} changed dramatically after re-watering (R^2=0.08 and 0.09). At a Ψ_{Xylem} of -0.8 MPa, we observed A_{SAT}, g_s and E to be 43%, 51% and 52% lower in drought-recovery seedlings compared to control seedlings (Fig. 5, Table 1). This reduced recovery of carbon assimilation and transpiration compares well to the 46% reduction of K_S in the drought-recovery seedlings (Fig. 4B), indicating that the persistence of xylem embolism was the main reason for the incomplete recovery of leaf gas exchange.

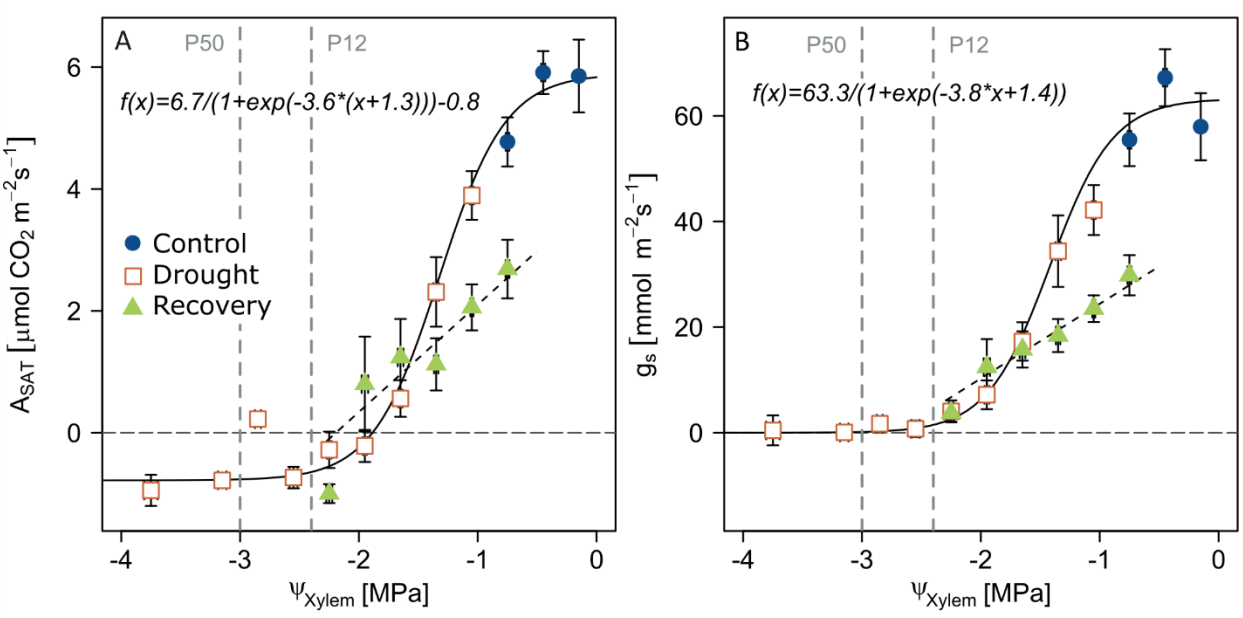

Fig. 5: Relationships of leaf gas exchange with xylem water potential Ψ_{Xylem}. Dependencies of light-saturated photosynthesis A_{SAT} (A) and stomatal conductance g_S (B) with xylem water potential Ψ_{Xylem} are given for the control treatment (including pre-stress data of the drought treatment; blue circles), drought progression (orange squares), and recovery (green triangles). Data are bin-averages for intervals of 0.3 MPa, mean ±SE are shown. P_{12} and P_{50} determined by Cavitron measurements are indicated. A sigmoidal function was fitted to control and drought data (A_{SAT} RMSE= 1.64; g_s RMSE= 20.9) and a linear regression to data of drought seedlings after re-watering (A_{SAT} R^2= 0.08; g_s R^2= 0.09). RMSE is root-mean-square error.

2.3 Discussion

The results of our study provide evidence for hydraulic impairments limiting the drought recovery of Scots pine seedlings. Both, hydraulic measurements on stem segments and micro-CT imaging on intact seedlings showed that embolized xylem tissue did not recover within 2 days or after 4 weeks following re-watering. Furthermore, we found no indication that C reserves were limiting hydraulic recovery. Leaf photosynthesis, transpiration and stomatal conductance also recovered partially. The underlying mechanism was that a persistently reduced stem hydraulic conductance restricted water transport and hence normal plant functioning.

2.3.1 Drought results in hydraulic limitations altering gas exchange and NSC dynamics

We dehydrated Scots pine seedlings to about 50% loss of hydraulic conductivity (Fig. 4B), which, as expected, did not result in tree death (Brodribb and Cochard, 2009). In a recent meta-analysis, a PLC higher than 60% was shown to be non-lethal in many tree species, including gymnosperms (Adams et al., 2017), and *Pinus taeda* saplings survived 72% PLC (Hammond et al., 2019). Our P_{50} values generally agreed with previous studies on Scots pine (Martínez-Vilalta et al., 2004; Poyatos et al., 2008; Torres-Ruiz et al., 2016). Torres-Ruiz et al. (2016) reported relatively similar P_{50} values for Cavitron measurements and 50% of embolized tracheid area obtained via micro-CT (-3.3 vs. -3.0 MPa). We found good agreement of PLC derived from Cavitron and pressure-flow analyses (Supplemental Fig. S1). The Cavitron curve, however, showed an earlier reduction in loss of conductivity at less negative Ψ_{Xylem} than PLA calculated from micro-CT images. We exclude differences in sampling time as the reason for this discrepancy (Charrier et al., 2018) as pressure-flow measurements compared quite well to the data derived from the Cavitron. The difference could rather be explained by the fact that PLA quantifies embolism visually and directly, but does not account for hydraulic conductivity. Therefore it probably overestimates embolism resistance compared to PLC in our study as water-filled tracheids, which are poorly connected to other water-filled tracheids, might appear as fully functional.

As shown in various earlier studies (e.g. Skelton et al., 2017; Birami et al., 2018), Scots pine reduced leaf gas exchange (A_{SAT}, g_S, and E) during the progression of drought alongside declining Ψ_{Xylem} (Fig. 1A-D). Stomata of seedlings were fully closed at a Ψ_{Xylem} of c. -2.4 MPa (Fig. 5B), which reduces water loss via transpiration and delays dehydration. The xylem tensions we observed at stomatal closure lies well within the reported range for pines (Martínez-Vilalta et al., 2004) and closely corresponds to P_{12} - generally related to the onset of embolism formation- which is consistent with previous studies (e.g. Li et al., 2015; Skelton et al., 2015).

In our study, partial stomatal closure reduced C uptake, and with progressing stomatal closure, light respiration exceeded A_{SAT} at Ψ_{Xylem} <-1.9 MPa. (Fig. 5A). This was further reflected in significantly decreasing starch concentrations in all tissues. By contrast, sugar concentrations did not decrease as seedlings needed to maintain metabolic and osmoregulatory processes (Fig. 2), likely at the cost of starch and other carbon reserves. With drought progression, sink activity can be reduced earlier than source activity, which leads to an accumulation of sugars in leaves (Muller et al., 2011) and, as transport is slowed during drought, also in the stem phloem. An additional mechanism sustaining sugar concentrations could be woody stem photosynthesis, which allows internal CO_2 recycling independent of stomata opening

(Vandegehuchte et al., 2015). Increased sugar concentrations in the wood may favor hydraulic functioning (Tomasella et al., 2019). Although there is no uniform pattern of NSC dynamics during drought (Hartmann and Trumbore, 2016), many previous studies have found starch concentrations to decline (Adams et al., 2017; Birami et al., 2018). This indicates that during drought stress, when net leaf carbon gain is suppressed, trees need to rely on reserve compounds.

2.3.2 No reversal of xylem embolism four weeks post-drought

Visual assessment via noninvasive micro-CT on Scots pine seedlings allowed for a proper estimation of air-filled versus water-filled areas within the stem xylem. Latewood showed more embolism than earlywood (Fig. 3, Supplemental Fig. S4), which agrees well with other studies on conifers (Mayr and Cochard, 2003; Choat et al., 2015, 2016; Umebayashi et al., 2016), and could be caused by the seemingly inflexible, rigid nature of the pit membrane, which results in a reduced ability to seal the pit aperture to prevent air-seeding (Petty and Preston, 1970; Domec and Gartner, 2002; Dalla-Salda et al., 2014). Latewood tracheids frequently show a lower pit density than earlywood, with pit borders reported to be larger than 15 µm in earlywood, but only 4 to 6 µm in latewood of *Picea sitchensis* and *P. orientalis* (Domec et al., 2006; Usta and Hale, 2006). Therefore, quantitative pit characteristics do not seem to explain the low embolism resistance of latewood compared to earlywood. The concentric distribution of embolized tracheids, however, could be explained by the occurrence of bordered pits in radial walls of tracheids (Dalla-Salda et al., 2014; Choat et al., 2016). Most of our control seedlings (and also dehydrated ones) revealed air-filled tracheids in the inner section of the xylem around the pith, which has also been reported previously for well-watered trees (Choat et al., 2016; Torres-Ruiz et al., 2016) and could have resulted from fast wood growth during early developmental stages of the plant, and tracheids with only partial secondary wall thickening.

Drought-recovery seedlings showed no reduction of PLA after two days and four weeks of re-watering (Fig. 3B-D, Fig. 4A). As hypothesized, results from the pressure-flow technique and dye staining agreed with micro-CT measurements, revealing that embolized xylem did not refill and hydraulic conductivity did not recover within four weeks post-drought (Fig. 4). This confirms previous findings on other conifer species. For instance, Choat et al. (2015) reported a lack of refilling in *Sequoia sempervirens* two weeks post-drought using micro-CT. Furthermore, no evidence of embolism refilling in *Pinus thunbergii* and three other conifer species using cryo-scanning electron microscopy was found (Utsumi et al., 2003; Umebayashi et al., 2016). Moreover, Brodribb et al. (2010) detected no evidence of refilling in *Callitris rhomboidea*, as did Hammond et al. (2019) using intrusive methods for *Pinus taeda*. In contrast, reversal of

winter embolism caused by a combination of strong drought and freeze-thaw cycles has been observed repeatedly (McCulloh et al., 2011; Mayr et al., 2014, 2020). In our study, soil drought was released via re-watering of the soil. Other studies, in which needle and bark tissues were re-wetted, however, reported at least partial embolism reversal (Laur and Hacke, 2014; Earles et al., 2016). Therefore, the type of re-wetting and also the timing of the drought experiment late in the season could play a role in the ability of trees to refill embolized xylem conduits. We did not measure predawn water potential here, but night-time conditions were relatively cool and moist, presumably preventing water loss by transpiration. Therefore, it is reasonable to assume that atmospheric conditions have not limited the ability to refill embolism in our study. Since the physiological parameters measured in the re-watered seedlings reached a plateau after 27 days, it seems unlikely that refilling would occur after a longer recovery period. Moreover, the timescale of seasonal refilling contrasts strongly with reports on daily refilling processes in conifers (Klein et al., 2018, 2016), which seems highly unlikely.

Reasons for the lack of xylem refilling may include the low proportion of parenchyma in the secondary xylem and relatively low NSC reserves in stems compared to angiosperms (Johnson et al., 2012; Morris et al., 2016), in which refilling has been proved (Salleo et al., 2009; Charrier et al., 2016; Gleason et al., 2017). In our study, we did not find any evidence of starch mobilization to coincide with re-watering. Directly after stress release, low wood starch concentrations could potentially have limited the lowering of the osmotic potential in the embolized conduit. However, 5 days after re-watering, drought-recovery seedlings had reached similar wood starch concentrations as the control seedlings, and soluble sugar concentrations surpassed the values of control seedlings. In addition, we found no clear relationship between starch and soluble sugar concentrations of relevant tissues with K_S, PLA or RWC_{Needle} (Supplemental Fig. S3). This indicates that the availability of NSC reserves was not a limiting factor in embolism repair, however, since no refilling occurred in our study, we cannot answer our second hypothesis.

2.3.3 Impaired hydraulic functionality affects C metabolism post-drought

Following stress release, we observed leaf gas exchange increasing slowly for about 9 days, then remaining unchanged during the following 2.5 weeks (Fig. 1A-C). Starch and soluble sugar concentrations increased strongly in all tissues along with carbon uptake 5 days after re-watering (Fig. 2). This may indicate that sink activities, e.g. growth, was still inhibited shortly after stress release. Other studies have shown that reserve formation is associated with a growth inhibition due to low water potentials (Muller et al., 2011) or active upregulation via the synthesis of starch or lipids (Dietze et al., 2014). Storage formation in needles and bark, which we have observed to occur during recovery, might indicate a conservative strategy to support

survival of subsequent drought periods (Galiano et al., 2017; Weber et al., 2019). Furthermore, storing of NSC in the bark might be important to fuel longitudinal growth and basal area increment of stems in the following year, as has been observed previously for branches (Kagawa et al., 2006), presumably to restore hydraulic conductivity in the long-term. In contrast, the observed consumption of root NSC in drought-recovery seedlings might suggest an immediate upregulation of repair and regrowth of root tissues, indicating the preference of resource investments to restore water and nutrient uptake (Hagedorn et al., 2016; Galiano et al., 2017; Cuneo et al., 2020). To transport assimilates to source organs, functional phloem loading and transport are needed. We observed that starch and soluble sugars increased in root tissues after re-watering, which indicates phloem functionality. This was also supported by the delayed but full recovery of RWC_{Needle}, which might restore the functionality of carbon transport via symplastic loading and unloading (Lalonde et al., 2003). The recovery of RWC_{Needle} indicates the repair of extra-xylary tissues (Laur and Hacke, 2014), which also plays an important role in buffering temporary water deficits (Charra-Vaskou et al., 2012).

Considering leaf gas exchange, we found a higher WUE_i in drought-recovery seedlings compared to control seedlings, which has previously been explained by an improved mesophyll conductance following drought release (Cano et al., 2014). In agreement, a meta-analysis found a complete recovery of photosynthesis to be more often reported than that of g_S (Ruehr et al., 2019), which results in a higher WUE_i during recovery than before stress. In our study, we did not observe a complete recovery of A_{SAT} or g_s throughout the 4-week recovery period, even though Ψ_{Xylem} increased quickly and steeply (Fig. 1). However, Ψ_{Xylem} also did not recover fully, which agrees with findings on severely drought-stressed *Callitris rhomboidea* (Brodribb et al., 2010). Similar to our study, fast increase of water potential but not leaf gas exchange post-drought has been reported in many earlier studies (Ruehr et al., 2019). An initial delay in the recovery of g_S might be the result of abscisic acid (ABA) – a phytohormone inducing stomatal closure – being maintained at high concentrations in the leaves for several hours after re-wetting (Brodribb and McAdam, 2013). Furthermore, impaired biochemical capacity (Cano et al., 2014), metabolic constraints (Hagedorn et al., 2016; Adams et al., 2017; Ruehr et al., 2019) and an impaired hydraulic system (Brodribb and Cochard, 2009; Brodribb et al., 2010; Skelton et al., 2017) might be the underlying reasons. The results of our study support hydraulic impairment as the most limiting factor of leaf gas exchange recovery, thereby confirming our hypothesis. Following stress release, we found the relationship between Ψ_{Xylem} and leaf gas exchange to differ compared to drought stress conditions (Fig. 5). In particular, g_S was much lower at the same Ψ_{Xylem} during recovery than before stress was applied. This suggests that leaf gas exchange was primarily limited by the embolism-induced lower hydraulic conductivity post-drought. Due to the impaired ability of the seedlings to transport water,

stomata could not fully open, which enabled the maintenance of moderate Ψ_{Xylem}. Overall, the 46% reduction of K_S caused by embolism corresponds quite well to transpiration being c. 50% lower in drought recovery compared to control seedlings.

We did not observe K_S to recover within one month. This indicates a lack of refilling of embolized tracheids, and also points towards a reduced growth of new xylem, albeit NSC concentrations were high. However, since our experiment was conducted during September to November, cambial activity and xylem formation had presumably already stopped at this time of the year (Gruber et al., 2009; Cuny and Rathgeber, 2016). In contrast, one might speculate that a similar experiment earlier during the season, could have resulted in K_S to recover (at least partially) along with wood formation. Xylem growth, resulting in recovery of hydraulic conductance, has been observed previously in conifers (Brodribb et al., 2010; Hammond et al., 2019) and angiosperms (Christensen-Dalsgaard and Tyree, 2014; Skelton et al., 2017). Considering the pine seedlings studied here, we assume that new wood formation in the next growing season would allow for the regain of at least partial hydraulic functioning and an improved overall whole-plant carbon gain, while considering that xylem development typically takes several weeks or even months (Cuny et al., 2014). This is also suggested by a recently developed model that predicts the repair of the hydraulic system to depend on secondary growth of xylem, which is limited by available NSC reserves (Trugman et al., 2018), and tree death would occur if reserves become critically depleted. In a recently developed conceptual framework, the tight coordination between hydraulic and metabolic recovery has been indicated (Ruehr et al., 2019). If stress results in an impaired functionality or tissue damage, recovery will be delayed and depends on repair mechanisms and/or growth of new functional tissue. In our study, we could clearly show that damage to the hydraulic system via embolism formation is not easily repaired, and that recovery may rely on formation of new xylem. This indicates that not only the intensity of stress, but also its frequency can critically affect tree survival, as production of new functional tissue might be too slow before the onset of the next drought event.

2.4 Conclusion

Our study demonstrates that a drought causing 50% loss in xylem hydraulic conductivity critically impairs metabolic and hydraulic functioning of Scots pine seedlings. While this did not result in mortality of the seedlings during a one-month recovery period, it might, in case of lacking recovery, culminate in tree death later on. We found no indication of a recovery of stem hydraulic conductivity, and no reversal of xylem embolism either directly after re-wetting or one month later. These results were supported by both intrusive and nonintrusive methods, and we therefore recommend the application of low-cost intrusive techniques such as pressure-

flow measurements and dye-injection experiments to determine hydraulic conductivity and visualize embolism of conifer xylem. Despite no refilling of embolized tracheids after re-watering, leaf gas exchange partially recovered, which was tightly connected to the reduced water transport capacity. Moreover, seedlings recovered slowly based on their carbohydrate dynamics, and it needs to be proven if there will be a delayed growth of new xylem.

Our study provides novel information on how drought-induced damage of the hydraulic system affects both carbon uptake and NSC dynamics in Scots pine. Based on our findings, we highlight the need for a better physiological understanding of the role of growth processes and carbon reserves in order to predict hydraulic functioning and growth performance after drought. Recent observations (e.g. DeSoto et al., 2020) have shown that mortality of mature trees can be linked to many years of reduced growth performance induced by stress, indicating that an incomplete recovery leaves trees more vulnerable to future drought events.

2.5 Material and Methods

2.5.1 Plant material and growth conditions

Potted 2-year-old seedlings of *Pinus sylvestris* (provenance: foothills of the Alps, Germany) were obtained from a local tree nursery and transplanted in larger pots (5 liter, 15 cm in diameter, 25 cm in height) in May 2017 in a mixture of fine sand, medium grained sand, gravel and vermiculite (1:2:1:2). 12 g of slow-release fertilizer (Osmocote® Exact Standard 5-6M fertilizer 15-9-12+2MgO+TE, ICL Specialty Fertilizers, The Netherlands) was added to all pots, supplemented by 0.14 ml liquid fertilizer (Compo® Complete, 6+4+6(+2) NPK(MgO), Hornbach, Germany) to ensure immediate nutrient supply.

Seedlings were grown under controlled conditions in a greenhouse at the Institute of Meteorology and Climate Research (IMK-IFU) in Garmisch-Partenkirchen, Germany (708 m a.s.l., 47°28′32.9″N, 11°3′44.2″E). The greenhouse was equipped with highly UV-transmissive glass. To supplement outside light, we used sodium vapor lamps (T-agro 400W, Philips, Hamburg, Germany). Air temperature and relative humidity were controlled automatically within the chamber (CC600, RAM Regel- und Messtechnische Apparate GmbH, Herrsching, Germany), in which ventilation and air-conditioning units allowed for homogenous air conditions. The seedlings were frequently rearranged within the greenhouse compartment. Air temperature and relative humidity were monitored at canopy height with relevant sensors (CS215, Campbell Scientific Inc., Logan, Utah, US, enclosed in aspirated radiation shields of type 43502, Young, Traverse City, MI, USA), alongside the measurement of photosynthetic active radiation (PAR; PQS 1, Kipp & Zonen, Delft, The Netherlands). All seedlings were watered to field capacity every second to third day.

2.5.2 Experimental design

The drought treatment was initiated on September 1, 2017, by withholding irrigation until a predetermined drought level was reached (Fig. 6). Subsequently, seedlings were re-watered to field capacity at around 6 pm and watered every second day. During the first 18 days of the drought treatment, day-night-oscillation of relative humidity was between 56%±8 (mean±SD) and 72%±4%, and air temperature oscillated between 13°C±1°C during the night and 20°C±5°C during the day (Supplemental Fig. S2). After 18 days, air temperature was increased by ca. 6°C and relative humidity decreased by about 25%, resulting in a maximum vapor pressure deficit of c. 3 kPa. During the day, PAR averaged between 700 and 1000 µmol m^{-2} s^{-1}. Furthermore, to achieve a predetermined drought level before re-watering, drying was enhanced by ventilators. We targeted a Ψ_{Xylem} causing 40-50% PLC to ensure that drought stress would be severe but not lethal since > 50% PLC may lead to mortality in conifers (Brodribb and Cochard, 2009). To estimate this Ψ_{Xylem}, we generated a vulnerability curve using the Cavitron technique (Cochard, 2002; Supplemental Methods S1), and found a P_{50} for Scots pine at -3.01 MPa (P_{12} at -2.42 MPa; Supplemental Fig. S1), which was defined as our target Ψ_{Xylem}.

For micro-CT measurements, a subset of randomly selected control (n=15) and drought-treated seedlings (n=30) was transported to the KARA synchrotron facility near Karlsruhe (for details see Section 2.5.6). Measurements were done immediately before and 2 days after re-watering. Between measurements, seedlings were placed outside in natural light conditions, where air temperature ranged between 10°C and 25°C, and relative humidity was between 50% and 98% (see Supplemental Fig. S2B for details). Note that another subset of control (n=15) and drought-treated seedlings (n=30) that had not reached the target Ψ_{Xylem} yet, was left in the greenhouse. These seedlings were re-watered 8 days later, when they had reached the target Ψ_{Xylem} (Fig. 6). During the recovery phase, temperature in the greenhouse was about 21°C ±2°C during the day and 15°C ±1°C in the night, and relative humidity ranged between 52% ±6% and 65% ±6% (Fig. S2A), thereby not exceeding a vapor pressure deficit of 1.8 kPa during the day and 1 kPa during the night. To asses if refilling of embolized conduits is a gradual process over time, micro-CT measurements on the second subset of seedlings were conducted 27 days after re-watering. We purposely chose another subset of seedlings to avoid possible artifacts from X-ray radiation on tree health (Cochard et al., 2015; Petruzzellis et al., 2018). Control and drought seedlings scanned via micro-CT were on average 53.3±4.5 cm and 51.5±3.2 cm in height with a stem diameter of c. 10.4±1 mm and 10.0±0.8 mm, respectively.

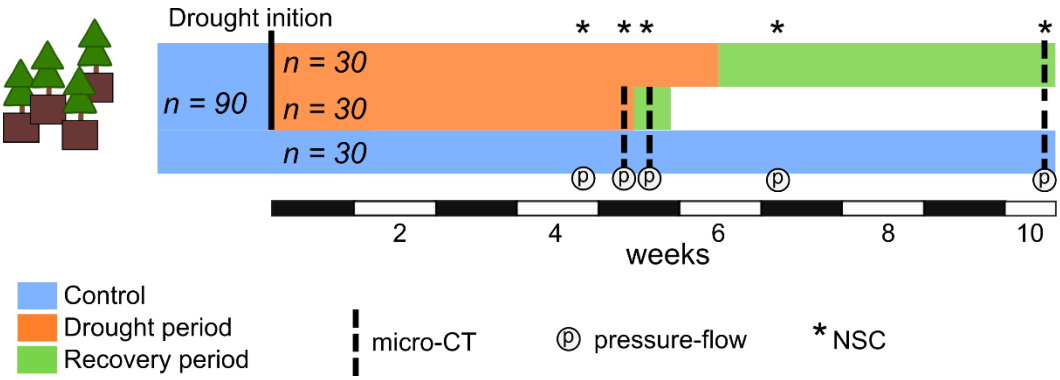

Fig. 6: Experimental design. Depicted are three subsets of seedlings used for (1) a long period of drought recovery (top bar), (2) a short recovery period (middle bar), and (3) control seedlings. Timing of micro-CT, pressure-flow and nonstructural carbohydrate (NSC) measurements are indicated.

2.5.3 Midday water potential and relative needle water content

We measured Ψ_{Xylem} from non-transpiring needle fascicles of 6 control and 10-12 drought-recovery seedlings typically at noontime directly after leaf gas exchange measurements (see 2.5.4). Furthermore, Ψ_{Xylem} of all seedlings measured via micro-CT was determined before scanning of seedlings. Transpiration of needles was prevented by enclosing a current-year shoot in a nontransparent plastic bag for 1 h before measurements. Two needle fascicles were sampled from each of the shoots, immediately measured with a Scholander pressure chamber (Model 1000 Pressure Chamber Instrument, PMS Instrument Company, Albany, Oregon, USA) and values averaged. We tested for agreement between Ψ_{Xylem} from needles of bagged shoots and Ψ_{Xylem} from branches of the same individual and found strong correlation (r=0.99, P<0.001, n=6).

During the drought period, Ψ_{Xylem} was measured at time intervals of 2 to 6 days, followed by more frequent measurements when Ψ_{Xylem} reached values closer to the target Ψ_{Xylem}. Directly after re-watering until 2 days later, Ψ_{Xylem} was measured daily. With progression of the recovery period, measurement intervals were prolonged. Assessing Ψ_{Xylem} was often accompanied by measurements of RWC_{Needle}. For this, two needle fascicles per seedling (n=6 control and n=10-12 drought-recovery seedlings) were placed in plastic bags to avoid moisture loss, and sample mass was determined immediately (W_{fresh}), after hydrating needles in purified water for 48 h (W_{turgid}), and after drying at 70°C for at least 48 h (W_{dw}). The time until needles were fully hydrated was predetermined by saturation curves for dehydrated and control seedlings. RWC_{Needle} was then calculated according to Chen et al. (2010) as follows:

$$\mathrm{RWC_{Needle}}(\%) = 100 \cdot \frac{(W_{\mathrm{fresh}} - W_{\mathrm{dw}})}{W_{\mathrm{turgid}} - W_{\mathrm{dw}}} \quad (1).$$

2.5.4 Leaf gas exchange

Leaf gas exchange measurement campaigns were coordinated with Ψ_{Xylem} measurements. Light-saturated photosynthesis (A_{SAT}) [µmol CO_2 $m^{-2}s^{-1}$], transpiration (E) [mmol $m^{-2}s^{-1}$] and stomatal conductance (g_s) [mol $m^{-2}s^{-1}$] were measured using a portable leaf-gas exchange system (Li-6400 , LI-COR Inc., Lincoln, NE,USA) equipped with a light source (6400-40 Leaf Chamber Fluorometer). The same fully developed current-year needle cohorts were measured throughout the experiment, and we only switched to other needle cohorts if signs of damage became obvious. The measured projected needle area was known by filling the leaf cuvette (2 cm^2) completely with needles and avoiding overlap as much as possible. Each measurement campaign lasted from 10 to 12 am, and leaf gas exchange of 6 control and 10-12 drought-recovery seedlings was measured under predetermined saturated light conditions of 1200 µmol m^{-2} s^{-1} PPFD and a CO_2 concentration of 400 ppm. Conditions inside the leaf cuvette were kept constant, with an average leaf temperature of 25.5°C, relative humidity of 46.5% and vapor pressure deficit of 2 kPa. 5 days after re-watering, we resumed leaf gas exchange measurements of those seedlings that were not measured at the micro-CT facility (Fig. 6, top bar). We calculated intrinsic water-use efficiency (WUE_i in µmol CO_2 mol^{-1} H_2O) as a measure of photosynthetic efficiency as follows:

$$\mathrm{WUE_i} = \frac{A_{\mathrm{SAT}}}{g_{\mathrm{s}}} \quad (2).$$

2.5.5 Nonstructural carbohydrate measurements

Plant available carbon reserves were determined by analyzing NSC concentrations in samples of needles, roots, stem bark (including cambium) and stem wood (n=5-8 per tissue and time step), according to Landhäusser et al. (2018). Collection of samples was coordinated with hydraulic conductivity measurements (see 2.5.7) and was done in the afternoon (3 to 4 pm) as follows. Samples were immediately microwaved for 120 s to stop enzyme activity (Landhäusser et al., 2018), oven dried at 70°C for 78 h and then ball milled to fine powder (MM200, Retsch, Haan, Germany). Approximately 10 mg per sample was extracted in 80% (v/v) ethanol at 90°C for 10 min. The supernatant was used for quantifying NSCs by High-Performance Anion Exchange Chromatography with Pulsed Amperic Detection (HPAE-PAD), an Ion Chromatography method. For starch digestion and quantification, the residual pellet was cleaned and dried at 60°C to eliminate the remaining ethanol. Starch was converted to soluble oligosaccharides by using α-amylase from *Bacillus licheniformis* (Sigma cat. no. A4551) for 2 h at 85°C. Solids were separated by centrifugation at 13,000 g for 1 min and glucans in the supernatant were hydrolyzed to glucose with amyloglucosidase from *Aspergillus niger* (Sigma cat. no. ROAMYGLL) for 2 h at 55°C. The resulting product glucose hydrolysate

was again quantified by HPLC. Results were multiplied by 0.9 to obtain the starch concentration.

2.5.6 Visualization of embolism via micro-CT

To visualize embolized tracheids in secondary xylem of intact plants, we conducted micro-CT measurements at the IMAGING beamline at the KARA Synchrotron of the Karlsruhe Institute of Technology (KIT), Germany. We performed micro-CT scans of the seedlings a) after drought stress (n=12), b) two days after re-watering (recovery; n=10), and c) four weeks after re-watering using another set of seedlings which had not been exposed to X-ray radiation before (n=12). Further, we measured d) control seedlings from both subsets (n=12) and e) compared synchrotron-based PLA with the Cavitron vulnerability curve by additionally dehydrating seedlings (n=15, Supplemental Fig. S1). Note that some of these additionally dehydrated seedlings, which were either stressed until reaching P_{12} values (i.e., Ψ_{Xylem} of -1.5 to -2.4 MPa) or exposed to higher drought stress (Ψ_{Xylem} > -3.6 MPa), were also scanned twice (after drought stress and two days after re-watering). This was done in order to determine if the degree of embolism has an influence on potential refilling mechanisms (Supplemental Fig. S4 D,E,K,L).

Before each micro-CT measurement, we determined Ψ_{Xylem} and leaf gas exchange, and then placed each seedling in a custom-built plant holder, which was fixed to an air-bearing stage. Branches and needles were wrapped in cling film to avoid movement that could blur the image. The white-beam spectrum (used for the tomography experiments) was filtered with 1 mm Al. The X-ray projections of the tomography scan were recorded with an indirectly converting X-ray area detector composed of a 200-µm-thick LuAG:Ce scintillator, an Optique Peter white beam microscope providing a magnification of 2x and a PCO.DIMAX camera with 2016 × 2016 pixels, with a physical pixel size of 11 µm. The effective pixel size was 5.5 µm and the effective field of view 11.0 mm × 11.08 mm. For each tomography experiment 6,000 projections over 360 degrees were taken to increase the available field of view. The distance between the sample and the detector (propagation distance) was set to 230 mm. Scan time per sample was about 3 min. The tomographies were acquired with a frame rate between 40 fps up to 70 fps. During micro-CT scans, we used an infrared camera (PI 450, Optris, Germany) to observe stem temperature, which remained approximately between 24 and 26°C. The scanned region was at a stem height of approx. 4-5 cm above the soil surface and we marked this area in order to scan seedlings after re-watering at the same height. As soon as all micro-CT scans were completed, seedlings were cut and a sample of the stem (ca. 6 cm) that included the scanned area, was dried for about 1 day to produce a fully dehydrated stem cross-section (reference scan). Additionally, the piece of the stem above the scanned area was used for further

hydraulic measurements (see 2.5.7). Samples from stem, roots and needles were taken for NSC analysis (see 2.5.5).

Images were reconstructed according to Vogelgesang et al. (2016), and the middle slice per sample was automatically selected for quantitative analysis in ImageJ/Fiji image-processing freeware, a Java-based distribution of ImageJ (www.fiji.sc; Schindelin et al., 2012; Rueden and Eliceiri, 2019). We assessed the percentage of air-filled versus water-filled stem xylem conduits by excluding the pith, the primary xylem and the resin channels, as well as other nonconductive areas as determined by the reference scan. Brightness and contrast were modified for each sample individually to improve the detection of water- versus air-filled conduits, and thus estimate PLA. Differentiation into air versus water-filled tracheids was confirmed by dye staining on the same samples analyzed by micro-CT (Supplemental Methods S2).

2.5.7 Stem xylem hydraulic conductivity

Hydraulic conductivity measurements on stem segments of 6-12 seedlings per treatment were conducted using the pressure-flow method (Sperry and Tyree, 1988). Firstly, stem segments were wrapped in cling film, placed in tightly sealed plastic bags and kept frozen at -18°C for c. 10 days until analyses were conducted. Prior test measurements revealed that freezing of samples had no effect on K_S by correlating K_S from frozen with fresh stem segments of the same individuals ($r=0.94$, $P<0.001$, $n = 8$).

For hydraulic conductivity measurements, frozen samples were emerged in distilled water and slowly thawed. Finally, they were cut back underwater, the bark was removed at the sample ends, and 2-3 mm were cut off at both ends with a sharp carving knife to remove exuded resin, which could interfere with flow measurements. The obtained stem segments were about 6-10 cm long and had a diameter of ca. 7-9 mm. Up to 5 samples were fastened to a fivefold valve (Luer-lock system; neoLab Migge Laborbedarf-Vertriebs GmbH, Heidelberg, Germany), and an infusion bag with distilled, filtered (0.22 µm pore size) and degassed water with 0.005% (v/v) Micropur water purifier (Katadyn Products, Wallisellen, Switzerland) was connected to the water flow system. The measurement pressure was 0.004 MPa, and the flow rate was determined for each stem segment separately using a mass flow meter (mini-CORI-FLOW M13, Bronkhorst, Montigny les Cormeilles, France). K_S was calculated based on the cross-sectional area of the xylem and length of the sample. We further tested if K_S differed between controls and samples previously exposed to X-ray radiation. We obtained similar results and thus merged them. To generate a vulnerability curve, we dehydrated additional seedlings ($n=9$), and PLC was obtained by relating K_S to that of control seedlings (Supplemental Fig. S1).

2.5.8 Data analyses and statistics

All data analyses were performed in 'R' version 3.6.1 (R Core Team, 2019). To test for significant differences between the control and drought treatment, we used the Wilcoxon rank-sum test to account for small and unequal sample sizes. Considering several groups, we applied the Kruskal-Wallis test followed by the Bonferroni post-hoc analysis. A p-value <0.05 was considered significant. Treatment effects on leaf gas exchange, Ψ_{Xylem} and RWC_{Needle} were further assessed by fitting linear-mixed effects models (lme; lmerTest package, Kuznetsova et al., 2017) using time and treatment as fixed effects and tree number as random factor to account for repeated measurements in time. Model selection was based on the Akaike's information criterion corrected for small sample size (AICc), and the models with the lowest AICc, i.e. the most parsimonious model, was selected (Burnham and Anderson, 2002). This was followed by the post-hoc Tukey multiple comparisons test of means (Lenth et al., 2020). Tukey's HSD for significant difference between treatments is reported.

To test for dependencies between Ψ_{Xylem} and gas exchange parameters (A_{SAT}, g_s), we used regression analyses. We fitted a sigmoidal function to data from pre-stress and drought. Furthermore, we tested for effects of changes in NSC concentration on hydraulic parameters such as K_S, PLA, Ψ_{Xylem} and RWC_{Needle} by plotting these variables versus starch and soluble sugar concentration of the relevant tissues. Further, correlation analyses were performed using Spearman's rank correlation.

For selected variables, the % treatment effect (TE) of the drought treatment was calculated as follows:

$$\mathrm{TE}\ (\%) = 100 \cdot \frac{(\mathrm{mean}_{\mathrm{drought}} - \mathrm{mean}_{\mathrm{control}})}{\mathrm{mean}_{\mathrm{control}}} \quad (3)$$

where *mean* is the treatment average per measurement time-point.

Acknowledgements

We would like to thank Birgit E. Dämon for assistance with hydraulic measurements, Eliana Häfele and Tamara Wittmann for experimental support and assistance at the synchrotron facility. Furthermore, we are grateful to Daniel Nadal-Sala for help with statistical data analyses and to 3 anonymous reviewers for their constructive feedback on an earlier version of the manuscript.

Funding information

This study was supported by the German Research Foundation through its Emmy Noether Program (RU 1657/2-1) and by the Austrian Science Fund (FWF) I3724-B32.

Author contributions

R.R. and N.K.R. designed the study with support from S.J., S.M. and H.H.; R.R. and N.K.R. conducted the experiment; R.R., A.C., M.Z., T.F. and N.K.R. performed micro-CT measurements and analyses; H.H. conducted NSC analyses and R.R. performed all other measurements and analyzed the data with support from N.K.R, S.M., H.H. and S.J.; R.R. wrote the original draft of the article with contributions from N.K.R. and all other co-authors.

2.6 Supplemental material

Supplemental figures

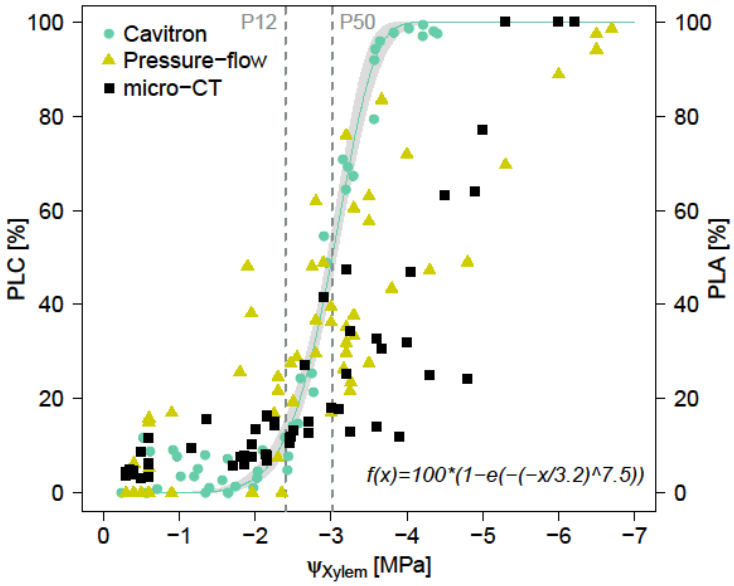

Fig. S1: Percent loss of hydraulic conductivity (PLC) as a function of xylem water potential (Ψ_{Xylem}) for Scots pine seedlings determined by the centrifuge-based Cavitron method (turquoise points) compared with results from a pressure-flow method (yellow triangles) and with percent loss of water-conducting area (PLA) based on micro-CT images (black squares). P_{12} and P_{50} of the vulnerability curve generated by the Cavitron technique are highlighted. Note that distribution of data points derived from pressure-flow and micro-CT are not ideal to calculate vulnerability estimates.

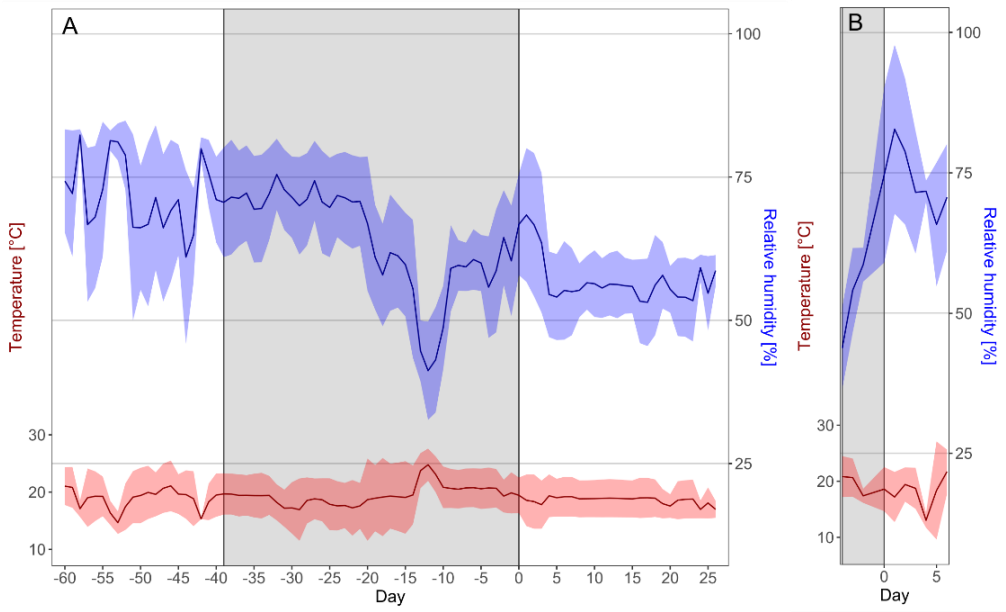

Fig. S2: Air temperature and relative humidity during the experiment and 3 weeks before initiating drought stress. Environmental conditions shown for (A) the seedlings in the greenhouse and (B) for the seedlings transported to Karlsruhe for micro-CT measurements at the end of drought and after re-watering. Data are daily averages and shaded areas depict ±SD. The grey boxes represent the drought period.

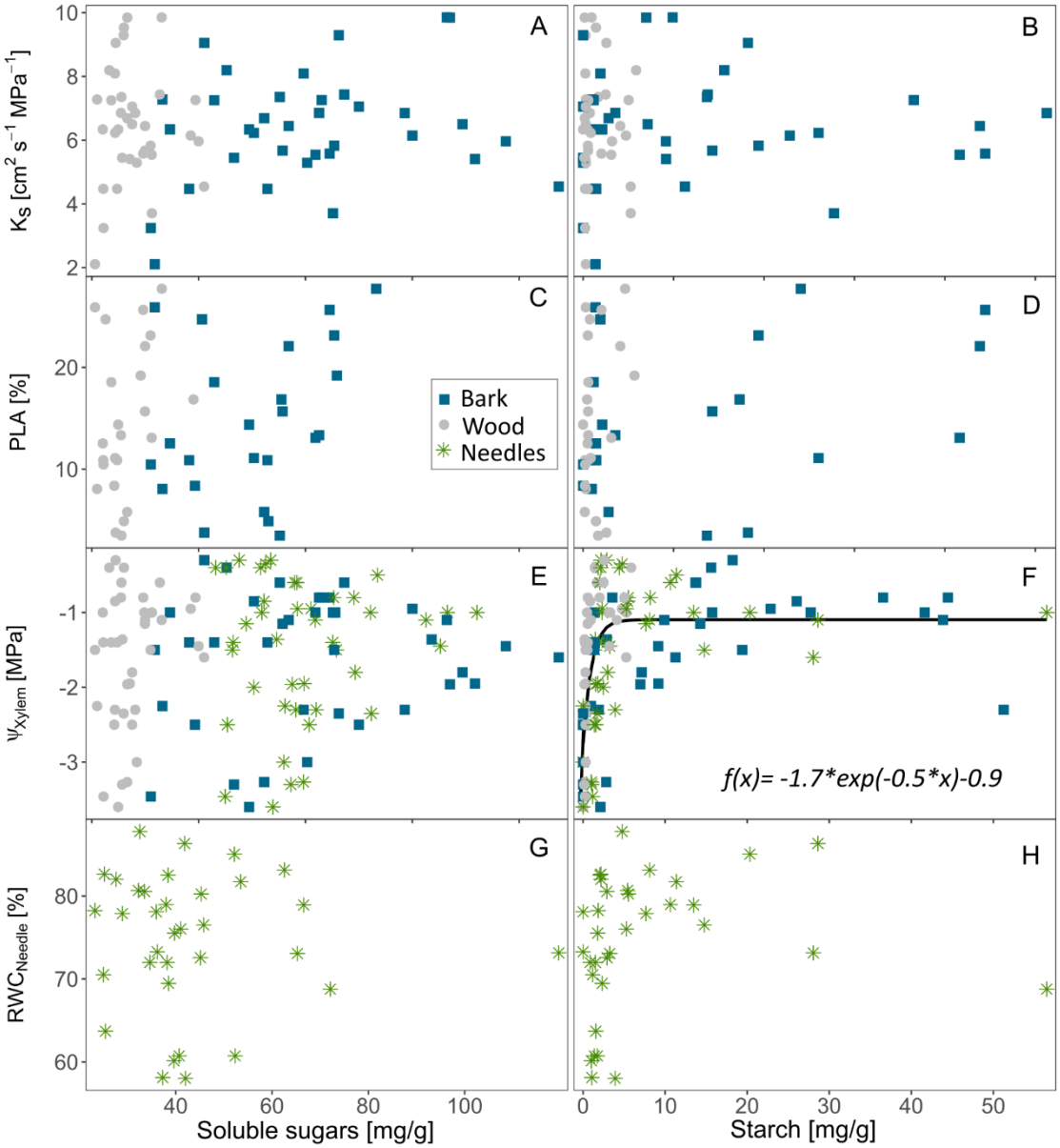

Fig. S3: Tissue-specific relationships of soluble sugars (left panels) and starch (right panels) with hydraulic conductivity K_S (A,B), percent loss of water-conducting area PLA (C,D), stem xylem water potential Ψ_{Xylem} (E,F) and relative needle water content RWC_{Needle} (G,H) during the experiment. Regression model for significant relationship between starch and Ψ_{Xylem} is fitted (including all tissues; R^2= 0.33).

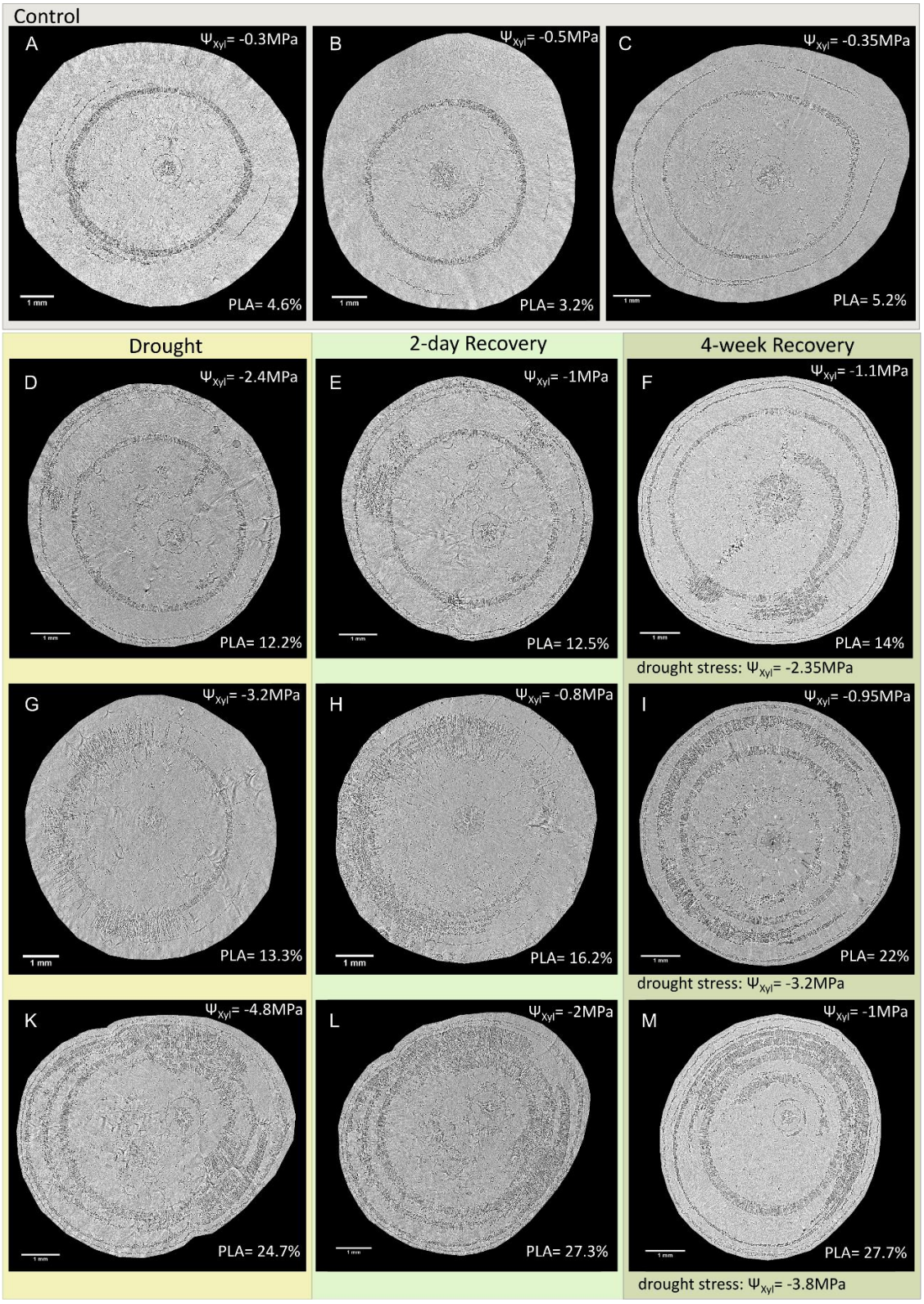

Fig. S4: Transverse X-ray tomography images of stem xylem of several control seedlings of *Pinus sylvestris* (A-C), differently stressed seedlings at the end of drought stress (D,G,K), the same ones 2 days after re-watering (E,H,L) and another set of seedlings 4 weeks after re-watering with Ψ_{Xylem} during drought stress given below the image (F,I,M). Embolized conduits are observed as black and water-filled conduits as grey. Stem xylem water potential (Ψ_{Xyl}) and percent loss of water-conducting area (PLA) are given.

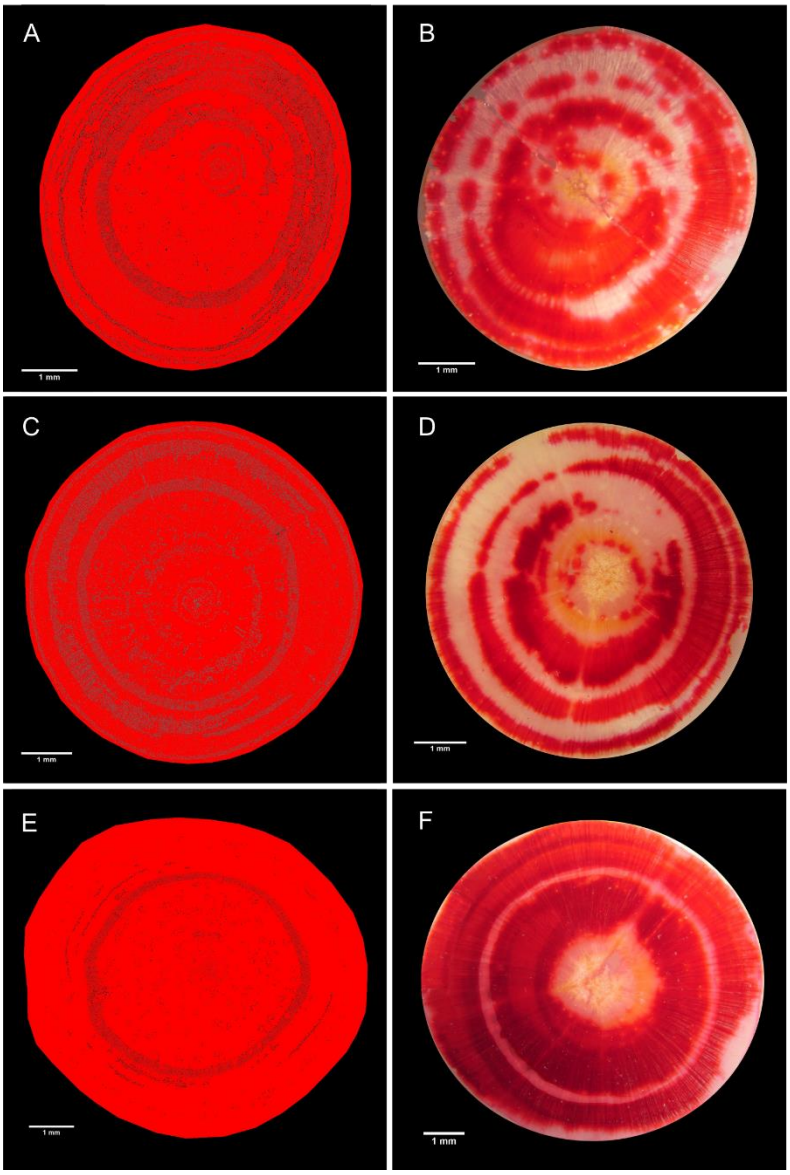

Fig. S5: Transverse sections of micro-CT images (left: A,C,E) and dye stained stem xylem segments (right: B,D,F) from the same individual show similar patterns of embolism formation. Left: Embolized tracheids are marked in black, water-filled tracheids are observed as red. Right: Xylem area not stained was embolized.

Supplemental methods

Methods S1: Percent loss of hydraulic conductivity via Cavitron

The resistance of the xylem to embolism formation was assessed using the Cavitron technique (Cochard, 2002). Measurements were conducted on the 2.5-year-old seedlings (n=5) two months before initiating the drought treatment as follows. Fresh, saturated stem segments of about 15 cm length were decorticated at both ends submerged in purified water and additionally recut 2-3 mm with a sharp carving knife. Previously prepared stem segments were fixed into a custom-made, honeycomb 15 cm rotor and positioned in a Sorvall RC-5 centrifuge (Thermo Fisher Scientific, Waltham, MA, USA). Stem ends were placed in cuvettes with outlets fitted inside the rotor. Distilled, filtered (0.22 µm pore size) and degassed water with 0.005% (v/v) Micropur water purifier (Katadyn Products, Wallisellen, Switzerland) preventing microbial growth, was used for the measurements. The centrifugal force of the Cavitron increases the negative pressure in the stem while the hydraulic conductance and loss thereof (PLC) is measured concurrently. Measurements started at a force of about -0.25 MPa, which was gradually increased until minimum hydraulic conductivity (K_S) was reached. We fitted a Weibull function to the data as re-parameterized by (Ogle et al., 2009) using the fitplc package (Duursma and Choat, 2017), and determined the Ψ_{Xylem} at which 12% (P_{12}) and 50% (P_{50}) hydraulic conductivity is lost (Fig. S2).

Methods S2: Dye staining experiments

Dye staining experiments were performed on stem segments of about 6-10 cm length to visualize water-conductive areas. Samples originating from the same seedlings that were previously measured using micro-CT were used to assess if the conductive area would be similar between dye-injected stems and micro-CT scanned stems. Stems were perfused with an aqueous solution of Safranin 1:5 (0.02%; Sigma-Aldrich, cat. no. S-2255) for about one hour. After 30 minutes, slices were cut on a sliding microtome and used for light microscopy observation of dye distribution. Photographs were taken to visually compare with micro-CT images.

3 Tree allocation dynamics beyond heat and hot drought stress reveal changes in carbon storage, belowground translocation and growth

---

This chapter has been submitted (2021) to *New Phytologist* as: Rehschuh, R. [1], Rehschuh, S.[1], Gast, A.[1], Jakab, A. [1], Lehmann, M.M. [2], Saurer M. [2], Gessler, A. [2,3], and Ruehr, N.K.[1]: Tree allocation dynamics beyond heat and hot drought stress reveal changes in carbon storage, belowground translocation and growth.

[1] Karlsruhe Institute of Technology, KIT Campus Alpin, Institute of Meteorology and Climate Research- Atmospheric Environmental Research, Garmisch-Partenkirchen, Germany

[2] Swiss Federal Research Institute WSL, Research Unit Forest Dynamics, 8903 Birmensdorf, Switzerland

[3] ETH Zurich, Department of Environmental System Sciences, 8092 Zurich, Switzerland

Summary

- Heatwaves combined with drought affect tree functioning with yet to be determined legacy effects on carbon (C) and nitrogen (N) allocation.
- We continuously monitored shoot and root gas exchange, $\delta^{13}CO_2$ of respiration and stem growth in well-watered and drought-treated *Pinus sylvestris* (Scots pine) seedlings exposed to increasing daytime heat stress (max. 42°C) and enhanced evaporative demand. Following stress release, we used $^{13}CO_2$ canopy pulse-labeling, supplemented by soil-applied ^{15}N to determine allocation to plant compartments, respiration and the soil microbial biomass (SMB) during 2.5 weeks.
- Well-watered previously heat treated seedlings rapidly translocated recent C along the long-distance path, to root respiration (R_{root}; 7.1 h) and SMB (3 d). Further, ^{13}C accumulated in branch cellulose, suggesting secondary growth enhancement as a compensatory response. Contrary, recovering drought-heat seedlings retained ^{13}C in needles, delayed C translocation to R_{root} (13.8 h) and incorporated ^{13}C into starch rather than cellulose, alongside reduced N uptake and aboveground allocation.
- C and N allocation during early recovery are affected by stress type and impact. While C uptake increased quickly in both treatments, hot drought stress reduced the above-belowground coupling and starch accumulated in leaves at the expense of growth. This indicates that C allocation during early recovery depends on phloem translocation capacity.

Keywords: ^{13}C, cellulose, respiration, heat stress, ^{15}N, recovery, Scots pine, starch

3.1 Introduction

The Earth's forests play an important role in the global carbon (C) cycle by removing a large amount of CO_2 from the atmosphere (Pan et al., 2011; Le Quéré et al., 2018). Worldwide, forests store about 653 billion tons of C, which approximates to anthropogenic CO_2 emissions of about 75 years (Klein & Schulz, 2011). However, the ability of forests to regulate C and nutrient cycling is tightly linked to climatic conditions (Rennenberg et al., 2006), which are projected to change rapidly within the 21st century (Coumou et al., 2013; IPCC, 2018). Heatwaves under wet conditions, but also hot droughts associated with high vapor pressure deficit (VPD) have become more common (Hao et al., 2013; Stéfanon et al., 2014), and thus intensify climatic stress on forests globally (Grossiord et al., 2020; McDowell et al., 2020).

Heatwaves directly impact plant physiological processes by influencing enzymatic activity, membrane integrity (Schrader et al., 2004; Rennenberg et al., 2006; Sage et al., 2008), as well as mitochondrial and dark respiration (Teskey et al., 2015). The impacts of heatwaves depend on water availability (Ruehr et al. 2016) and heat combined with drought affect plants even more since evaporative demand intensifies (Kumarathunge et al., 2020). Trees are able to regulate water loss by closing stomata, therefore limiting tree internal pressure and dehydration (Tyree & Sperry, 1989). However, reduced stomatal conductance decreases CO_2 uptake via photosynthesis (Rennenberg et al., 2006; Ruehr et al., 2016; Birami et al., 2018), which can influence C and N allocation dynamics (Ruehr et al., 2009; Blessing et al., 2015; Schönbeck et al., 2020) and growth rates (Bauweraerts et al., 2014; Teskey et al., 2015; Ruehr et al., 2016). A negative whole-plant C balance might arise if respiration costs for metabolic maintenance exceed C assimilation rates. Consequently, tree functioning needs to be sustained by nonstructural carbohydrates (NSC) and other C storage pools. A depletion of these pools might affect the ability of trees to recover and withstand subsequent stress events (McDowell et al., 2008).

Further, severe heatwaves and drought can result in metabolic impairment and functional damage, which clearly delays recovery pace (Ruehr et al., 2019). Several stress legacy impacts have been reported, including decreased water transport due to persisting embolism, i.e. the blockage of xylem tracheids by air bubbles (Rehschuh et al., 2020), reduced leaf biomass (Ruehr et al., 2016; Timofeeva et al., 2017), and reduced stem growth rates (Anderegg et al., 2015b), which have been linked to tree mortality processes (Trugman et al., 2018). However, the underlying mechanisms, particularly the involvement of C assimilation and reserve mobilization in tree recovery are far from being resolved (Martínez-Vilalta et al., 2016). Little is known on C allocation patterns post-stress, and results from a few studies on temperate tree species provide contrasting results. While Zang et al. (2014) and Galiano et al. (2017) recorded an increased allocation of recent assimilates aboveground, Hagedorn et al.

(2016) and Joseph et al. (2020) found an enhanced allocation belowground possibly due to an upregulation of repair mechanisms in roots.

Following stress release, a first step in gaining functionality is to upregulate photosynthesis. Recent assimilates might directly fuel metabolic demands and/or are used to fill carbohydrate storages (Galiano et al., 2017). Long-distance transport from source to sink organs depends on sink demand and phloem transport capacity, including phloem loading and unloading (Lalonde et al., 2003; De Schepper et al., 2013; Sevanto, 2018). Phloem functionality, however, might be impaired by drought stress (Sevanto, 2014, 2018) and eventually recovers slowly once stress is released. This could hinder repair processes and regrowth of new functional tissue. To replace and regrow tissues lost or impaired during stress, C and N translocation from source to sink organs is essential (Rennenberg et al., 2006; Gessler et al., 2017). However, root N uptake can be reduced by drought and heat stress due to impaired root functioning (Fotelli et al., 2004; Gessler et al., 2005, 2017; Giri et al., 2017). Despite this, information on the ability of trees to acquire and allocate N post-stress is scarce. An imbalanced nutritional status can affect tissue growth, plant functioning and resistance. $^{13}CO_2$ and ^{15}N-labeling allow to obtain a comprehensive picture of C and N allocation dynamics (Millard and Grelet, 2010; Epron et al., 2012). ^{13}C-labeling has been used in a variety of experiments particularly focusing on impacts of seasonal changes (Dannoura et al., 2011; Epron et al., 2012), drought events (Ruehr et al., 2009; Zang et al., 2014; Hagedorn et al., 2016), elevated temperatures (Blessing et al., 2015; Drake et al., 2019), and recovery from drought (Zang et al., 2014; Hagedorn et al., 2016; Galiano et al., 2017; Joseph et al., 2020). ^{15}N tracer studies have evaluated the remobilization of N for seasonal growth (Millard & Grelet, 2010), the capacity for N uptake and cycling dependent on the internal N status (Dyckmans and Flessa, 2001; Schönbeck et al., 2020), and during drought and heat stress (Aaltonen et al., 2016; Dannenmann et al., 2016; Giri et al., 2017). Yet, studies on the combined C and N allocation dynamics post heat and hot drought stress in temperate tree species are lacking, while this knowledge is crucial to improve our ability of predicting forests' resilience under climate change.

Scots pine (*Pinus sylvestris* L.), one of the most widespread conifers globally, has suffered lately from extreme climate events causing tree mortality (Buras et al., 2018; Jaime et al., 2019; Schuldt et al., 2020). This has raised concerns about the resilience of this important timber species. Here, we exposed Scot pine seedlings to heat and hot drought scenarios while constantly monitoring above- and belowground gas exchange. Following stress release, we applied $^{13}CO_2$ and ^{15}N labeling to closely follow C and N allocation patterns during a 3-week recovery period. We were particularly interested in the different responses of above-belowground C and N cycling post-stress and addressed the following hypotheses: 1) translocation speed of recently assimilated C to belowground is enhanced post-heat, but

delayed post drought-heat, 2) recent C will be strongly invested into repair and growth, if stress impairment occurs, and 3) N uptake and allocation are strongly coupled to the C metabolism post-stress.

3.2 Material and Methods

3.2.1 Plant material and growth conditions

We obtained bare-rooted 3-year-old *Pinus sylvestris* seedlings (Provenance 85115, Franconia, Germany) from a tree nursery in March 2018. Seedlings were placed in separate pots (6.8 L) in C-free potting substrate, containing fine quartz sand (0.1-1.2 mm), medium-grained sand (1-2.5 mm), gravel (3-5.6 mm) and vermiculite (2:2:1:2). Additionally, 12 g of long-term fertilizer (Osmocote® Exact Standard 5-6M fertilizer 15-9-12+2MgO+TE, ICL Specialty Fertilizers, The Netherlands) was added per pot, and liquid fertilizer applied monthly for immediate nutrient supply (Compo® Complete, 6+4+6(+2) NPK(MgO), Hornbach, Germany). To mimic a typical forest soil microbial community, we applied a microbial wash by adding 8 L of deionized water to 8 kg of forest soil (Franconia, Germany), and soaked roots before potting. Finally, 100 ml of the liquid supernatant of the microbial wash was added to each pot after filtering (40 µm). We also added 100 ml mycorrhiza inoculate (*Laccaria laccata*) per pot, inducing a mycorrhization rate of c. 50% after 6 months.

During plant acclimation and the whole experiment (see Fig. 1a for timeline), seedlings were kept under controlled conditions in a glasshouse facility in Garmisch-Partenkirchen, Germany (708 m a.s.l., 47°28′32.9″N, 11°3′44.2″E). The glasshouse is equipped with highly UV-transmissive glass. Inside light was supplemented with sodium vapor lamps during daytime (T-agro 400W, Philips, Hamburg, Germany) and photosynthetic active radiation recorded automatically (PAR; PQS1, Kipp&Zonen, Delft, The Netherlands).

Air temperature and relative humidity were adjusted to pre-defined conditions within the glasshouse compartment (CC600, RAM Regel- und Messtechnische Apparate GmbH, Herrsching, Germany), and measured automatically at canopy height (CS215, Campbell Scientific Inc., Logan, Utah, US). Seedlings were frequently relocated within the compartment. An individual drip irrigation system (Rain Bird, Azusa, CA, USA) served to adjust the watering automatically. During plant acclimation, all seedlings were watered daily to achieve a soil water content (SWC) close to field capacity (at 22%), monitored continuously (EC5, Meter Group, USA). Temperature was on average 20.7°C (day: 22.9°C; night: 17.4°C). To mimic a long-term drought after needle elongation was completed, irrigation was reduced in 25 seedlings on August 02, 2018, reaching a SWC ~10% (Fig. S1). At the end of the 6-week-drought (before placing seedlings in the tree gas exchange chambers), needle water potential (Ψ_{Needle}) was -1.4±0.05 MPa compared to -0.6±0.03 MPa in well-watered seedlings.

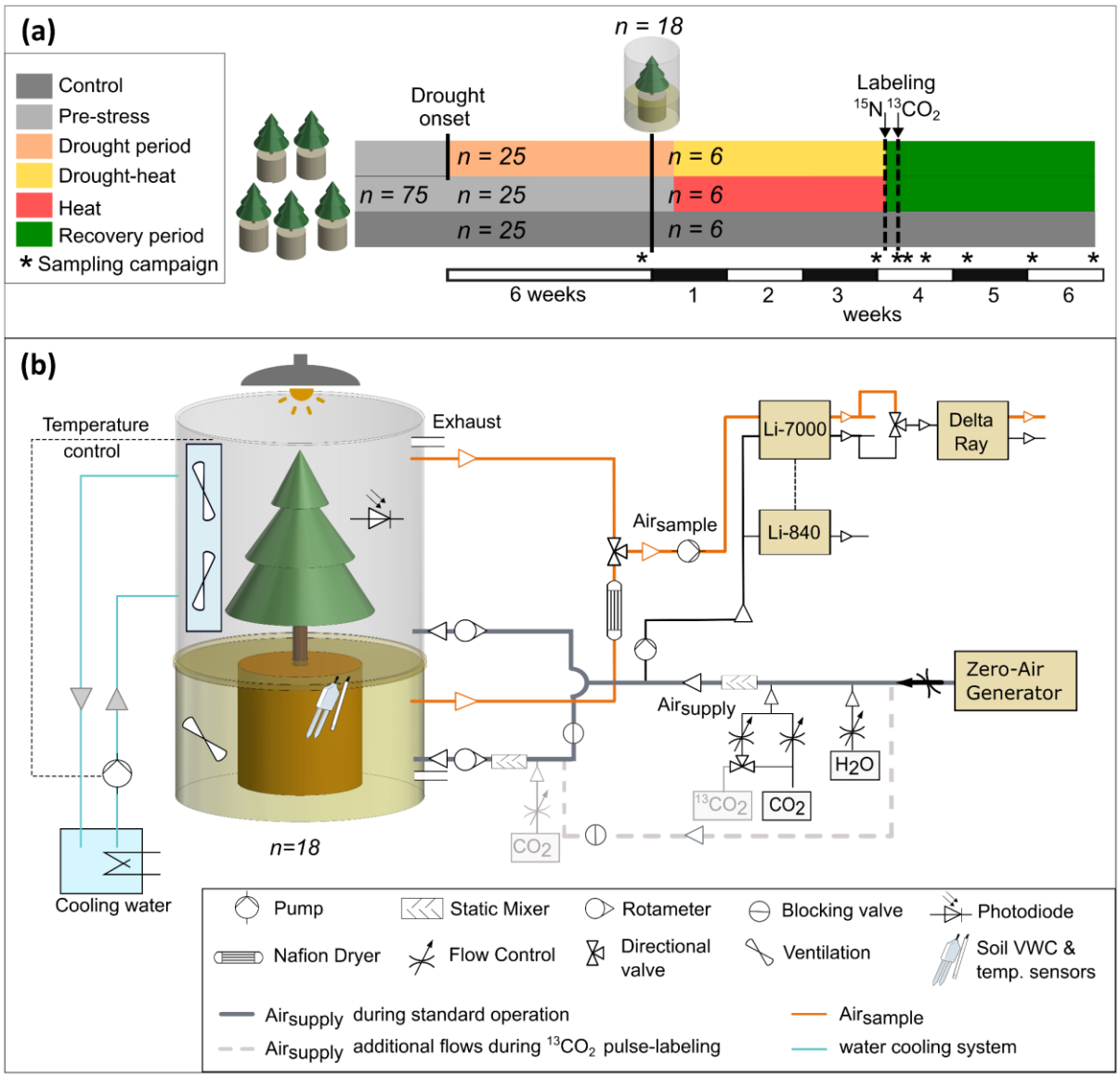

Fig. 1: (a) Experimental timeline and (b) schematic of the open gas-exchange chamber system (n=18 chambers with seedlings and 2 empty chambers). (a) Seedlings were acclimated for 5 months after potting (light gray) before drought stress was initiated in randomly selected seedlings (orange). 6 weeks later, 6 seedlings per treatment were randomly selected and transferred to the individual tree chambers where daytime heat stress was applied in the heat (middle bar) and the drought-heat (upper bar) treatment. In order to keep the numbers of replicates sufficient, we were not able to investigate a drought-only treatment. Timing of labeling and manual sampling campaigns are depicted. (b) An individual tree chamber is shown exemplarily, and arrows indicate the direction of air and water flow. Absolute CO_2 and H_2O concentrations were measured by a Li-840, connected to a Li-7000 for differential measurement of Air_{supply} and Air_{sample}. The associated $^{13}CO_2$ signature was measured by an isotope ratio infrared spectrometer (Delta Ray). Photosynthetic active radiation (PAR), air and soil temperature and soil moisture were continuously recorded and each seedling was equipped with an automatic drip irrigation system. Because seedlings were potted in C-free substrate and we corrected for potentially occurring microbial respiration (see Methods S2.2), the belowground flux was considered as root respiration (R_{root}).

Experimental conditions

On September 18, 2018, 18 seedlings (n=6 drought, n=12 well-watered) were transferred to individual gas exchange chambers placed in a glasshouse compartment and assigned to three treatments (n=6 each): control (well-watered), heat (well-watered) and drought-heat (drought pre-stressed; for tree growth parameters see Table 1).

Table 1: Tree height, stem diameter, biomass and needle area of 3-year-old *Pinus sylvestris* seedlings in the tree chambers (n=6 per treatment). Dry weight of total tree biomass, branches, stems, roots and needles, as well as needle area were determined at the end of the experiment. Soil microbial biomass (SMB) C and total dissolved nitrogen (TDN) in the soil are given for the end of the stress period (n=3 per treatment). Data are given as treatment averages ±SE. A significant difference between treatments was observed for soil microbial biomass C in drought-heat only (P<0.01; Kruskal-Wallis and Bonferroni post-hoc test). sdw= soil dry weight.

Treat-ment	Tree height [cm]	Stem diam. [mm]	Total biomass [g]	Bran-ches [g]	Stem [g]	Root [g]	Need-le [g]	Needle area [m^2]	SMB-C [µg g^{-1} sdw]	TDN [mg kg^{-1} sdw]
Control	57.3± 1.8	16.4± 0.6	113.6±4. 5	21.8± 1.5	16.4 ±1.0	36.3 ±1.1	39.1± 2.9	0.17±0. 01	65.0±6. 8	159.7±9 3.7
Heat	57.5± 1.9	15.9± 0.5	126.3±1 2.8	23.4± 2.6	17.4 ±2.0	35.8 ±3.5	47.6± 4.6	0.18±0. 01	61.2±3. 6	83.8± 33.3
Drought-heat	58.1± 3.6	14.9± 0.4	107.6±7. 6	18.7± 1.2	14.0 ±0.5	28.7 ±1.9	46.1± 6.7	0.20±0. 03	26.2±4. 1	172.9±7 6.7

We adjusted temperature and VPD based on a natural hot drought in 2003 and control conditions on 30-year-averages in Franconia, Bavaria (Methods S1, Fig. S2). Following five days of acclimation, air temperature in the stress treatments was steadily increased by 2-3°C during daytime within 20 days to finally reach maximum temperatures of 41.5°C. Pre-defined maximum temperatures per period (Fig. 2, Table S1) were maintained for min. 6 h daily (see Rehschuh and Ruehr, 2021). Daytime VPD increased alongside air temperature (Fig 2b), but less in the heat compared to the drought-heat treatment due to increasing transpiration rates, affecting chamber humidity (Fig. S3). Note that nighttime air temperatures and VPD did not differ between treatments due to technical constraints. Because soil compartments were passively cooled (and the entire glasshouse compartment was heated), mean soil temperature increased in all treatments, but remained <30°C. An automated drip irrigation system allowed to maintain SWC at field capacity in the control and heat treatment by watering 4-times daily (300 ml in total; Fig. 2). Drought-heat treated seedlings were irrigated daily at 5 am (70 ml), and the amount was reduced steadily until SWC was c. 5%. On October 13, stress was released, and drought-heat seedlings re-watered manually to field capacity (Fig 2d). During the recovery phase, environmental parameters were adjusted to control conditions.

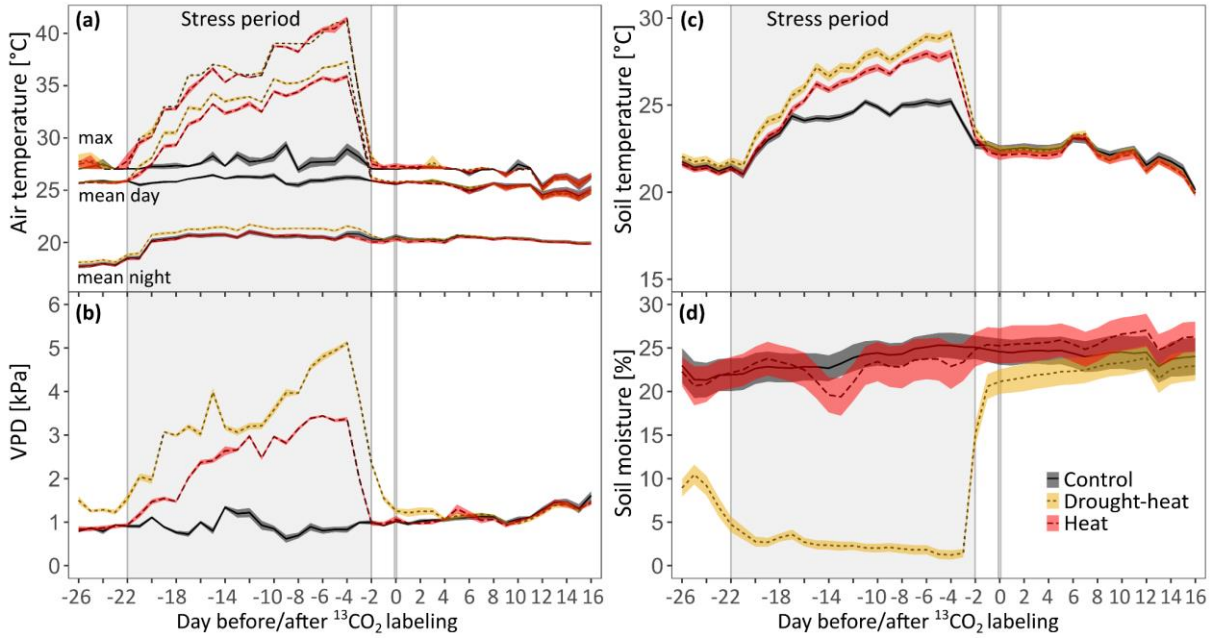

Fig. 2: Environmental conditions during the chamber experiment for (a) daytime (PAR >100 µmol m^{-2} s^{-1}) and nighttime mean and daily maximum air temperature, (b) daily daytime average vapor pressure deficit (VPD), (c) daily average soil temperature, and (d) daily average soil moisture. Shown are treatment averages and shaded areas are ±SE (n=6 per treatment). The gray boxes represent the stress period, and the vertical gray line indicates the day of the experiment (day 0) on which seedlings were $^{13}CO_2$ pulse-labeled. During the entire period, average daytime PAR was between 350 and 550 µmol m^{-2} s^{-1} in all treatments. Note that VPD in the drought-heat treatment was highest due to low tree transpiration rates. PAR= photosynthetic active radiation. For diurnal patterns see Rehschuh and Ruehr (2021).

3.2.2 Individual tree gas exchange chambers

Chamber design and measurements

We closely followed shoot and root gas exchange (H_2O and CO_2) and $\delta^{13}CO_2$ during stress and recovery using a custom-built gas exchange chamber system (Birami et al., 2020; Gattmann et al., 2020; Fig. 1b). Briefly, each individual tree chamber consisted of a separate temperature-controlled (Table S1) transparent shoot and opaque root compartment. Each compartment included the root or shoot part of an individual seedling and was tightly sealed against each other to ensure gas tightness (for details see Methods S2.1). Additionally, stem growth was recorded half-hourly by point dendrometers (DD-S, Ecomatik, Dachau, Germany), fixed to each stem at 5-10 cm height.

The supply air (Air_{supply}) was constantly delivered to the chamber system at c. 430 ppm CO_2 and 8 mmol H_2O during acclimation and recovery (see also Methods S2.2). During heat stress, [H_2O] was reduced to 4 mmol in all treatments to avoid high humidity and condensation. $\delta^{13}CO_2$ of Air_{supply} was kept constant at 0.28±0.006‰ $\delta^{13}C$ (except during pulse-labeling). The isotopic

ratios (*R*) are expressed in δ notation (‰) relative to the international standard Vienna Pee Dee Belemnite (VPDB) for $\delta^{13}C$ and atmospheric N_2 for $\delta^{15}N$ (for solid samples only):

$$\delta^{13}\mathrm{C} \text{ or } \delta^{15}\mathrm{N} = \left(\frac{R_{\mathrm{sample}}}{R_{\mathrm{standard}}} - 1\right) \cdot 1000‰ \quad (1).$$

Shoot compartments were supplied with c. 13 L min^{-1} and root compartments with c. 3 L min^{-1}. Sample air (Air_{sample}) was drawn back at 500 ml min^{-1}, and each compartment measured every 120 min. We organized the measurement sequence as to avoid frequent switching between shoot and root compartments. Absolute H_2O and CO_2 concentrations were measured by a gas analyzer (Li-840, LI-COR, Lincoln, NE, USA), connected to a differential gas analyzer (Li-7000, LI-COR), allowing for determining the concentration differences in Air_{supply} and Air_{sample} in 10 s intervals over 80 s. The associated $\delta^{13}CO_2$ of Air_{supply} and Air_{sample} was determined by an isotope ratio infrared spectrometer (IRIS, Delta Ray, Thermo Fisher Scientific) at 80 ml min^{-1} and measurements averaged over 60 s. Air_{supply} was measured alternately between shoots and roots every 40 min, and remained relatively constant. Referencing was performed hourly using a commercially available reference gas with $\delta^{13}C$=-9.86±0.3‰ (160402, Thermo Fisher Scientific). The gas analyzers and the infrared spectrometer were calibrated with calibration gases before the experiment according to the manufacturers' recommendations.

To correct for offsets between Air_{supply} and Air_{sample} not caused by plant gas exchange, two chambers were operated without trees but containing pots with potting substrate. The offset in shoot compartments was 1.3±0.01 µmol CO_2 mol^{-1} and 0.1±0.003 mmol H_2O mol^{-1}. The not-tree derived flux in root compartments was slightly larger with 3.9±0.03 µmol CO_2 mol^{-1} and could be due to microbial activity. These offsets were removed from the data accordingly.

For calculations of gas exchange fluxes and the isotopic signature see Methods S2.3.

3.2.3 $^{13}CO_2$ pulse-labeling and ^{15}N labeling

$^{13}CO_2$ pulse-labeling was performed on October 15, 2018, i.e. two days after stress release when C uptake of drought-heat seedlings was within 70% of control seedlings. Shoot compartments were pulse-labeled for 4 h during the period of highest photosynthetic activity, starting at 9:15 am. For this, we mixed 99% enriched $^{13}CO_2$ (364592-10L-EU, Sigma-Aldrich, Taufkirchen, Germany) directly to Air_{supply} of shoot compartments (Fig. 1b), resulting in a [CO_2] of c. 400 ppm at 45 atom% $^{13}CO_2$ (equals $\delta^{13}CO_2$ of 75,000‰). The root compartments received the same, non-enriched air as before (see Fig. S4). To avoid memory effects on infrared spectroscopy measurements from highly enriched $\delta^{13}CO_2$, we applied longer flushing (10 min) when switching between shoot and root compartments during and 24 h after labeling. We derived ^{13}C-uptake per treatment, which compared well between a flux and a biomass based approach (Table 2).

Table 2: ^{13}C-uptake determined from gas exchange measurements for the 4-hour pulse and from excess ^{13}C of needle biomass sampled directly after labeling (for details see Methods S2.3). Data are treatment averages ±SE (n=6). No significant differences between treatments were observed.

Treatment	Photosynthetic ^{13}C-uptake [mg ^{13}C]	Needle biomass [mg ^{13}C]
Control	72.5±5.1	61.6±8.4
Heat	74.1±5.1	68.4±7.6
Drought-heat	50.0±7.9	60.7±11.1

C translocation rates were estimated from the time difference between the beginning of pulse-labeling and label appearance in root respiration (R_{root}), while considering stem length. Label appearance was defined individually per chamber based on a threshold calculated from pre-labeling variability of $\delta^{13}C$ ($SD_{pre\text{-}labeling}$) as follows: $2 \cdot 1.65 \cdot \mathrm{SD}_{\mathrm{pre-labeling}}$ (Salomón et al., 2021).

To further derive information on the nutrient uptake capacity of roots and within-tree N allocation post-stress, we applied double-labeled $^{15}NH_4{}^{15}NO_3$ (98% enriched, 366528-1G, Sigma-Aldrich, Taufkirchen, Germany) as follows. Stress was released and seedlings were re-watered close to field capacity on October 13 at 5 am. Subsequently, we applied 170 ml of a 0.37 mM ^{15}N solution (5.1 mg ^{15}N) per seedling, evenly distributed around the stem.

3.2.4 Sample collection and preparation

To quantify dynamics in NSC and the isotopic signatures of bulk (^{13}C and ^{15}N), water-soluble compounds (WSC), starch and cellulose (^{13}C), we subsampled needles, fine roots (diameter ≤2 mm) and branches of each seedling per individual tree chamber (n=18). To minimize disturbance of continuous measurements, each seedling was sampled directly after gas exchange was quantified. Further, to assess pre-labeling variability, samples were taken one day before stress release. Following $^{13}CO_2$ pulse-labeling, we sampled immediately after labeling (needles), 8 h, 15 h (needles), 27 h, 78 h, 7 d, 11 d, and 16 d after the start of labeling. We sampled between 3 and 4 pm, except for the 8 h and 15 h step. Branches were immediately separated into xylem and phloem (including the cambium), but one part was kept intact for cellulose extraction (and cut in pieces later). Root samples were rinsed with distilled and filtered water (dH_2O), and excess water removed. Plant biomass samples were immediately frozen in liquid N_2 and stored at -80°C until freeze-drying (Alpha 24 LSC; Martin Christ Gefriertrocknungsanlagen GmbH, Osterode am Harz, Germany) and grinding to fine powder (MM200, Retsch, Haan, Germany).

At the end of the experiment, seedlings were harvested and separated into needles, roots, branches and stems before oven-drying at 70°C for 48 h. Dry weight (DW; Table 1) was used to calculate ^{13}C and ^{15}N excess. Regarding stem xylem, we estimated the DW of the outer tree

ring based on stem xylem weight. Total leaf area per tree was derived from needle biomass and a subsample of predetermined specific leaf area (g cm^{-2}; Li-3100, LI-COR Inc., Lincoln, Nebraska, USA). Except for soil microbial biomass (SMB) C, differences in tissue biomass between treatments were not significant.

3.2.5 Nonstructural carbohydrate analysis

We determined total NSC concentrations from 10 mg of plant material (needles, roots, branch phloem and xylem; n=5-6 per treatment), i.e. soluble sugars (Glucose, Fructose, and Sucrose) and starch, according to Landhäusser et al. (2018). After extraction in 80% ethanol and specific enzymatic reactions, absorption was determined by a spectrophotometer at an absorption of 340 nm (Epoch 2, BioTek, Winooski, Vermont, USA; for details see Methods S3).

3.2.6 Water-soluble compounds, starch and cellulose extraction

For $\delta^{13}C$ analyses, WSC (n=6) and starch (n=3) were extracted from 40-60 mg of dry homogenized biomass (needles, roots, branch phloem and xylem) following standard protocols (Richter et al., 2009; Lehmann et al., 2015; see Methods S4). WSC were extracted in 1.5 ml deionized water at 85°C for 30 min. Starch was enzymatically extracted from the remaining pellets using heat-stable α-amylase. For $\delta^{13}C$ analysis of cellulose (n=5-6), c. 15 mg of cut plant material (branches, stems, fine roots) was step-wise extracted in Teflon filters using 5% NaOH and 7% acidified $NaClO_2$ at 60°C (Galiano et al., 2017). Cellulose was then homogenized by an ultrasonic transducer (Laumer et al., 2009).

3.2.7 Soil microbial biomass extraction

$\delta^{13}C$ of the SMB was determined from soil samples taken close to roots (n=3), while timing was coordinated with plant biomass sampling. Soil samples were immediately frozen at -20°C. To extract SMB, we applied a chloroform fumigation extraction method (Vance et al., 1987, see Methods S5). $\delta^{13}C$ of fumigated and non-fumigated samples was determined by isotope ratio mass spectrometry, and total organic C by an infrared TOC analyzer (DIMATEC, Essen, Germany). $\delta^{13}C$ of SMB ($\delta^{13}C_{MB}$) was then calculated as follows:

$$\delta^{13}C_{MB}\,(‰) = \frac{\delta^{13}C_F \cdot C_F - \delta^{13}C_{NF} \cdot C_{NF}}{C_F - C_{NF}} \quad (2),$$

where F are values from fumigated and NF from nonfumigated extracts. Total soil microbial C was calculated as (total C_F – total C_{NF})/0.45 (Vance et al., 1987).

3.2.8 Isotope ratio mass spectrometry

For determining the isotopic compositions and C and N contents of solid samples, c. 1 mg of homogenized bulk material and cellulose, and c. 10 mg of freeze-dried soil extracts were

weighed into tin capsules. Liquid solutions of WSC and starch samples were pipetted into tin capsules and subsequently oven-dried at 70°C for 12 h, resulting in c. 0.5 mg DW. The samples were then combusted to CO_2 and N_2 in an elemental analyzer (EA1110 CHN, Carlo Erba, Milan, Italy) coupled to an isotope-ratio mass-spectrometer (Delta XL, Thermo Scientific, Bremen, Germany). For calibration, laboratory and international standards with known $\delta^{13}C$ and $\delta^{15}N$ were used, resulting in a precision of 0.2‰ for $\delta^{13}C$ and 0.3‰ for $\delta^{15}N$. Additionally, $\delta^{13}C$ and $\delta^{15}N$ of solid material and $\delta^{13}C$ of gas flux data was converted to atom%. For calculations of atom%, excess $^{13}C/^{15}N$ (amount of label in pools and biomass) and a ^{13}C mass balance see Methods S6.

3.2.9 Needle water potential and needle temperature

To assess drought severity, we measured Ψ_{Needle} of mature needles (n=6 per treatment) before dawn and at noontime using a pressure chamber (Model 1000, PMS Instruments, Albany, Oregon, USA). Measurements were performed before placing seedlings in the tree chambers, at the end of stress and during initial and final recovery. Since irrigation took place in the morning, predawn Ψ_{Needle} was occasionally lower than midday Ψ_{Needle} in drought-treated seedlings, wherefore we report the minimum Ψ_{Needle} per measurement day.

Needle temperature was measured during the most severe stress and final recovery (n=6 per treatment) around 1 pm using an infrared camera (PI 450, Optris, Germany). Images were analyzed using the manufacturer's software by setting needle emissivity to 0.97 and adjusting background radiation according to air temperature.

3.2.10 Statistical data analysis

All data analyses and statistics were conducted in 'R' version 3.6.1 (R Core Team, 2019). Stem increment rates were determined by fitting linear regression models to dendrometer data. Considering drought-heat seedlings, the model was fitted from day 5 until the end of the recovery period, i.e. when seedlings grew post-stress and passed the pre-stress baseline. Significant differences between slopes of fitted lines per treatments were analyzed using least-squares means (package lsmeans:lstrends; Lenth, 2017). To test for significant differences between treatments at discrete time points (used for non-continuous data and $^{13}C/^{15}N$ in plant tissues and compounds), we used the Kruskal-Wallis followed by the Bonferroni post-hoc test for small sample size.

To analyze overall treatment effects per time period for continuous measurements (e.g. gas exchange, $\delta^{13}C$ of respiration, stem increment), linear-mixed effects models were applied (lme; lmerTest package; Kuznetsova et al., 2017). We assigned treatment and time period (pre-drought, initial and final stress, initial recovery until $^{13}CO_2$ labeling, recovery (labeling peak), recovery and additionally the final recovery) as fixed effect and chamber as random factor. The

lme model with the lowest Akaike's information criterion corrected for small sample size (AICc) was chosen (Burnham & Anderson, 2002), and the post-hoc Tukey's HSD applied for multiple comparisons of means to determine differences between treatments (package emmeans; Lenth et al., 2020).

We estimated the mean residence time (MRT) and half-life time (HLT) of the ^{13}C-label in respiration, relevant tissues and their compounds by using the following exponential decay function:

$$N(t) = N_0 e^{-\lambda t} \quad (3),$$

where $N(t)$ is $\delta^{13}C$ at time t and N_0 is the initial $\delta^{13}C$ at the labeling peak (here t=0), and λ is the decay constant. The MRT and HLT ($t_{1/2}$) were determined as follows:

$$MRT = \frac{1}{\lambda} \text{ and } t_{1/2} = \frac{\ln(2)}{\lambda} \quad (4),$$

We additionally fit curves to ^{13}C dynamics of tissues and compounds to improve the visualization of ^{13}C trajectories over time. Models were selected based on the lowest AICc. We calculated the deviance to compare the fitted model to the null model, and determined the percentage explained by the best-fit model (reported here, Fuentes et al., 2018). All statistical tests were considered significant if P<0.05.

3.3 Results

3.3.1 Stress impacts and gas exchange recovery

Stress impacts on tree biomass were small, as drought was initiated after needle growth was completed (Table 1). However, the pre-drought treatment resulted in a tendency of reduced root biomass. Gas exchange was affected by drought as observed in lower net assimilation (A_{net}) and shoot dark respiration ($R_{shoot\ night}$) compared to control seedlings (Tukey's HSD, P>0.1, Fig. 3a-b). With increasing daytime air temperatures and VPD, A_{net}, $R_{shoot\ night}$ and root respiration (R_{root}) declined strongly (Tukey's HSD, P<0.01, see Table S2 for p-values per period). The larger stress impacts under drought-heat were also observed in low Ψ_{needle} (-2.70±0.13 MPa; P<0.01, Table 3), strong stem diameter shrinkage (Tukey's HSD, P<0.01, Fig. 3d), and 4.6°C warmer maximum needle temperatures compared to the heat treatment (P<0.001). In contrast, in the well-watered heat treated seedlings the effects of high daytime temperatures were small and resulted in A_{net} declining to c. 70% of control values, reflected in slowly decreasing $R_{shoot\ night}$ (note night-time temperatures were on average c. 20°C in all treatments) and stem growth, while R_{root} initially increased and then acclimated with higher temperatures (Tukey's HSD P>0.1, Table S2, Fig. 3).

Table 3: Minimum needle water potential (Ψ_{Needle}) and maximum and mean needle temperature at the end of stress, 1-day recovery and at the end of the recovery period. Data are treatment averages ±SE (n=6).

Parameter	Treatment	End of stress	1-day recovery	End of recovery
Ψ_{Needle} [MPa]	Control	-0.56±0.07	-0.44±0.04	-0.61±0.03
	Drought-heat	-2.70±0.13	-0.98±0.13	-0.66±0.04
	Heat	-0.58±0.08	-0.50±0.07	-0.64±0.02
Maximum needle temperature [°C]	Control	31.83±0.45	-	28.09±0.28
	Drought-heat	45.80±0.43	-	28.23±0.24
	Heat	41.16±0.90	-	27.98±0.16
Mean needle temperature [°C]	Control	29.56±0.16	-	26.68±0.31
	Drought-heat	44.29±0.48	-	26.58±0.34
	Heat	39.66±0.59	-	26.12±0.12

Consequently, following stress release, A_{net}, $R_{shoot\ night}$ and R_{root} recovered fast in heat seedlings (Fig. 3), and did not differ from the control during the recovery period (Tukey's HSD, P>0.1). Additionally, stem growth rates increased above the control during the last week of recovery (heat: 0.043 mm d^{-1} vs. control: 0.035 mm d^{-1}; P<0.001).

Post drought-heat, A_{net} and $R_{shoot\ night}$ increased sharply, alongside increasing Ψ_{needle} (Table 3). A_{net} reached about 60% and $R_{shoot\ night}$ 75% of control values two days post-stress (Tukey's HSD, P<0.001), with A_{net} recovering to c. 80% within the following 4 days (Tukey's HSD, P<0.05), while $R_{shoot\ night}$ recovered fully. Alongside, R_{root} also increased and tended to exceed the control at the end of the recovery period (Tukey's HSD, P>0.1). Stem diameter width remained below pre-stress values until 6 d after stress release, marking the onset of secondary growth. In the remaining recovery period, stem growth rates (0.066 mm d^{-1}) accelerated above control rates (P<0.001).

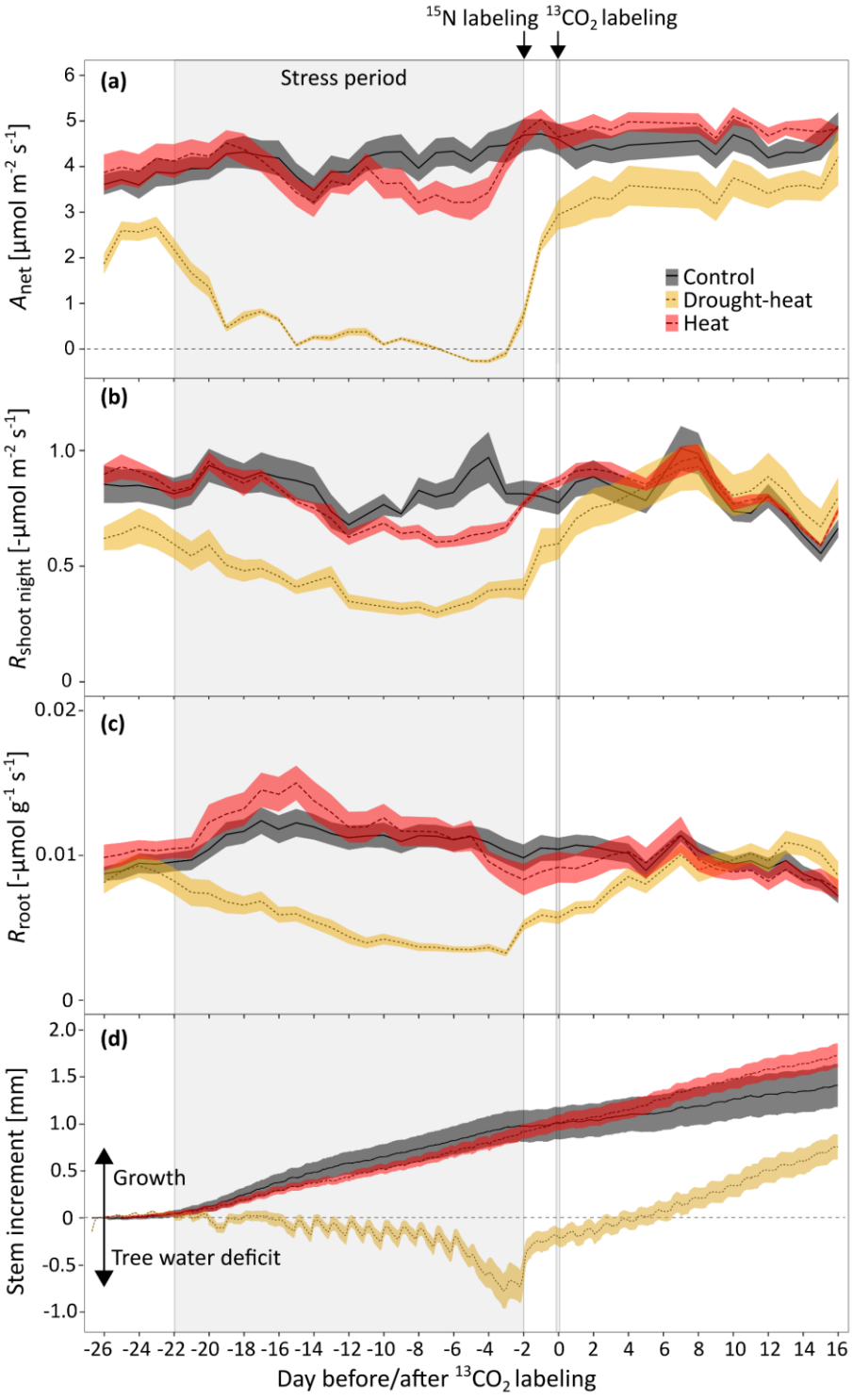

Fig. 3: Dynamics of daily averaged (a) net canopy assimilation (A_{net}), (b) shoot dark respiration ($R_{shoot\ night}$), and (c) root respiration (R_{root}), as well as (d) half-hourly changes in stem increment of Scots pine seedlings. Data are treatment averages and shaded areas show ±SE (n=6). The gray boxes represent the stress period, and with stress release ^{15}N was applied (day -2). The vertical gray line indicates when seedlings were $^{13}CO_2$ pulse-labeled (day 0). In d), data above 0 indicate stem growth, and below 0, tree water deficit. Note that nighttime temperatures did not differ between treatments.

3.3.2 Dynamics of ^{13}C in respiration, water-soluble compounds and soil microbial biomass

We closely monitored the dynamics of ^{13}C progression post-stress (Fig. 4). In R_{root}, the first signal of ^{13}C arrived in the heat (7.06±0.8 h), tightly followed by the control (8.3±0.3 h) and about 6 h later in the drought-heat treatment (13.8±0.3 h; P<0.01). This resulted in a 40% lower C translocation velocity in seedlings recovering from drought-heat compared to control seedlings (P<0.01; heat: 4.14±0.38 cm h^{-1}, control: 3.40±0.20 cm h^{-1}, drought-heat: 1.98±0.13 cm h^{-1}), alongside increased MRTs and HLTs (Table 4). The $\delta^{13}C$ peak in R_{root} was reached in both, the heat and control treatment one day after $^{13}CO_2$ labeling, i.e. after 36 and 37 h (Fig. 4b). In drought-heat seedlings, the peak became apparent 24 h later and at a much lower intensity (866±104‰ compared to 2352±119‰ in control; Tukey's HSD, P<0.001). Generally, we found re-occurring diurnal $\delta^{13}C$ peaks in R_{root} during night. In contrast, in $R_{shoot\ night}$ the label peak occurred simultaneously in all treatments (at 4 am; c.18 h after $^{13}CO_2$ labeling), but at different intensities and was lowest post drought-heat (Fig. 4a). Further, $\delta^{13}C$ of $R_{shoot\ night}$ leveled-off faster in the heat and control treatment, whereas the MRT was increased post drought-heat (Table 4).

Respiration of recent assimilates is based on fast C pools such as WSC, including soluble sugars, sugar alcohols, organic acids and amino acids. Consistent with WSC supplying respiratory processes, we found an initially fast decline of WSC $\delta^{13}C$ in aboveground tissues of control and heat seedlings (Fig. 4, for ^{13}C excess see Fig. S5). In root WSC of these seedlings, highest $\delta^{13}C$ occurred 2 days after labeling (Fig. 4f), corresponding with the label-peak in R_{root}. In heat seedlings, $\delta^{13}C$ in phloem and xylem WSC was larger compared to the other treatments within one day post-labeling (Fig. 4d-e), corresponding to a tendency of faster C translocation and lower MRT. In drought-heat seedlings, slower ^{13}C dynamics were reflected in longer MRTs of ^{13}C in WSC in most pools (Table 4). The $\delta^{13}C$ dynamics of SMB showed a much slower trajectory that appeared uncoupled from the WSC dynamics (Fig. 4g, ^{13}C excess: Fig. S6).

Table 4: Treatment-specific mean residence time (MRT) and half-life time (HLT) in respiration, different tissues and compounds of ^{13}C assimilated two days after stress release. Values are derived following the $\delta^{13}C$ peak during a 16 day period after $^{13}CO_2$ pulse-labeling. The 95% confidence intervals are given in brackets, and R^2 of the fitted exponential decay function (Eqn. 3) is indicated (n=6 per treatment and time step for respiration, bulk and WSC; n=3 for starch). MRT and HLT are only provided in case the fitted model was significant.

Organ/ Tissue	Flux/ Compound	Treatment	MRT [d]	HLT [d]	R^2
Shoot	respiration	Control	2.3 (2.1, 2.5)	1.6 (1.4, 1.7)	0.90
		Heat	2.4 (2.3, 2.5)	1.7 (1.6, 1.8)	0.91
		Drought-heat	4.0 (3.7, 4.4)	2.8 (2.5, 3.0)	0.86
Roots	respiration	Control	2.6 (2.4, 2.7)	1.8 (1.7, 1.9)	0.94
		Heat	2.7 (2.5, 2.9)	1.9 (1.7, 2.0)	0.93
		Drought-heat	4.9 (4.4, 5.4)	3.4 (3.1, 3.7)	0.85
Needles	WSC	Control	1.6 (1.4, 1.9)	1.1 (0.9, 1.3)	0.95
		Heat	1.4 (1.2, 1.8)	1.0 (0.8, 1.2)	0.83
		Drought-heat	4.0 (3.0, 5.8)	2.8 (2.1, 4.0)	0.89
Phloem	WSC	Control	2.8 (2.2, 3.9)	1.9 (1.5, 2.7)	0.79
		Heat	2.2 (1.5, 3.8)	1.6 (1.1, 2.6)	0.82
		Drought-heat	6.9 (4.2, 18.8)	4.8 (2.9, 13.0)	0.37
Xylem	WSC	Control	4.4 (3.5, 6.1)	3.1 (2.4, 4.3)	0.87
		Heat	3.4 (2.3, 6.1)	2.3 (1.6, 4.2)	0.88
		Drought-heat	4.1 (3.1, 6.2)	2.8 (2.1, 4.3)	0.84
Roots	WSC	Control	7.9 (5.3, 15.5)	5.5 (3.6, 10.7)	0.55
		Heat	7.6 (4.5, 24.8)	5.3 (3.1, 17.2)	0.52
		Drought-heat	10.5 (7.3, 18.8)	7.3 (5.0, 13.0)	0.58
Needles	starch	Control	5.5 (3.5, 13.1)	3.8 (2.4, 9.1)	0.69
		Heat	0.6 (0.2, 1.6)	0.4 (0.2, 1.1)	0.72
		Drought-heat	6.6 (4.8, 10.7)	4.6 (3.3, 7.4)	0.79
Needles	bulk	Control	1.5 (1.3, 1.8)	1.0 (0.9, 1.2)	0.62
		Heat	1.8 (1.4, 2.6)	1.3 (0.9, 1.8)	0.64
		Drought-heat	9.8 (7.0, 15.8)	6.8 (4.8, 10.9)	0.62
Phloem	bulk	Control	6.1 (3.9, 13.3)	4.2 (2.7, 9.2)	0.35
		Heat	12.3 (7.4, 35.4)	8.5 (5.1, 24.5)	0.25
		Drought-heat	-	-	-

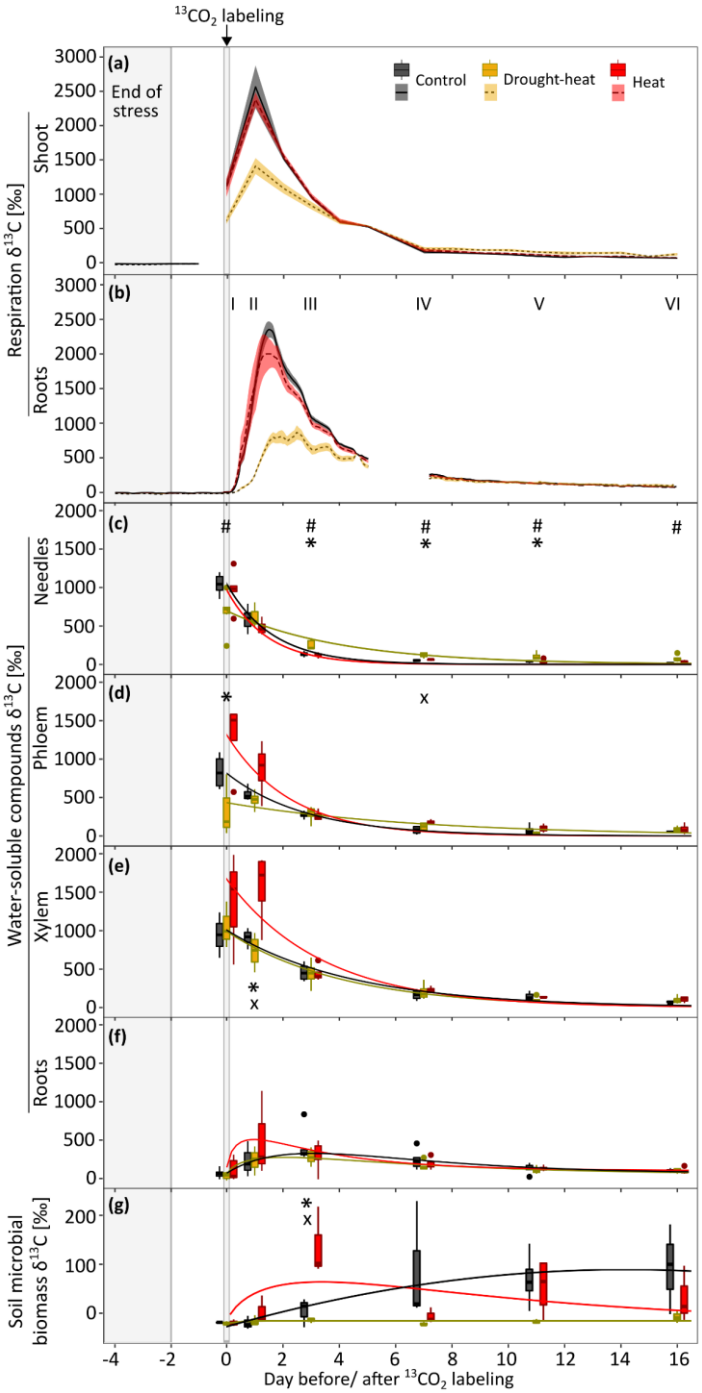

Fig. 4: Dynamics of $\delta^{13}C$ in respiration, water-soluble compounds (n=6) and soil microbial biomass (n=3) during the recovery period. Shown are $\delta^{13}C$ of (a) shoot night respiration, (b) root respiration, water-soluble compounds (WSC) in (c) needles, (d) branch phloem, (e) branch xylem and (f) roots, as well as (g) soil microbial biomass. Data are daily means of $\delta^{13}C$ in shoot night respiration and hourly means of $\delta^{13}C$ in root respiration; shown are treatment averages and shaded areas indicate ±SE. The gray box represents the end of the stress period and the vertical gray line indicates $^{13}CO_2$ pulse-labeling on day 0 two days after stress release. Tissue and soil sampling intervals are highlighted by roman letters (I-VI). Note that reported WSC and microbial biomass data on day 0 are for samples taken 8 h after labeling start. Symbols indicate significant differences (P<0.05) between treatments per sampling campaign (Kruskal-Wallis and Bonferroni post-hoc test) as follows: drought-heat vs. control (#), heat vs. control (x), and drought-heat vs. heat (∗). The curve with the best fit is given per treatment (see Table S3).

3.3.3 C allocation to starch and cellulose

The $\delta^{13}C$ progression in starch and cellulose reflects the allocation of recent assimilates to storage and growth (Figs. 5, S7, S8). While drought stress reduced starch concentrations, starch increased during recovery and was larger than the control in most tissues towards the

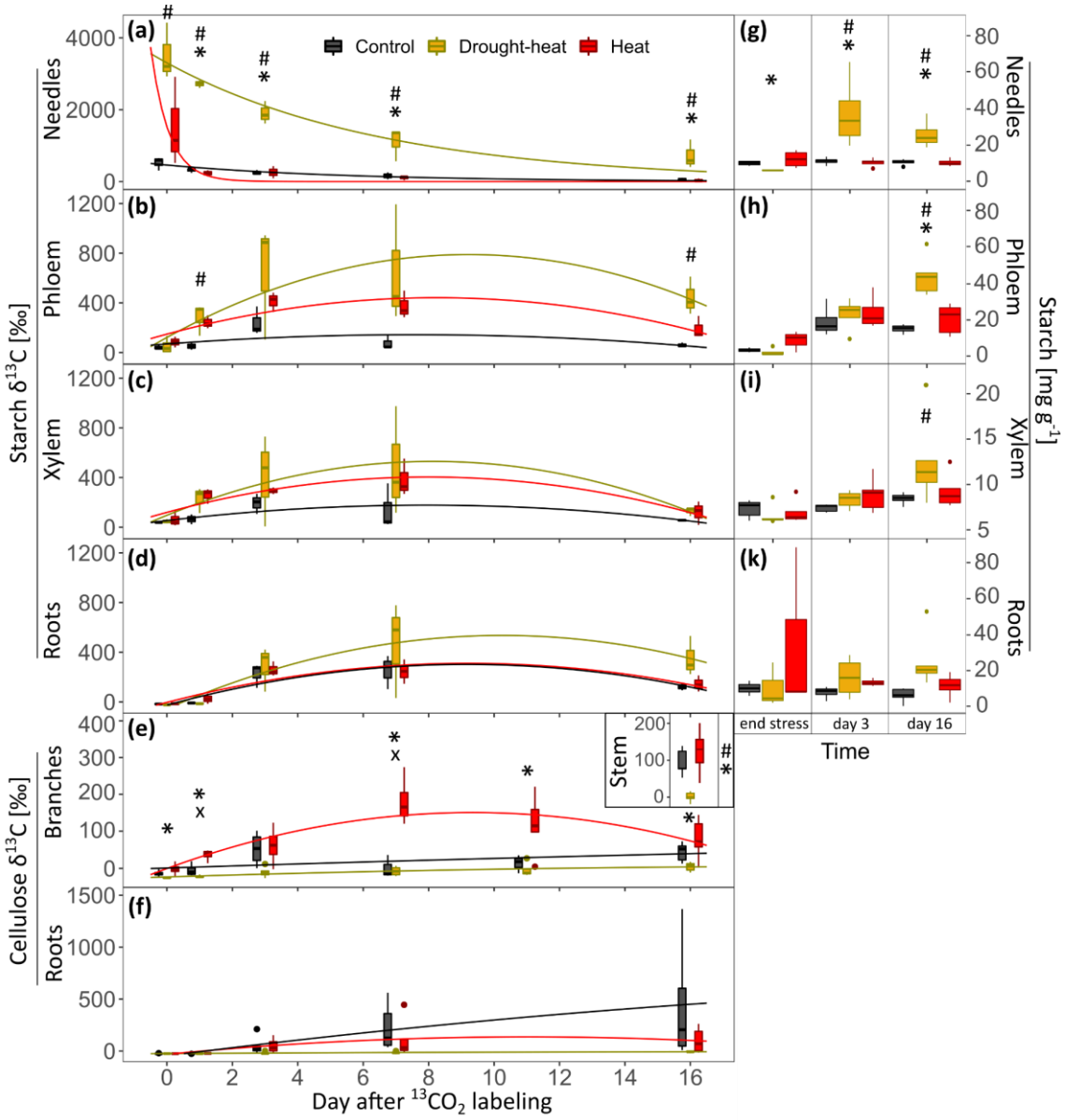

Fig. 5: Treatment-specific dynamics in $\delta^{13}C$ of starch and cellulose following $^{13}CO_2$ pulse-labeling (a-f), as well as starch concentrations at the end of stress and during recovery (g-k). Shown is $\delta^{13}C$ of starch in (a) needles, (b) branch phloem, (c) branch xylem and (d) roots (n=3 per treatment), as well as of cellulose in (e) branches (phloem and xylem), stems (only for day 16, see inserted panel) and (f) roots (n=6 per treatment). Starch concentrations are depicted for (g) needles, (h) branch phloem, (i) branch xylem and (k) roots (n=5-6 per treatment). Seedlings were $^{13}CO_2$ pulse-labeled on day 0. Note that data on day 0 are from sampling 8 h after the start of labeling. Symbols indicate significant differences (P<0.05) between treatments within one sampling campaign (Kruskal-Wallis and Bonferroni post-hoc test; drought-heat vs. control (#), heat vs. control (x), and drought-heat vs. heat (∗)). The regression with the best fit is depicted per treatment (see Table S3).

end of the recovery period (Fig. 5g-k). Contradictory, we found little treatment-specific differences in soluble sugar concentrations (Fig. S9). Drought-heat seedlings strongly allocated recent C to starch and the $\delta^{13}C$ progression of needle starch revealed a longer MRT and HLT in drought-heat compared to heat and control seedlings (Fig. 5a, Table 4). In contrast, needle starch $\delta^{13}C$ of recovering heat seedlings decayed rapidly and MRT was lowest, displaying a rapid translocation to sink tissues. This was congruent with higher $\delta^{13}C$ in branch cellulose, indicating fast allocation to growth (Fig. 5e). Control seedlings preferentially invested ^{13}C into root cellulose, whereas drought-heat seedlings incorporated little ^{13}C into cellulose. This indicates a delayed recovery of growth post drought-heat, consistent with an apparent absence of stem increment during the initial 6 days of recovery (Fig. 3d).

3.3.4 ^{13}C allocation dynamics and overall patterns

After stress release, treatment-specific differences in allocation patterns became apparent in the relative distribution and temporal dynamics of ^{13}C excess in tissue bulk biomass (Fig. 6, see also Figs. S10, S11). Whereas in drought-heat seedlings the relative fraction of ^{13}C remained high in needles (at c. 60%) during the entire recovery period (consistent with a 5-times longer MRT; Table 4), a more dynamic picture emerged in heat and control seedlings. Here, the relative fraction of ^{13}C in needles declined dramatically within 3 d after labeling and evenly distributed among tissues (Fig. 6). Considering long-term recovery, relatively less ^{13}C-label was allocated to roots but to branch and stem tissues post-heat compared to control seedlings.

To summarize the ^{13}C allocation to respiration, plant tissues and compounds, we derived an isotopic mass balance. This included cumulative ^{13}C release via respiration (Fig. S12) and transfer to the SMB, and remaining ^{13}C in plant tissues/compounds 16 d after $^{13}CO_2$ pulse-labeling (i.e., 18 d after stress release; Fig. 7). A general pattern emerged, showing that in combination with drought, ^{13}C retention increased (Tukey's HSD, $P<0.05$ drought-heat vs. control) and ^{13}C release via R_{root} decreased during recovery (Tukey's HSD, drought-heat: $P<0.01$). While control seedlings favored ^{13}C investment into R_{root} and root growth, this was not apparent in seedlings recovering from heat or drought-heat stress. In the heat treatment, we found preferred ^{13}C allocation to branch and stem cellulose, suggesting secondary woody growth. Contrary, drought-heat seedlings hardly invested ^{13}C into growth, but NSC storage. Alongside, a larger fraction of ^{13}C was respired aboveground (Figs. 7, S12b), likely because of ^{13}C retention in WSC, easily available for respiration. The reduced translocation belowground in drought-heat seedlings after re-watering became further apparent in low allocation of ^{13}C to SMB.

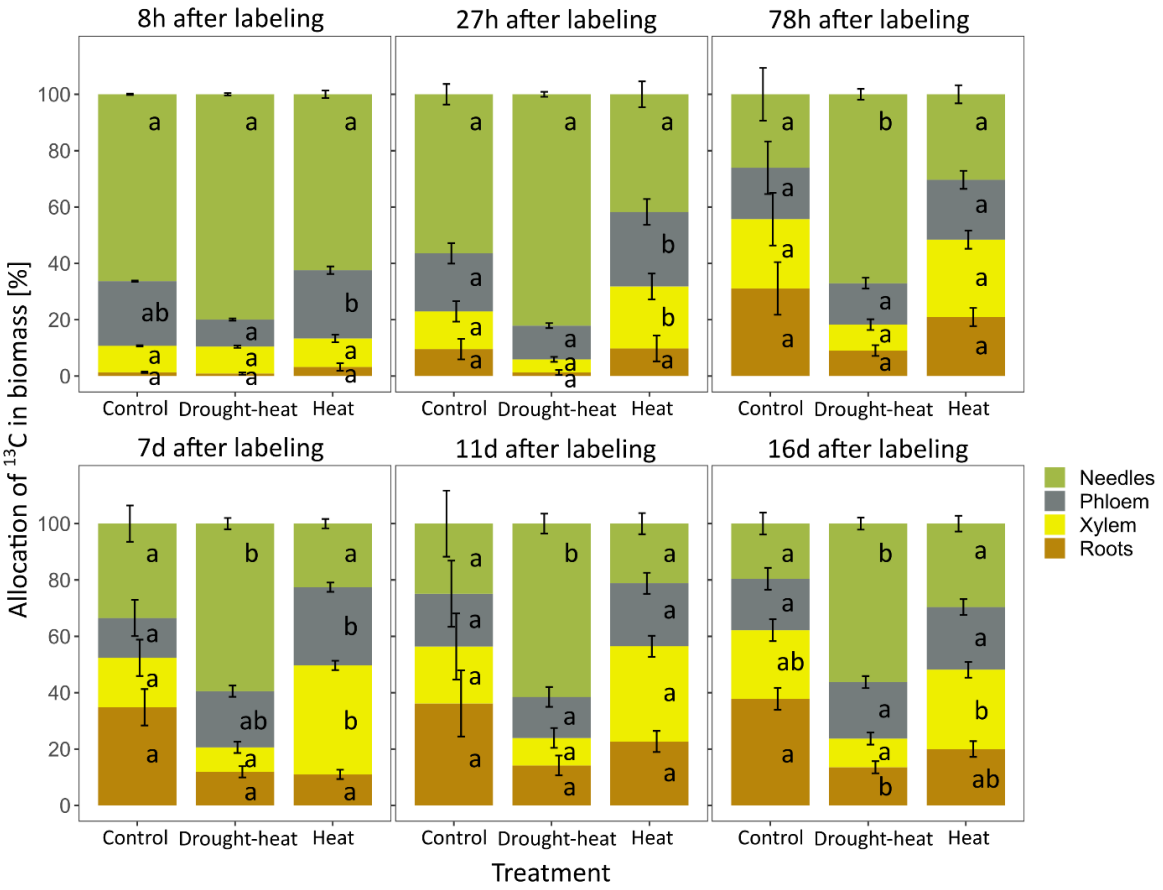

Fig. 6: Post-stress distribution of total ^{13}C present in the plant at each measurement time point within the different plant organs. Shown are the fractions of ^{13}C excess in biomass of needles (green), phloem (gray), xylem (yellow), and roots (brown) in *Pinus sylvestris* seedlings during recovery progression. Tissue-specific biomass was determined at the end of the experiment. The fraction of ^{13}C excess in phloem and xylem was estimated from branch and stem biomass. Error bars represent standard errors (n = 4-6). Different lowercase letters indicate significant differences between treatments per tissue and sampling campaign (Kruskal-Wallis and Bonferroni post-hoc test). For absolute bulk $\delta^{13}C$ and ^{13}C excess values see Figs. S10 and S11.

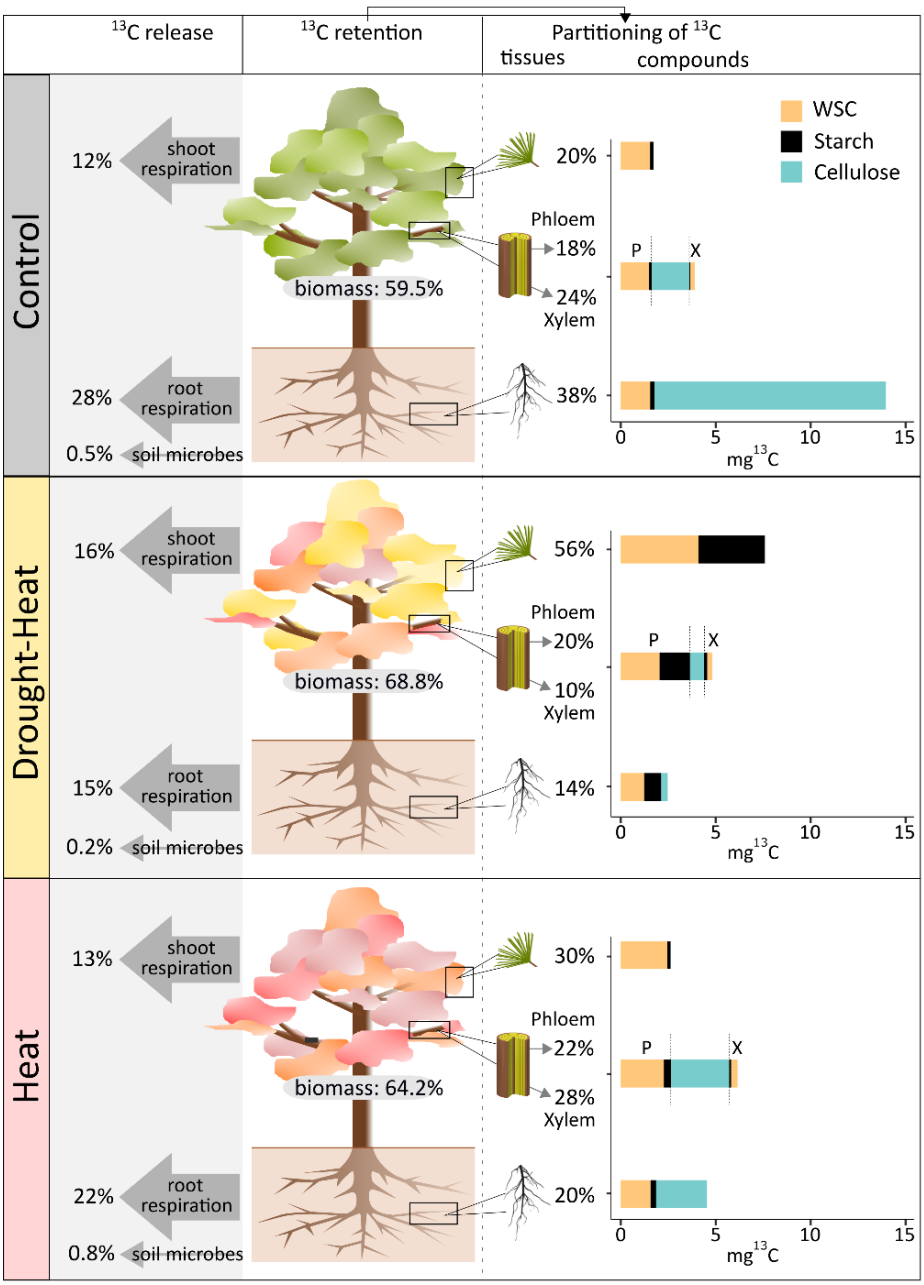

Fig. 7: Overview of treatment-specific carbon allocation during stress recovery in *Pinus sylvestris* seedlings. The isotopic mass balance is based on ^{13}C uptake during $^{13}CO_2$ pulse-labeling, ^{13}C release (respiration and soil microbial biomass) and ^{13}C retention in tree biomass of at the end of the recovery period, 18 days after stress release, i.e. 16 days after pulse-labeling. Percentage of ^{13}C released is derived from total ^{13}C uptake relative to cumulative shoot and root respiration, and ^{13}C ingested by soil microbes (see Methods S6). Shoot respiration includes day- and nighttime, while shoot day respiration was interpolated from shoot night respiration. Percent of ^{13}C retention in biomass was derived from ^{13}C release assuming a closed C balance. Additionally, the partitioning of ^{13}C between needles, xylem and phloem (including branches and stem), and roots is indicated (^{13}C partitioning- tissues), and the amount of label (in mg ^{13}C) allocated to water-soluble compounds (WSC), starch, and cellulose in these tissues is shown (^{13}C partitioning- compounds). Note that compounds for woody xylem/phloem are depicted in one bar showing the amount of ^{13}C in WSC and starch separately (indicated as P= phloem and X= xylem), whereas the amount of ^{13}C in cellulose is shown for the entire stem/branch biomass. Also note that cellulose was not measured in needles, as seasonal needle elongation was completed.

3.3.5 Tissue-specific dynamics of ^{15}N

The inhibition of above-belowground coupling was further reflected in a reduced ^{15}N uptake capacity of recovering drought-heat seedlings (Fig. 8d). Here, we report ^{15}N excess to account for total N differences between treatments (Fig. S13). Clearly, seedlings recovering from drought-heat assimilated significantly less ^{15}N than control seedlings (Fig. 8a-c). In contrast, the ^{15}N dynamics of heat seedlings followed closely the trajectories of control seedlings, albeit missing a distinct ^{15}N peak in root tissues. The transient character of ^{15}N in roots and xylem was underlined by the bell-shaped temporal trajectories. 9 d post ^{15}N-labeling, ^{15}N had been incorporated in needle and phloem tissues as curves leveled off.

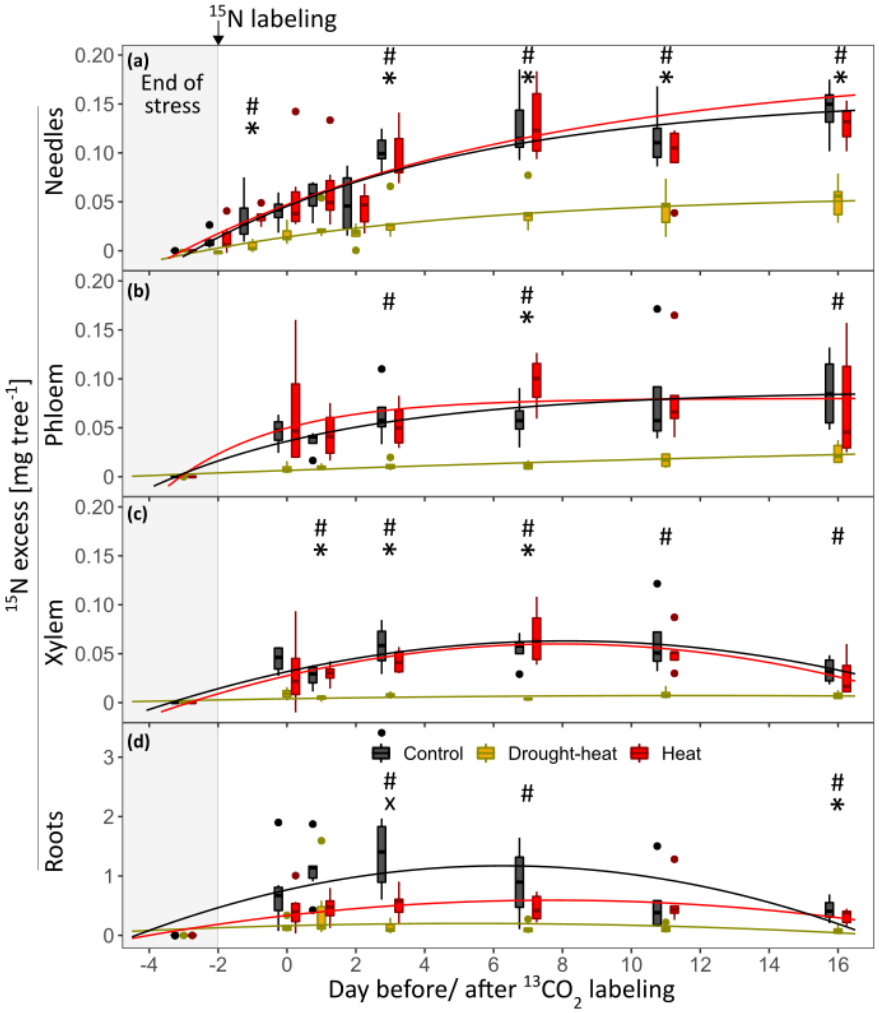

Fig. 8: Dynamics of ^{15}N excess of bulk material in (a) needles, (b) phloem, (c) xylem and (d) roots for the end of stress and recovery period per treatment (n=6). The gray box represents the end of the stress period, and the ^{15}N label was applied to the soil upon stress release on day -2 (= 2 days before $^{13}CO_2$ pulse-labeling). Note that background values on day -3 are also displayed. Tissue-specific biomass was determined at the end of the experiment, and ^{15}N excess in phloem and xylem includes branch and stem biomass. Symbols indicate significant differences (P<0.05) between treatments per sampling campaign (Kruskal-Wallis and Bonferroni post-hoc test) as follows: drought-heat vs. control (#), heat vs. control (x), and drought-heat vs. heat (∗). The curve with the best fit is given for each treatment (see Table S3).

3.4 Discussion

3.4.1 Stress impact and above-belowground coupling during recovery

Under well-watered conditions, the impacts of high daytime temperature (<43°C) and VPD on *P. sylvestris* seedlings were small. In combination with drought, resulting in higher leaf temperatures and VPD, stress impacts became severe and C loss exceeded C uptake. Remarkably, throughout the heatwave we found an acclimation of respiration, which seemed to closely follow C uptake dynamics (Fig. 3). Such acclimation processes have been reported previously in response to warming (Jarvi and Burton, 2013; Birami et al. 2020, 2021). For detailed information on temperature-related dynamics of gas exchange in the same seedlings see Rehschuh and Ruehr (2021).

Following heat release, tree C exchange recovered quickly in well-watered seedlings as shown previously (Ameye et al., 2012; Ruehr et al., 2019). Despite this nearly instantaneous recovery of C uptake and respiration, we found C allocation patterns to differ from control seedlings. Within 1 d after $^{13}CO_2$ labeling, we observed a preferential allocation of recent assimilates to WSC in phloem and xylem and a tendency for faster C translocation to R_{root} in heat seedlings compared to the control (Fig. 4b,d-e). Based on the leakage-retrieval mechanism during phloem transport (van Bel, 2003; Thorpe et al., 2005), sugars and other carbohydrates are retrieved from phloem sieve tubes to feed the lateral sinks along the pathway, supporting growth and tissue maintenance (De Schepper et al., 2013; Deslauriers et al., 2014). Thus, the detected large ^{13}C signal in xylem WSC shortly post-heat could indicate support for secondary growth, consistent with ^{13}C allocation to branch cellulose 1 d after labeling (Fig. 5e). In addition, a fast above-belowground coupling became evident in SMB, where ^{13}C peaked already 3 d post-labeling (Fig. 4g). C release via root exudates can support seedling growth indirectly via improved soil microbial functioning and nutrient cycling (Wagg et al., 2014; Rennenberg and Dannenmann, 2015; Gessler et al., 2017).

Heat combined with drought resulted in higher needle temperatures due to reduced evaporative cooling (Drake et al. 2018), and much larger impacts on overall tree performance (see Rehschuh and Ruehr (2021) for impacts on tree hydraulics). This was observed in a stark reduction of respiration and stem diameter shrinkage (Fig. 3), in agreement with previous studies (Ruehr et al., 2016; Birami et al., 2018). Hydraulic measurements further showed that stem hydraulic conductivity decreased by 25% under drought-heat (Rehschuh and Ruehr, 2021). These, in comparison to the heat seedlings, larger stress impacts were reflected in a much slower recovery of C cycling, stem growth and Ψ_{Needle} with evident consequences for C allocation. A substantially longer MRT and HLT of ^{13}C in needles and $R_{shoot\ night}$ (Table 4) could indicate that the metabolism was still operating in stress mode. The delayed translocation of recent C from source to sink organs is likely driven by reduced phloem translocation caused

by impaired phloem loading and/or reduced sink activity. Both could result in a passive overflow of NSC in aboveground organs, as observed here (Fig. 5). Impaired phloem functionality can reduce the source-sink coupling (Sevanto, 2014, 2018) under drought (Ruehr et al., 2009; Blessing et al., 2015; Hesse et al., 2019) and post-drought (Zang et al., 2014; Galiano et al., 2017). Damage to the hydraulic system in drought-heat seedlings (Rehschuh and Ruehr, 2021) and a close link between xylem and phloem functioning (Hölttä et al. 2009) supports impaired phloem transport. This is further supported by large shrinkage and slow expansion of stem diameter width to before-stress conditions (7 d after rewetting), indicating a rather slow hydration and repair of phloem sieve tubes.

Further, low sink activity might explain the reduced source-sink coupling as suggested by the tendency of lower root biomass under drought-heat. According to the pressure-flow hypothesis, phloem flow is driven by pressure differences between source and sink tissues (Münch 1930). If C demand for growth and maintenance is low in sink tissues, phloem transport will decrease, supported here by initially low secondary growth likely due to persisting drought-induced meristem inactivation and lower ^{13}C allocation to R_{root} (Fig. 4b, 5e-f). While limited C allocation to SMB has been reported under drought stress (Ruehr et al., 2009; Hagedorn et al., 2016; Joseph et al., 2020), our findings are in contrast to Hagedorn et al. (2016) and Joseph et al. (2020), who found an enhanced C allocation to belowground sinks post-drought. Therefore, it should be noted that the timing of pulse-labeling might strongly affect the results. In Hagedorn et al. (2016) e.g., ^{13}C pulse-labeling was conducted 14 d after re-wetting in beech seedlings, when soil respiration exceeded photosynthesis and the above-belowground coupling was fast. In our study, pulse-labeling was conducted 2 d after stress release, when the tree metabolism still appeared to operate in stress mode and phloem functionality was impaired. In summary, we can confirm our first hypothesis. In heat treated seedlings C sink allocation was fast, while drought-heat stress delayed phloem translocation to belowground during early recovery.

3.4.2 C allocation to storage, repair and growth

We found drought-heat but not heat seedlings to allocate significant amounts of C to starch during the entire recovery period (Figs. 5, 7). This has been shown previously following drought (Galiano et al., 2017; Rehschuh et al., 2020) and heat stress (Marias et al., 2017). However, the underlying processes remain largely elusive. C stored in starch is a source for growth and dark respiration (Smith and Stitt, 2007), the latter conforming with peaks in night $\delta^{13}C$ of R_{root} in drought-heat seedlings. We suggest that shortly after stress release, C passively overflowed to storage due to reduced phloem translocation (see above) at the expense of growth (Fig. 5e-f; Sala et al., 2012; Dietze et al., 2014; Galiano et al., 2017. Later, c. 8 d after re-wetting, when respiration rates had recovered, accumulating starch in branches and roots indicates a more

active process and underlines the importance of starch in tree fitness and survival (Thalmann and Santelia, 2017).

The dominant allocation of ^{13}C to starch in drought-heat seedlings resulted in a very low incorporation into root, branch and stem cellulose (Fig. 5e-f). In agreement, stem diameter remained below pre-stress values during the initial 6 d post-stress, when a large fraction of ^{13}C had already been allocated. This was in stark contrast to previously heat treated seedlings, which upregulated aboveground woody growth immediately, as observed in stem increment rates and ^{13}C allocation to branch and stem cellulose (Figs. 3d, 5e). The reasons could involve increased cambial activity and cell division under elevated temperatures, thus enhancing stem growth (Gričar et al., 2007; Gričar, 2013; Balducci et al., 2016). Growth is initiated by cell division, involving cellulose accumulation during the formation of new cell walls (Drakakaki, 2015). This step is followed by cell enlargement, wall thickening and secondary wall formation, involving intensive cellulose synthesis (Cuny et al., 2014, 2019). In our study, we suggest that heat stress enhanced cell division, while once stress was released, cell enlargement continued, typically taking about 9 d in Scots pine (Cuny et al., 2014).

In drought-heat seedlings, stem growth was accelerated in the second half of the recovery period. Hardly any ^{13}C in stem cellulose at the end of the experiment suggests that C skeletons for growth were supplied by older storage compounds including lipids, or more likely, C assimilated after pulse-labeling. The delayed growth recovery is in line with observed repair of cambial activity taking 2-4 weeks post drought-heat in *Picea mariana* saplings (Balducci et al. 2013). Enhanced stem growth promotes a reestablishment of the plant hydraulic system via new functional xylem (Trugman et al., 2018). Further, stress-induced stem growth compensation have been reported post drought and heat (Balducci et al., 2016; Ruehr et al., 2016) by an extension of xylogenesis processes. These compensatory measures are important for photosynthetic processes in the long-term by optimizing water transport to needles. Concurrently, repairing root functionality would be highly important. In drought-heat seedlings, low ^{13}C allocation to root cellulose and R_{root}, but R_{root} tending to exceed control rates at the end of the experiment indicates a delayed upregulation of root growth and rhizosphere activity. Based on our results, we suggest that during initial recovery, growth was limited by impaired phloem functioning, which repair enhanced the recovery of respiratory activity and growth later.

In summary, we partially refute our second hypothesis as short-term growth post drought-heat was inhibited, while stem growth appeared to be a strong C sink later on, concurrently with the recovery of above- and belowground respiration, indicating repair mechanisms.

3.4.3 Coupling of C and N metabolism

Post-stress, N uptake and allocation was closely coordinated with C allocation dynamics. In recovering heat seedlings, large investments of C into branch and stem growth were consistent with the enhanced allocation of N to aboveground tissues (Fig. 8; Rennenberg et al., 2006; Gessler et al., 2017). In contrast, control seedlings allocated most ^{13}C to roots (Figs. 5f, 7) and revealed largest N uptake. This provides additional evidence for roots as a dominant C sink during autumn (Endrulat et al., 2010; Blessing et al., 2015) to enhance water and nutrient uptake. Additionally, N might be invested into storage proteins that can be remobilized for growth in spring (Palacio et al., 2018).

Further, low N uptake and transport to aboveground post drought-heat supports low root activity and the inhibition of short-term growth (Fig. 8; Palacio et al., 2018). N uptake is operated at the whole-plant level by a cycling pool of N as a bidirectional exchange between the xylem and phloem within leaves, roots and the long-distance transport path. This ensures the signaling of the actual N demand to regulate nutrient supply (Herschbach et al., 2012; Rennenberg and Dannenmann, 2015). Low growth activity typically results in low N demand. The reduced N uptake as observed here could result from amino compounds (particularly glutamine) accumulating in roots (Geβler et al., 2004b), associated with stress-induced impairment of root functioning (Schönbeck et al., 2020).

Overall, we found a close coordination of C and N cycling post-stress, confirming our third hypothesis. This was reflected in lower N uptake and aboveground allocation in seedlings where growth processes were not activated yet.

3.5 Conclusion

In well-watered Scots pine seedlings exposed to moderate daytime heat stress, C uptake and respiration recovered quickly. Accordingly, translocation of recent C to belowground was fast and growth, i.e. ^{13}C allocation to branch cellulose, upregulated quickly. In contrast, combined heat and drought resulted in higher leaf temperatures and substantially affected tree physiological functioning, reflected in a delayed and reduced allocation of recent C to belowground following stress release. The underlying causes may include impaired phloem functioning and/or reduced C sink strength. This is consistent with a delayed increase of respiration, low ^{13}C allocation to cellulose and low N uptake during initial recovery. Later during recovery, stem diameter changes indicate enhanced secondary growth, not captured by the label.

The initially delayed translocation from source to sink organs following release from hot drought stress could have substantial consequences for tree functioning and nutrient uptake. If such a decoupling emerges relevant for forest regeneration, it should be considered in stress legacy

modeling, while accounting for seasonality. To further elucidate the reversibility of stress damage and impairment of C and N cycling, we call for experiments addressing the impacts and timing of single and compound stressors during different recovery stages.

Acknowledgements

We are particularly grateful to Rudolf Meier, Benjamin Birami, Juliane Bachmann and Paula Hainz for technical and experimental support. Furthermore, we like to thank Manuela Oettli and Ulrike Ostler for isotopic MS analyses. This study was supported by the German Research Foundation through its Emmy Noether Program (RU 1657/2-1). We further acknowledge funding by the German Federal Ministry of Education and Research (BMBF), through the Helmholtz Association and its research program ATMO. MML was supported by the SNF Ambizione grant (No. 179978).

Author contributions

RR and NKR designed the study. RR conducted the experiment with support from A Gast, SR, AJ and NKR. RR, AJ and SR conducted extractions for isotopic mass spectrometry and performed NSC analyses. RR analyzed the data with support from SR, MML and NKR. RR wrote the original draft with reviewing and editing from NKR and all other co-authors.

3.6 Supplemental material

Supplemental methods

Methods S1: Implementation of heat-drought scenarios

In the stress treatments, we based the adjustment of environmental conditions on a natural drought event linked with heat waves. Data for such a natural hot drought was obtained from a meteorological station of the *German Meteorological Service* in Franconia, Bavaria. In this region, high mortality rates of Scots pine have been reported recently due to extreme weather events (Gößwein et al., 2017; Walentowski et al., 2017; Buras et al., 2018). We analyzed air temperature, relative humidity and vapor pressure deficit (VPD) during the growing season of extraordinary dry and hot years (2003, 2015) in Weißenburg-Emetzheim (435 m a.s.l., N49° 1′ 38,28″ E10° 58′ 55,2″), and identified August 2003 as a good example for a hot and dry month (Fig. S2). This was also reflected in growth reductions of up to 50% in some European forests after the 2003 summer (Bertini et al., 2011). Environmental control conditions were adjusted according to long-term averages of August 1986-2016, i.e. to 30-year-means, and constant soil moisture.

Methods S2: Tree gas exchange chambers

S2.1 Chamber design

The cylindrical tree gas exchange chambers were separated into a root and a shoot compartment by a polyamide disc. Stems were mounted through an opening and a double-sealed polyamide spacer and additional plastic putty (Teroson, Düsseldorf, Germany) ensured gas tightness between the shoot and root compartment. For the shoot enclosures (inner diameter 29 cm, height: 55-65 cm; flexible depending on tree height), transparent acrylic glass (4 mm; PMMA XT, Sahlberg, Feldkirchen, Germany) was used. The root chamber was made from lightproof polyvinyl chloride (inner diameter: 30 cm, height: 29 cm), and was equipped with two ventilators (252N, ebm-papst, St. Georgen, Germany). Soil temperature (TS 107, Campbell Scientific, Inc. USA) and moisture (EC5, Meter Group, USA) were continuously measured. Air temperature in each shoot compartments was measured and regulated by fast-response thermocouples (5SC-TTTI-36-2M, Newport Electronics GmbH, Deckenpfronn, Germany) connected to a water cooling system (for details see Birami et al. (2020)). Photosynthetic active radiation (PAR) in the shoot compartments was determined by individual photodiodes (G1118, Hamamatsu Photonics, Hamamatsu, Japan), which were calibrated previously with a high-precision PAR sensor (PQS 1, Kipp & Zonen, Delft, the Netherlands). Data was automatically logged every 10 min (CR1000, Campbell Scientific, Inc. USA).

S2.2 Gas exchange measurements

Gas exchange was measured via an open system. Because air was supplied to the chamber compartments at a much higher rate than drawn back to the analyzers, the pressure inside the chambers was slightly above ambient to ensure that outside air was not entering. Excess air could leave the chambers via an exhaust vent.

Supply air (Air_{supply}) was provided by an oil-free screw compressor (SLD-S 7.5, Renner Kompressoren GmbH, Güglingen, Germany), which was connected to a condensation trap (DFX9, FST GmbH, Essen, Germany) and adsorption columns (DPS 8 MZ, FST GmbH, Essen, Germany), and provided in total 300 L min^{-1} of almost CO_2-free air with a dew point of -60°C at 8 bar (abs). We added a predefined concentration of CO_2 (F-201CV-500, Bronkhorst, Ruurlo, Netherlands), and H_2O by an evaporator mixer (CEM W-303B-330-K, Bronkhorst, Ruurlo, Netherlands) to Air_{supply} using two mass flow controllers (M13-RGD-33-O-S and F-201CV-500, Bronkhorst, Ruurlo, Netherlands). Well-mixing of air and water was enabled by a static mixer (SVMW-J-19/19-10-C, Schumacher Verfahrenstechnik GmbH, Germany). Each shoot compartment received c. 13 L min^{-1} and every root chamber c. 3 L min^{-1} of Air_{supply} (GZ-32461-56 and -52, Cole-Parmer GmbH, Wertheim, Germany). At the end of the experiment, we determined the exact flow rates for each chamber compartment used for calculations of gas exchange fluxes. Air_{sample} was drawn back from the compartments at 500 ml min^{-1} (NMP830KNDC, KNF Neuberger GmbH, Freiburg, Germany). To avoid condensation, Air_{sample} from the belowground compartments was dried (Nafion® tubing, Gasmet Technologies GmbH, Karlsruhe, Germany). Four valve units (EUTA-SD16MWE, Vici AG International) and two three-way valves (0330, Bürkert GmbH & Co. KG, Ingelfingen, Germany) enabled switching between chambers and compartments.

$\delta^{13}CO_2$ was measured by the Delta Ray at a flow rate of 80 ml min^{-1}. To start a cycle of measurements, an external trigger signal was applied for coordination with differential gas analyses. Each measurement lasted for 60 s, and between measurements, lines were flushed for 70 s. The Delta Ray measured Air_{supply} and Air_{sample} iteratively using a three-way valve. Air_{sample} of shoot and root compartments was measured each in blocks of 6-7 to avoid long flushing times during labeling (due to memory effects of the highly enriched $\delta^{13}CO_2$ signal in shoot compartments). For calibration, two commercially available calibration gases were used (Ref.1: $\delta^{13}C$= -9.86±0.3‰ and Ref.2: $\delta^{13}C$= - 27.8±0.3‰, 160402 and 141101, Thermo Fisher Scientific).

S2.3 Gas exchange and isotopic calculations

Gas exchange data were analyzed based on plausibility, and outliers were identified by inspecting day and night-time measurements separately for each chamber. Values outside 1.5 times the interquartile range above the upper and below the lower quartile were then removed

(c. 6.6% of CO_2 and 8.1% of H_2O gas exchange data). Measurements were then interpolated per chamber by gap filling. Between day 5 and 7 after labeling, measurements were not available due to technical failure and daily fluxes were calculated from linear interpolation.

Above- and belowground gas exchange per tree was calculated according to concentration differences of CO_2 and H_2O of Air_{supply} and Air_{sample}. Transpiration (E) in mol s^{-1} m^{-2} was calculated as follows:

$$E = \frac{\dot{m}(W_{\text{sample}} - W_{\text{supply}})}{area_{needle}\,(1 - W_{\text{sample}})} \quad (1),$$

where $\dot{m}$ is air mass flow (mol s^{-1}) into the chamber compartment, and W_{supply} and W_{sample} are the H_2O concentrations of Air_{supply} and Air_{sample}, respectively. $Area_{needle}$ is the total needle area in m^2.

CO_2 fluxes, i.e. net assimilation A_{net} and shoot respiration R_{shoot} in µmol s^{-1}, as well as root respiration R_{root} in µmol s^{-1} were calculated as follows:

$$\mathrm{CO_2\ flux} = (-\dot{m}\,\Delta\mathrm{C}) - (E\,C_{sample}) \quad (2),$$

where ΔC is the difference between the CO_2 concentration of Air_{sample} and Air_{supply}. Additionally, A_{net} was based on total needle area, and R_{root} on *g* DW of total root biomass.

The daily C uptake by A_{net} and C loss for $R_{shoot\ night}$ and R_{root} was derived by summing up hourly means (in mg C d^{-1} $tree^{-1}$).

$\delta^{13}CO_2$ of night-time R_{shoot} and R_{root} was calculated according to the following equation:

$$\delta^{13}\mathrm{CO_2}(‰) = \frac{\delta^{13}\mathrm{C_{sample}} \cdot C_{\text{sample}} - \delta^{13}\mathrm{C_{supply}} \cdot C_{\text{supply}}}{C_{\text{sample}} - C_{\text{supply}}} \quad (3),$$

where $\delta^{13}C$ is the isotopic signature of CO_2 and C is the CO_2 concentration of Air_{sample} or Air_{supply}.

To establish a mass balance of ^{13}C measurements, we assumed day-time R_{shoot} to equal night-time R_{shoot} and estimated daily sums by multiplying averaged night-time R_{shoot} by day light hours, here 16 h.

We estimated label uptake (in mg ^{13}C) during pulse-labeling per seedling as follows:

$$^{13}\mathrm{C\ uptake} = \frac{C_{\text{uptake}} \cdot (\mathrm{atom\%_{Air\ supply}} - \mathrm{atom\%_{background}})}{100} \quad (4),$$

where C uptake is net photosynthesis in mg C determined by the Delta Ray (since it is not blind for ^{13}C). $Atom\%_{Air\ supply}$ and $atom\%_{background}$ are the average ^{13}C concentrations during the 4-hour pulse and before labeling in Air_{supply} (Table S4), respectively.

Further, we assessed the isotopic signature of current and last year needles (bulk material) sampled directly after $^{13}CO_2$ labeling. Excess ^{13}C (mg per seedling) of bulk needle material (see Methods S6) compared well with ^{13}C-values derived from C uptake (see Table 2).

Methods S3: Nonstructural carbohydrate (NSC) analysis

For the determination of total NSC concentrations, 10 mg per sample was used for the extraction in 80% ethanol at 80°C for 10 min, and after centrifugation at 13,000 g for 3 min, the supernatant was transferred into a new reaction vial. This step was repeated 3 times, and the remaining pellets were used for the quantification of starch concentrations. For this, pellets were suspended in 1 ml dH_2O, heated to 95°C for 2 h and then cooled to room temperature. Further, α-amlylase from *Bacillus licheniformi*s (Sigma cat. no. A4551) was added to the samples, which were then heated at 85°C for 90 min. After cooling to room temperature and centrifugation, an amyloglucosidase reagent (25mM sodium acetate buffer (pH 4.5) and amyloglucosidase from *Aspergillus niger* (Sigma 10115-1G-F)) was added and samples heated at 55°C for 90 min. After cooling and centrifugation, glucose detection was carried out. For this, two solutions were prepared (with and without enzyme). In a buffer solution of MgCl and Tris-HCl, ATP, NAD+, glucose-6-phosphate (Sigma G8404-2KU) and hexokinase (Roche 1142632001) were dissolved. The other solution contained the buffer MgCl and Tris-HCl. Finally, these solutions were added to the samples, and absorption was determined by a spectrophotometer at an absorption of 340 nm (Epoch 2, BioTek, Winooski, Vermont, USA).

For soluble sugar analysis, the reaction vials containing the extracts, were placed in a centrifugal vacuum concentrator (Model 5301, Eppendorf, Germany) to remove the ethanol. Subsequently, 1 ml dH_2O was added. The samples were digested using invertase from *Saccharomyces cerevisiae* (Sigma-Aldrich I4504-250mg) by incubating at 55°C for 35 min. Finally, the glucose detection was carried out similar to starch quantification, but here, isomerase from *Streptomyces murinus* (Sigma-Aldrich P5381-1KU) was used additionally to ensure fructose break down to glucose.

Methods S4: Extraction of water-soluble compounds (WSC), starch and cellulose

For $\delta^{13}C$ analysis of WSC and starch, 40-60 mg of dry homogenized biomass was extracted in 1.5 ml deionized water at 85°C for 30 min. After cooling and centrifugation at 10,000 g for 2 min, the supernatant liquid (WSC) was pipetted into a new reaction vial. The remaining pellets were dissolved in 1 ml deionized water for starch extraction by enzymatic hydrolysis. For this, pellets were incubated 4 times with 1.5 ml of a Methanol-Chloroform-Water solution (MCW, 12:5:3, v/v/v) for 10 min at 70°C; in between, samples were centrifuged (10,000 g, 2 min). Subsequently, pellets were washed with deionized water, bench-dried overnight, and finally

oven-dried at 60°C for 1 h to completely remove chloroform. Pellets were then dissolved in deionized water, and incubated at 100 °C for 15 min to gelatinize starch. After cooling, α-amylase (EC 3.2.1.1, Sigma-Aldrich) was added, and samples heated at 85°C for 2 h to hydrolyze starch. Samples were centrifuged (10,000 g, 2 min), and the supernatant liquid was transferred to centrifugation filters (Vivaspin 500, Sartorius, Göttingen, GER) to remove enzymatic residues by centrifugation at 12,000 g for 50 min.

For cellulose extraction, closed Teflon filter bags (Fiber Filter Bags F57, Ankom Technology, Macedon, NY, USA) were placed in a 5% NaOH solution, and heated twice at 60°C for 2 h. Further, a 7% $NaClO_2$ solution, acidified with 96% acetic acid (pH of 4-5) was added to the samples, and heated to 60°C. The solution was renewed every 10 h, with extraction times ranging from 20-40 h. Finally, Teflon filter bags were oven-dried at 60°C for 12 h. Following, samples were soaked in deionized water for a few hours and homogenized by an Ultrasonic transducer. After freezing, samples were freeze-dried for 36 h.

Methods S5: Soil microbial biomass extraction

For $\delta^{13}C$ analysis of the soil microbial biomass, biomass residues and bigger stones were removed from soil samples, which were then divided into 4 subsamples of 10 g, of which 2 parts were fumigated for 24 h with chloroform (stabilized with Methanol and 1-Methyl-buten) vapor, whereas the others were not fumigated. After vigorous shaking in 50 ml K_2SO_4 for 30 min extracts were filtered using vacuum pumps and glass fiber filters (0.03 M for determination of ^{13}C and 0.5 M for C content measurements). Fumigated and non-fumigated 0.03 M extracts were freeze-dried and weighed into tin capsules for isotopic analysis (c. 10 mg). 0.5 M extracts were immediately frozen for later analysis of total organic C by an infrared TOC analyzer (DIMATEC, Essen, Germany). The gravimetric soil water content was determined from c. 10-20 g samples before and after oven-drying at 105°C for 24 h.

Methods S6: Isotope ratio mass spectrometry

To calculate excess ^{13}C/ excess ^{15}N (mg per seedling) added by pulse-labeling to dry weight in bulk material, tissue compounds (WSC, starch, cellulose), the soil microbial biomass and respiration, we determined atom%:

$$\text{atom\%} = \frac{100 \cdot R_{\text{standard}} \cdot \left(\frac{\delta}{1000}+1\right)}{1 + R_{\text{standard}} \cdot \left(\frac{\delta}{1000}+1\right)} \quad (5),$$

where R_{standard} of 0.0111802 is the isotope ratio ($^{13}C/^{12}C$) of the VPDB and 0.003677 of $^{15}N/^{14}N$ of atmospheric N_2.

Subsequently, we used the following equation to calculate excess ^{13}C/ excess ^{15}N (mg per seedling):

$$\text{excess } {}^{13}C/{}^{15}N_{sample} = \frac{\text{atom\%}_{\text{sample}} - \text{atom\%}_{\text{background}}}{100} \cdot \text{DW} \cdot \frac{X\%}{100} \quad (6),$$

where $\text{atom\%}_{background}$ is the atom% of the background value per tree (for single tissue compounds averaged per treatment; for background permil values see Table S4), *X*% is the percentage of C or N in the sample, and DW is dry weight of a plant tissue or tissue compound per tree (the latter averaged per treatment and time step). DW of WSC and cellulose was determined during preparation for ^{13}C analyses. Starch content was measured as described in section “Nonstructural carbohydrate analysis” for applicable or nearest sampling campaigns.

^{13}C excess of SMB (µg g^{-1} of dry soil) was determined as follows:

$$\text{excess } {}^{13}C_{microbes} = \frac{\text{atom\%}_{\text{sample}} - \text{atom\%}_{\text{background}}}{100} \cdot \text{TOC} \quad (7),$$

where TOC is the total organic C content of SMB.

Further, we calculated excess ^{13}C of shoot night and root CO_2 efflux as follows:

$$\text{excess } {}^{13}C_{respiration} = \frac{\text{atom\%}_{\text{sample}} - \text{atom\%}_{\text{background}}}{100} \cdot \text{F} \quad (8),$$

where F is the shoot or rather root CO_2 efflux (in mg C h^{-1} $tree^{-1}$).

To assess the overall allocation of recent assimilates (^{13}C mass balance), we calculated daily cumulative sums of excess $^{13}C_{respiration}$ per tree and referred this daily $^{13}CO_2$ loss to total $^{13}CO_2$ uptake during pulse-labeling (see Fig. S12). We determined the fraction of ^{13}C retained in tree biomass as follows: (^{13}C uptake −cumulative ^{13}C respired −^{13}C in SMB), where ^{13}C in SMB was determined from the $\delta^{13}C$ peak in SMB.

Supplemental tables

Table S1: Pre-defined maximum air temperatures for the different treatments per time period (Days of experiment).

Time period		Temperature [°C]		
Days of experiment	Length [d]	Control	Drought-heat	Heat
-27 to -23	5	28	28	28
-22 to -20	3	28	30	30
-19 to -18	2	28	33	33
-17 to -11	7	28	36	36
-10 to -8	3	28	38	38
-7 to -4	4	28	41	41
-3	1	28	35	35
-2 to 16	19	28	28	28

Table S2: Results of the Tukey post-hoc test of overall treatment comparisons per time period derived by linear-mixed effects models (lme) for continuous measurements, i.e. for net assimilation (A_{net}), shoot night respiration ($R_{shoot\ night}$), root respiration (R_{root}), stem diameter, $\delta^{13}C$ of shoot night respiration ($R_{shoot\ night}$ $\delta^{13}C$) and $\delta^{13}C$ of root respiration (R_{root} $\delta^{13}C$). Shown are the p-values for all treatment comparisons for the specified periods, while significant values (P<0.05) are highlighted in bold. Note that p-values are additionally given for the final recovery days. DH = Drought-heat.

Para-meter	Treatment		Pre-drought (day -26 to -23)	Initial stress (day -22 to -9)	Final stress (day -8 to -3)	Initial recovery (day -2 to 0)	Recovery (labeling peak) (day 1 to 6)	Reco-very (day 7 to 16)	Final Reco-very (day 14 to 16)
A_{net} [µmol m^{-2} s^{-1}]	Control -	Heat	1	1	0.438	1	0.99	0.99	0.95
	Control -	DH	0.12	**<.0001**	**<.0001**	**<.0001**	**0.013**	0.55	0.75
	Heat -	DH	**0.015**	**<.0001**	**<.0001**	**<.0001**	0.12	0.09	0.13
$R_{shoot\ night}$ [µmol m^{-2} s^{-1}]	Control -	Heat	1	1	0.15	1	1	1	1
	Control -	DH	0.28	**0.0011**	**<.0001**	**0.003**	1	1	0.99
	Heat -	DH	0.055	**0.003**	**0.011**	**0.019**	0.73	1	0.98
R_{root} [µmol g^{-1} s^{-1}]	Control -	Heat	1	0.93	1	0.98	1	1	1
	Control -	DH	0.98	**0.006**	**0.0001**	**0.005**	0.28	1	0.98
	Heat -	DH	0.65	**0.0004**	**0.0001**	0.08	0.58	1	0.97
Stem diameter [mm]	Control -	Heat	1	1	1	1	1	1	0.7081
	Control -	DH	1	0.39	**<.0001**	**<.0001**	**<.0001**	**<.0001**	**0.0006**
	Heat -	DH	1	0.75	**<.0001**	**<.0001**	**<.0001**	**<.0001**	**<.0001**
$R_{shoot\ night}$ $\delta^{13}C$ [‰]	Control -	Heat	1	1	1	1	1	1	1
	Control -	DH	1	1	1	1	**<.0001**	1	1
	Heat -	DH	1	1	1	1	**<.0001**	1	1
R_{root} $\delta^{13}C$ [‰]	Control -	Heat	1	1	0.95	0.07	**<.0001**	1	1
	Control -	DH	1	**0.002**	**<.0001**	**<.0001**	**<.0001**	1	1
	Heat -	DH	1	**0.0006**	**<.0001**	**0.002**	**<.0001**	1	1

Table S3: Functions and percentages explained by the best-fit models for curves fitted to $\delta^{13}C$ and $\delta^{15}N$ data per plant tissue (or soil), compound and treatment. $\delta^{13}C$ of plant bulk material, starch, water-soluble compounds (WSC), cellulose and soil microbial biomass was analyzed, as well as $\delta^{15}N$ of plant bulk material.

Stable isotope	Plant tissue/ Soil	Compound	Treatment	Function	Percent explained by model
$\delta^{13}C$	Needles	bulk	Control	198.96918 exp(-0.66596 x)	90.2
			Heat	192.14530 exp(-0.54420 x)	73.5
			Drought-heat	172.62263 exp(-0.10232 x)	54.1
	Needles	starch	Control	460.23357 exp(-0.18023 x)	70.2
			Heat	1524.880 exp(-1.797 x)	56.2
			Drought-heat	3304 exp(-1.504e-01 x)	82.9
	Needles	WSC	Control	1049.5253 exp(-0.6145 x)	95.8
			Heat	970.40844 exp(-0.69438 x)	92.5
			Drought-heat	697.82963 exp(-0.24854 x)	79.2
$\delta^{13}C$	Phloem	bulk	Control	129.95734 exp(- 0.16472 x)	53.1
			Heat	191.11294 exp(-0.08127 x)	33.6
			Drought-heat	-0.111974 x^2 +0.005882 x+67.239624	7.8
	Phloem	starch	Control	-1.297 x^2+19.604 x+69.4646	13.8
			Heat	-4.318 x^2+71.192 x +148.297	59.3
			Drought-heat	-7.848 x^2+144.799 x+121.541	40.4
	Phloem	WSC	Control	816.74066 exp(-0.35466 x)	89.2
			Heat	1317 exp(-4.467e-01 x)	79.7
			Drought-heat	433.36873 exp(-0.14537 x)	49.2
$\delta^{13}C$	Xylem	bulk	Control	-0.4681 x^2+6.6821 x+63.8207	20.7
			Heat	-1.2223 x^2+18.4311 x+101.757	17.2
			Drought-heat	46.05464 exp(-0.09776 x)	13.1
	Xylem	starch	Control	-1.9702 x^2+31.242 x+53.6546	25.4
			Heat	-4.4677 x^2+71.314 x+119.5968	62.8
			Drought-heat	-6.569 x^2+106.795 x+96.152	35.2
	Xylem	WSC	Control	1008 exp(-2.243e-01 x)	88.4
			Heat	1671 exp(-2.943e-01 x)	76.4
			Drought-heat	991.48184 exp(-0.24368 x)	83.1
$\delta^{13}C$	Roots	bulk	Control	-1.5949 x^2+29.8391 x+9.6528	21.3
			Heat	-0.9515 x^2+16.7138 x+24.5477	19.1
			Drought-heat	-0.4719 x^2+9.9217 x-5.9764	33.8
	Roots	starch	Control	-3.9068 x^2+71.5627 x-25.7156	66.1
			Heat	-3.724 x^2+68.4544 x-3.9172	69.4
			Drought-heat	-5.618 x^2+115.179 x-55.225	55.8

Stable isotope	Plant tissue/ Soil	Compound	Treatment	Function	Percent explained by model
$\delta^{13}C$	Roots	WSC	Control	$68.7829+229.0654\ x^{0.9929}\ \exp(-0.3256\ x^{0.9929})$	75.0
			Heat	$103.2197+1116.2640\ x^{0.7003}\ \exp(-1.0136\ x^{0.7003})$	34.5
			Drought-heat	$48.0748+364.4244\ x^{0.7325}\ \exp(-0.5879\ x^{0.7325})$	56.2
	Roots	Cellulose	Control	$-0.5703\ x^2+40.1437\ x-45.9271$	33.2
			Heat	$-1.3788\ x^2+30.4124\ x-31.298$	26.4
			Drought-heat	$-0.04167\ x^2+1.78167\ x-24.48492$	48.4
$\delta^{13}C$	Branches	Cellulose	Control	$-0.02622\ x^2+2.85035\ x+1.06107$	18.3
			Heat	$-1.7353\ x^2+32.4272\ x-0.2887$	49.6
			Drought-heat	$-0.06511\ x^2+2.73916\ x-23.17578$	44.2
$\delta^{13}C$	Soil	Microbial biomass	Control	$-0.5759\ x^2+16.3868\ x-27.7366$	37.7
			Heat	$-19.7915+83.2105\ x^{0.7325}\ \exp(-0.3252\ x^{0.8272})$	21.5
			Drought-heat	$-5.982\ \exp(-1.898\ x)-15.502$	7.6
$\delta^{15}N$	Needles	bulk	Control	$-0.26424\ x^2+7.50206\ x+26.20588$	74.9
			Heat	$-71.98795\ \exp(-0.09359\ x)+96.82214$	53.9
			Drought-heat	$-0.07822\ x^2+2.21258\ x+8.02655$	80.2
$\delta^{15}N$	Phloem	bulk	Control	$-63.7716\ \exp(-0.2741\ x)+150.4731$	46.4
			Heat	$-52.30025\ \exp(-0.3263\ x)+146.2306$	16.8
			Drought-heat	$-80.66929\ \exp(-0.0267\ x)+93.33215$	62.1
$\delta^{15}N$	Xylem	bulk	Control	$-1.283\ x^2+21.937\ x+117.824$	46.1
			Heat	$-1.3307\ x^2+22.4281\ x+97.6201$	21.0
			Drought-heat	$-0.06559\ x^2+2.22483\ x+15.72772$	40.5
$\delta^{15}N$	Roots	bulk	Control	$-9.568\ x^2+120.331\ x+704.693$	30.8
			Heat	$-4.912\ x^2+75.423\ x+380.926$	27.0
			Drought-heat	$-1.87\ x^2+21.647\ x+203.929$	6.1

Supplemental Table S4: Background values for $\delta^{13}C$ of respiration, tissues and their compounds, and soil microbial biomass, as well as $\delta^{15}N$ of tissue bulk material sampled one day before stress release per treatment. Note that the data do not reflect typical natural abundance vales since supply air to the tree chambers was slightly enriched in $\delta^{13}C$ ($\delta^{13}C$= 0.28‰).

Plant tissue (organ)/ Soil	Flux/Compound	Treatment	$\delta^{13}C$	$\delta^{15}N$
Shoot	Respiration	Control	-16.54±1.44	-
		Heat	-15.38±1.87	-
		Drought-heat	-24.82±1.48	-
Roots	Respiration	Control	-6.72±1.04	-
		Heat	-9.78±1.46	-
		Drought-heat	-16.91±0.48	-
Needles	bulk	Control	-28.49±0.20	0.97±0.20
		Heat	-28.08±0.28	0.94±0.50
		Drought-heat	-28.04±0.36	1.76±0.30
Needles	starch	Control	-23.44±0.49	-
		Heat	-22.21±1.66	-
		Drought-heat	-25.62±3.89	-
Needles	WSC	Control	-27.75±0.20	-
		Heat	-27.92±0.35	-
		Drought-heat	-28.39±0.45	-
Phloem	bulk	Control	-27.7±0.29	-0.14±0.19
		Heat	-27.69±1.00	0.28±0.56
		Drought-heat	-27.64±0.29	0.21±0.30
Phloem	starch	Control	-26.43±0.87	-
		Heat	-26.37±0.39	-
		Drought-heat	-27.01±0.98	-
Phloem	WSC	Control	-27.22±0.80	-
		Heat	-28.83±0.29	-
		Drought-heat	-29.14±0.29	-
Xylem	bulk	Control	-27.02±0.78	-0.12±0.30
		Heat	-27.22±0.46	0.19±0.85
		Drought-heat	-27.88±0.52	1.90±1.23
Xylem	starch	Control	-23.31±2.50	-
		Heat	-26.08±2.35	-
		Drought-heat	-24.75±0.66	-
Xylem	WSC	Control	-25.48±0.73	-
		Heat	-25.99 ±0.59	-
		Drought-heat	-26.55±0.31	-
Roots	bulk	Control	-26.07±0.62	4.19±1.07
		Heat	-24.49±0.82	5.83±0.96
		Drought-heat	-25.80±0.49	2.42±0.59
		Control	-24.51±0.58	-

Plant tissue (organ)/ Soil	Flux/Compound	Treatment	$\delta^{13}C$	$\delta^{15}N$
Roots	starch	Heat	-20.55±0.46	-
		Drought-heat	-26.46±2.0	-
Roots	WSC	Control	-23.97±0.97	-
		Heat	-22.31±0.57	-
		Drought-heat	-23.43±0.36	-
Roots	Cellulose	Control	-25.27±0.90	-
		Heat	-23.25±0.93	-
		Drought-heat	-24.54±0.98	-
Branches	Cellulose	Control	-26.07±0.41	-
		Heat	-25.62±0.45	-
		Drought-heat	-26.88±0.40	-
Soil	Microbial biomass	Control	-22.70±0.90	-
		Heat	-23.21±1.45	-
		Drought-heat	-23.81±3.56	-

Supplemental figures

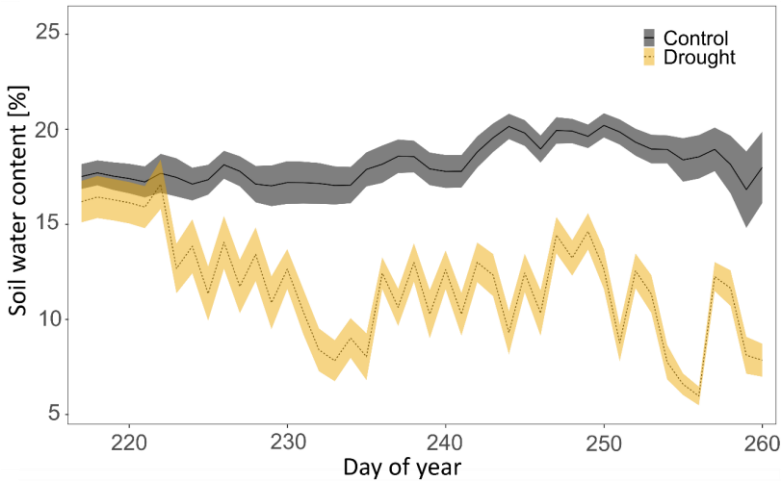

Fig. S1: Daily average soil water content during the pre-drought and drought period (1.5 months before the start of the tree chamber experiment). Shown are treatment averages and shaded areas indicate ±SE (n=6).

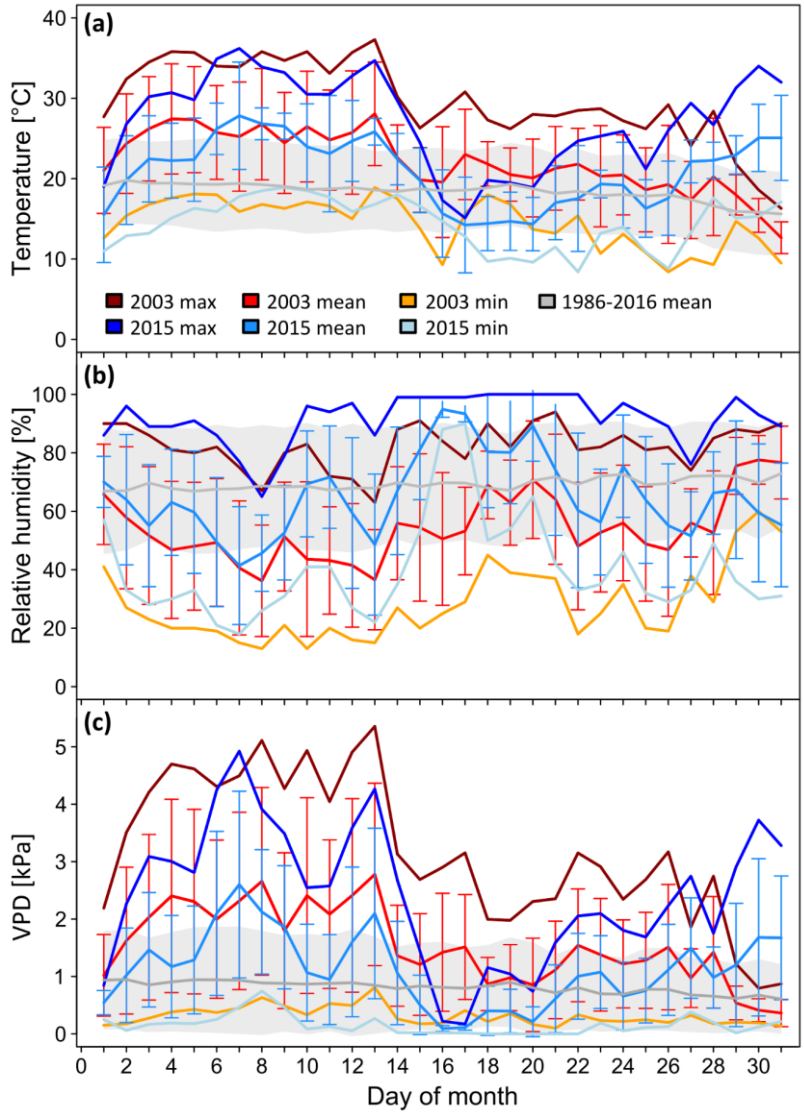

Fig. S2: (a) August daily mean, maximum and minimum temperature, (b) relative humidity and (c) vapor pressure deficit (VPD) of extremely dry and hot years (2013 and 2015), and 30-year averages (1986-2016) for Weißenburg- Emetzheim, Franconia, Germany, where Scots pine forest mortality has been observed recently. Data was obtained from the meteorological station of the *German Meteorological Service* and used as reference for the adjustment of the environmental conditions during the experiment.

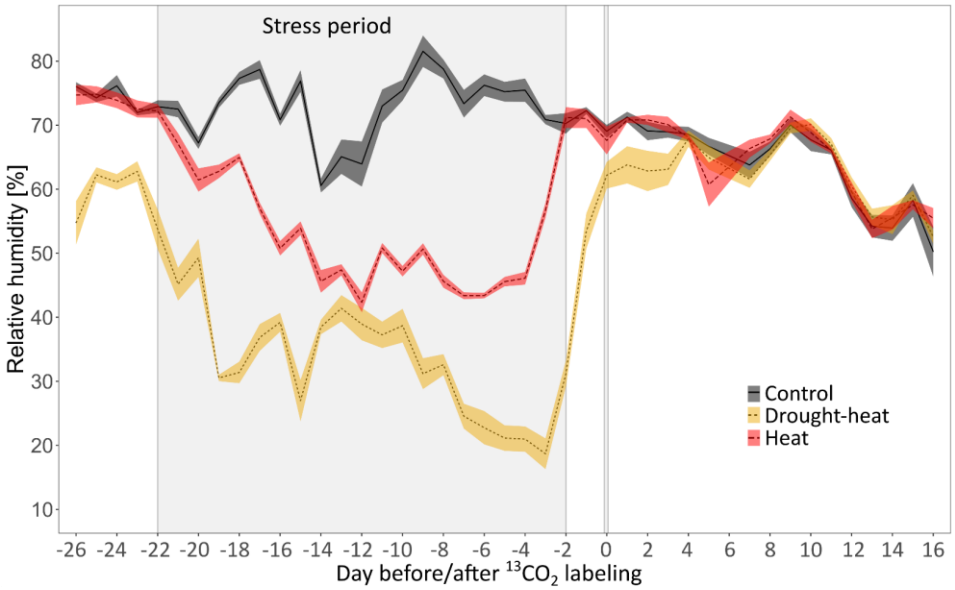

Fig. S3: Relative humidity (RH) during the experiment for PAR >100 µmol m^{-2} s^{-1}. Shown are treatment averages and shaded areas are ±SE (n=6). The gray box represent the stress period; and the vertical gray line indicates the day of the experiment (day 0) on which seedlings were $^{13}CO_2$ pulse-labeled. Note that RH in the drought-heat treatment was lowest due to low tree transpiration rates.

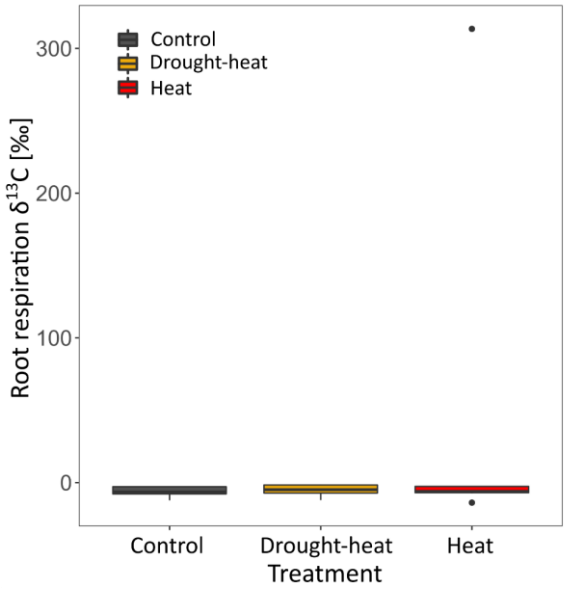

Fig. S4: $\delta^{13}C$ in root respiration during the 4h $^{13}CO_2$ labeling pulse per treatment (n=6). Note that in one chamber of the Heat treatment, $\delta^{13}C$ was enriched due to a small leak between the shoot and the root compartment, but this had no effect for the determination of the arrival time of the label in root respiration.

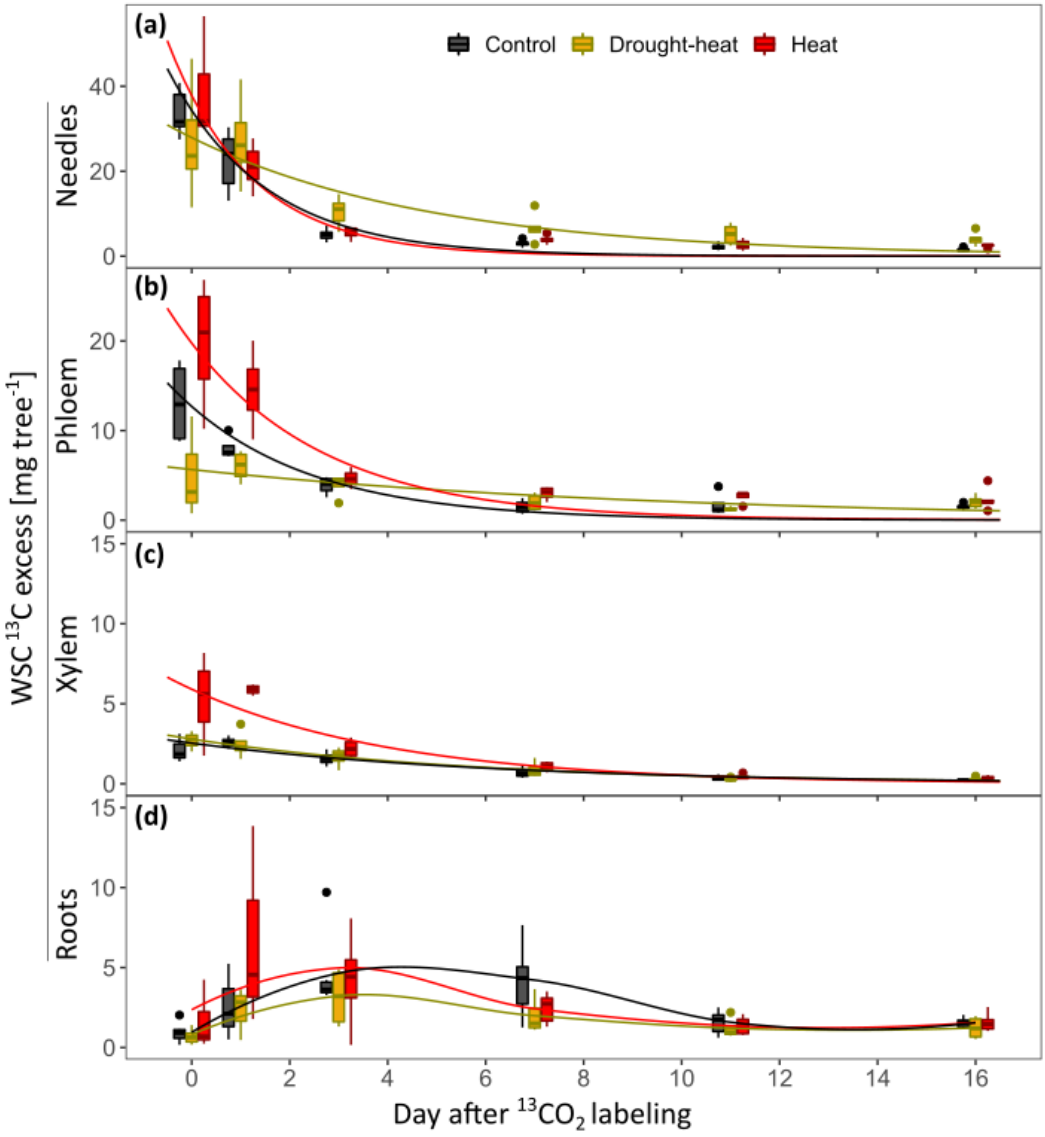

Fig. S5: Treatment-specific dynamics in ^{13}C excess of water-soluble compounds (WSC) in (a) needles, (b) branch and stem phloem, (c) branch and stem xylem and (d) roots (n=6 per treatment). Seedlings were $^{13}CO_2$ pulse-labeled on day 0. Note that data on day 0 are for 8 h after the start of labeling.

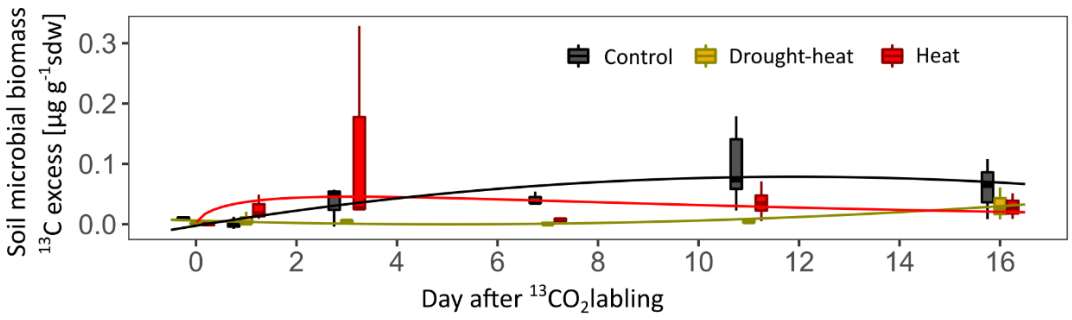

Fig. S6: Dynamics in ^{13}C excess of soil microbial biomass per treatment (n=3). Seedlings were $^{13}CO_2$ pulse-labeled on day 0. Note that data on day 0 are for 8 h after the start of labeling. sdw= soil dry weight.

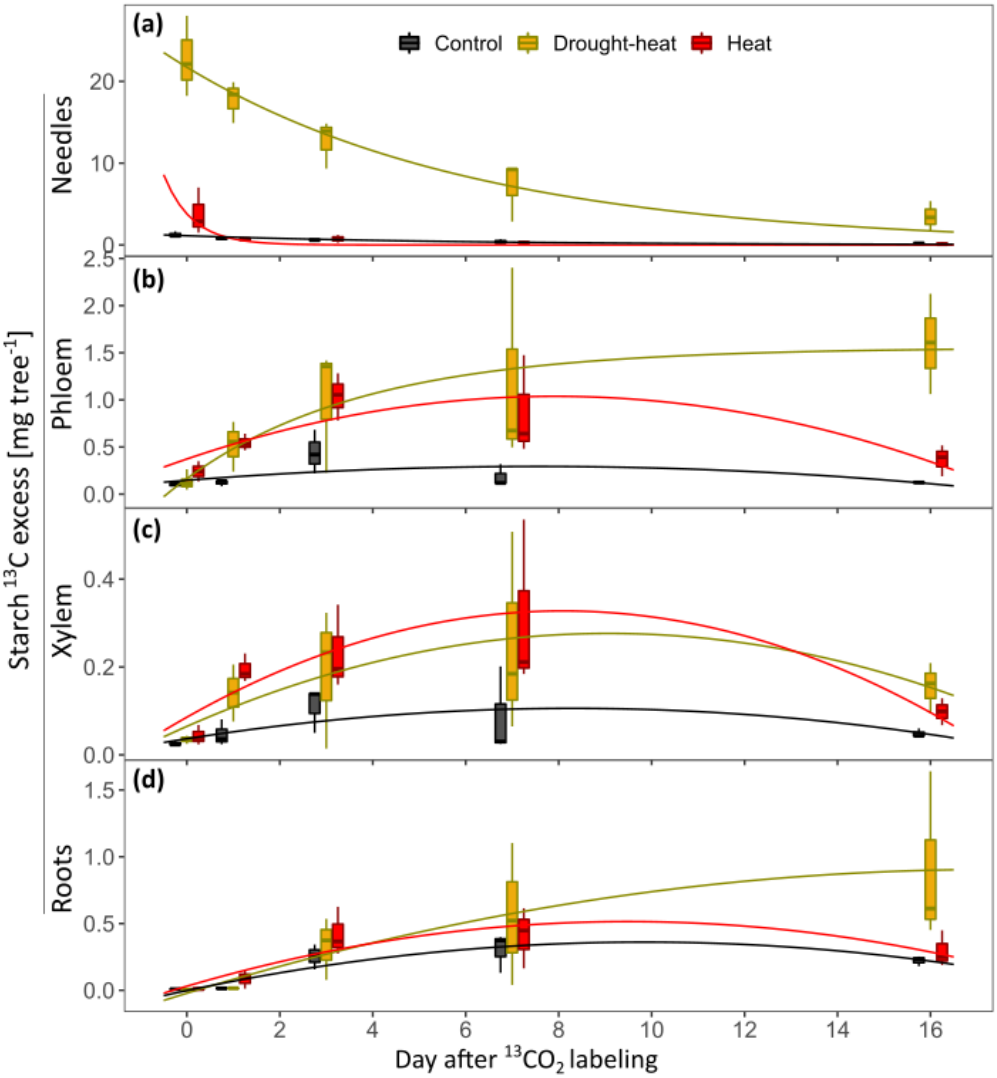

Fig. S7: Treatment-specific dynamics in ^{13}C excess of starch in (a) needles, (b) branch and stem phloem, (c) branch and stem xylem and (d) roots (n=3 per treatment). Seedlings were $^{13}CO_2$ pulse-labeled on day 0. Note that data on day 0 are for 8 h after the start of labeling.

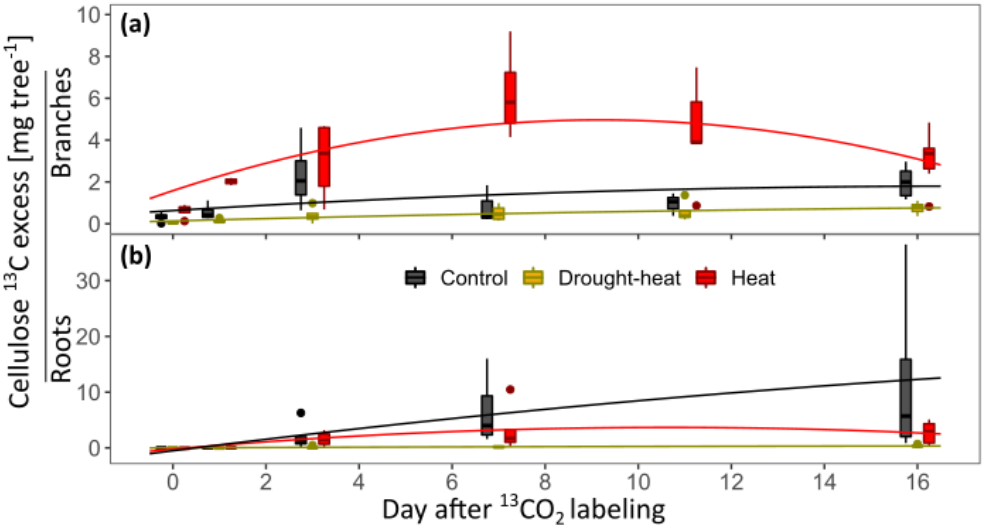

Fig. S8: Treatment-specific dynamics in ^{13}C excess of cellulose in (a) branches and stems, and (b) in roots (n=5-6 per treatment). Seedlings were $^{13}CO_2$ pulse-labeled on day 0. Note that data on day 0 are for 8 h after the start of labeling.

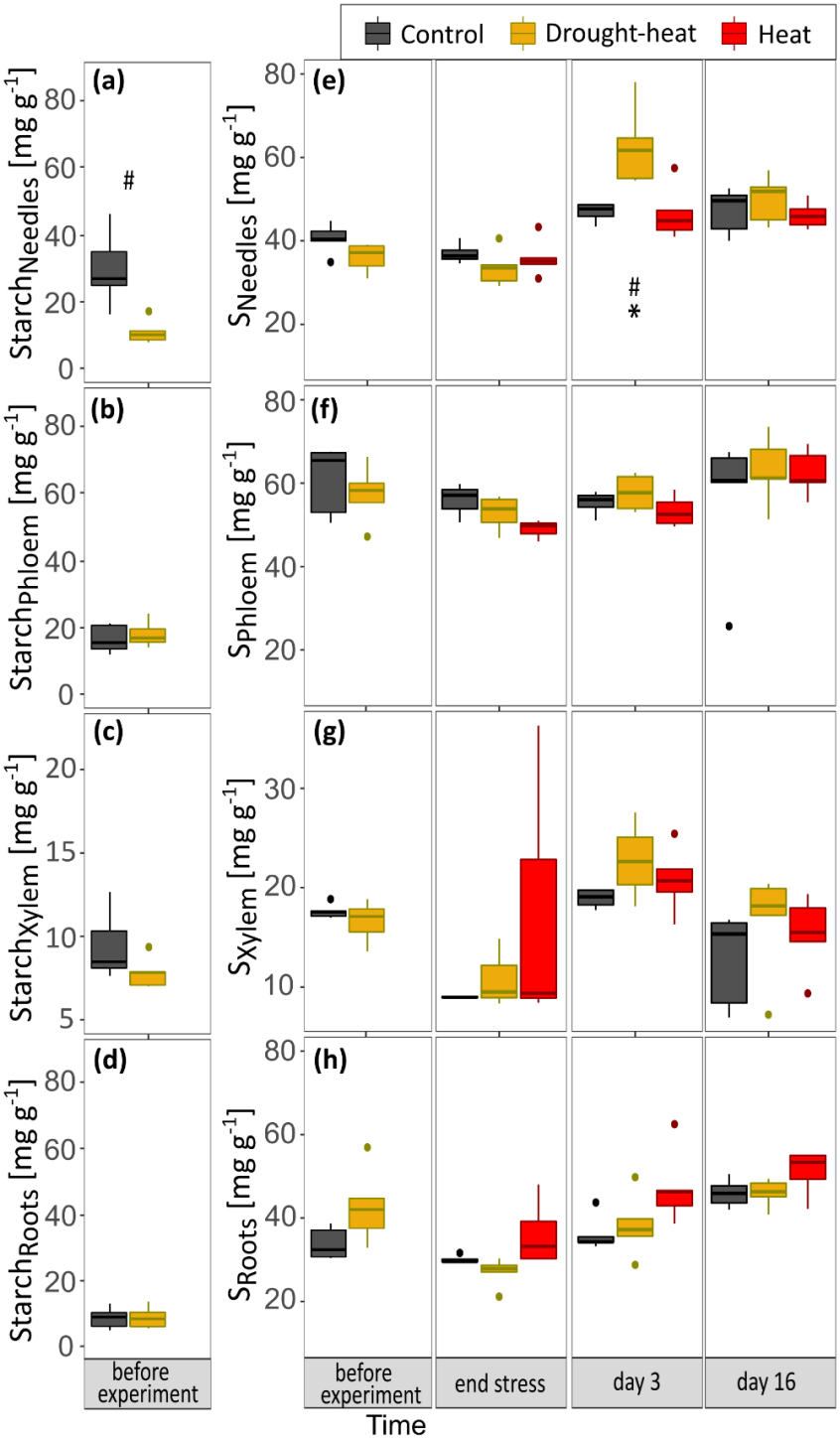

Fig. S9: Treatment- and tissue-specific nonstructural carbohydrate dynamics during stress and recovery (n= 5-6). Starch (a-d) and soluble sugar (e-h) concentrations are shown before the chamber experiment started (before experiment). Soluble sugar concentrations are also shown for the end of stress on day -3 (natural abundance sample taking), on day 3 (5 days after stress release) and at the end of the recovery phase on day 16. Symbols indicate significant differences (P<0.05) between treatments per sampling campaign (Kruskal-Wallis and Bonferroni post-hoc test) as follows: drought-heat vs. control (#), and drought-heat vs. heat (∗). S= Soluble sugars.

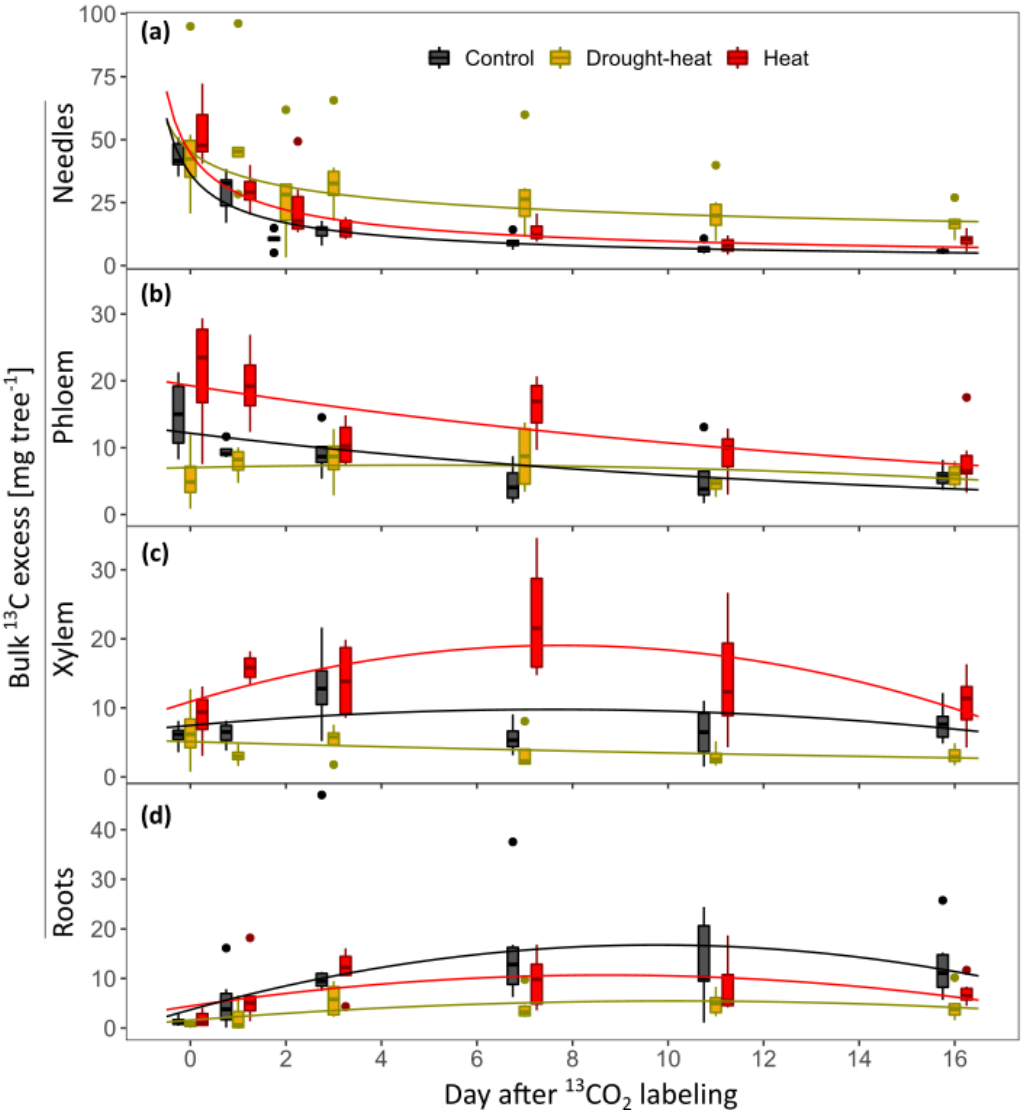

Fig. S10: Treatment-specific dynamics in ^{13}C excess of bulk material in (a) needles, (b) branch and stem phloem, (c) branch and stem xylem and (d) roots (n=6 per treatment). Seedlings were $^{13}CO_2$ pulse-labeled on day 0. Note that data on day 0 are for 8 h after the start of labeling.

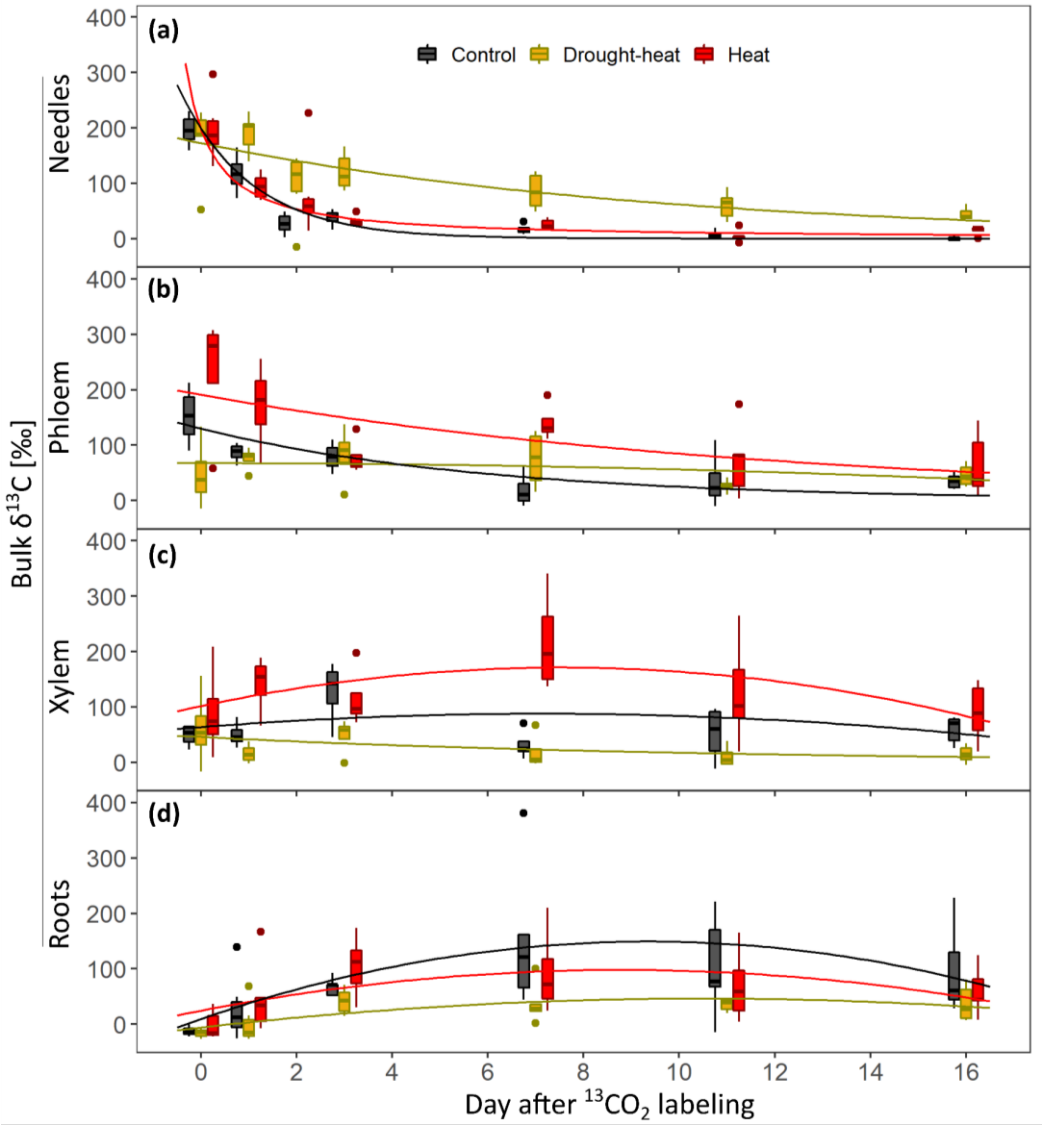

Fig. S11: Treatment-specific dynamics in $\delta^{13}C$ of bulk material in (a) needles, (b) branch phloem, (c) branch xylem and (d) roots (n=6 per treatment). Seedlings were $^{13}CO_2$ pulse-labeled on day 0. Note that data on day 0 are for 8 h after the start of labeling.

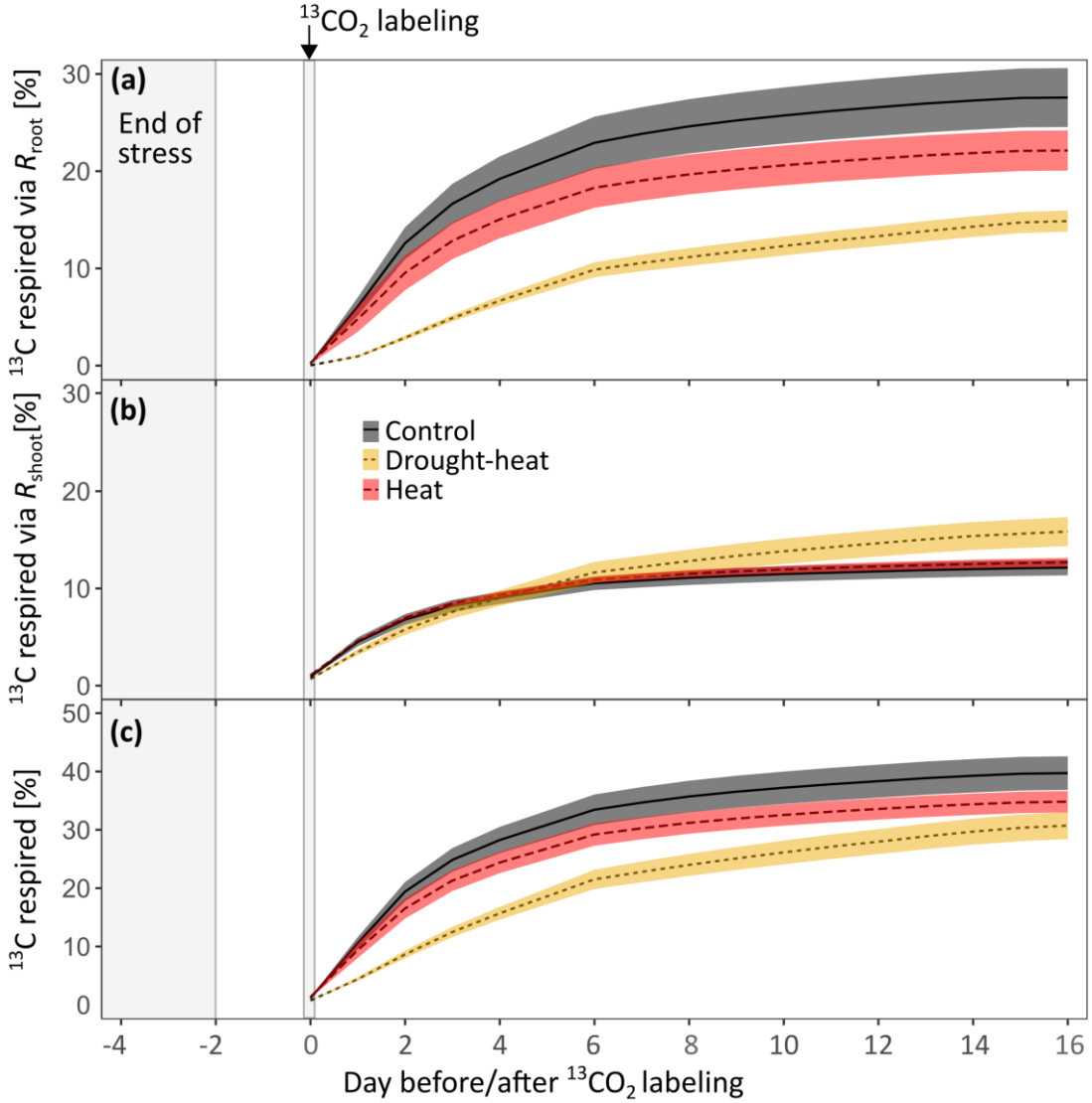

Fig. S12: Cumulative fluxes of respired ^{13}C via (a) root respiration (R_{root}), (b) shoot respiration (R_{shoot}; includes day and night), and (c) total respired ^{13}C via R_{shoot} and R_{root} during the chase period. Data are treatment averages and shaded areas show ±SE (n=6 per treatment). The gray box depicts the end of the stress period and the vertical gray line indicates $^{13}CO_2$ pulse-labeling on day 0 two days after stress release.

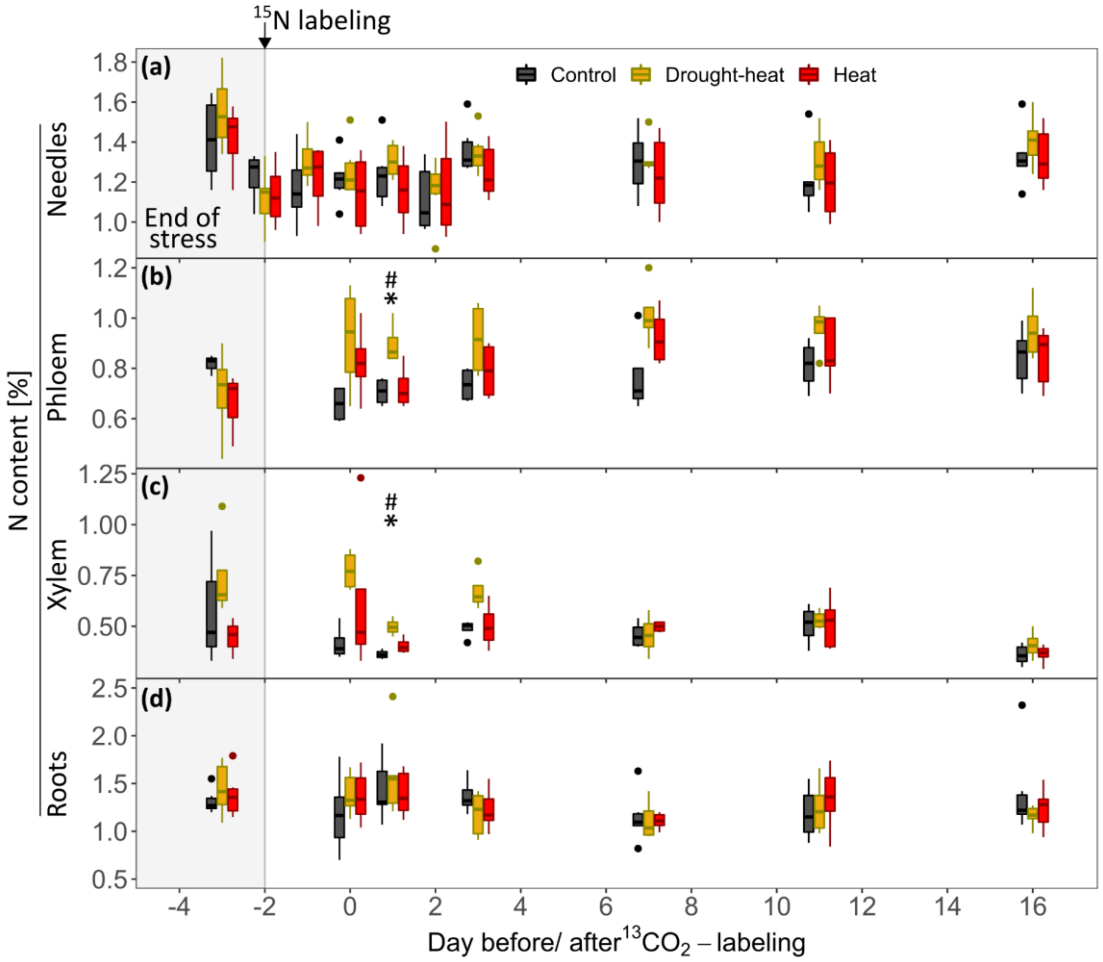

Fig. S13: Dynamics of the nitrogen (N) content in (a) needles, (b) branch phloem, (c) branch xylem and (d) roots for the end of stress and recovery period per treatment (n=6). The ^{15}N label was applied to the soil on day -2 (= 2 days before $^{13}CO_2$ pulse-labeling). Note that natural abundance values on day -3 are also displayed. Symbols indicate significant differences (P<0.05) between treatments per sampling campaign (Kruskal-Wallis and Bonferroni post-hoc test) as follows: drought-heat vs. control (#), and drought-heat vs. heat (∗).

4 Unrevealing water and carbon relations during and after heat and hot drought stress in *Pinus sylvestris*

This chapter has been submitted as pre-print to bioRxiv (2021), and is intended to be submitted to *Tree Physiology* as: Rehschuh, R. [1] and Ruehr, N.K.[1]: Unrevealing water and carbon relations during and after heat and hot drought stress in *Pinus sylvestris.* doi.org/10.1101/2021.06.29.450316

[1] Karlsruhe Institute of Technology KIT, Institute of Meteorology and Climate Research-Atmospheric Environmental Research, Garmisch-Partenkirchen, Germany

Abstract

Forests are increasingly affected by heatwaves, often co-occurring with drought, with consequences for water and carbon (C) cycling. However, our ability to project the resilience of trees to an intensification of hot droughts remains limited. Here, we used single tree cuvettes (n=18) allowing us to investigate transpiration (E), net assimilation (A_{net}), root respiration (R_{root}) and stem diameter change in Scots pine seedlings during gradually intensifying heat or drought-heat stress (max. 42°C), and post-stress. Further, we assessed indicators of stress impacts and recovery capacities.

Under heat stress, well-watered seedlings prevented overheating of leaves effectively via increased E, while under drought-heat leaf temperatures increased to 46°C. However, leaf electrolyte leakage was negligible, but F'_v/F'_m declined alongside A_{net} moderately in heat but strongly in drought-heat seedlings, in which respiration exceeded C uptake. Further, the decrease of needle water potential (Ψ_{Needle}) to -2.7 MPa and relative needle water content (RWC_{Needle}) under drought-heat reflected a decline of leaf hydraulic conductance (K_{Leaf}) by 90% and stem hydraulic conductivity (K_S) by 25%. Alongside, we observed pronounced stem diameter shrinkage.

Heat stress alone resulted in low functional impairment and all measured parameters recovered fast. In contrast, larger impacts following combined heat and drought led to the incomplete recovery of K_{Leaf} and K_S. Despite A_{net} tended to be reduced albeit F'_v/F'_m had recovered, the seedlings' net C balance reached control values 2 d after stress release and stem growth rates exceeded control rates in the 2nd week post-stress. This indicates that a new equilibrium of C uptake and release was maintained at the tree level, slowly supporting regaining of stress-induced losses.

In summary, we highlight that under moderate heatwaves with low functional impairment, recovery is fast in Scots pine, while in combination with drought hydraulic and thermal stress are intensified, resulting in functional damage and delayed recovery processes. The

incomplete recovery of hydraulic conductance indicates limited water transport capacities that could become critical under repeated heat events.

Keywords: electrolyte leakage, heat and drought stress, leaf hydraulic conductance, photosynthesis, root respiration, recovery, Scots pine, stem hydraulic conductivity, transpiration

4.1 Introduction

In the past two decades, extreme summer heatwaves and drought periods, combined with high vapor pressure deficit (VPD; Grossiord et al., 2020), have been increasing in Central Europe (Ciais et al., 2005; Ionita et al., 2017; IPCC, 2018). This has increased the pressure on forests, thus reducing primary productivity and enhancing hydraulic constraints, which might lead to decreased vitality and/or tree death in the long-term (Anderegg et al., 2019; McDowell et al., 2020; Schuldt et al., 2020; Arend et al., 2021). Global climate change is forecasted to continue and includes -besides the ecological aspect- the decline of economically important tree species (Hanewinkel et al., 2013) such as Scots pine (*Pinus sylvestris* L.). Although considered a rather drought-resistant species in Central Europe (Ellenberg and Leuschner, 2010), heat waves and drought spells are increasingly limiting its survival, causing c. 40% of the European forest mortality events (Allen et al., 2010).

Studies on the resistance of conifers to thermal stress are limited (Escandón et al., 2016). Further, few experimental studies have focused on the responses of trees to a combination of heat and drought stress (e.g. Zhao et al., 2013; Bauweraerts et al., 2013, 2014; Birami et al., 2020; Kumarathunge et al., 2020), and even less have addressed subsequent recovery trajectories (Ruehr et al., 2016, 2019; Birami et al., 2018). In general, our understanding of tree physiological recovery from combined heat waves and drought stress is very limited (Ruehr et al., 2019), thus hindering our ability of forecasting tree responses to climatic extremes. Recently, Ruehr et al. (2019) suggested that recovery trajectories depend on stress impact, indicating that physiological recovery will be slower if stress causes functional impairment and/or damage. Hence, to understand recovery trajectories, the physiological stress impacts need to be quantified properly.

High temperatures affect the water and carbon (C) relations of trees. C uptake via photosynthesis is closely linked to stomatal conductance (g_s) and water loss via transpiration (E). During heat, increasing E can cool leaves if soil water is not limiting, while stomata have been found to remain at least partially open (Urban et al., 2017b; De Kauwe et al., 2018; Drake et al., 2018). Drought stress, however, exacerbates during heat waves as the evaporative demand increases, forcing water loss from trees. Drought-induced stomatal closure typically delays the decrease of tree-internal water potentials to critical values, but impedes transpirational leaf cooling, thus leading to higher leaf temperatures (Scherrer et al., 2011;

Birami et al., 2018; Drake et al., 2018). As a result of high temperatures, photosynthetic processes might be affected by decreased activity of Rubisco activase and photosystem II (PSII), reduced CO_2 solubility, and inhibited electron transport (Schrader et al., 2004; Smith and Stitt, 2007; Sage et al., 2008; von Caemmerer and Evans, 2015; Birami et al., 2018). Excessive leaf temperatures may further lead to cell membrane damages in leaves, typically observed via electrolyte leakage (Saelim and Zwiazek, 2000; Correia et al., 2013; Escandón et al., 2016). This often involves the buildup of reactive oxygen species (Demidchik et al., 2014; Larkindale and Knight, 2002), which have been shown to even further impair cell membranes and proteins (O'Kane et al., 1996). The impairment of extra-xylary leave tissues, resulting in leaf hydraulic conductance (K_{Leaf}) decline, has been found manifold in response to drought, with leaf xylem embolism formation at higher levels of dehydration (e.g. Cochard et al., 2004; Brodribb and Cochard, 2009; Johnson et al., 2009; Skelton et al., 2017). Less information on hydraulic responses to high temperature stress exist and responses of K_{Leaf} range from no effect to extreme heat stress (Drake et al., 2018) to increases under modest temperature increments related to changes in the viscosity of water and the symplastic conductance (Sellin and Kupper, 2007; Way et al., 2013).

Besides direct impacts of high temperature and drought on assimilation (A_{net}), also respiratory processes are affected (Gauthier et al., 2014; Birami et al., 2020). Root respiration (R_{root}) provides energy for maintenance and growth, necessary for root water and ion uptake (Atkin et al., 2000a). However, under heat and hot drought, R_{root} has been found to decline, with reduced C availability being one of the reasons (Birami et al., 2020). Yet, C is also necessary to sustain aboveground growth. So far, the knowledge of growth processes in response to heat waves remains elusive, and should be evaluated in combination with water limitation (Ruehr et al., 2016). Under both, heat and drought-heat, stem diameter has been shown to level off or decrease, with larger effects occurring under water limitation (Bauweraerts et al., 2014; Ruehr et al., 2016). Large proportions (>90%) of stem diameter fluctuations result from swelling or shrinkage of the elastic bark, indicating tree water deficits (Zweifel et al., 2000; Zweifel and Häsler, 2000). The tree water status in combination with gas exchange measurements could reveal important evidence on tree physiological mechanisms and processes.

In addition to evaluating stress effects, information about recovery dynamics are crucial for estimating the resilience of trees and forests to climatic change in order to adapt long-term forest management. Stress impacts may leave physiological functions impaired for weeks and even years post-stress (Ruehr et al., 2019; Rehschuh et al., 2020; Schuldt et al., 2020). Depending on stress severity (Ruehr et al., 2019), this includes the persistent reduction of gas exchange (Duarte et al., 2016; Ruehr et al., 2016; Birami et al., 2018; Rehschuh et al., 2020), often associated with the impairment of the photosynthetic apparatus (Ameye et al., 2012; Birami et al., 2018) or the lack/only partial recovery of the hydraulic system (Brodribb et al.,

2010; Rehschuh et al., 2020). Further, stem increment rates have been shown to remain low (Anderegg et al., 2015b; Rehschuh et al., 2017), particularly due to the reduction of leaf area and C reserves during stress (Galiano et al., 2011). Therefore, the rapid recovery of net C gain plays an important role during recovery, as it provides energy and C skeletons for repair and regrowth processes.

Here we tested the impacts of a heatwave on the hydraulic and metabolic recovery of well-watered and drought-treated *Pinus sylvestris* seedlings. For this, seedlings were placed in individual gas exchange chambers and exposed to a heat and a hot drought scenario, followed by a recovery period, while continuously measuring above- and belowground CO_2 and H_2O gas exchange, and stem diameter change. Our objectives were to quantify the dynamics of (1) water relations during heat stress, in particular the cooling capacity of transpiration, (2) leaf temperature stress impact and recovery of leaf and branch hydraulic parameters, and (3) the interplay of hydraulic processes with carbon relations, and the effect on stem diameter change. We further investigated parameters related to functional integrity of leaves such as the maximum light-adapted quantum yield of the photosystem II (F'_v/F'_m) and electrolyte leakage. To provide a complete picture of carbon and water relations, we analyzed the diurnal dynamics within several temperature regimes, as well as the initial and final recovery phase of the experiment. The following hypotheses were tested:

1) Low transpiration rates during heat waves result in higher thermal stress leading to tissue damage.

2) Metabolic and hydraulic recovery will be fast if stress does not result in functional impairment and/or damage.

3) Stress-induced reductions of hydraulic properties will be directly linked to the recovery of the tree C balance and stem growth.

4.2 Material and Methods

4.2.1 Plant material and growth conditions

3-year-old *Pinus sylvestris* seedlings originating from a tree nursery in Middle Franconia (provenance 85115), Germany, were potted in round pots (18 cm in height, 22 cm in diameter) in March 2018. To assess the whole-tree C balance (net C uptake = net photosynthesis-respiration) we used a C-free potting substrate, i.e. a mixture of fine quartz sand (0.1-1.2 mm), medium-grained sand (1-2.5 mm), gravel (3-5.6 mm) and vermiculite in a relation of 2:2:1:2. The substrate was enriched with 12 g of slow-release fertilizer (Osmocote® Exact Standard 5-6M fertilizer 15-9-12+2MgO+TE, ICL Specialty Fertilizers, The Netherlands) per pot and liquid fertilizer (Compo® Complete, 6+4+6(+2) NPK(MgO), Hornbach, Germany) added monthly during the growing season. During the entire adjustment and experimental period, seedlings

were kept in a scientific greenhouse facility in Garmisch-Partenkirchen, Germany (708 m asl, 47°28′32.9″N, 11°3′44.2″E) with highly UV-transmissive glass. Additionally, growth lamps (T-agro 400W, Philips, Hamburg, Germany) were used to supplement outside light. Photosynthetic active radiation (PAR) inside the greenhouse was measured continuously (PQS 1, Kipp & Zonen, Delft, The Netherlands), reaching daytime averages of 350 to 550 µmol m^{-2} s^{-1} (16 h daylight length).

Seedlings were randomly assigned to a well-watered control, a well-watered heat and a combined drought-heat treatment, in which we assessed stress and recovery trajectories. After needle elongation was completed (August 02, 2018), seedlings assigned to the drought-heat treatment were subjected to a 1.5-month drought period, keeping the soil water content (SWC) close to 10% (EC5, Meter Group, USA) before heat stress was initiated. SWC was adjusted automatically by a drip irrigation system (Rain Bird, Azusa, CA, USA), and was close to field capacity at 22% in the control treatment. Throughout the pre-drought period, air temperature and relative humidity (RH; CS215, Campbell Scientific, Logan, UT) were maintained constant (CC600, RAM Regel- und Messtechnische Apparate GmbH, Herrsching, Germany) between well-watered and drought treated seedlings (daytime: temp.: 22.95±0.07 °C; RH: 71.6±0.5%; nighttime: temp.: 17.36±0.02°C; RH: 81.8±0.8%).

On September 18, 2018, we started the experiment in the gas exchange chambers. Seedlings used for the control, heat and drought-heat treatment were on average 57.3±1.8 cm (±SE), 57.5±1.9 cm and 58.1±3.6 cm in height, and had a stem diameter of 16.4±0.6 cm, 15.9±0.5 cm and 14.9±0.4 cm, respectively. To realistically adjust the environmental conditions in the stress treatments to extreme heat events, we analyzed daily and hourly data (air temperature, RH, VPD) from the *German Meteorological Service* of climatically extreme years in Weißenburg-Emetzheim, Franconia, Germany (435 m a.s.l., N49° 1′ 38,28″ E10° 58′ 55,2″). Around this area, Scots pine dieback had been observed after the hot dry summer in 2015 (Gößwein et al., 2017; Walentowski et al., 2017). As we found the period from August 07- 13, 2003 to reveal the most intense climate extremes, we analyzed diurnal hourly averages for this period (Fig. S1) to base the climatic conditions in the tree chambers on these data. We stepwise increased the air temperature in the stress treatments over 20 days (30°C, 33°C, 35°C, 38°C and 40/41°C period) after acclimating the seedlings in the tree chambers for 5 d at 26°C, with VPD increasing concurrently to max. 6 kPa in the drought-heat treatment, but remaining lower (max. c. 4 kPa) in the heat treatment due to larger transpiration rates and thus higher humidity (Fig. 1a-b, Fig. 2a). Air temperatures were maintained at the targeted maximum values for min. 6 h per day. Soil temperature increased with a timely offset to air temperature, and also increased slightly in the control treatment, because soil compartments could only be cooled passively (Fig. 1c). During night time, air and soil temperatures decreased to c. 15-20°C in all treatments.

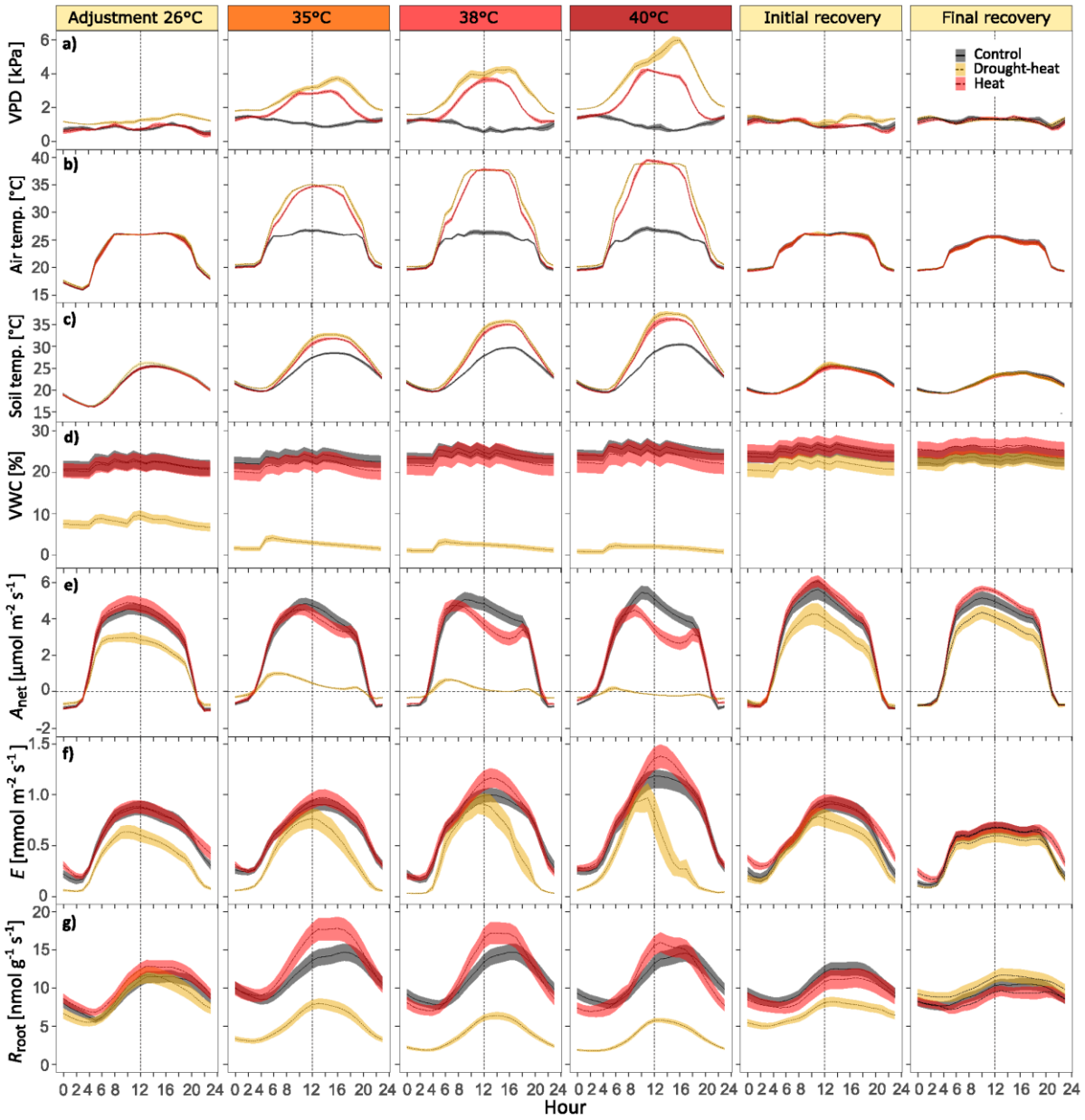

Fig. 1: Diurnal dynamics of treatment-averaged hourly a) vapor pressure deficit (VPD), b) air temperature c) soil temperature, d) soil volumetric water content (VWC), e) net assimilation (A_{net}), f) transpiration (E), and g) root respiration (R_{root}) for different periods. Before heat stress, during adjustment (26°C, 4 days), temperature increments (35°C, 7 days; 38°C, 3 days and 40°C, 4 days), the initial (26°C, day 28-30) and final recovery period (26°C, day 40-42). Daytime length was 16 h (4:30 – 20:30 CET). Shown are treatment averages and shaded areas are ±SE (n = 6 per treatment).

The conditions in the control treatment were adjusted according to August 30-year-averages (1986-2016) in Weißenburg-Emetzheim, and maintaining SWC close to field capacity by watering 4x daily c. 75 ml, respectively (Fig. 1d). A similar SWC was achieved in the heat treatment, while the amount had to be increased slightly due to higher transpiration rates. In the drought-heat treatment, seedlings were irrigated 2x daily during acclimation (c. 50 ml, respectively) and only at 5 am during the heat stress period (70 ml), while the water supply was further steadily reduced.

To analyze recovery processes, seedlings were re-watered to field capacity at 5 am on October 13, 2018, and temperature and VPD were down-regulated to control conditions (Fig. 1a-d, Fig. 2a, see initial and final recovery period).

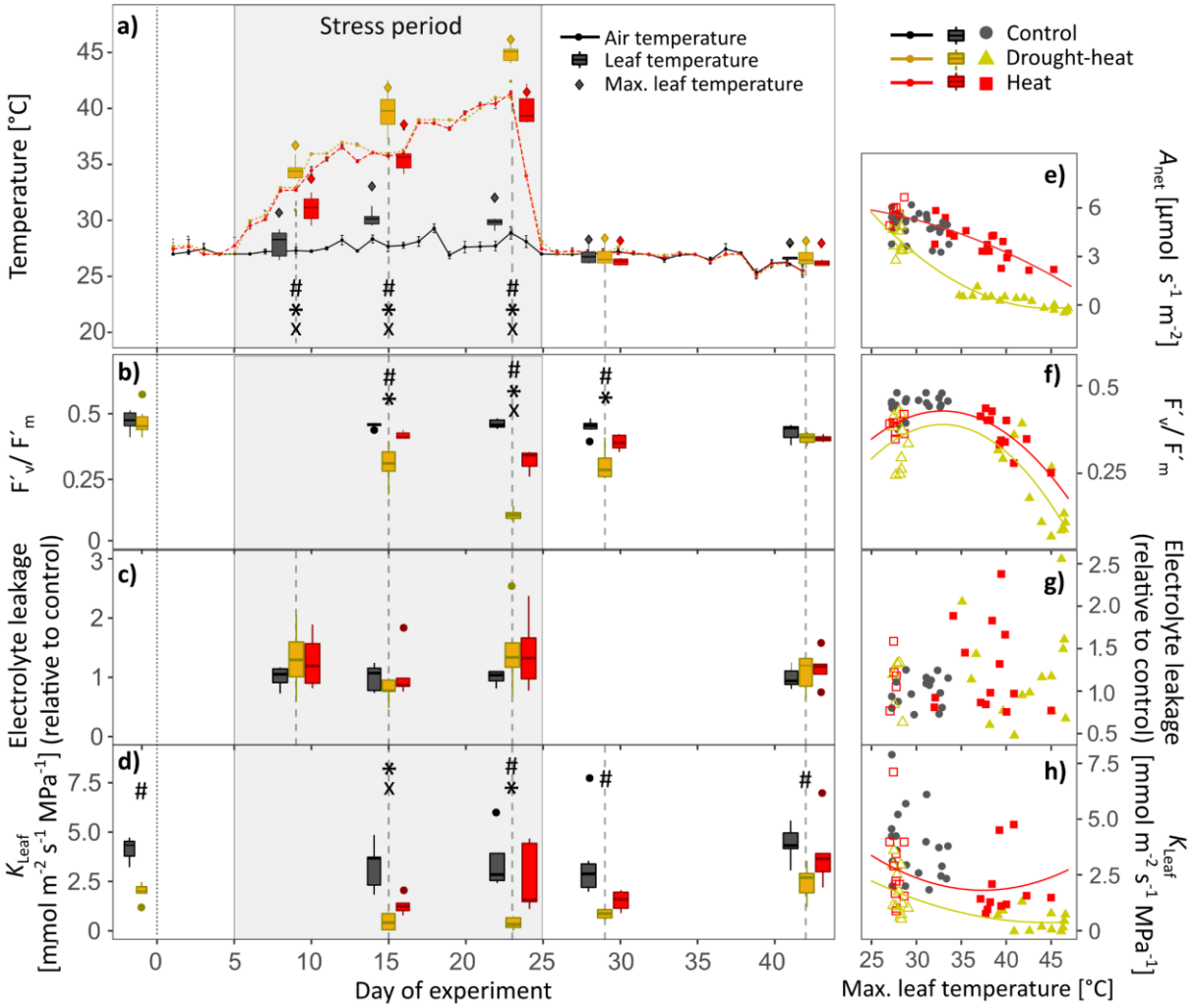

Fig. 2: Dynamics of air and leaf temperature and stress indicators during the experimental phase in Scots pine seedlings. Shown are a) air temperature, mean and maximum leaf temperature, b) maximum light adapted quantum yield of photosystem II ($F´_v/F´_m$), c) electrolyte leakage and d) leaf hydraulic conductance (K_{Leaf}) during stress progression and recovery (n = 5-6 per treatment). In e-h) the relationships of A_{net}, $F´_v/F´_m$, electrolyte leakage and K_{Leaf} with maximum leaf temperature during stress and recovery are shown per seedling and treatment. The gray boxes represent the stress period. Symbols indicate significant differences (P<0.05) between treatments per sampling campaign (Kruskal-Wallis and Bonferroni post-hoc test) as follows: drought-heat vs. control (#), heat vs. control (x), and drought-heat vs. heat (∗). Note that data before day 0 are for measurements 2 weeks before the chamber experiment started and that drought-heat seedlings were drought pre-stressed for 1.5 months. Open symbols in e-h) indicate measurements during the recovery period. Polynomial curves were fitted for the drought-heat and heat treatment if applicable (for functions see Supplemental Table S1).

4.2.2 Tree gas exchange chambers

For continuous monitoring of above- and belowground gas exchange (H_2O and CO_2) during the drought and heat period and the recovery phase, we randomly selected 12 well-watered (subsequently assigned to n=6 control and n=6 heat treated) and 6 drought pre-treated seedlings (assigned to the drought-heat treatment), and placed them in individual tree chambers within the greenhouse compartment. The tree chambers were divided into a translucent temperature-controlled shoot compartment, which was gas-tightly sealed from an opaque root compartment (for further details on materials and technical operation of the chamber system see Birami et al. 2020 or Chapter 3). Air temperature was predefined for the different treatments and days and regulated within each shoot compartment separately by fast-response thermocouples (5SC-TTTI-36-2M, Newport Electronics GmbH, Deckenpfronn, Germany) and based on a water-cooling principle. PAR was recorded per chamber by photodiodes (G1118, Hamamatsu Photonics, Hamamatsu, Japan), calibrated in advance with a PAR sensor (PQS 1, Kipp & Zonen, Delft, the Netherlands). Soil temperature and moisture were continuously logged (TS 107, Campbell Scientific, Inc. USA and EC 5, Meter Group, USA, respectively), and data recorded in 10 min intervals (CR1000, Campbell Scientific, Inc. USA). In addition, stem diameter change was measured half-hourly by dendrometers (DD-S, Ecomatik, Dachau, Germany), attached to each stem at approximately 5-10 cm above the soil surface.

4.2.3 Gas exchange measurements and calculations

Above- and belowground chamber compartments were constantly supplied with air (Air_{supply}) from an oil-free screw compressor by adding a pre-defined CO_2 (c. 430 ppm) and H_2O concentration (8 mmol during the adjustment and recovery period; 4 mmol during the stress period). Each of the 20 shoot and root compartments received c. 13 L min^{-1} and 3 L min^{-1} of air flow, respectively.

Firstly, absolute [CO_2] and [H_2O] of Air_{supply} and sample air (Air_{sample}) were quantified by a gas analyzer (Li-840, LI-COR, Lincoln, NE, USA). Subsequently, a differential gas analyzer determined the differences between Air_{supply} and Air_{sample} (Li-7000, LI-COR, Lincoln, USA). We used two empty tree chambers (no trees but pots with the same potting substrate) to correct for fluctuations in [CO_2] and [H_2O] not caused by plant gas exchange. Subsequently, offsets were removed from the data. Every compartment was measured once every 2 h for c. 80 sec, while data was logged every 10 sec. The following equations were used to calculate gas exchange fluxes: Transpirational loss of H_2O (E) in mol m^{-2} s^{-1} was calculated as follows:

$$E = \frac{\dot{m}\,(W_{\text{sample}} - W_{\text{supply}})}{area_{needle}\,(1 - W_{\text{sample}})} \quad (1),$$

where ṁ is air mass flow (mol s^{-1}), W_{supply} is [H_2O] in Air_{supply}, and W_{sample} is [H_2O] in Air_{sample}. $Area_{needle}$ is the total needle area of the shoot in m^2.

Stomatal conductance g_s in mmol m^{-2} s^{-1} was calculated accordingly:

$$g_s = \frac{E\left(1000 - \frac{W_{needle}+W_{sample}}{2}\right)}{W_{needle}-W_{sample}} \quad (2),$$

where W_{needle} is the needle H_2O vapor concentration, which was deduced from saturated vapor pressure (kPa) at the prevailing air temperature (°C) and atmospheric pressure p (kPa). This method of determining g_s assumes well mixed air within the shoot compartment and therefore, neglects the boundary layer conductance.

Net assimilation (A_{net}) and soot respiration (R_{shoot}) in µmol m^{-2} s^{-1} and root respiration (R_{root}) in µmol s^{-1} g^{-1} DW (dry weight) were calculated by the equation for CO_2 fluxes:

$$CO_2 \text{ flux} = (-\ \dot{m} \cdot \Delta C) - (E \cdot C_{sample}) \quad (3),$$

where ΔC is the difference between [CO_2] of Air_{supply} and Air_{sample}, C_{sample} is [CO_2] of Air_{sample}. E was included to correct for dilution by transpiration. Further, A_{net} was related to total needle area, and R_{root} to g DW of total root biomass. Whole-tree daily net C uptake (in mg C d^{-1} $tree^{-1}$) was then calculated from daily sums (calculated by summing up hourly means) by subtracting daily C loss (R_{root} and R_{shoot}) from daily C uptake via assimilation:

$$\text{Net C uptake} = C_{uptake} - (R_{shoot} + R_{root}) \quad (4).$$

4.2.4 Leaf temperature

To assess temperature and indirect drought effects, we measured leaf temperature (n=6 per treatment) between 1 and 2 pm using an infrared camera (PI 450, Optris, Germany). Leaf temperature was evaluated about weekly during the stress period, and two times during the recovery phase (initial and final recovery). Mean and maximum leaf temperatures were determined from images using the manufacturer's software. For this, we corrected for background radiation using air temperature during measurements and set emissivity to 0.97.

4.2.5 F'_v/F'_m

We measured maximum light adapted quantum yield of photosystem II (F'_v/F'_m) using a portable leaf-gas exchange system (Li-6400, LI-COR Inc., Lincoln, NE, USA), supplemented with a fluorescence head (6400-40 Leaf Chamber Fluorometer). Measurements (n=6 per treatment) were conducted between 9 am and 1 pm about 2 weeks before placing the seedlings in the tree chambers (only drought stress), during drought and/or heat stress and during the recovery phase, coordinated with leaf temperature measurements. For this, we clamped needles into the leaf cuvette, covering it completely (2 cm^2), but avoiding overlapping

of needles as much as possible. We used predetermined saturated light conditions of 1200 µmol m^{-2} s^{-1} PPFD and a reference [CO_2] of 400 ppm. Leaf temperature, RH and VPD were kept constant during measurements, and averaged 26°C, 52% and 1.5 kPa in the control and 29°C, 37% and 3 kPa in the heat and drought-heat treatment.

4.2.6 Electrolyte Leakage

To assess cell membrane stability, we quantified electrolyte leakage of needles following Mena-Petite et al. (2003). Sampling of 10 needle fascicles on 5 seedlings per treatment was done in coordination with leaf temperature measurements, between 10 and 12 am. The samples were immediately wrapped in moist paper towels and subsequently washed in a petri dish filled with deionized water to remove solutes from needle surfaces. Excess water was removed and needles were cut into segments of c. 1 cm length, excluding the needle sheath. The needle segments were weighed and transferred to falcon tubes (Isolab, Laborgeräte GmbH, Eschau, Germany) with 20 ml of distilled water of known electrical conductivity (EC_{dist}). Electrical conductivity was determined with a conductivity electrode (1480–90 Cole-Palmer Instruments; Chicago, I., USA). Subsequently, falcon tubes were placed inside a desiccator. To facilitate electrolyte leakage, a vacuum was created by withdrawing air. Samples were kept in the dark for 24 h at room temperature. Then, samples were shaken and EC_{final} was measured. Subsequently, samples were heated to 100°C for 10 min to destroy all living cells and maximize leakage. After samples were cooled to room temperature, EC_{total} was determined. 24 h- electrolyte leakage was then calculated as follows:

$$\mathrm{EC} = \frac{\mathrm{EC_{final}} - \mathrm{EC_{dist}}}{\mathrm{EC_{total}} - \mathrm{EC_{dist}}} \cdot 100 \quad (5),$$

which was then related to needle weight and expressed relative to control seedlings.

4.2.7 Leaf hydraulic conductance (K_{Leaf})

K_{Leaf} was measured between 10 and 12 am on 5-6 seedlings per treatment, coordinated with F'_v/F'_m measurements. We adjusted the evaporative flux method used by Sack and Scoffoni (2012) to measure single needles of seedlings as follows. Needle fascicles were detached from branches under water and placed with their base in Eppendorf tubes filled with distilled and filtered water (0.22 µm pore size). After an adjustment time of c. 20 min in ventilated air to enhance *E* under constant light conditions (800-1000 µmol m^{-2} s^{-1} PAR), *E* of a single needle fascicle was measured using a portable leaf-gas exchange system (Li-6400, LI-COR Inc., Lincoln, NE, USA) equipped with a light source (6400-40 Leaf Chamber Fluorometer) under saturated light conditions of 1200 µmol m^{-2} s^{-1} PAR and [CO_2] of 400 ppm until stable conditions were reached. Temperature and RH during acclimation and measurement corresponded to conditions inside the tree chambers per treatment and measurement time

point. After measuring *E*, the same needle fascicles were placed in nontransparent plastic bags to equilibrate for 20 min whereupon Ψ_{Needle} was determined using a Scholander pressure chamber (Model 1000, PMS Instruments, Albany, Oregon, USA). The projected needle area (A_{Leaf}) of the enclosed needle segments was determined using a leaf area meter (Li-3100, LI-COR Inc., Lincoln, Nebraska, USA). K_{Leaf} in mmol m^{-2} s^{-1} MPa^{-1} was then calculated as follows:

$$K_{\mathrm{Leaf}} = \frac{E}{\Psi_{\mathrm{Needle}} \cdot A_{\mathrm{Leaf}}} \quad (6).$$

4.2.8 Needle water potential (Ψ_{Needle}) and relative needle water content (RWC_{Needle})

To assess tree water status, we measured predawn and midday Ψ_{Needle} of mature needles of 6 seedlings per treatment using a Scholander pressure chamber (Model 1000, PMS Instruments, Albany, Oregon, USA). We report daily minimum Ψ_{Needle} since predawn Ψ_{Needle} was measured before the automatic irrigation and hence sometimes slightly lower than midday Ψ_{Needle}. Measurements of Ψ_{Needle} were coordinated with RWC_{Needle} measurements. For this, we sampled two needle fascicles per seedling (n=6 per treatment), placed them in a plastic bag to avoid evaporation and immediately determined fresh weight (W_{fresh}). After soaking them in purified water at room temperature for 48 h (as predetermined from saturation curves), turgid weight (W_{turgid}) was measured, then needles placed in an oven at 70°C for 48 h, and consequently dry weight (W_{dw}) determined. RWC_{Needle} was calculated as follows:

$$\mathrm{RWC}_{\mathrm{Needle}}\ (\%) = 100 \cdot \frac{W_{\mathrm{fresh}} - W_{\mathrm{dw}}}{W_{\mathrm{turgid}} - W_{\mathrm{dw}}} \quad (7).$$

4.2.9 Biomass and needle area

We sampled the biomass of the seedlings (n=6 per treatment) at the end of the experiment and took a subsample to determine stem hydraulic conductivity (see below). Biomass was then separated into leaf, root, branch and stem tissues and oven-dried for 48 h at 70°C to determine dry weight (DW).

Leaf area of each tree was derived from leaf biomass and predetermined specific leaf area (gDW cm^{-2}). On a subsample of fresh needles, specific leaf area was measured using an area meter (Li-3100, LI-COR Inc., Lincoln, Nebraska, USA), and its dry mass determined. Total leaf area per tree was then calculated via this leaf area index.

4.2.10 Stem xylem hydraulic conductivity (K_S)

A part of each stem was wrapped in cling film and frozen immediately in plastic bags at -18°C to determine K_S (n=6 per treatment) by applying the pressure-flow method (Sperry and Tyree, 1988), as described more detailed in Rehschuh et al. (2020). In short, frozen samples were

thawed in distilled water, cut back underwater with sharp instruments, and the bark was peeled off. Samples were fixed in a fivefold valve (Luer-lock system; neoLab Migge Laborbedarf-Vertriebs GmbH, Heidelberg, Germany), and exposed to a natural pressure of water flow to determine in-situ degree of embolism. A mass flow meter (mini-CORI-FLOW M13, Bronkhorst, Montigny les Cormeilles, France) served to measure the flow rate of each stem segment individually. By considering the xylem cross-sectional area and sample length, we then determined K_S.

4.2.11 Statistical data analysis

Gas exchange data were quality-checked per chamber, and outliers identified separately for day- and nighttime measurements based on the widely applied boxplot approach. For this, values outside 1.5 times the interquartile range above the upper and below the lower quartile were removed. Between day 32 and 34, daily net C uptake was calculated from linear interpolation due to data unavailability because of technical constraints. For diurnal progression analysis of gas exchange data and depiction of environmental variables, we hourly averaged data from several key experimental periods (adjustment period at 26°C, temperature stages (35°C, 38°C and 40°C), initial stable and final recovery period).

Data processing and statistical analyses were performed in 'R' version 3.6.1 (R Core Team, 2019). Differences between treatments (significant if $P<0.05$) were determined per measurement campaign for discretely measured parameters (e.g. leaf temperature, F'_v/F'_m, K_{Leaf}) by applying the Kruskal-Wallis followed by the Bonferroni post-hoc test, therefore accounting for small sample sizes.

Treatment effects on continuous data (gas exchange measurements, net C uptake) were assessed by applying linear-mixed effects models (lme; lmerTest package; Kuznetsova et al., 2017). Treatment and time period were assigned as fixed effect and chamber as random factor. Time periods included the adjustment period, the different temperature steps, initial and final recovery. For diurnal measurements, we further considered day- and nighttime. We selected the model with the lowest Akaike's information criterion corrected for small sample size (AICc; Burnham and Anderson, 2002), i.e. the most parsimonious model. Further, we used the post-hoc Tukey's multiple comparisons test of means for the determination of differences between treatments (package emmeans; Lenth et al., 2020). Tukey´s HSD is reported here.

Further, we analyzed leaf temperature dependencies of A_{net}, F'_v/F'_m, electrolyte leakage and K_{Leaf}, and relationships of Ψ_{Needle} with gas exchange parameters (A_{net}, net C uptake, E). Additionally, we tested for the relationships of net C uptake with stem diameter change during stress and recovery separately. Where applicable, we fitted polynomial or sigmoidal functions for better visualization of relationships. Fitted curves for stem diameter change in relation to C

uptake during recovery were analyzed for significant differences between treatments by comparing their coefficients.

4.3 Results

Drought stress was initiated after needle growth was completed and no significant differences between treatments in needle biomass and area were found (Fig. S2). However, a modest effect of the prolonged drought became visible as the root:shoot ratio (-25%), root (-23%) and woody biomass (-15%) tended to be lower than in control seedlings.

4.3.1 Tree gas exchange, net C uptake and stem diameter change during stress and recovery

During daytime, increases in air temperature enhanced VPD (Fig. 1a-b). This increase in VPD was larger in the drought-heat treatment due to lower transpiration rates, which reduced the RH inside the tree chambers. Nighttime temperatures, however, did not differ largely between treatments, and were maintained close to 20°C.

The diurnal course of E and A_{net} in drought-treated seedlings remained below the control already before the heatwave was initiated (Tukey's HSD, $P<0.01$, see Table S2 for p-values; Fig. 1e-f). With increasing temperatures and VPD, E in drought-heat seedlings approximated control values during the morning hours, but decreased dramatically in the course of the day, intensified with stress progression (Tukey's HSD, $P<0.05$ for 38°C and $P<0.001$ for 40°C period). In well-watered heat treated seedlings, E increased with a rise in air temperature and VPD, despite declining g_s (Fig. S3). This was reflected in diurnal dynamics of A_{net}, which decreased to about 70% of control values during periods of high air temperature and VPD (Tukey's HSD, $P<0.001$ for 40°C period; Fig. 1a-b) between 10 am and 4 pm, followed by a slight increase later (Fig. 1e). Under the combined drought and heat stress, we found a strong decline in A_{net}, which was reflected in partial or full stomatal closure (Fig. S4), with g_s being lower at the same VPD and air temperature compared to the heat treatment (Fig. S3).

R_{root} largely followed diurnal soil temperature patterns (Fig. 1c,g, Fig. S5). Over the 20-day heat period, R_{root} initially increased under well-watered conditions, but when 40°C prevailed, the difference to control seedlings diminished, indicating some kind of adjustment. In the drought-heat treatment, R_{root} declined with an increase in soil temperatures and was about three times lower than in the control during day- and nighttime throughout the 35°C to 40°C period (Tukey's HSD, $P<0.01$; Fig. 1g).

The daily net C uptake appeared to be moderately sensitive to heat under well-watered conditions, particularly when air temperatures reached >38°C and VPD rose >3 kPa (Fig. 3a, see also Fig. S6 for daily means of A_{net}, R_{shoot} and R_{root} per tree). The effect on the C balance

was more apparent when heat was combined with drought. While net C uptake and stem growth (Fig. 3a-b) continued under heat, net C uptake decreased in drought-heat treated seedlings, resulting in a negative C balance (Tukey's HSD, $P<0.001$ compared to heat and control). This was reflected in stem growth cessation and phloem shrinkage due to water deficits (Fig. 3b).

With stress release on day 25 of continuous gas exchange measurements, we observed a fast response of E and net C uptake (Tukey's HSD, $P>0.1$ for stress treatments compared to control; Table S2). In the heat treatment, net C uptake tended to exceed that of the control seedlings by c. 10%, also reflected in higher daily stem increment rates ($P>0.05$; Fig. 3c). Net C uptake in drought-heat treated seedlings reached control values within 2 days, while A_{net} remained c. 20% below control rates (Tukey's HSD, $P<0.05$ for initial and $P=0.08$ for final recovery period; Fig. 1e). The fast recovery of tree net C uptake can be explained by an initially slow recovery of R_{root} (Tukey's HSD, $P<0.05$ compared to control, Fig. 1g) and a tendency for a lower root:shoot ratio (i.e. R_{root} at the tree level did not fully recover, see Fig. S6). Alongside, stem growth rates exceeded those of the control during the second half of the recovery period largely independent of net C uptake ($P<0.05$; Fig. 3c).

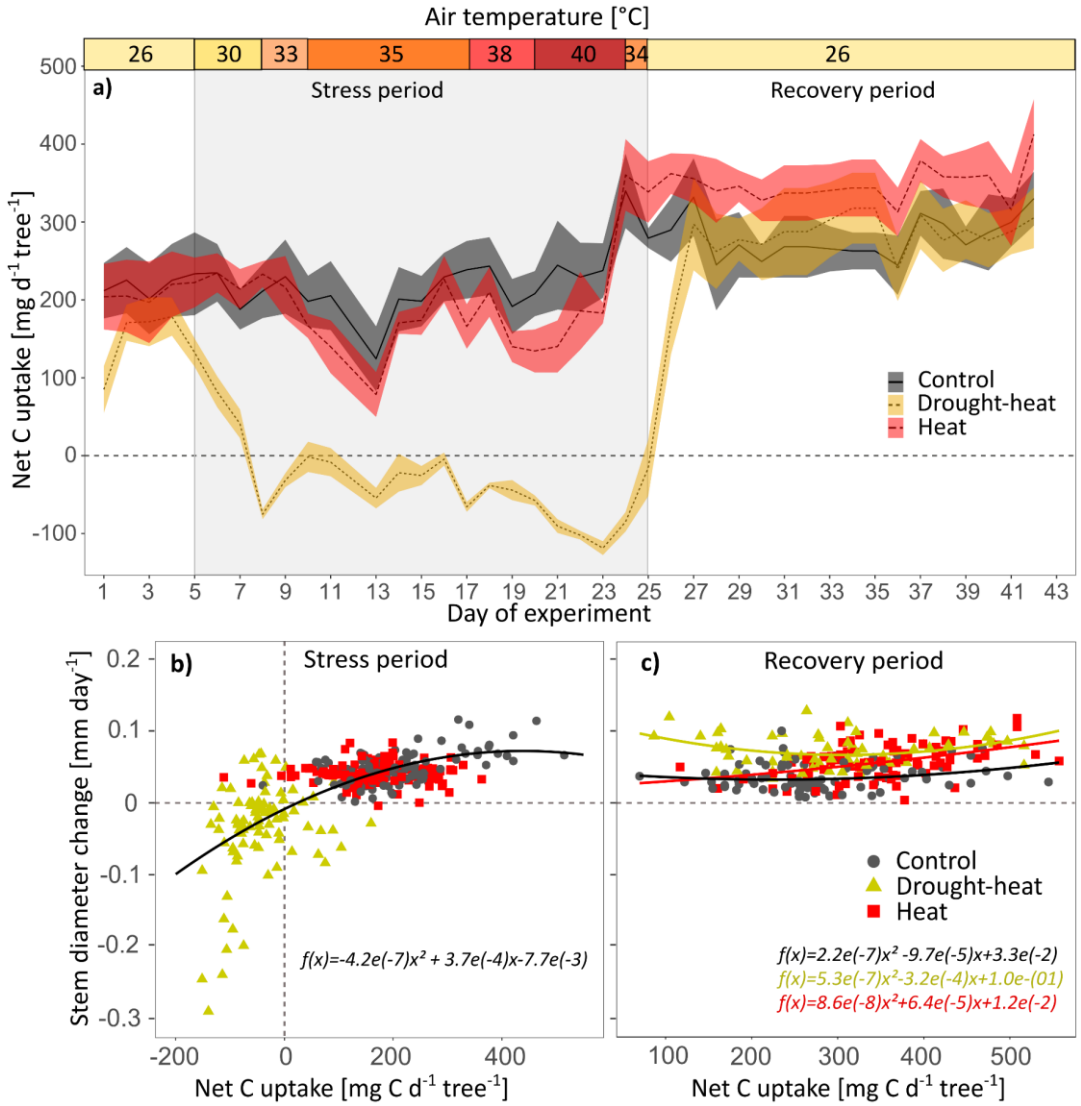

Fig. 3: Daily net carbon (C) uptake of Scots pine seedlings during the entire experiment (a) and in relation to stem diameter change during stress (b) and recovery (c). The daily net C uptake per seedling was derived by summing hourly means of C uptake by photosynthesis minus C release by shoot and root respiration. In a), the shaded areas show ±SE (n = 6). Mean daytime air temperature is given for the stress treatments, while control seedlings were at 26-28°C. In b) and c) diurnal stem diameter changes per seedling and treatment are shown. Negative stem diameter change was caused by stem shrinking due to water deficits. The rehydration period after stress release (6 days) was excluded for the recovery period.

4.3.2 Stress impairment and delayed recovery

Because the degree of evaporative cooling from transpiration differed among treatments, seedlings exposed to combined heat and drought experienced substantially (3-4.5°C) higher leaf temperatures than heat treated well-watered seedlings at the same air temperature (Fig. 2a, Fig. S7). Leaf temperatures were significantly higher compared to the control in both stress treatments, while in well-watered heat treated seedlings evaporative cooling maintained leave temperature below maximum air temperature.

The effect of high leaf temperatures was also apparent in the decline of A_{net} and simultaneous decrease in photosystem II activity (here F'_v/F'_m; Fig. 2e-f). F'_v/F'_m was not affected by the pre-drought, but decreased strongly in response to heat and water limitation within the course of the experiment, reaching 80% lower values than the control ($P<0.05$; Fig. 2b). Heat treated seedlings were less affected, but F'_v/F'_m also decreased by 30% compared to the control ($P<0.05$). These effects were fully reversed within the recovery period in both stress treatments, with a delay in drought-heat seedlings. While the relationship between A_{net} and leaf temperature differed under heat and drought-heat (including recovery), F'_v/F'_m showed a rather similar response pattern to leaf temperature within the two stress treatments (Fig. 2f). In contrast to large stress effects on photosystem II, we found no apparent needle cell damage from heat stress on well-watered and drought-treated seedlings as electrolyte leakage only tended to be increased on day 23 when highest leaf temperatures were reached, but did not differ significantly from the control (Fig. 2c,g).

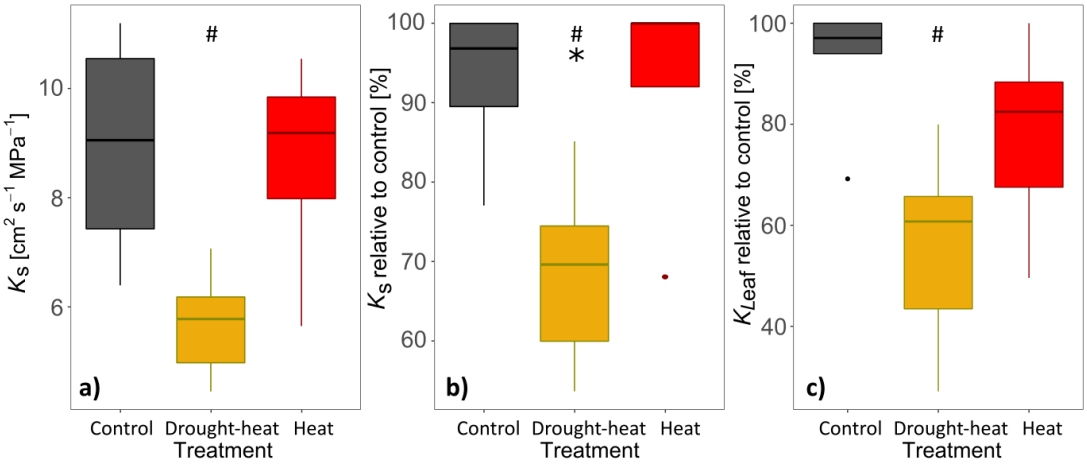

Fig. 4: a) Treatment-specific stem hydraulic conductivity (K_S), b) K_S relative to average control values, and c) leaf hydraulic conductance (K_{Leaf}) relative to average control values measured on the last day of the recovery period, 18 days after re-watering (n=5-6). Symbols indicate significant differences (P<0.05) between drought-heat and control (#), and between drought-heat and heat (∗) (Kruskal-Wallis & Bonferroni post-hoc test).

Further, hydraulic parameters were affected mildly under well-watered conditions, but strongly under water limitation. K_{Leaf} was reduced during the initial drought period, and continued to decline with heat initiation in both stress treatments (Fig. 2d), reaching c. 90% lower values in the drought-heat treatment compared to the control ($P<0.05$). This decline was partially associated with high leaf temperatures (Fig. 2h). While the other stress-related parameters recovered fully, K_{Leaf} did not reach control values in drought-heat treated seedlings until the end of the experiment ($P<0.05$). Similarly, K_S was c. 25% lower post drought-heat compared to the control at the end of the experiment, indicating that K_S did not recover ($P<0.05$, Fig. 4a-b). However, the stress impacts were less apparent than for K_{Leaf} (Fig. 4c).

The combination of drought and heat stress had large impacts on Ψ_{Needle}, which decreased to -2.70±0.13 MPa (P<0.05, Fig. 5a). While heat stress alone did not affect Ψ_{Needle}, RWC_{Needle} declined significantly in the heat treatment compared to the control during the hottest days (Fig 5b). In the drought-heat treatment, the decline in RWC_{Needle} was more pronounced and appeared earlier during the experiment. Ψ_{Needle} and RWC_{Needle} recovered to control values nearly immediately following stress release.

Further, a close relationship of A_{net}, net C uptake and E with Ψ_{Needle} was apparent in the drought-heat treatment (Fig. 6). A_{net} halted or turned negative (i.e. shoot respiration and photorespiration exceeded assimilation) at a Ψ_{Needle} of c. -1.16 MPa, while the tree net C uptake turned negative slightly earlier at a Ψ_{Needle} of c. -1.08 MPa. This indicates the dominant role of tree hydraulic processes in limiting gas exchange rates during hot droughts. The recovery of these gas exchange parameters appeared to largely follow the increase in Ψ_{Needle}, with a tendency of somewhat lower E in previously drought-heat treated seedlings.

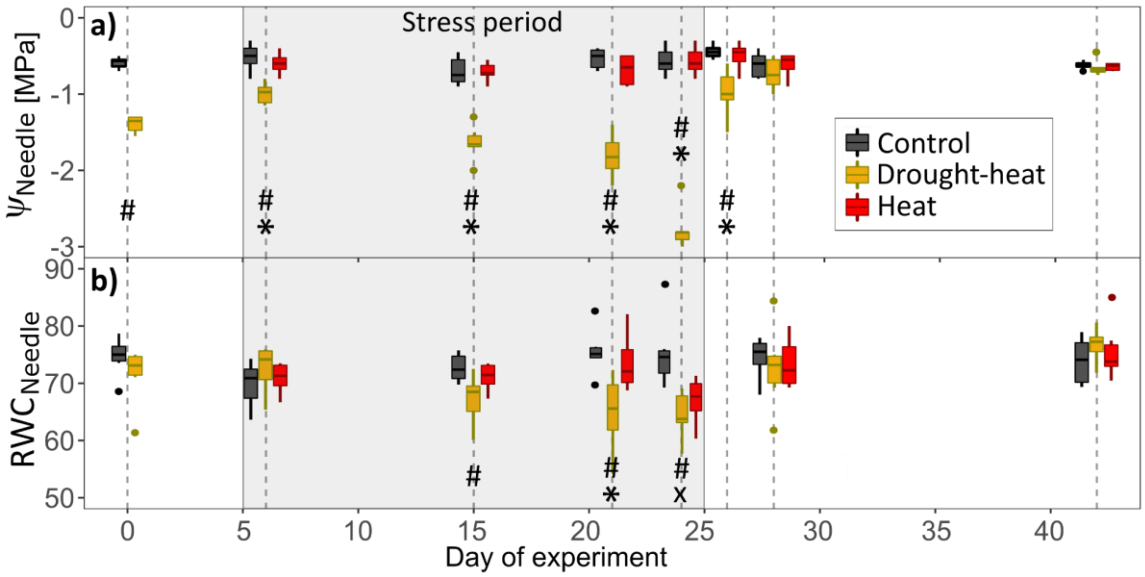

Fig. 5: Treatment-specific dynamics of a) needle water potential (Ψ_{Needle}, n=6) and b) relative needle water content (RWC_{Needle}, n=6) during stress and recovery. The gray boxes represent the stress period. Symbols indicate significant differences (P<0.05) between treatments per measurement campaign (Kruskal-Wallis and Bonferroni post-hoc test) as follows: drought-heat vs. control (#), heat vs. control (x), and drought-heat vs. heat (∗). Note that drought-heat seedlings were drought pre-stressed for 1.5 months before the start of the main experiment (day 1).

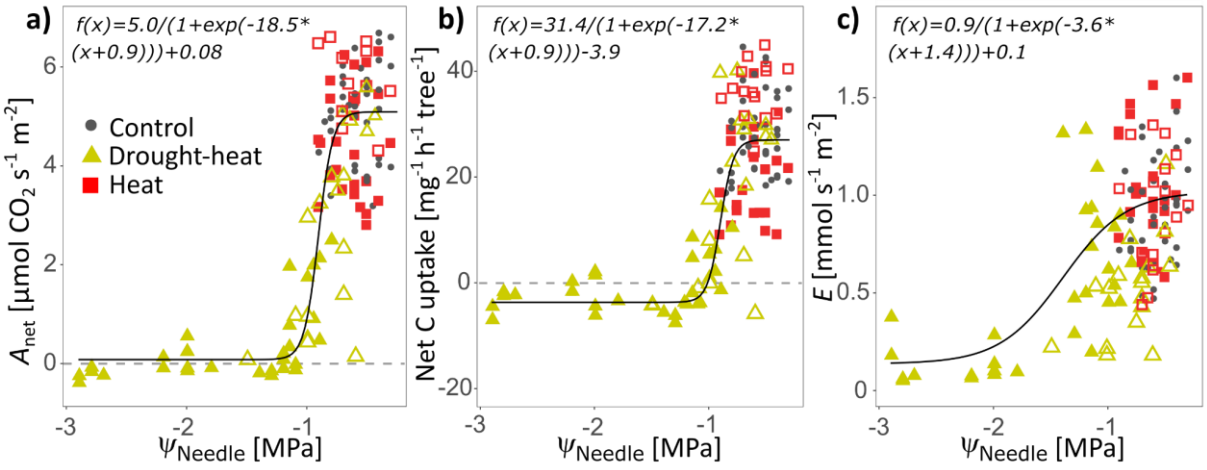

Fig. 6: Dependencies of a) net assimilation (A_{net}), b) net C uptake, and c) transpiration (E) with needle water potential (Ψ_{Needle}) measured at noon per seedling during stress and recovery. The different treatments are highlighted and open symbols indicate measurements during the recovery period. Sigmoidal functions were fitted to drought-heat (excluding recovery) and control measurements. Root-mean-square error: A_{net} 0.86; Net C uptake: 6.15; E: 0.30.

4.4 Discussion

We closely monitored stress and recovery responses of Scots pine seedlings exposed to heat and hot drought stress. All seedlings successfully survived the heatwave, while additional drought delayed recovery as observed in photosynthetic and hydraulic responses. Moreover, we found all seedlings to recover overall net C uptake quickly, indicating that a new equilibrium between C uptake and release appeared largely independent of lasting hydraulic impairment.

4.4.1 Thermal stress but no needle damage

A gradually increasing heatwave over 20 d resulted in daytime temperatures above 40°C during 3 d. Heat stress under well-watered conditions affected the hydraulic system moderately, but in combination with drought, stress impacts intensified. Both, on a diurnal scale and in the course of the heatwave, we found E to increase with rising air temperatures in well-watered seedlings (Fig. 1f; Ameye et al., 2012; Ruehr et al., 2016). Under water-limiting conditions and high VPD, E decreased strongly during the second half of the day to prevent extensive water loss and high xylem tensions, alongside declining g_s (Fig. S3; Ruehr et al., 2016; Birami et al., 2018; Zhao et al., 2013). This is in contrast to Urban et al. (2017b, 2017a), who found g_s to increase with rising temperatures, even under low soil water content. Stomatal adjustment affects evaporative cooling of transpiring leaves, thus decreasing leaf temperatures. In our study, well-watered heat seedlings were able to keep leaf temperatures below maximum air temperatures (Fig. 2a), as E increased despite declining g_s. Under drought-heat, the limited capacity of needle cooling due to reduced E resulted in higher leaf temperatures (max. 46°C) during early afternoon. Although tree mortality has been reported

following hot drought stress (Allen et al., 2010; Balducci et al., 2013; Teskey et al., 2015) and leaf temperatures similar to our study (47°C in Birami et al. (2018)), we did not find negative effects on seedling survival nor direct tissue damage, which was also supported by negligible effects on electrolyte leakage in needle tissues (Fig. 2c,g). In part, this might have been prevented by relatively high *E* rates during early mornings in drought-heat seedlings, buffering some of the excessive needle temperature stress. Moreover, the duration of the temperature exposure is important, while the heatwave resulted in a total of 18 h at c. 40°C air temperature. However, in well-watered seedlings of *Pinus radiata* at air temperatures and heat exposure comparable to our study, significant effects on the increase of electrolyte leakage were observed (Escandón et al., 2016). The discrepancy might result from the gradual increase of temperatures in our study compared to the immediate temperature increment from 25°C to 40°C in Escandón et al. (2016), allowing the seedlings to acclimate cell membrane stability to thermal stress (Saelim and Zwiazek, 2000).

While it is difficult to clearly disentangle the impacts of high temperatures on our drought treatment, we did not find direct needle damage albeit the very high leaf temperatures during periods of low transpiration (early afternoon). Hence, we found a remarkable thermal resistance of Scots pine needles to temperatures of 46°C during several hours and have to partially reject our first hypothesis.

4.4.2 Tree hydraulics during stress and recovery

Both, the heat and drought-heat treatment affected K_{Leaf} (Fig. 2d). In response to heat alone, the decline was modest and could be related to the high temperatures and/or increases in VPD. Most likely, heat stress affected K_{Leaf} in extra-xylary tissues due to tissue shrinkage, cell collapse and/or the reduction in aquaporin activity (Cochard et al., 2004; Scoffoni et al., 2014; Sack et al., 2016), consistent with the decline of RWC_{Needle} (Fig. 5b). In the drought-heat treatment, K_{Leaf} declined further alongside large reductions in Ψ_{Needle} and RWC_{Needle}, indicating that leaf xylem embolism must have appeared later during stress progression (Lo Gullo et al., 2005; Brodribb and Cochard, 2009; Johnson et al., 2009). The role of embolism was further supported by 25% reduced K_S at the end of the experiment in drought-heat seedlings (Fig. 4a-b). That stem xylem embolism reversal does not occur in Scots pine following drought release has been reported recently (Rehschuh et al., 2020). We also suggest embolism as underlying reason for the incomplete recovery of K_{Leaf} within the 18d-recovery-period (Fig. 4c). If solely extra-xylary tissues had been affected, we could assume K_{Leaf} to recover faster alongside RWC_{Needle} and Ψ_{Needle} (Brodribb and Cochard, 2009; Laur and Hacke, 2014) due to hydration not related to refilling of xylem embolism. In agreement, in previously heat treated seedlings, we observed a fast recovery of RWC_{Needle} and K_{Leaf}, supported by full K_S integrity (Fig. 4a-b). This agrees with a recent stress-recovery framework by Ruehr et al. (2019), indicating that

xylem embolism delays hydraulic recovery, while outside xylem conductance can be recovered quickly. Additionally, the larger response of K_{Leaf} than K_S in response to water limitation indicates the higher vulnerability of distal organs such as leaves compared to stems (Brodribb and Cochard, 2009; Bartlett et al., 2016) in highly segmented trees such as Scots pine.

Overall, we show that under heat stress the impact on the hydraulic system became particularly apparent in drought-treated seedlings, resulting in needle and stem xylem embolism, which did not recover fully.

4.4.3 Metabolic responses during stress and recovery

The stress imposed by high temperatures was further reflected in the C metabolism of the seedlings. A_{net} declined moderately in response to higher leaf temperatures (c. 40°C) in well-watered seedlings (Fig. 1e, Fig. 2e; Bernacchi et al., 2002; Birami et al., 2020), while in the combined heat and drought treatment, A_{net} decreased strongly with stress progression and declining Ψ_{Needle} (Fig. 6a), concurrently with a heavy decline in g_s (Fig. S4; Ruehr et al., 2016; Birami et al., 2018). Under optimal water supply and heat, g_s also decreased (Fig. S3), which resulted in a close maintenance of Ψ_{Needle} in isohydric pines. A_{net} was modulated by a strong diurnal pattern in both stress treatments as apparent in larger C uptake during the cooler morning hours, directly after irrigation (Bauweraerts et al., 2013; Drake et al., 2018). The A_{net} decline was accompanied by a decrease in F'_v/F'_m under heat stress in well-watered (Ameye et al., 2012; Guha et al., 2018) and with a more severe reduction in drought-treated seedlings (Fig. 2b; Birami et al., 2018). Other chlorophyll fluorescence parameters, i.e. electron transfer rate, effective photosystem II quantum yield and coefficients of photochemical fluorescence quenching have been shown to reveal strong decreases under heat and drought stress (Ameye et al., 2012; Birami et al., 2018). F'_v/F'_m serves to assess stress impacts of the photosynthetic apparatus (Netto et al., 2005). Its decrease can be seen as a protective mechanism, i.e. a photoprotective process, which eliminates excess excitation energy, thus inhibiting the formation of harmful free radicals (Murchie and Lawson, 2013). The observed fast recovery of F'_v/F'_m in the heat treatment is in line with previous studies (Ameye et al., 2012; Birami et al., 2018; Guha et al., 2018), but the recovery rate in drought-heat seedlings was lower. In summary, we found A_{net} to increase quickly to c. 80% of control rates alongside increasing F'_v/F'_m. This indicates that neither single nor compound stress had substantially harmed the photosynthetic apparatus.

Regarding R_{root}, we found at first an increase in well-watered heat treated seedlings with rising temperatures (Fig. 1g, Fig. S5, Fig. S6) as commonly observed (Burton et al., 2002; Jarvi and Burton, 2013; Birami et al., 2020). The subsequent decline at soil temperatures >34°C is in agreement with a study on Aleppo pine seedlings, where R_{root} peaked at 31–34°C (Birami et al., 2020). This might indicate a respiratory acclimation response as shown also in a study on

sugar maple (Jarvi and Burton, 2013). In drought-heat seedlings, R_{root} decreased strongly with drought progression, but apparently showed no large temperature sensitivity (Fig. S5). Explanations for declining respiration might be downregulated growth, lower availability of C, and at the cellular level limitation of substrates or adenylate control (Atkin and Tjoelker, 2003; Dusenge et al., 2019; O'Leary et al., 2019; Birami et al., 2020). Further, decreased C transport to sink organs might play a role due to reduced water cycling (Ruehr et al., 2009; Blessing et al., 2015). Despite lower R_{root} under drought-heat, the whole-tree C balance turned negative, which was hence dominated by a strong drop in A_{net} (Fig. 3a, Fig. S6; Zhao et al., 2013), with A_{net} and C uptake halting or turning negative at a Ψ_{Needle} of c. -1.0 MPa (Fig. 6a-b).

Following heat release in well-watered seedlings, the full recovery of shoot gas exchange is in agreement with a fully functional stem xylem (Fig. 4a-b). In contrast, delayed A_{net} recovery following drought-heat stress might be related to persistent reductions of K_{Leaf} and K_S compared to control seedlings (Brodribb and Cochard, 2009; Skelton et al., 2017; Rehschuh et al., 2020). R_{root} increased slowly during recovery from drought-heat stress, but surpassed control values at the end of the 18d-recovery-period (Fig. 1g). This reveals the enhancement of belowground repair mechanisms and root development to reestablish a fully functional root system (Davidson et al., 2006; Hagedorn et al., 2016), most likely to prepare for further stress periods.

Overall, we show that under heat stress, the C metabolism was affected moderately in well-watered and strongly in drought-treated seedlings. The decline of F'_v/F'_m in both treatments indicates a protective mechanism of the photosynthetic apparatus, and its full recovery points towards no persistent photosynthetic damage. Alongside, A_{net} and respiration rates recovered almost fully, indicating a quick restoration of the C metabolism. This largely confirms our second hypothesis.

4.4.4 Coupling of net C uptake and stem diameter change during stress and recovery

Stress-induced changes in water cycling and net C uptake simultaneously affected stem diameter change (Fig. 3). During the entire stress period, little stem growth appeared in drought-heat treated seedlings as cambium activity decreases at high xylem tension and low turgor (Abe et al., 2003; Balducci et al., 2013, 2016; Deslauriers et al., 2014), in agreement with the negative C balance (Fig. 3b). Further, stem shrinkage can be related to increased tree water deficit in phloem and xylem tissues. Under heat stress, the positive but reduced daily net C balance translated into slightly reduced stem growth as reported previously to occur under heatwaves (Bauweraerts et al., 2014; Ruehr et al., 2016). Following heat stress release, larger stem growth rates compared to control in well-watered seedlings were supported by a slight overcompensation of A_{net} and the associated higher daily net C balance (Fig. 1e, Fig. 3),

reflecting stress compensatory responses (Balducci et al., 2016; Ruehr et al., 2016). Interestingly, in drought-heat seedlings, the C balance also recovered fast and reached control rates 2 d after rewetting. As A_{net} showed a tendency to remain below control rates while R_{root} recovered (on a tissue basis), this could be due to a relatively lower sink demand, as root biomass and the root:shoot ratio tended to be on average lower in drought-heat seedlings. The fast recovery of net C uptake suggests that the seedlings rebalanced C uptake and release, appearing largely independent of the reduced recovery of hydraulic conductance. We suggest that persistently lower K_S and K_{Leaf} in drought-heat seedlings did not translate into limitations of A_{net} and E under the generally low VPD conditions during the recovery period. During low VPD, the hydraulic system is operating far away from its maximum capacity, hence relatively small reductions in conductance as observed here have little effect on the water transport system. However, if another heat event occurred before the hydraulic system was fully restored, the persisting reductions of K_S and K_{Leaf} should limit E more strongly, thus reducing evaporative cooling and increasing thermal stress. Therefore, environmental conditions during recovery are an important factor to consider when drawing conclusions on the underlying mechanisms of stress legacy. In agreement, larger stem growth rates in drought-heat seedlings compared to control post-stress support a preference for the restoration of maximum hydraulic conductivity over the long-term (Brodribb and Cochard, 2009; Balducci et al., 2013).

Opposing to our third hypothesis, this indicates a fast regulation of the tree net C balance, appearing independent of hydraulic impairments under the recovery conditions applied here. However, enhanced stem growth post drought-heat supports the repair of the hydraulic system to restore maximum K_S and thus increase resistance to future stress conditions.

4.5 Conclusion

Our study demonstrated that heat in combination with drought amplified the impacts on the carbon and water balance of Scots pine seedlings compared to heat stress alone. Well-watered heat treated seedlings were able to mitigate temperature stress by sustained evaporative cooling, while g_s and A_{net} declined moderately. This was also reflected in post-stress dynamics, indicating a fast recovery following heat stress with a slight overcompensation of net C uptake. In contrast, we found a delayed recovery of R_{root} and A_{net} after drought-heat release, while the photosynthetic apparatus appeared undamaged albeit high temperatures. Nonetheless, the net C balance in drought-heat seedlings recovered within 2 d after stress release, suggesting that a new equilibrium between C uptake and release was established. This was largely independent of the much slower recovery of K_{Leaf} and K_S, most likely because the water transport system operated far away from its maximum capacity during the recovery conditions. Stem growth, however, might have been upregulated in order to produce new conductive tissues to repair the impaired hydraulic system. While our study

shows that Scots pine seedlings are able to survive leaf temperatures of 46°C alongside drought, it also indicates that seedlings are vulnerable to subsequent stress periods as the integrity of the hydraulic system, including supporting biomass, were not fully restored.

Acknowledgements

We particularly thank Andreas Gast, Andrea Jakab, Benjamin Birami and Barbara Beikircher for technical and experimental support and advice. This study was supported by the German Research Foundation through its Emmy Noether Program (RU 1657/2-1) and by the German Federal Ministry of Education and Research (BMBF) through the Helmholtz Association and its research program ATMO.

Author contributions

RR and NKR designed the study. RR conducted the experiment and measurements, and analyzed the data with support from NKR. RR wrote the original draft with reviewing and editing from NKR.

4.6 Supplemental material

Supplemental figures

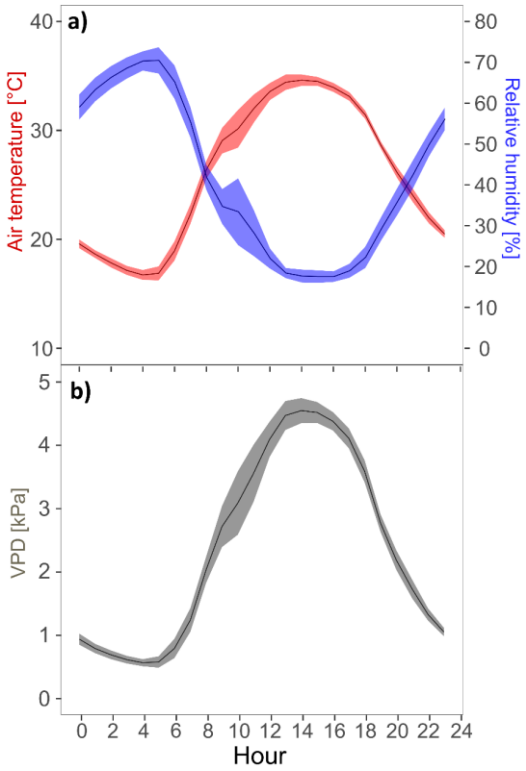

Fig. S1: Diurnal progression of a) air temperature and relative humidity and b) vapor pressure deficit (VPD) averaged per hour for a heat period in August 2003 (07. - 13.08.) in Weißenburg- Emetzheim, Franconia, Germany. Around this place, Scots pine forest dieback has been reported following severe climate events. Data is from the meteorological station of the *German Meteorological Service*. Shown are hourly averages and shaded areas are ±SE.

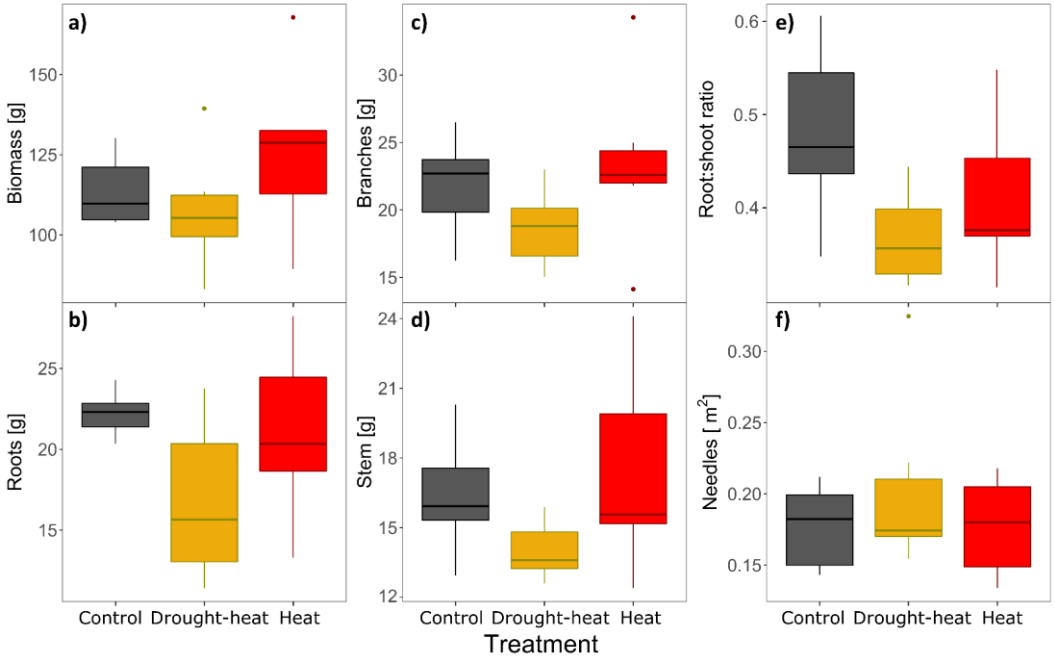

Fig. S2: Biomass, root:shoot ratio and needle area of 3-year-old *Pinus sylvestris* seedlings in the tree chambers (n=6 per treatment). Dry weight of a) total tree biomass, b) roots, c) branches and d) stems, as well as e) root:shoot ratio, and f) needle area were determined at the end of the experiment. No significant difference between treatments was observed (Kruskal-Wallis test).

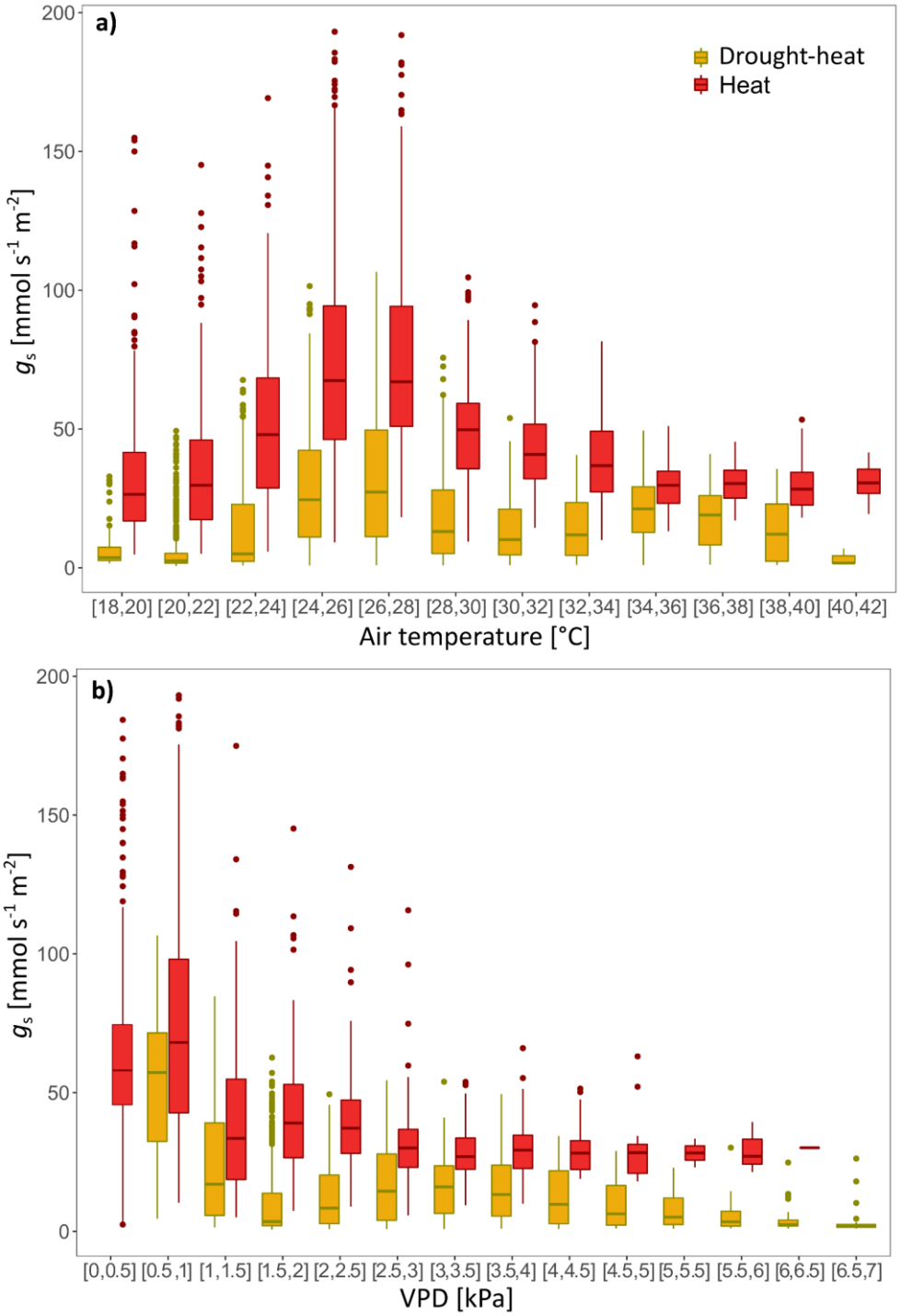

Fig. S3: Dependency of stomatal conductance (g_s) on a) air temperature and b) vapor pressure deficit (VPD) for the stress treatments (n=6). Data are bin-averaged in temperature classes of 2°C and VPD classes of 0.5 kPa.

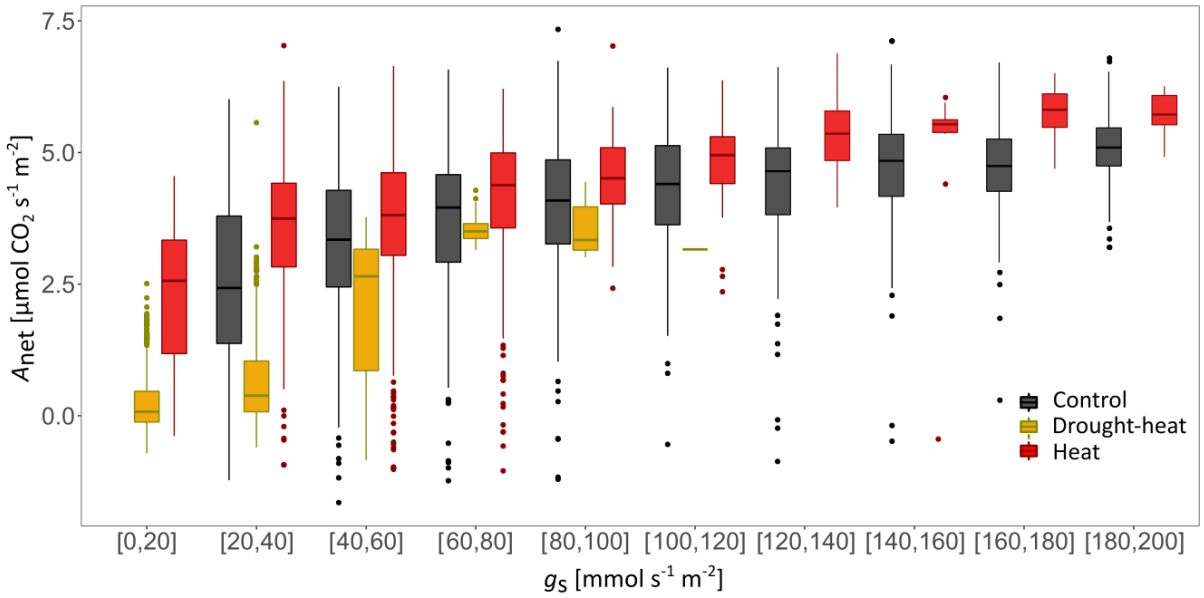

Fig. S4: Dependency of net assimilation (A_{net}) on stomatal conductance (g_s) per treatment (n=6) during stress and control conditions. Data are bin-averaged in g_s classes of 20 mmol s^{-1} m^{-2} (PAR>100 µmol m^{-2} s^{-1}).

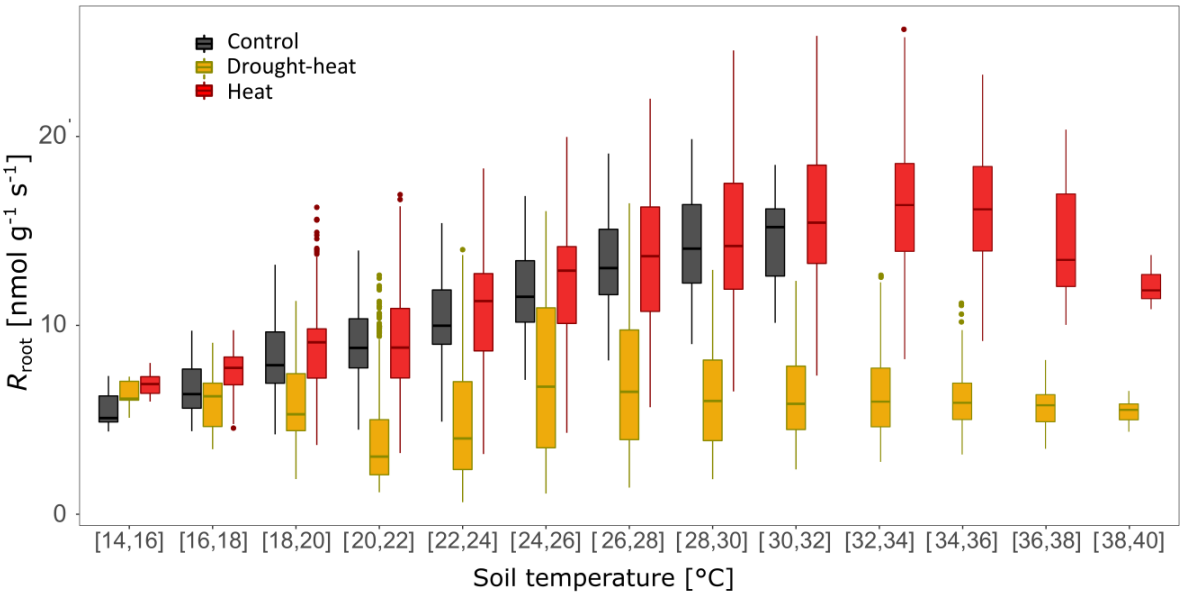

Fig. S5: Dependency of root respiration (R_{root}) on soil temperature per treatment (n=6) during stress and control conditions. Data are bin-averaged in soil temperature classes of 2 °C.

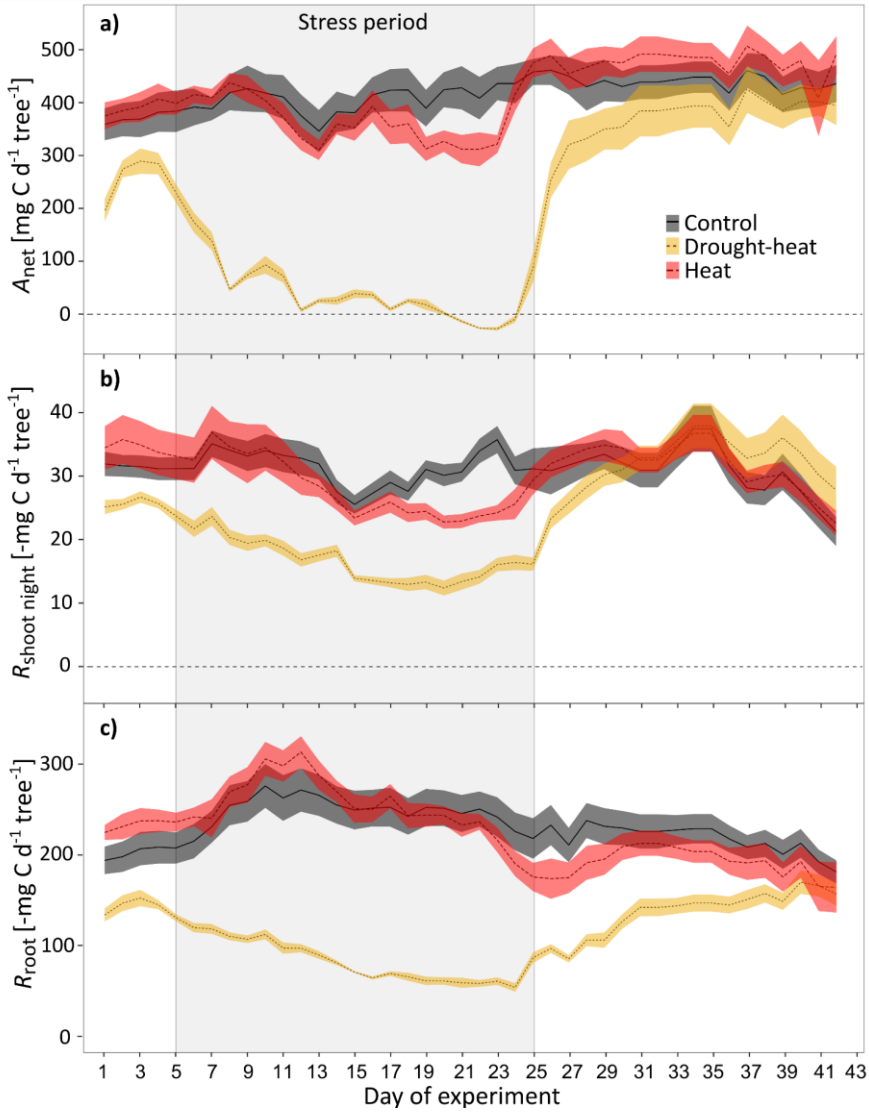

Fig. S6: Dynamics of daily-averaged a) net canopy assimilation (A_{net}), b) shoot dark respiration ($R_{shoot\ night}$), and c) root respiration (R_{root}) of Scots pine seedlings. Data are treatment averages and shaded areas show ±SE (n=6). The gray boxes represent the stress period.

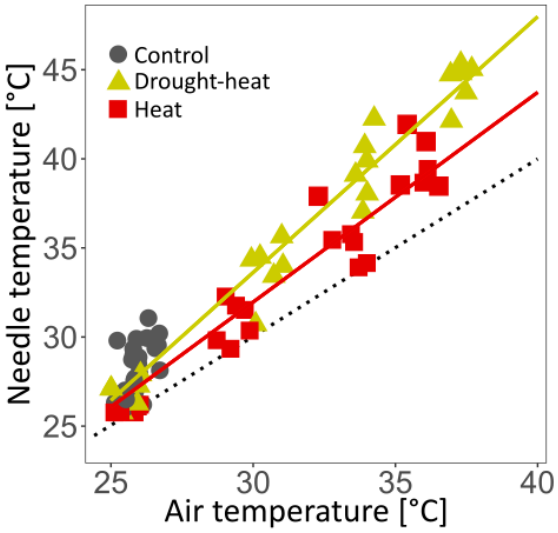

Fig. S7: Leaf temperature was strongly correlated with air temperature for the heat (r^2= 0.93, p<0.05) and drought-heat treatment (r^2= 0.96, p<0.05), with well-watered seedlings (heat treatment) showing a higher capacity for leaf cooling. The dashed line shows the 1:1 relationship.

Supplemental tables

Table S1: Functions for curves fitted to relationships of A_{net}, F'_v/F'_m and K_{Leaf} with leaf temperature for the heat and drought-heat treatment.

Correlation of max. leaf temperature with:	Heat	Drought-heat
A_{net}	f(x)= -0.005 x^2 + 0.17 x +4.93	f(x)= 0.015 x^2 -1.38 x + 30.67
F'_v/F'_m	f(x)= -0.001 x^2 + 0.08 x -0.96	f(x)= -0.002 x^2 +0.10 x -1.32
K_{Leaf}	f(x)= 0.01 x^2 -0.74 x +15.68	f(x)= 0.005 x^2 -0.42 x +9.86

Table S2: Results of the Tukey post-hoc test of overall treatment comparisons per time period derived by linear-mixed effects models (lme) for continuous measurements, i.e. for net assimilation (A_{net}; daytime) and shoot night respiration ($R_{shoot\ night}$; nighttime), transpiration (E), root respiration (R_{root}) and net C uptake. Shown are p-values for all treatment comparisons for day and nighttime (diurnal measurements) and for the entire day for net C uptake. Significant p-values (P<0.05) are highlighted in bold. Tested periods include adjustment (26°C, day 1-4), temperature increments (35°C, day 10-16; 38°C, day 17-19; and 40°C, day 20-23), the initial (26°C, day 28-30) and final recovery period (26°C, day 40-42). DH= Drought-heat.

Parameter	Treatment		Adjustment (daytime)	Adjustment (nighttime)	35°C period (daytime)	35°C period (nighttime)	38°C period (daytime)	38°C period (nighttime)	40°C period (daytime)	40°C period (nighttime)	Initial recovery (daytime)	Initial recovery (nighttime)	Final recovery (daytime)	Final recovery (nighttime)
A_{net} / $R_{shoot\ night}$ [µmol m^{-2} s^{-1}]	Control -	Heat	0.93	0.99	0.99	0.99	0.83	0.83	**0.0063**	0.99	0.83	0.99	0.55	0.99
	Control -	DH	**0.0014**	0.97	**<.0001**	**<.0001**	**<.0001**	**<.0001**	**<.0001**	**0.0096**	**0.0183**	0.98	0.08	0.98
	Heat -	DH	**0.0001**	0.93	**<.0001**	**<.0001**	**<.0001**	**<.0001**	**<.0001**	**0.0375**	**0.0009**	0.91	**0.0013**	0.8
E [mm m^{-2} s^{-1}]	Control -	Heat	0.99	0.96	0.99	0.99	0.974	1	0.89	0.43	0.71	0.99	0.94	0.94
	Control -	DH	**0.0031**	**0.0433**	0.058	0.058	**0.0394**	**0.0362**	**0.0001**	**<.0001**	0.95	0.43	0.87	0.87
	Heat -	DH	**0.002**	**0.0087**	**0.024**	**0.024**	**0.0097**	**0.0351**	**<.0001**	**<.0001**	0.25	0.26	0.42	0.42
R_{root} [µmol g^{-1} s^{-1}]	Control -	Heat	0.81	0.97	0.25	0.99	0.41	0.98	0.9	0.84	0.85	0.98	0.89	0.99
	Control -	DH	1	0.91	**0.0014**	**0.0015**	**<.0001**	**0.0002**	**<.0001**	**0.0001**	**0.0168**	0.07	0.87	0.86
	Heat -	DH	0.79	0.56	**<.0001**	**0.0007**	**<.0001**	**0.0005**	**<.0001**	**0.0006**	0.13	0.22	0.33	0.72
Net C uptake [mg d^{-1} $tree^{-1}$]	Control -	Heat	1		0.99		0.99		0.95		0.95		0.84	
	Control -	DH	0.07		**0.0006**		**<.0001**		**<.0001**		0.18		1	
	Heat -	DH	0.08		**0.0097**		**0.0006**		**0.0001**		**0.0061**		0.95	

5 Synthesis

Extreme drought and heat events alter the water, nutrient and carbon (C) cycling of trees (Sippel et al., 2018; Dannenmann et al. 2016, Brodribb et al., 2020), which might affect their biomass allocation and growth potential (Teskey et al., 2015), as well as reveal lagged effects following stress release (Anderegg et al., 2015; Ruehr et al., 2016, 2019; Birami et al., 2018). The capacity of trees to recuperate from stress (Galiano et al., 2011), however, is crucial for their survival. Hence trees must acclimate physiologically and adapt phenotypically, e.g. by increasing hydraulic recovery potentials. In this thesis, the impacts of extreme climatic events on the physiological functioning and recovery performance of Scots pine seedlings were investigated. For this, I applied drought, heat and combined drought and heat stress in a series of two experiments, aiming at investigating the following objectives: **(1)** To evaluate drought-induced xylem embolism and potential refilling after re-watering, and to examine the coupling with leaf gas exchange and carbon metabolism, **(2)** To determine legacy effects of heat and hot drought on C allocation, and identify the coupling with the plant N metabolism, and **(3)** To evaluate the impacts of heat and hot drought stress on C and water relations, and their repercussions on stem growth during and post-stress.

In order to answer these queries, extensive experimental and laboratory analyses were conducted. To provide a comprehensive picture of abiotic stress impacts and recovery dynamics, I used micro-CT, conventional hydraulic, nonstructural carbohydrate (NSC) and leaf gas exchange measurements, supplemented by $^{13}CO_2$ and ^{15}N labeling, as well as isotopic analyses of plant tissues and soil samples. The results from three studies, presented in this thesis, emerged.

In the following, the hypotheses formulated under 1.6 will be answered.

(1) Under combined drought and heat stress, the impacts on the hydraulic and metabolic processes and other processes regarding tree functional integrity are larger than under single stressors.

In this thesis, I showed that stress impacts largely depend on stress intensity. Stronger constrains on hydraulic and metabolic processes were found in drought-treated seedlings, i.e. under average temperature **(Chapter 2)** as well as under heat **(Chapters 3 and 4;** see Fig. 1 for a summary of stress effects on measured parameters compared to control). While in well-watered seedlings transpiration (*E*) increased under a heat wave to enhance leaf cooling, drought-treated seedlings were exposed to much higher leaf temperatures (max. 46°C) as evaporative cooling was strongly limited in the second half of the day **(Chapter 4)**.

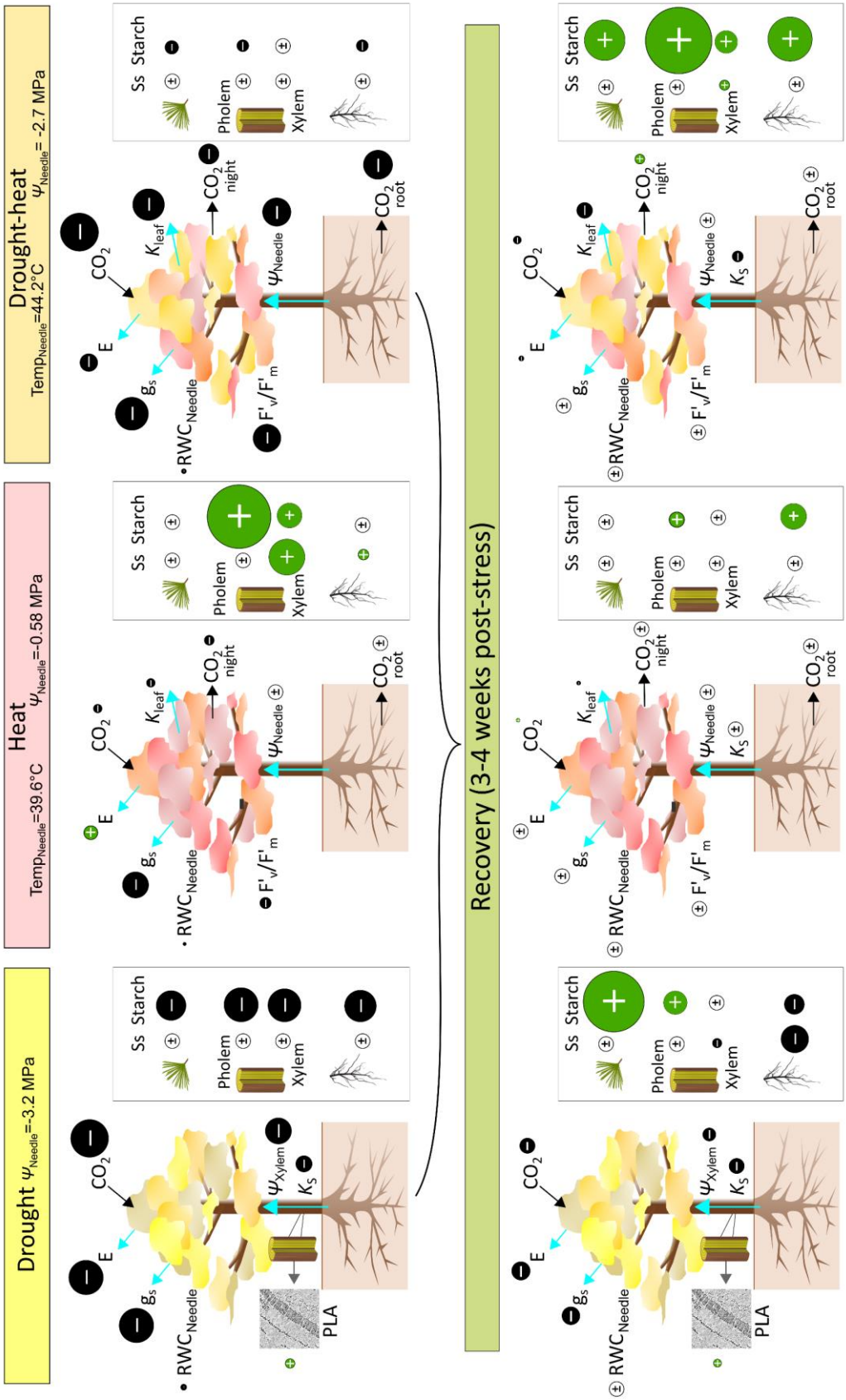

Fig. 1: Overview of hydraulic and metabolic processes and parameters analyzed during drought (experiment 1, Chapter 2), heat and drought-heat stress (experiment 2, Chapter 3 and 4) as well as after stress release (3-4 weeks post-stress). The size of the circles indicates the degree by which the parameters deviate from the control: Black circles (-) depict a reduction and green circles (+) show an increase compared to control. (±) indicates negligible or no deviation from the control.

In experiment 1 (2017), drought-treated seedlings were stressed to a Ψ_{Xylem} of c. -3.2 MPa, resulting in c. 50% PLC based on a previously determined vulnerability curve (Supplemental Fig. S1, **Chapter 2).** In experiment 2 (2018), drought-heat treated seedlings reached a min. needle water potential (Ψ_{Needle}) of -2.7 MPa **(Chapters 3 and 4)**. Since Ψ_{Needle} is related to the stem xylem water potential (Ψ_{Xylem}) at higher drought stress levels, i.e. when plants reduce transpiration to a very low level, it can be assumed that c. 25-30% PLC occurred in these seedlings as determined from the PLC curve. This corresponds well with the 25% reduction in stem hydraulic conductivity (K_S) compared to control seedlings (measured *in vivo* on stem segments). Contrary, heat alone (max. 42°C) caused no reduction in Ψ_{Needle} and K_S (see Fig. 2 for hydraulic and metabolic stress responses).

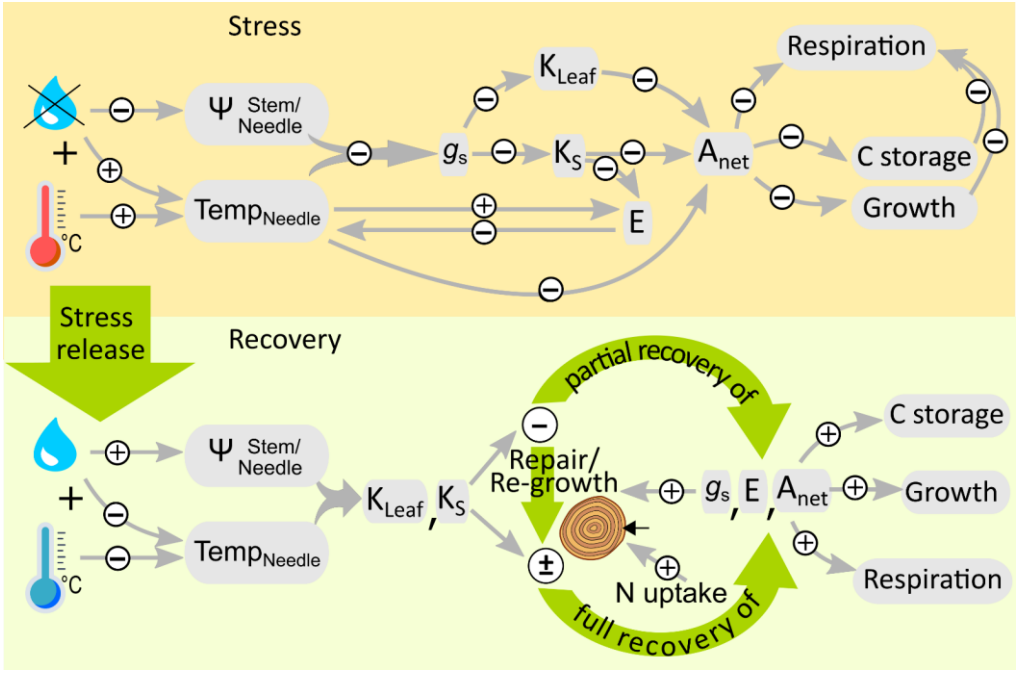

Fig. 2: Flowchart representing stress and recovery dynamics of Scots pine seedlings. Shown are plant physiological processes (hydraulic and metabolic) changing in response to water limitation and/or heat stress, as well as the dependency of gas exchange recovery and related parameters on tree hydraulic functionality. Reduced K_S relates to the build-up of xylem embolism. Since refilling of drought-induced embolized tracheids did not occur in Scots pine (i.e. K_S remained lower than in control seedlings), full recovery of gas exchange should be related to regrowth of stem xylem tissue. This assumes that the photosynthetic apparatus and metabolic enzymes were not damaged largely. (-) indicates a reduction, (+) an increase, and (±) indicates negligible or no deviation from the control.

The C metabolism was closely related to tree hydraulics during stress (Fig. 2). I further analyzed the CO_2 signature of shoot night ($R_{shoot\ night}$) and root respiration (R_{root}) during stress (i.e. before pulse-labeling) in experiment 2 **(Chapters 3 and 4)**. A continuous increase of $\delta^{13}C$ in $R_{shoot\ night}$ and R_{root} was observed within the first 7 d in all treatments when seedlings were placed in the tree chambers (Fig. 3), resulting from C uptake of the slightly enriched supply air (Air_{suppy}; difference in $\delta^{13}C$ ca. 9‰). This indicated that the pre-drought stress period for 1.5

months (final Ψ_{Needle} was -1.4±0.05 MPa compared to -0.6±0.03 MPa in control) did not largely affect C allocation to respiration (in later drought-heat treated seedlings; Tukey´s HSD>0.1). Larger stress levels, i.e. combined drought and heat stress applied in the following resulted in significantly lower discrimination against $^{13}CO_2$ compared to the control treatment (Tukey's HSD, P<0.001 for 35°C to 40°C period; Fig. 3a), consistent with strongly reduced stomatal conductance (g_s) and net assimilation (A_{net}) due to large hydraulic stress **(Chapter 4)**. g_s decline has been shown to result in a lower intercellular CO_2 concentration (c_i), inducing ^{13}C discrimination to decrease (Olivas-García et al., 2000; Klein et al., 2005). Regarding $\delta^{13}C$ in $R_{shoot\ night}$, drought-heat seedlings showed more depleted $\delta^{13}C$ at the end of the stress period (40°C period, Tukey's HSD, P >0.1; Fig. 3b). This indicates that older reserves were used for

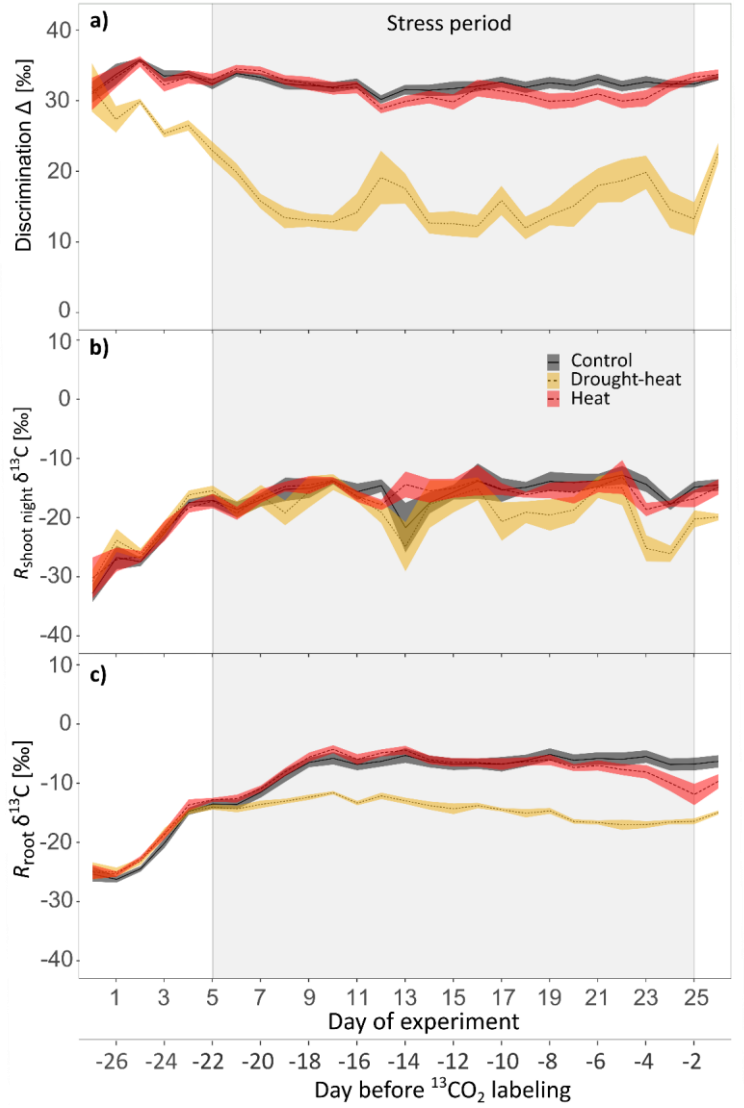

Fig. 3: Treatment-specific dynamics of a) photosynthetic ^{13}C discrimination, b) $\delta^{13}C$ in shoot night respiration, and c) $\delta^{13}C$ in root respiration measured in the tree chambers during the end of the pre-drought, within the stress period and 2 days after stress release, i.e. before $^{13}CO_2$ labeling (n=6 per treatment). Data are daily means shown as treatment averages and shaded areas indicate ±SE. The gray boxes represent the stress (heat) period. Note that the data do not reflect typical natural abundance vales since supply air to the tree chambers was slightly enriched in $\delta^{13}C$ ($\delta^{13}C$= 0.28‰).

maintenance respiration with a higher ^{12}C amount, most likely due to overall C uptake limitation (of the slightly enriched air) due to water shortage (see Fig. 1e in **Chapter 4)**. Strong reductions in C uptake over c. 30 d **(Chapter 2:** drought stress) and 20 d **(Chapter 3:** drought-heat stress) were reflected in most tissues in strong and moderate declines of starch, i.e. storage pools, respectively (Figs. 1 and 2).

After day 7 (day -20), $\delta^{13}C$ of R_{root} in control and heat treated seedlings further increased, reaching c. 20‰ difference compared to the beginning of the tree chamber experiment. This suggests that the respired fraction consisted mainly of recently assimilated C and new C incorporated into root tissues, thus revealing that C uptake and transfer was not limited by heat if water was not limiting. This coincides with Högberg et al. (2001) who reported soil respiration to be fueled by c. 40% by current assimilates in Scots pine forests. In contrast, drought-heat stress resulted in reduced transport of newly assimilated C to roots and R_{root} as seedlings respired older C reserves, which were more depleted in ^{13}C (Tukey's HSD, $P<0.001$ for 35°C to 40°C period; Fig. 3c). This is confirmed by previous $^{13}CO_2$-labeling studies on European beech under water limitation, in which longer mean residence times of ^{13}C in leaf respiration and a slower transfer to roots and into the soil were reported (Ruehr et al., 2009; Zang et al., 2014; Hagedorn et al., 2016).

Under the heat wave in experiment 2, the C metabolism and hydraulic functioning of seedlings under well-watered conditions were only moderately affected, resulting from g_s decrease in response to increasing VPD following temperature increases **(Chapters 3 and 4).** However, air temperatures remained <43°C. If temperatures would have been slightly higher, larger effects would likely have occurred even under well-watered conditions. Large damages to needle tissues of conifers typically occur at leaf temperatures ~47°C (Colombo, 1992; Bigras, 2000), and heat stress has been shown to result in leaf shedding (Filewod and Thomas, 2014; Ruehr et al., 2016) or even in tree death, often associated with water limitation (Allen et al., 2010; Balducci et al., 2013; Birami et al., 2018).

Based on the results presented in this thesis, soil water availability is of great importance during heatwaves, independent of whether single or multiple stress occurs, thus rejecting the hypothesis. Tree responses to episodic heat and drought events, however, may be buffered by soils with a high water holding capacity, i.e. clayey soils or soils containing large amounts of soil organic matter. If trees are able to reach water-saturated deep soil layers, this will be less dependent on episodic drought events (Mu et al., 2021; Nadal-Sala et al., 2021).

(2) Embolism formation in stem xylem of Scots pine is not fully reversible one month after drought stress, and must therefore be compensated by stem growth.

One of the main findings of experiment 1 was the inability of Scots pine to refill drought-induced embolized tracheids within 1 month, consistent with no significant increase of K_S at the end of the recovery period **(Chapter 2)**. This was confirmed by micro-CT and conventional hydraulic methods. Similarly, K_S in drought-heat treated seedlings of experiment 2 did not recover to control values within almost 3 weeks albeit the lower reduction in K_S (c. 25% reduction; **Chapter 4)**, compared to a 46% reduction in experiment 1 **(Chapter 2)**. This shows that xylem embolism refilling in Scots pine does not depend on the level of embolism formation, which was also observed in additional seedlings stressed to a lower drought level (higher Ψ_{Xylem}) in experiment 1 (see Supplemental Fig. S4 in **Chapter 2)**. The incapacity of Scots pine to refill embolized xylem, and its reliance on xylem regrowth to recover the hydraulic transport capacity, is supported by the strong growth enhancement resuming c. one week post-stress in previously drought-heat treated seedlings of experiment 2 **(Chapters 3 and 4).** While stem growth was still hindered shortly post-stress as observed by low ^{13}C-label incorporation into cellulose, growth rates significantly exceeded those of control seedlings one week post-stress **(Chapter 3)**. The regrowth of new functional xylem should thus enable an increase of K_S in the mid-term, which is indispensable to restore the functionality of the tree hydraulic system. The results of the thesis therefore support the hypothesis.

(3) Leaf gas exchange recovery is delayed following drought, heat or combined stress once embolism has developed in leaf or stem xylem.

Particularly the results of experiment 1 revealed that the recovery of leaf gas exchange was delayed because hydraulic integrity was not restored **(Chapter 2)**. Drought-induced loss of K_S by c. 46% corresponded well with persistently reduced E, light-saturated photosynthesis (A_{SAT}) and g_s four weeks after stress release by 52%, 43% and 51% compared to control seedlings, respectively. Therefore, large damages to the hydraulic system indicate that the full restoration of leaf gas exchange is only possible via the regrowth of functional stem xylem, thus increasing the water transport capacity to leaves in the long-term (Fig. 2). In experiment 2, heat treated well-watered seedlings did not suffer from large hydraulic impairments and leaf gas exchange recovered fast after stress release **(Chapters 3 and 4)**. In contrast, in drought-heat seedlings, leaf hydraulic conductance (K_{Leaf}) had not recovered within the 18-day-recovery period, suggesting that besides impairments to extra-xylary tissues, embolism had developed in leaves. The relatively low reduction of K_S (25% compared to control; **Chapter 4)** in comparison to experiment 1 (46% reduction, **Chapter 2)**, however, might not have largely affected the recovery of A_{net} as it recovered quickly alongside E, almost reaching control values within 3 weeks. The absence of significant electrolyte leakage in leaf tissues under drought-heat and

the full recovery of F'_v/F'_m indicates that the photosynthetic apparatus was not damaged despite the high leaf temperatures reached (46°C). Because the tree net C balance recovered rapidly within 2 days post drought-heat, it can be assumed that the seedlings rebalanced C uptake and C release, given the tendency towards lower root biomass post-stress. This appeared independent of the slower recovery of K_{Leaf} and K_S, presumably due to the low VPD conditions during recovery. Tree exposure to higher VPD, however, should push the hydraulic system closer to its maximum capacity, and persistent impairments should become more evident; also if larger impairments occurred as observed in experiment 1. Therefore, if K_S and/or K_{Leaf} are not restored before a new stress event occurs, trees will likely suffer from larger reductions in leaf gas exchange. This might result in a feedback mechanism of recurrent stressors that may lead to slow tree decline and lagged tree death (e.g. Gea-Izquierdo et al., 2021; Preisler et al., 2021).

(4) Translocation of recently assimilated C to the belowground is enhanced shortly post-heat, but delayed post drought-heat. Recent C will be strongly invested into repair and growth, if stress impairment occurs.

The $^{13}CO_2$ pulse-labeling experiment two days post-stress **(Chapter 3)** revealed that well-watered heat treated seedlings allocated recent C faster to branch phloem and xylem water-soluble compounds (WSC) compared to control seedlings (within several hours), to R_{root} (7.1 h compared to 8.3 h in control) and the soil microbial biomass (SMB; 3 d compared to 7 d in control). Fast C allocation to xylem WSC was based on the leakage-retrieval mechanism during phloem transport (van Bel, 2003; Thorpe et al., 2005), and supports strong C investments into secondary growth of branches post-heat, as observed in high ^{13}C amounts in branch cellulose (see also Fig. 7, **Chapter 3**, for a summary of C allocation patterns at the end of the recovery period). This might relate to enhanced cell division during elevated temperatures and cell enlargement following stress release, and reflects a compensatory process of stress-induced reductions in stem growth. Following drought-heat release, however, the stress-induced deceleration and reduction of C transport to R_{root} and the belowground (Fig. 3c) still persisted 2 days post-stress (detection of ^{13}C in R_{root} 13.8 h after $^{13}CO_2$ pulse-labeling and negligible C allocation to SMB; **Chapter 3)**. This might be attributed to hydraulic limitations, impaired phloem loading and transport, and/or low sink strength. Short-term growth of above- and belowground systems appeared to be inhibited during initial recovery as observed in low ^{13}C allocation to cellulose, probably resulting from persistent meristem inactivation at lower water potentials and higher tissue temperatures. The reduced above-belowground coupling shortly after drought-heat stress supports the strong accumulation of ^{13}C in needle biomass, apparent particularly in needle starch. This might indicate passive C overflow to storage compartments because the photosynthetic apparatus

had to continue working to dissipate the light energy, while the C transport capacity to other organs was limited.

Further, starch concentrations increased strongly in needle and bark tissues 4 weeks post-drought **(Chapter 2)** and in all tissues c. 3 weeks post drought-heat **(Chapter 3**, see Fig. 1: Recovery). In previously heat treated well-watered seedlings smaller non-significant increases of starch concentrations were observed in root and phloem tissues. The resumption of stem growth in drought-heat seedlings in the second recovery week and delayed but full recovery of R_{root} **(Chapters 3 and 4)** suggests that starch was accumulated actively later on. Increased storage formation might therefore serve as a safety measure for future stress periods, while enabling C remobilization for metabolism, growth and defense in periods of low photosynthetic uptake.
Therefore, the first part of the hypothesis can be confirmed, while the second part has to be rejected because growth was not fueled by C assimilated shortly post drought-heat.

(5) N uptake and allocation are in sync with the tree C metabolism post-stress.

Chapter 3 successfully revealed that a close link exists between the tree C and N metabolism post-stress. This strong coupling during early recovery was reflected by significant correlations between ^{13}C excess of branch cellulose and ^{15}N excess of branch bulk material (Fig. 4). Large allocation of N to the aboveground biomass in previously heat treated seedlings was consistent with enhanced C allocation to branch and stem growth **(Chapter 3)**. Contrary, seedlings recovering from drought-heat stress invested little C into short-term growth, reflected in low N uptake and transport to the aboveground biomass. This might have been caused by the drought-induced decrease in root activity and reduced demand for N in aboveground organs due to continued growth inhibition shortly after stress.

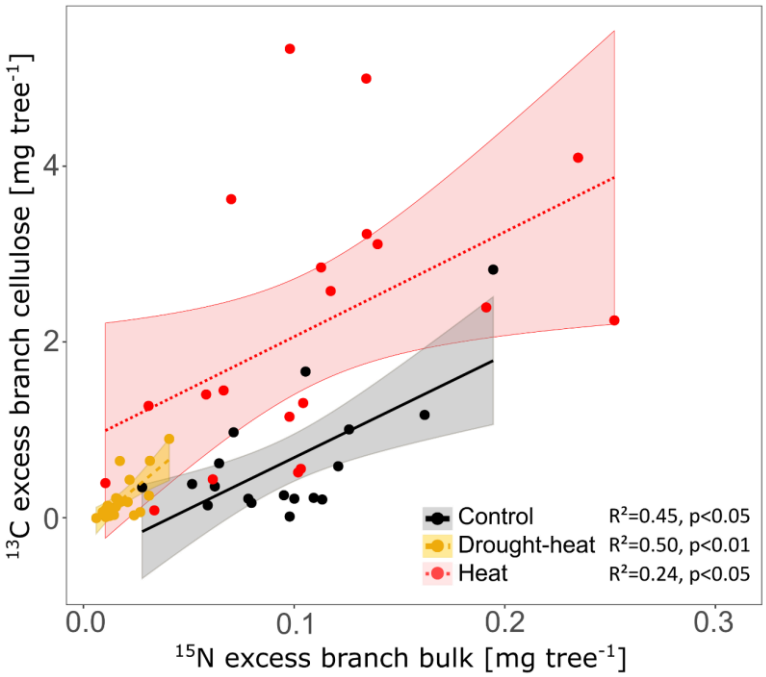

Fig. 4: Treatment-specific relationships between ^{13}C excess of branch cellulose and ^{15}N excess of branch bulk material (phloem and xylem) post-stress indicate a close coupling between the C and N metabolism in Scots pine seedlings after stress release.

5.1 Research advances and limitations of the study- research needs

The greenhouse experiments conducted in the scope of this thesis allowed for the tight control of abiotic drivers **(Chapters 2-4)**. Since environmental conditions were based on past weather extremes in regions, where Scots pine dieback has been reported in recent years, close-to-realistic results were generated. However, potential biotic stress impacts (e.g. Seidl et al., 2017) had to be neglected, which could have amplified abiotic stressors impacts on trees. Therefore, manipulative experimental setups in the greenhouse allow for the investigation of tree responses to individual abiotic stressors, but in turn, decouple the tree from its natural environment. In the present thesis, seedlings instead of mature trees were analyzed due to a more convenient handling, as well as technical and financial limitations. Concurrently, it should be borne in mind that the extrapolation of results to mature trees remains critical. Since noticeable differences in C dynamics between seedlings and mature trees have been reported (see Hartmann et al., 2018a), field studies on mature trees and ecosystem flux measurements should be integrated to provide reliable results at the forest and ecosystem level. So far, however, the use of mature trees to test for a xylem refilling mechanism after re-watering via micro-CT is hardly possible by keeping trees intact to avoid cutting artefacts. These novel methods can therefore provide detailed pictures about seedlings or saplings only **(Chapter 2)**. Further, the gas exchange chamber system allowed to determine the whole-tree C balance during stress and recovery and to capture the complete ^{13}C allocation to root and shoot respiration within 2.5 weeks post-stress **(Chapter 3).** During labeling, the tree chambers

allowed for a tight control of the enriched air residing in the shoot compartments, which prevented the penetration of labeled air into soil pores. In in-situ experiments, this is often one of the main problems during labeling (Subke et al., 2006; Bahn et al., 2009) and could lead to misinterpretations of label detection in soil respiration. Further, ^{13}C labeling and whole-tree C allocation studies on mature trees are scarce (Klein and Hoch, 2015; Joseph et al., 2020), and often do not capture the entire C fluxes and pools (e.g. Keel et al., 2007; Andersen et al., 2010), wherefore results on seedlings can provide a basis for stress and resilience modeling. In particular, stress legacy effects on hydraulic properties and C metabolism and allocation, which possibly lead to growth limitation and/or mortality, are still insufficiently addressed in current models (Anderegg et al., 2015; Merganičová et al., 2019). However, the effect of xylem refilling (Sperry & Love, 2015) and tree growth responses post-drought (Trugman et al., 2018; Itter et al., 2019) have started to be implemented in modeling approaches. Based on the factors outlined above, it could be demonstrated that experiments under controlled greenhouse conditions are valuable to contribute to our understanding of mechanistic responses and processes in C and water cycling during stress and recovery, while the results should be supplemented by field-based data on mature trees.

As demonstrated successfully, canopy $^{13}CO_2$ labeling and soil-applied ^{15}N are valuable tools to disentangle C and N allocation processes during post-stress recovery **(Chapter 3)**. Nonetheless, when applying $^{13}CO_2$ pulse-labeling, one should consider that a detailed picture of the allocation of C assimilated within a short time frame, here within 4 h (two days after stress release), can only be provided. To quantify C dynamics later during the recovery period (including C assimilated later post-stress), it is therefore of importance to measure additional physiological parameters such as stem diameter increment or starch and sugar concentrations. For example, without determining the change in stem diameter following stress release by dendrometers in experiment 2, we would not have captured the strong increase in C allocation to growth later during the recovery period in drought-heat treated seedlings **(Chapter 3).** To disentangle C and/or N allocation changes and recovery pace, further stable isotope labeling studies could therefore focus on different recovery stages. $^{13}CO_2$ pulse-labeling e.g. two weeks after stress release should have resulted in a very different C allocation pattern, especially regarding ^{13}C in stem cellulose, and presumably also in root cellulose. These dynamics might also increasingly be affected by the rising atmospheric CO_2 concentration (Patra et al., 2005; Le Quéré et al., 2018).

Further, in **Chapter 3**, we suggested several reasons and mechanism to be responsible for the differences in C allocation in previously stressed compared to control seedlings, particularly the reduced C transfer to the belowground in previously drought-heat treated seedlings. To test for the given reasons, further studies should focus on the quantification of phloem damage,

which might be responsible for reduced phloem loading and C transport to other organs. Root damage and growth during and post-stress should also be analyzed qualitatively and quantitatively to evaluate reductions in root sink strength. For this, minirhizotron techniques and imagery, including machine learning approaches to detect and segment roots, would provide a welcome possibility (Johnson et al., 2001; Yu et al. 2020). To analyze long-term recovery and resilience, longer observation periods (e.g. for another growing season) would be necessary. In both experiments, it would have been interesting to analyze K_S recovery via growth of sufficient xylem tissue and whether this compensation would ultimately have enabled the full recovery of leaf gas exchange **(Chapters 2 and 4)**. However, this can certainly depend on other factors, including root vitality and hydraulic conductance.

Other important points of interest represent the water, C and N interactions between trees during and post stress to evaluate the potential support of stressed trees by little or non-stressed neighbors, e.g. favored by deeper rooting depths. This aspect is neglected by investigating the responses of single isolated trees. Hydraulic redistribution, i.e. the passive flow of water through roots, can provide water to neighboring drought-stressed trees (Hafner et al., 2017, 2021; Töchterle et al., 2020). So far, the relevance and extent of hydraulic redistribution still needs to be proven, particularly under field conditions (Hafner et al., 2017, 2021). Similarly, C and N exchange between trees via belowground connections, i.e. roots or mycorrhizal networks, might be of importance for tree fitness at the population level. The transfer of C and/or N from non-stressed plants to e.g. NSC-limited neighbors might enhance their survival. Therefore, further labeling experiments (^{2}H, ^{13}C, ^{15}N) could serve to elucidate water, C and N transfer between trees particularly in response to drought and/or thermal stress, as well as post-stress. This would improve our understanding of the functionality of the forest as a whole ecosystem and its resilience to stress, especially if environmental conditions become more extreme in the future.

5.2 Conclusion and outlook

The findings of this thesis significantly contributed to expand knowledge on hydraulic processes as well as C and N cycling during and post-stress in Scots pine. Since vegetation models still overestimate the recovery potential of trees (Anderegg et al., 2015) and lack reliable input on the fundamentals of plant physiological processes, particularly following stress events (Lukac et al. 2010; Merganičová et al., 2019), the results presented here can potentially improve stress legacy modeling. ^{13}C and ^{15}N labeling were found to considerably enable the quantification of C and N allocation post-stress. This study provides a glimpse of allocation dynamics, while the results largely depend on the timing of labeling, and heat and drought events can further vary largely in intensity, duration and frequency. Adjusting environmental

conditions to past extreme climatic events, however, most likely resulted in close-to-realistic stress and recovery scenarios.

The thesis demonstrated that Scots pine seedlings are able to survive a loss of stem hydraulic conductivity up to 50% and leaf temperatures of 46°C during several hours. Further, it showed that drought-induced stem xylem embolism repair does not occur via short-term refilling of embolized tracheid. This indicates that the full recovery of leaf gas exchange should only be possible via the growth of sufficient functional stem tissue. The labeling experiments revealed an initially reduced above-belowground coupling of C and N cycling post drought-heat, most likely due to lasting limitations of phloem functioning and sink strength. Short-term growth was still inhibited, while larger stem growth rates in the second week post drought-heat compared to control point to preferences in C allocation by aiming at a functional stem xylem. Following release from water limitation, we also found seedlings to increasingly invest into starch, which may indicate storage pools as a backup for future stress periods. Overall, soil water shortage was found to be the dominating factor in response to heat waves, causing higher leaf temperatures and larger effects on metabolic functioning and hydraulic conductance at the stem-leaf continuum, thus delaying recovery and leaving seedlings more vulnerable to subsequent stress periods. A larger intensity and longer duration of the heatwave, however, might have also affected post-stress recovery in well-watered seedlings more strongly by depleting C reserves or reducing enzyme activity.

In summary, the outlined novel findings as well as limitations allow to give rise to the following research to provide a more comprehensive picture of tree recovery following single and compound stress:

- Quantification of stress damage, i.e. of phloem transport, root and stem meristems
- Long-term recovery in greenhouse experiments: Monitoring delayed recovery of stress-induced parameters for another growing season
- Stable isotope labeling during several recovery stages and different seasons (also on mature trees in the field and various tress species)
- Water, C and N interactions between several trees during stress and recovery

6 References

Aaltonen, H., Lindén, A., Heinonsalo, J., Biasi, C., Pumpanen, J., 2016. Effects of prolonged drought stress on Scots pine seedling carbon allocation. Tree Physiology treephys;tpw119v1. https://doi.org/10.1093/treephys/tpw119

Adams, H.D., Zeppel, M.J.B., Anderegg, W.R.L., Hartmann, H., Landhäusser, S.M., Tissue, D.T., Huxman, T.E., Hudson, P.J., Franz, T.E., Allen, C.D. et al., 2017. A multi-species synthesis of physiological mechanisms in drought-induced tree mortality. Nature Ecology & Evolution 1, 1285-1291. https://doi.org/10.1038/s41559-017-0248-x

Akselsson, C., Westling, O., Alveteg, M., Thelin, G., Fransson, A.-M., Hellsten, S., 2008. The influence of N load and harvest intensity on the risk of P limitation in Swedish forest soils. Science of The Total Environment 404, 284–289. https://doi.org/10.1016/j.scitotenv.2007.11.017

Allen, C.D., Breshears, D.D., McDowell, N.G., 2015. On underestimation of global vulnerability to tree mortality and forest die-off from hotter drought in the Anthropocene. Ecosphere 6, art129. https://doi.org/10.1890/ES15-00203.1

Allen, C.D., Macalady, A.K., Chenchouni, H., Bachelet, D., McDowell, N., Vennetier, M., Kitzberger, T., Rigling, A., Breshears, D.D., Hogg, E.H. (Ted), Gonzalez, P., Fensham, R., Zhang, Z., Castro, J., Demidova, N., Lim, J.-H., Allard, G., Running, S.W., Semerci, A., Cobb, N., 2010. A global overview of drought and heat-induced tree mortality reveals emerging climate change risks for forests. Forest Ecology and Management 259, 660–684. https://doi.org/10.1016/j.foreco.2009.09.001

Ameye, M., Wertin, T.M., Bauweraerts, I., McGuire, M.A., Teskey, R.O., Steppe, K., 2012. The effect of induced heat waves on *Pinus taeda* and *Quercus rubra* seedlings in ambient and elevated CO_2 atmospheres. New Phytologist 196, 448–461. https://doi.org/10.1111/j.1469-8137.2012.04267.x

Anderegg, W.R.L., Anderegg, L.D.L., Kerr, K.L., Trugman, A.T., 2019. Widespread drought-induced tree mortality at dry range edges indicates that climate stress exceeds species´ compensating mechanisms. Glob. Change Biol. 25, 3793–3802. https://doi.org/10.1111/gcb. 14771

Anderegg, W.R.L., Flint, A., Huang, C., Flint, L., Berry, J.A., Davis, F.W., Sperry, J.S., Field, C.B., 2015a. Tree mortality predicted from drought-induced vascular damage. Nat. Geosci. 8, 367–371. https://doi.org/10.1038/ngeo2400

Anderegg, W.R.L., Kane, J.M., Anderegg, L.D.L., 2013a. Consequences of widespread tree mortality triggered by drought and temperature stress. Nature Clim Change 3, 30–36. https://doi.org/10.1038/nclimate1635

Anderegg, W.R.L., Plavcová, L., Anderegg, L.D.L., Hacke, U.G., Berry, J.A., Field, C.B., 2013b. Drought's legacy: multiyear hydraulic deterioration underlies widespread aspen forest die-off and portends increased future risk. Glob Change Biol 19, 1188–1196. https://doi.org/10.1111/gcb.12100

Anderegg, W.R.L., Schwalm, C., Biondi, F., Camarero, J.J., Koch, G., Litvak, M., Ogle, K., Shaw, J.D., Shevliakova, E., Williams, A.P., Wolf, A., Ziaco, E., Pacala, S., 2015b. Pervasive drought legacies in forest ecosystems and their implications for carbon cycle models. Science 349, 528–532. https://doi.org/10.1126/science.aab1833

Andersen, C.P., Ritter, W., Gregg, J., Matyssek, R., Grams, T.E.E., 2010. Below-ground carbon allocation in mature beech and spruce trees following long-term, experimentally enhanced O3 exposure in Southern Germany. Environmental Pollution 158, 2604–2609. https://doi.org/10.1016/j.envpol.2010.05.008

Angeles, G., Bond, B., Boyer, J.S., Brodribb, T., Burns, M.J., Cavender-Bares, J., Clearwater, M., Cochard, H., Comstock, J., Domec, J.C., 2004. The cohesion-tension theory. New Phytologist 163, 451–452. https://doi.org/10.1111/j.1469-8137.2004.01142.x

Arend, M., Link, R.M., Patthey, R., Hoch, G., Schuldt, B., Kahmen, A., 2021. Rapid hydraulic collapse as cause of drought-induced mortality in conifers. Proc. Natl. Acad. Sci. 118. https://doi.org/10.1073/pnas.2025251118

Atkin, O.K., Edwards, E.J., Loveys, B.R., 2000a. Response of root respiration to changes in temperature and its relevance to global warming. New Phytologist 147, 141–154. https://doi.org/10.1046/j.1469-8137.2000.00683.x

Atkin, O.K., Evans, J.R., Ball, M.C., Lambers, H., Pons, T.L., 2000b. Leaf respiration of snow gum in the light and dark. Interactions between temperature and irradiance. Plant Physiology 122, 915–924. https://doi.org/10.1104/pp.122.3.915

Atkin, O.K., Tjoelker, M.G., 2003. Thermal acclimation and the dynamic response of plant respiration to temperature. Trends Plant Sci. 8, 343–351. https://doi.org/10.1016/S1360-1385(03)00136-5

Bahn, M., Schmitt, M., Siegwolf, R., Richter, A., Brüggemann, N., 2009. Does photosynthesis affect grassland soil-respired CO_2 and its carbon isotope composition on a diurnal timescale? New Phytologist 182, 451–460.

Baker, H.S., Millar, R.J., Karoly, D.J., Beyerle, U., Guillod, B.P., Mitchell, D., Shiogama, H., Sparrow, S., Woollings, T., Allen, M.R., 2018. Higher CO_2 concentrations increase extreme event risk in a 1.5 °C world. Nature Clim Change 8, 604–608. https://doi.org/10.1038/s41558-018-0190-1

Balducci, L., Cuny, H.E., Rathgeber, C.B.K., Deslauriers, A., Giovannelli, A., Rossi, S., 2016. Compensatory mechanisms mitigate the effect of warming and drought on wood formation. Plant Cell Environ. 39, 1338–1352. https://doi.org/10.1111/pce.12689

Balducci, L., Deslauriers, A., Giovannelli, A., Rossi, S., Rathgeber, C.B.K., 2013. Effects of temperature and water deficit on cambial activity and woody ring features in *Picea mariana* saplings. Tree Physiology 33, 1006–1017. https://doi.org/10.1093/treephys/tpt073

Bartlett, M.K., Klein, T., Jansen, S., Choat, B., Sack, L., 2016. The correlations and sequence of plant stomatal, hydraulic, and wilting responses to drought. Proc. Natl. Acad. Sci. 113, 13098–13103. https://doi.org/10.1073/pnas.1604088113

Bartlett, M.K., Scoffoni, C., Sack, L., 2012. The determinants of leaf turgor loss point and prediction of drought tolerance of species and biomes: a global meta-analysis. Ecology Letters 15, 393–405. https://doi.org/10.1111/j.1461-0248.2012.01751.x

Bauweraerts, I., Ameye, M., Wertin, T.M., McGuire, M.A., Teskey, R.O., Steppe, K., 2014. Water availability is the decisive factor for the growth of two tree species in the occurrence of consecutive heat waves. Agric. For. Meteorol. 189–190, 19–29. https://doi.org/10.1016/j.agrformet.2014.01.001

Bauweraerts, I., Wertin, T.M., Ameye, M., McGuire, M.A., Teskey, R.O., Steppe, K., 2013. The effect of heat waves, elevated [CO_2] and low soil water availability on northern red oak (*Quercus rubra* L.) seedlings. Glob. Change Biol. 19, 517–528. https://doi.org/10.1111/gcb.12044

Bernacchi, C.J., Portis, A.R., Nakano, H., 2002. Temperature response of mesophyll conductance. Implications for the determination of Rubisco enzyme kinetics and for limitations to photosynthesis in vivo. Plant Physiology 130, 1992–1998.

Berry, J., Bjorkman, O., 1980. Photosynthetic response and adaptation to temperature in higher plants. Annu. Rev. Plant. Physiol. 31, 491–543. https://doi.org/10.1146/annurev.pp.31.060180.002423

Bertini, G., Amoriello, T., Fabbio, G., Piovosi, M., 2011. Forest growth and climate change: evidences from the ICP-Forests intensive monitoring in Italy. iForest 4, 262–267. https://doi.org/10.3832/ifor0596-004

Bigler, C., Bräker, O.U., Bugmann, H., Dobbertin, M., Rigling, A., 2006. Drought as an inciting mortality factor in Scots pine stands of the Valais, Switzerland. Ecosystems 9, 330–343.

Bigras, F.J., 2000. Selection of white spruce families in the context of climate change: heat tolerance. Tree Physiology 20, 1227–1234. https://doi.org/10.1093/treephys/20.18.1227

Birami, B., Bamberger, I., Ghirardo, A., Grote, R., Arneth, A., Gaona-Colmán, E., Nadal-Sala, D., Ruehr, N.K., 2021. Heatwave frequency and seedling death alter stress-specific emissions of volatile organic compounds in Aleppo pine. Oecologia. https://doi.org/10.1007/s00442-021-04905-y

Birami, B., Gattmann, M., Heyer, A.G., Grote, R., Arneth, A., Ruehr, N.K., 2018. Heat waves alter carbon allocation and increase mortality of Aleppo pine under dry conditions. Front. For. Glob. Change 1. https://doi.org/10.3389/ffgc.2018.00008

Birami, B., Nägele, T., Gattmann, M., Preisler, Y., Gast, A., Arneth, A., Ruehr, N.K., 2020. Hot drought reduces the effects of elevated CO_2 on tree water-use efficiency and carbon metabolism. New Phytologist. nph.16471. https://doi.org/10.1111/nph.16471

Birch, H.F., 1964. Mineralisation of plant nitrogen following alternate wet and dry conditions. Plant and Soil 20, 43–49.

Blankenship, R.E., 2014. Molecular mechanisms of photosynthesis. John Wiley & Sons.

Blessing, C.H., Werner, R.A., Siegwolf, R., Buchmann, N., 2015. Allocation dynamics of recently fixed carbon in beech saplings in response to increased temperatures and drought. Tree Physiology 35, 585–598. https://doi.org/10.1093/treephys/tpv024

Bonan, G.B., 2008. Forests and climate change: Forcings, feedbacks, and the climate benefits of forests. Science 320, 1444–1449.

Bouda, M., Windt, C.W., McElrone, A.J., Brodersen, C.R., 2019. In vivo pressure gradient heterogeneity increases flow contribution of small diameter vessels in grapevine. Nat. Commun. 10, 5645. https://doi.org/10.1038/s41467-019-13673-6

Bradshaw, C.J.A., Warkentin, I.G., 2015. Global estimates of boreal forest carbon stocks and flux. Global and Planetary Change 128, 24–30. https://doi.org/10.1016/j.gloplacha.2015.02.004

Bréda, N., Huc, R., Granier, A., Dreyer, E., 2006. Temperate forest trees and stands under severe drought: a review of ecophysiological responses, adaptation processes and long-term consequences. Ann. For. Sci. 63, 625–644. https://doi.org/10.1051/forest:2006042

Brodersen, C.R., McElrone, A.J., 2013. Maintenance of xylem network transport capacity: A Review of embolism repair in vascular plants. Frontiers in Plant Science 4. https://doi.org/10.3389/fpls.2013.00108

Brodersen, C.R., McElrone, A.J., Choat, B., Matthews, M.A., Shackel, K.A., 2010. The dynamics of embolism repair in xylem: In vivo visualizations using high-resolution computed tomography. Plant Physiology 154, 1088–1095. https://doi.org/10.1104/pp.110.162396

Brodribb, T.J., Bowman, D.J.M.S., Nichols, S., Delzon, S., Burlett, R., 2010. Xylem function and growth rate interact to determine recovery rates after exposure to extreme water deficit. New Phytologist 188, 533–542. https://doi.org/10.1111/j.1469-8137.2010.03393.x

Brodribb, T.J., Cochard, H., 2009. Hydraulic failure defines the recovery and point of death in water-stressed conifers. Plant Physiology 149, 575–584. https://doi.org/10.1104/pp.108.129783

Brodribb, T.J., McAdam, S.A.M., 2013. Abscisic acid mediates a divergence in the drought response of two conifers. Plant Physiology 162, 1370–1377. https://doi.org/10.1104/pp.113.217877

Brodribb, T.J., Powers, J., Cochard, H., Choat, B., 2020. Hanging by a thread? Forests and drought. Science 368, 261–266. https://doi.org/10.1126/science.aat7631

Bucci, S.J., Goldstein, G., Scholz, F.G., Meinzer, F.C., 2016. Physiological significance of hydraulic segmentation, nocturnal transpiration and capacitance in tropical trees: Paradigms revisited, in: Goldstein, G., Santiago, L.S. (Eds.), Tropical Tree Physiology, Tree Physiology. Springer International Publishing, Cham, pp. 205–225. https://doi.org/10.1007/978-3-319-27422-5_9

Buras, A., Rehschuh, R., Lange, J., Fonti., M., Fonti. P., Menzel, A., Gessler, A., von Arx, G., Treydte, K. & Rigling, A. (in preparation). Stable isotopes and xylem anatomy corroborate higher drought-susceptibility of Scots pine at the forest edge.

Buras, A., Schunk, C., Zeiträg, C., Herrmann, C., Kaiser, L., Lemme, H., Straub, C., Taeger, S., Gößwein, S., Klemmt, H.-J., Menzel, A., 2018. Are Scots pine forest edges particularly prone to drought-induced mortality? Environ. Res. Lett. 13, 025001. https://doi.org/10.1088/1748-9326/aaa0b4

Burnham, K., Anderson, D., 2002. Model selection and multi-model inference. Springer, New York.

Burton, A.J., Pregitzer, K.S., Ruess, R.W., Hendrick, R.L., Allen, M.F., 2002. Root respiration in North American forests: Effects of nitrogen concentration and temperature across biomes. Oecologia 131, 559–568.

Canny, M.J., 1998. Applications of the compensating pressure theory of water transport. Am. J. Bot. 85, 897–909. https://doi.org/10.2307/2446355

Cano, F.J., LóPez, R., Warren, C.R., 2014. Implications of the mesophyll conductance to CO_2 for photosynthesis and water-use efficiency during long-term water stress and recovery in two contrasting *Eucalyptus* species. Plant Cell Environ. 37, 2470–2490. https://doi.org/10.1111/pce.12325

Charra-Vaskou, K., Badel, E., Burlett, R., Cochard, H., Delzon, S., Mayr, S., 2012. Hydraulic efficiency and safety of vascular and non-vascular components in *Pinus pinaster* leaves. Tree Physiology 32, 1161–1170. https://doi.org/10.1093/treephys/tps071

Charrier, G., Delzon, S., Domec, J.-C., Zhang, L., Delmas, C.E.L., Merlin, I., Corso, D., King, A., Ojeda, H., Ollat, N., Prieto, J.A., Scholach, T., Skinner, P., van Leeuwen, C., Gambetta, G.A., 2018. Drought will not leave your glass empty: Low risk of hydraulic failure revealed by long-term drought observations in world's top wine regions. Sci. Adv. 4, eaao6969. https://doi.org/10.1126/sciadv.aao6969

Charrier, G., Torres-Ruiz, J.M., Badel, E., Burlett, R., Choat, B., Cochard, H., Delmas, C.E.L., Domec, J.-C., Jansen, S., King, A., Lenoir, N., Martin-StPaul, N., Gambetta, G.A., Delzon, S., 2016. Evidence for hydraulic vulnerability segmentation and lack of xylem refilling under tension. Plant Physiology 172, 1657–1668. https://doi.org/10.1104/pp.16.01079

Chen, J.-W., Zhang, Q., Li, X.-S., Cao, K.-F., 2010. Gas exchange and hydraulics in seedlings of *Hevea brasiliensis* during water stress and recovery. Tree Physiology 30, 876–885. https://doi.org/10.1093/treephys/tpq043

Choat, B., Badel, E., Burlett, R., Delzon, S., Cochard, H., Jansen, S., 2016. Noninvasive measurement of vulnerability to drought-induced embolism by X-ray microtomography. Plant Physiology 170, 273–282. https://doi.org/10.1104/pp.15.00732

Choat, B., Brodersen, C.R., McElrone, A.J., 2015. Synchrotron X-ray microtomography of xylem embolism in *Sequoia sempervirens* saplings during cycles of drought and recovery. New Phytologist 205, 1095–1105. https://doi.org/10.1111/nph.13110

Choat, B., Brodribb, T.J., Brodersen, C.R., Duursma, R.A., López, R., Medlyn, B.E., 2018. Triggers of tree mortality under drought. Nature 558, 531–539. https://doi.org/10.1038/s41586-018-0240-x

Choat, B., Jansen, S., Brodribb, T.J., Cochard, H., Delzon, S., Bhaskar, R., Bucci, S.J., Feild, T.S., Gleason, S.M., Hacke, U.G. et a., 2012. Global convergence in the vulnerability of forests to drought. Nature 491, 752–755. https://doi.org/10.1038/nature11688

Choat, B., Nolf, M., Lopez, R., Peters, J.M.R., Carins-Murphy, M.R., Creek, D., Brodribb, T.J., 2019. Non-invasive imaging shows no evidence of embolism repair after drought in tree species of two genera. Tree Physiology 39, 113–121. https://doi.org/10.1093/treephys/tpy093

Christensen-Dalsgaard, K.K., Tyree, M.T., 2014. Frost fatigue and spring recovery of xylem vessels in three diffuse-porous trees *in situ*: Frost fatigue in diffuse-porous trees. Plant Cell Environ. 37, 1074–1085. https://doi.org/10.1111/pce.12216

Ciais, Ph., Reichstein, M., Viovy, N., Granier, A., Ogée, J., Allard, V., Aubinet, M., Buchmann, N., Bernhofer, Chr., Carrara, A. et al. 2005. Europe-wide reduction in primary productivity caused by the heat and drought in 2003. Nature 437, 529–533. https://doi.org/10.1038/nature03972

Cochard, H., 2002. A technique for measuring xylem hydraulic conductance under high negative pressures. Plant Cell Environ. 25, 815–819. https://doi.org/10.1046/j.1365-3040.2002.00863.x

Cochard, H., Delzon, S., Badel, E., 2015. X-ray microtomography (micro-CT): a reference technology for high-resolution quantification of xylem embolism in trees. Plant, Cell & Environment 38, 201–206. https://doi.org/10.1111/pce.12391

Cochard, H., Froux, F., Mayr, S., Coutand, C., 2004. Xylem wall collapse in water-stressed pine needles. Plant Physiology 134, 401–408. https://doi.org/10.1104/pp.103.028357

Colombo, S.J., 1992. Clonal variation in heat tolerance and heat shock protein expression in black spruce. Silvae Genet. 41, 234–239.

Correia, B., Valledor, L., Meijón, M., Rodriguez, J.L., Dias, M.C., Santos, C., Cañal, M.J., Rodriguez, R., Pinto, G., 2013. Is the interplay between epigenetic markers related to the acclimation of Cork oak plants to high temperatures? PLoS ONE 8, e53543. https://doi.org/10.1371/journal.pone.0053543

Coumou, D., Robinson, A., Rahmstorf, S., 2013. Global increase in record-breaking monthly-mean temperatures. Clim. Change 118, 771–782. https://doi.org/10.1007/s10584-012-0668-1

Creek, D., Blackman, C.J., Brodribb, T.J., Choat, B., Tissue, D.T., 2018. Coordination between leaf, stem and root hydraulics and gas exchange in three arid-zone angiosperms during severe drought and recovery. Plant Cell Environ 41, 2869–2881. https://doi.org/10.1111/pce.13418

Cruiziat, P., Cochard, H., Ameglio, T., 2002. Hydraulic architecture of trees: main concepts and results. Ann. For. Sci. 59, 723–752. https://doi.org/10.1051/forest:2002060

Cui, M., Caldwell, M.M., 1997. A large ephemeral release of nitrogen upon wetting of dry soil and corresponding root responses in the field. Plant and Soil 191, 291–299.

Cuneo, I.F., Barrios-Masias, F., Knipfer, T., Uretsky, J., Reyes, C., Lenain, P., Brodersen, C.R., Walker, M.A., McElrone, A.J., 2020. Differences in grapevine rootstock sensitivity and recovery from drought are linked to fine root cortical lacunae and root tip function. New Phytologist nph.16542. https://doi.org/10.1111/nph.16542

Cuny, H.E., Fonti, P., Rathgeber, C.B.K., Arx, G., Peters, R.L., Frank, D.C., 2019. Couplings in cell differentiation kinetics mitigate air temperature influence on conifer wood anatomy. Plant Cell Environ. 42, 1222–1232. https://doi.org/10.1111/pce.13464

Cuny, H.E., Rathgeber, C.B.K., 2016. Xylogenesis: Coniferous trees of temperate forests are listening to the climate tale during the growing season but only remember the last words! Plant Physiology 171, 306–317. https://doi.org/10.1104/pp.16.00037

Cuny, H.E., Rathgeber, C.B.K., Frank, D., Fonti, P., Fournier, M., 2014. Kinetics of tracheid development explain conifer tree-ring structure. New Phytologist 203, 1231–1241. https://doi.org/10.1111/nph.12871

Dalla-Salda, G., Fernández, M.E., Sergent, A.-S., Rozenberg, P., Badel, E., Martinez-Meier, A., 2014. Dynamics of cavitation in a Douglas-fir tree-ring: transition-wood, the lord of the ring? J. Plant Hydraul. 1, 005. https://doi.org/10.20870/jph.2014.e005

Daniel, R.M., Danson, M.J., Eisenthal, R., Lee, C.K., Peterson, M.E., 2008. The effect of temperature on enzyme activity: new insights and their implications. Extremophiles 12, 51–59. https://doi.org/10.1007/s00792-007-0089-7

Dannenmann, M., Bimüller, C., Gschwendtner, S., Leberecht, M., Tejedor, J., Bilela, S., Gasche, R., Hanewinkel, M., Baltensweiler, A., Kögel-Knabner, I. et al. 2016. Climate change impairs

nitrogen cycling in European beech forests. PLOS ONE 11, e0158823. https://doi.org/10.1371/journal.pone.0158823

Dannenmann, M., Simon, J., Gasche, R., Holst, J., Naumann, P.S., Kögel-Knabner, I., Knicker, H., Mayer, H., Schloter, M., Pena, R., Polle, A., Rennenberg, H., Papen, H., 2009. Tree girdling provides insight on the role of labile carbon in nitrogen partitioning between soil microorganisms and adult European beech. Soil Biology and Biochemistry 41, 1622–1631. https://doi.org/10.1016/j.soilbio.2009.04.024

Dannoura, M., Maillard, P., Fresneau, C., Plain, C., Berveiller, D., Gerant, D., Chipeaux, C., Bosc, A., Ngao, J., Damesin, C., Loustau, D., Epron, D., 2011. In situ assessment of the velocity of carbon transfer by tracing ^{13}C in trunk CO2 efflux after pulse labelling: variations among tree species and seasons. New Phytologist 190, 181–192. https://doi.org/10.1111/j.1469-8137.2010.03599.x

Davidson, E.A., Janssens, I.A., Luo, Y., 2006. On the variability of respiration in terrestrial ecosystems: moving beyond Q_{10}. Glob. Change Biol. 12, 154–164. https://doi.org/10.1111/j.1365-2486.2005.01065.x

Davies-Colley, R.J., Payne, G.W., Elswijk, M. van, 2000. Microclimate gradients across a forest edge. New Zealand Journal of Ecology 24, 111–121.

De Baerdemaeker, N.J.F., Arachchige, K.N.R., Zinkernagel, J., Van den Bulcke, J., Van Acker, J., Schenk, H.J., Steppe, K., 2019. The stability enigma of hydraulic vulnerability curves: addressing the link between hydraulic conductivity and drought-induced embolism. Tree Physiology 39, 1646–1664. https://doi.org/10.1093/treephys/tpz078

De Kauwe, M.G., Medlyn, B.E., Pitman, A.J., Drake, J.E., Ukkola, A., Griebal, A., Pendall, E., Prober, S., Roderick, M., 2018. Examining the evidence for sustained transpiration during heatextremes (preprint). Biogeophysics: Ecohydrology. https://doi.org/10.5194/bg-2018-399

Demidchik, V., Straltsova, D., Medvedev, S.S., Pozhvanov, G.A., Sokolik, A., Yurin, V., 2014. Stress-induced electrolyte leakage: the role of K+-permeable channels and involvement in programmed cell death and metabolic adjustment. Journal of Experimental Botany 1259–1270.

De Schepper, V., De Swaef, T., Bauweraerts, I., Steppe, K., 2013. Phloem transport: a review of mechanisms and controls. Journal of Experimental Botany 64, 4839–4850. https://doi.org/10.1093/jxb/ert302

Deslauriers, A., Beaulieu, M., Balducci, L., Giovannelli, A., Gagnon, M.J., Rossi, S., 2014. Impact of warming and drought on carbon balance related to wood formation in black spruce. Ann. Bot. 114, 335–345. https://doi.org/10.1093/aob/mcu111

DeSoto, L., Cailleret, M., Sterck, F., Jansen, S., Kramer, K., Robert, E.M.R., Aakala, T., Amoroso, M.M., Bigler, C., Camarero, J.J., Čufar, K. et al., 2020. Low growth resilience to drought is related to future mortality risk in trees. Nat. Commun. 11, 545. https://doi.org/10.1038/s41467-020-14300-5

Dietze, M.C., Sala, A., Carbone, M.S., Czimczik, C.I., Mantooth, J.A., Richardson, A.D., Vargas, R., 2014. Nonstructural carbon in woody plants. Annu. Rev. Plant biology 65, 667–687. https://doi.org/10.1146/annurev-arplant-050213-040054

Dixon, H.H., Joly, J., 1895. On the ascent of sap. Philos. Trans. R. Soc. London 563–576.

Dlugokencky, E., Tans, P., 2021. Trends in atmospheric carbon dioxide, National Oceanic & Atmospheric Administration, Earth System Research Laboratory (NOAA/ESRL), available at: http:// www.esrl.noaa.gov/gmd/ccgg/trends/global.html, last access: 10 May 2021.

Domec, J.C., Gartner, B.L., 2002. How do water transport and water storage differ in coniferous earlywood and latewood? Journal of Experimental Botany 53, 2369–2379. https://doi.org/10.1093/jxb/erf100

Domec, Lachenbruch, Meinzer, 2006. Bordered pit structure and function determine spatial patterns of air-seeding thresholds in xylem of Douglas-fir (*Pseudotsuga menziesii; Pinaceae*) trees. Am. J. Bot. 93, 1588–1600. https://doi.org/10.3732/ajb.93.11.1588

Drakakaki, G., 2015. Polysaccharide deposition during cytokinesis: Challenges and future perspectives. Plant Sci. 236, 177–184. https://doi.org/10.1016/j.plantsci.2015.03.018

Drake, J.E., Furze, M.E., Tjoelker, M.G., Carrillo, Y., Barton, C.V.M., Pendall, E., 2019. Climate warming and tree carbon use efficiency in a whole-tree $^{13}CO_2$ tracer study. New Phytologist 222, 1313–1324. https://doi.org/10.1111/nph.15721

Drake, J.E., Tjoelker, M.G., Medlyn, B.E., Reich, P.B., Leigh, A., Pfautsch, S., Blackman, C.J., Lo, R., Duursma, R.A., Kumarathunge, D., Kauwe, M.G.D., Jiang, M., Nicotra, A.B., Tissue, D.T., Choat, B., Atkin, O.K., Barton, C.V.M., 2018. Trees tolerate an extreme heatwave via sustained transpirational cooling and increased leaf thermal tolerance. Glob. Change Biol. 24(6), 2390–2402.

Duarte, A.G., Katata, G., Hoshika, Y., Hossain, M., Kreuzwieser, J., Arneth, A., Ruehr, N.K., 2016. Immediate and potential long-term effects of consecutive heat waves on the photosynthetic performance and water balance in Douglas-fir. J. Plant Physiology 205, 57–66. https://doi.org/10.1016/j.jplph.2016.08.012

Dusenge, M.E., Duarte, A.G., Way, D.A., 2019. Plant carbon metabolism and climate change: elevated CO_2 and temperature impacts on photosynthesis, photorespiration and respiration. New Phytologist 221, 32–49. https://doi.org/10.1111/nph.15283

Duursma, R., Choat, B., 2017. fitplc - an R package to fit hydraulic vulnerability curves. J. Plant Hydraul. 4, 1–14. https://doi.org/10.20870/jph.2017.e002

Dyckmans, J., Flessa, H., 2001. Influence of tree internal N status on uptake and translocation of C and N in beech: a dual ^{13}C and ^{15}N labeling approach. Tree Physiology 21, 395–401. https://doi.org/10.1093/treephys/21.6.395

Earles, M.J., Sperling, O., Silva, L.C.R., McElrone, A.J., Brodersen, C.R., North, M.P., Zwieniecki, M.A., 2016. Bark water uptake promotes localized hydraulic recovery in coastal redwood crown: Localized hydraulic recovery via bark water uptake. Plant Cell Environ. 39, 320–328. https://doi.org/10.1111/pce.12612

Ellenberg, H., Leuschner, C., 2010. Vegetation Mitteleuropas mit den Alpen: in ökologischer, dynamischer und historischer Sicht, Vol. 8104. ed. Utb.

Endrulat, T., Saurer, M., Buchmann, N., Brunner, I., 2010. Incorporation and remobilization of 13C within the fine-root systems of individual *Abies alba* trees in a temperate coniferous stand. Tree Physiology 30, 1515–1527. https://doi.org/10.1093/treephys/tpq090

Epron, D., Bahn, M., Derrien, D., Lattanzi, F.A., Pumpanen, J., Gessler, A., Hogberg, P., Maillard, P., Dannoura, M., Gerant, D., Buchmann, N., 2012. Pulse-labelling trees to study carbon allocation dynamics: a review of methods, current knowledge and future prospects. Tree Physiology 32, 776–798. https://doi.org/10.1093/treephys/tps057

Escandón, M., Cañal, M.J., Pascual, J., Pinto, G., Correia, B., Amaral, J., Meijón, M., 2016. Integrated physiological and hormonal profile of heat-induced thermotolerance in *Pinus radiata*. Tree Physiology 36, 63–77. https://doi.org/10.1093/treephys/tpv127

Etzold, S., Ziemińska, K., Rohner, B., Bottero, A., Bose, A.K., Ruehr, N.K., Zingg, A., Rigling, A., 2019. One century of forest monitoring data in Switzerland reveals species- and site-specific trends of climate-induced tree mortality. Front. Plant Sci. 10, 307. https://doi.org/10.3389/fpls.2019.00307

FAO, 2020. Global forest resources assessment 2020. Rome.

Farquhar, G.D., Ehleringer, J.R., Hubick, K.T., 1989. Carbon isotope discrimination and photosynthesis. Annual review of plant biology 40, 503–537.

Farquhar, G.D., O'Leary, M., Berry, J., 1982. On the relationship between carbon isotope discrimination and the intercellular carbon dioxide concentration in leaves. Functional Plant Biol. 9, 121. https://doi.org/10.1071/PP9820121

Feller, U., Crafts-Brandner, S.J., Salvucci, M.E., 1998. Moderately High Temperatures Inhibit Ribulose-1,5-Bisphosphate Carboxylase/Oxygenase (Rubisco) Activase-Mediated Activation of Rubisco. Plant Physiology 116, 539–546.

Filewod, B., Thomas, S.C., 2014. Impacts of a spring heat wave on canopy processes in a northern hardwood forest. Glob Change Biol 20, 360–371. https://doi.org/10.1111/gcb.12354

Fisher, J.B., Badgley, G., Blyth, E., 2012. Global nutrient limitation in terrestrial vegetation. Global Biogeochem. Cycles 26, 2011GB004252. https://doi.org/10.1029/2011GB004252

Flexas, J., Medrano, H., 2002. Drought-inhibition of Photosynthesis in C3 Plants: Stomatal and Non-stomatal Limitations Revisited. Annals of Botany 89, 183–189. https://doi.org/10.1093/aob/mcf027

Fotelli, M.N., Rennenberg, H., Geßler, A., 2002. Effects of Drought on the Competitive Interference of an Early Successional Species (Rubus fruticosus) on Fagus sylvatica L. Seedlings: 15N Uptake and Partitioning, Responses of Amino Acids and other N Compounds. Plant biol 4, 311–320. https://doi.org/10.1055/s-2002-32334

Fotelli, M.N., Rienks, M., Rennenberg, H., Geßler, A., 2004. Climate and forest management affect 15 N-uptake, N balance and biomass of European beech seedlings. Trees - Struct. Funct. 18, 157–166. https://doi.org/10.1007/s00468-003-0289-4

Freschet, G.T., Violle, C., Bourget, M.Y., Scherer-Lorenzen, M., Fort, F., 2018. Allocation, morphology, physiology, architecture: the multiple facets of plant above- and below-ground responses to resource stress. New Phytol 219, 1338–1352. https://doi.org/10.1111/nph.15225

Friedlingstein, P., Jones, M.W., O'Sullivan, M., Andrew, R.M., Hauck, J., Peters, G.P., Peters, W., Pongratz, J., Sitch, S., Le Quéré, C., et al., 2019. Global Carbon Budget 2019. Earth Syst. Sci. Data 11, 1783–1838. https://doi.org/10.5194/essd-11-1783-2019

Fuentes, L., Duguy, B., Nadal-Sala, D., 2018. Short-term effects of spring prescribed burning on the understory vegetation of a *Pinus halepensis* forest in Northeastern Spain. Sci. Total Environ. 610–611, 720–731. https://doi.org/10.1016/j.scitotenv.2017.08.050

Galiano, L., Martínez-Vilalta, J., Lloret, F., 2011. Carbon reserves and canopy defoliation determine the recovery of Scots pine 4 yr after a drought episode. New Phytologist 190, 750–759. https://doi.org/10.1111/j.1469-8137.2010.03628.x

Galiano, L., Timofeeva, G., Saurer, M., Siegwolf, R., Martínez-Vilalta, J., Hommel, R., Gessler, A., 2017. The fate of recently fixed carbon after drought release: towards unravelling C storage regulation in *Tilia platyphyllos* and *Pinus sylvestris*: The fate of recently fixed C after drought release. Plant Cell Environ. 40, 1711–1724. https://doi.org/10.1111/pce.12972

Gattmann, M., Birami, B., Nadal Sala, D., Ruehr, N.K., 2020. Dying by drying: Timing of physiological stress thresholds related to tree death is not significantly altered by highly elevated CO_2. Plant Cell Environ. pce.13937. https://doi.org/10.1111/pce.13937

Gaul, D., Hertel, D., Borken, W., Matzner, E., Leuschner, C., 2008. Effects of experimental drought on the fine root system of mature Norway spruce. Forest Ecology and Management 9.

Gauthier, P.P.G., Crous, K.Y., Ayub, G., Duan, H., Weerasinghe, L.K., Ellsworth, D.S., Tjoelker, M.G., Evans, J.R., Tissue, D.T., Atkin, O.K., 2014. Drought increases heat tolerance of leaf respiration in *Eucalyptus globulus* saplings grown under both ambient and elevated atmospheric [CO_2] and temperature. Journal of Experimental Botany 65, 6471–6485. https://doi.org/10.1093/jxb/eru367

Gea-Izquierdo, G., 2021. Holm oak death is accelerated but not sudden and expresses drought legacies. Science of the Total Environment 754, 12.

Gentine, P., Guérin, M., Uriarte, M., McDowell, N.G., Pockman, W.T., 2016. An allometry-based model of the survival strategies of hydraulic failure and carbon starvation. Ecohydrol. 9, 529–546. https://doi.org/10.1002/eco.1654

Gessler, A., Jung, K., Gasche, R., Papen, H., Heidenfelder, A., Börner, E., Metzler, B., Augustin, S., Hildebrand, E., Rennenberg, H., 2005. Climate and forest management influence nitrogen balance of European beech forests: microbial N transformations and inorganic N net uptake capacity of mycorrhizal roots. Eur. J. For. Res. 124, 95–111. https://doi.org/10.1007/s10342-005-0055-9

Gessler, A., Schaub, M., McDowell, N.G., 2017. The role of nutrients in drought-induced tree mortality and recovery. New Phytologist 214, 513–520. https://doi.org/10.1111/nph.14340

Gessler, A., Schneider, S., Von Sengbusch, D., Weber, P., Hanemann, U., Huber, C., Rothe, A., Kreutzer, K., Rennenberg, H., 1998. Field and laboratory experiments on net uptake of nitrate and ammonium by the roots of spruce *(Picea abies*) and beech (*Fagus sylvatica*) trees. New Phytologist. 138, 275–285. https://doi.org/10.1046/j.1469-8137.1998.00107.x

Geβler, A., Keitel, C., Nahm, M., Rennenberg, H., 2004a. Water shortage affects the water and nitrogen balance in central European beech forests. Plant Biology 6, 289–298. https://doi.org/10.1055/s-2004-820878

Geβler, A., Kopriva, S., Rennenberg, H., 2004b. Regulation of nitrate uptake at the whole-tree level: interaction between nitrogen compounds, cytokinins and carbon metabolism. Tree Physiology 24, 1313–1321. https://doi.org/10.1093/treephys/24.12.1313

Giri, A., Heckathorn, S., Mishra, S., Krause, C., 2017. Heat stress decreases levels of nutrient-uptake and -assimilation proteins in tomato roots. Plants 6, 6. https://doi.org/10.3390/plants6010006

Gleason, S.M., Wiggans, D.R., Bliss, C.A., Young, J.S., Cooper, M., Willi, K.R., Comas, L.H., 2017. Embolized stems recover overnight in Zea mays: The role of soil water, root pressure, and nighttime transpiration. Front. Plant Sci. 8, 662. https://doi.org/10.3389/fpls.2017.00662

Gößwein, S., Lemme, H., Buras, A., Schunk, C., Menzel, A., Straub, C., Mette, T., Taeger, S., 2017. Kiefernschäden in Bayern. LWF Aktuell 112, 12–13.

Gričar, J., 2013. Influence of temperature on cambial activity and cell differentiation in *Quercus Sessiliflora* and *Acer Pseudoplatanus* of different ages. Drv. Ind. 64, 95–105. https://doi.org/10.5552/drind.2013.1246

Gričar, J., Zupančič, M., Čufar, K., Oven, P., 2007. Regular cambial activity and xylem and phloem formation in locally heated and cooled stem portions of Norway spruce. Wood Sci. Technol. 41, 463–475. https://doi.org/10.1007/s00226-006-0109-2

Grossiord, C., Buckley, T.N., Cernusak, L.A., Novick, K.A., Poulter, B., Siegwolf, R.T.W., Sperry, J.S., McDowell, N.G., 2020. Plant responses to rising vapor pressure deficit. New Phytologist 226, 1550–1566. https://doi.org/10.1111/nph.16485

Gruber, A., Zimmermann, J., Wieser, G., Oberhuber, W., 2009. Effects of climate variables on intra-annual stem radial increment in *Pinus cembra* (L.) along the alpine treeline ecotone. Ann. For. Sci. 66, 503–503. https://doi.org/10.1051/forest/2009038

Guha, A., Han, J., Cummings, C., McLennan, D.A., Warren, J.M., 2018. Differential ecophysiological responses and resilience to heat wave events in four co-occurring temperate tree species. Environ. Res. Lett. 13, 065008. https://doi.org/10.1088/1748-9326/aabcd8

Gupta, S.K., Ram, J., Singh, H., 2018. Comparative Study of Transpiration in Cooling Effect of Tree Species in the Atmosphere. GEP 06, 151–166. https://doi.org/10.4236/gep.2018.68011

Hacke, U.G., Sperry, J.S., 2003. Limits to xylem refilling under negative pressure in *Laurus nobilis* and *Acer negundo*: Refilling under negative pressure. Plant, Cell & Environment 26, 303–311. https://doi.org/10.1046/j.1365-3040.2003.00962.x

Hafner, B.D., Hesse, B.D., Grams, T.E.E., 2021. Friendly neighbours: Hydraulic redistribution accounts for one quarter of water used by neighbouring drought stressed tree saplings. Plant Cell Environ 44, 1243–1256. https://doi.org/10.1111/pce.13852

Hafner, B.D., Tomasella, M., Häberle, K.-H., Goebel, M., Matyssek, R., Grams, T.E.E., 2017. Hydraulic redistribution under moderate drought among English oak, European beech and Norway spruce determined by deuterium isotope labeling in a split-root experiment. Tree Physiology 37, 950–960. https://doi.org/10.1093/treephys/tpx050

Hagedorn, F., Joseph, J., Peter, M., Luster, J., Pritsch, K., Geppert, U., Kerner, R., Molinier, V., Egli, S., Schaub, M., Liu, J.-F., Li, M., Sever, K., Weiler, M., Siegwolf, R.T.W., Gessler, A., Arend, M., 2016. Recovery of trees from drought depends on belowground sink control. Nat. Plants 2. https://doi.org/10.1038/nplants.2016.111

Hammond, W.M., Yu, K., Wilson, L.A., Will, R.E., Anderegg, W.R.L., Adams, H.D., 2019. Dead or dying? Quantifying the point of no return from hydraulic failure in drought-induced tree mortality. New Phytologist 223, 1834–1843. https://doi.org/10.1111/nph.15922

Hanewinkel, M., Cullmann, D.A., Schelhaas, M.-J., Nabuurs, G.-J., Zimmermann, N.E., 2013. Climate change may cause severe loss in the economic value of European forest land. Nat. Clim. Change 3, 203–207. https://doi.org/10.1038/nclimate1687

Hao, Z., AghaKouchak, A., Phillips, T.J., 2013. Changes in concurrent monthly precipitation and temperature extremes. Environ. Res. Lett. 8, 034014. https://doi.org/10.1088/1748-9326/8/3/034014

Harfouche, A., Meilan, R., Altman, A., 2014. Molecular and physiological responses to abiotic stress in forest trees and their relevance to tree improvement. Tree Physiology 34, 1181–1198. https://doi.org/10.1093/treephys/tpu012

Hartmann, H., Adams, H.D., Hammond, W.M., Hoch, G., Landhäusser, S.M., Wiley, E., Zaehle, S., 2018a. Identifying differences in carbohydrate dynamics of seedlings and mature trees to improve carbon allocation in models for trees and forests. Environmental and Experimental Botany 152, 7–18. https://doi.org/10.1016/j.envexpbot.2018.03.011

Hartmann, H., McDowell, N.G., Trumbore, S., 2015. Allocation to carbon storage pools in Norway spruce saplings under drought and low CO2. Tree Physiology 35, 243–252. https://doi.org/10.1093/treephys/tpv019

Hartmann, H., Moura, C.F., Anderegg, W.R.L., Ruehr, N.K., Salmon, Y., Allen, C.D., Arndt, S.K., Breshears, D.D., Davi, H., Galbraith, D., Ruthrof, K.X., Wunder, J., Adams, H.D., Bloemen, J., Cailleret, M., Cobb, R., Gessler, A., Grams, T.E.E., Jansen, S., Kautz, M., Lloret, F., O'Brien, M., 2018b. Research frontiers for improving our understanding of drought-induced tree and forest mortality. New Phytologist 218, 15–28.

Hartmann, H., Trumbore, S., 2016. Understanding the roles of nonstructural carbohydrates in forest trees – from what we can measure to what we want to know. New Phytologist 211, 386–403. https://doi.org/10.1111/nph.13955

Herschbach, C., Gessler, A., Rennenberg, H., 2012. Long-distance transport and plant internal cycling of N- and S-compounds, In: Lüttge, U., Beyschlag, W., Büdel, B., Francis, D. (Eds.), Progress in Botany Vol. 73, Progress in Botany. Springer Berlin Heidelberg, Berlin, Heidelberg, pp. 161–188. https://doi.org/10.1007/978-3-642-22746-2_6

Hesse, B.D., Goisser, M., Hartmann, H., Grams, T.E.E., 2019. Repeated summer drought delays sugar export from the leaf and impairs phloem transport in mature beech. Tree Physiology 39, 192–200. https://doi.org/10.1093/treephys/tpy122

Hoch, G., Richter, A., Körner, Ch., 2003. Non-structural carbon compounds in temperate forest trees. Plant, Cell & Environment 26, 1067–1081. https://doi.org/10.1046/j.0016-8025.2003.01032.x

Högberg, P., Nordgren, A., Buchmann, N., Taylor, A.F.S., Ekblad, A., Högberg, M.N., Nyberg, G., Ottosson-Löfvenius, M., Read, D.J., 2001. Large-scale forest girdling shows that current photosynthesis drives soil respiration. Nature 411, 789–792. https://doi.org/10.1038/35081058

Holbrook, N.M., Ahrens, E.T., Burns, M.J., Zwieniecki, M.A., 2001. In vivo observation of cavitation and embolism repair using magnetic resonance imaging. Plant Physiology 126, 27–31. https://doi.org/10.1104/pp.126.1.27

Holopainen, J., 2004. Multiple functions of inducible plant volatiles. Trends in Plant Science 9, 529–533. https://doi.org/10.1016/j.tplants.2004.09.006

Hölttä, T., Mencuccini, M., Nikinmaa, E., 2009. Linking phloem function to structure: Analysis with a coupled xylem–phloem transport model. Journal of Theoretical Biology 259, 325–337. https://doi.org/10.1016/j.jtbi.2009.03.039

Hubau, W., Lewis, S.L., Phillips, O.L., Affum-Baffoe, K., Beeckman, H., Cuní-Sanchez, A., Daniels, A.K., Ewango, C.E.N., Fauset, S., Mukinzi, J.M., et al., 2020. Asynchronous carbon sink saturation in African and Amazonian tropical forests. Nature 579, 80–87. https://doi.org/10.1038/s41586-020-2035-0

Ionita, M., Tallaksen, L.M., Kingston, D.G., Stagge, J.H., Laaha, G., Van Lanen, H.A.J., Scholz, P., Chelcea, S.M., Haslinger, K., 2017. The European 2015 drought from a climatological perspective. Hydrol. Earth Syst. Sci. 21, 1397–1419. https://doi.org/10.5194/hess-21-1397-2017

IPCC, 2018. Summary for policymakers. In: Global Warming of 1.5°C.

Itter, M.S., D'Orangeville, L., Dawson, A., Kneeshaw, D., Duchesne, L., Finley, A.O., 2019. Boreal tree growth exhibits decadal-scale ecological memory to drought and insect defoliation, but no negative response to their interaction. J Ecol 107, 1288–1301. https://doi.org/10.1111/1365-2745.13087

Ivans, C.Y., Leffler, A.J., Spaulding, U., Stark, J.M., Ryel, R.J., Caldwell, M.M., 2003. Root responses and nitrogen acquisition by *Artemisia tridentata* and *Agropyron desertorum* following small summer rainfall events. Oecologia 134, 317–324. https://doi.org/10.1007/s00442-002-1089-z

Jacob, D., Petersen, J., Eggert, B., Alias, A., Christensen, O.B., Bouwer, L.M., Braun, A., Colette, A., Déqué, M., Georgievski, G., et al. 2014. EURO-CORDEX: new high-resolution climate change projections for European impact research. Reg Environ Change 14, 563–578. https://doi.org/10.1007/s10113-013-0499-2

Jaime, L., Batllori, E., Margalef-Marrase, J., Pérez Navarro, M.Á., Lloret, F., 2019. Scots pine (*Pinus sylvestris* L.) mortality is explained by the climatic suitability of both host tree and bark beetle populations. For. Ecol. Manag. 448, 119–129. https://doi.org/10.1016/j.foreco.2019.05.070

Jarvi, M.P., Burton, A.J., 2013. Acclimation and soil moisture constrain sugar maple root respiration in experimentally warmed soil. Tree Physiology 33, 949–959. https://doi.org/10.1093/treephys/tpt068

Jensen, K.H., Berg-Sørensen, K., Bruus, H., Holbrook, N.M., Liesche, J., Schulz, A., Zwieniecki, M.A., Bohr, T., 2016. Sap flow and sugar transport in plants. Rev. Mod. Phys. 88, 035007. https://doi.org/10.1103/RevModPhys.88.035007

Johnson, D.M., McCulloh, K.A., Woodruff, D.R., Meinzer, F.C., 2012. Hydraulic safety margins and embolism reversal in stems and leaves: Why are conifers and angiosperms so different? Plant Sci. 195, 48–53. https://doi.org/10.1016/j.plantsci.2012.06.010

Johnson, D.M., Meinzer, F.C., Woodruff, D.R., Mcculloh, K.A., 2009. Leaf xylem embolism, detected acoustically and by cryo-SEM, corresponds to decreases in leaf hydraulic conductance in four evergreen species. Plant Cell Environ. 32, 828–836. https://doi.org/10.1111/j.1365-3040.2009.01961.x

Johnson, M.G., Tingey, D.T., Phillips, D.L., Storm, M.J., 2001. Advancing fine root research with minirhizotrons. Environmental and Experimental Botany 45, 263–289. https://doi.org/10.1016/S0098-8472(01)00077-6

Jonsson, M., Bengtsson, J., Gamfeldt, L., Moen, J., Snäll, T., 2019. Levels of forest ecosystem services depend on specific mixtures of commercial tree species. Nat. Plants 5, 141–147. https://doi.org/10.1038/s41477-018-0346-z

Joseph, J., Gao, D., Backes, B., Bloch, C., Brunner, I., Gleixner, G., Haeni, M., Hartmann, H., Hoch, G., Hug, C. et al. 2020. Rhizosphere activity in an old-growth forest reacts rapidly to changes in soil moisture and shapes whole-tree carbon allocation. Proc. Natl. Acad. Sci. 117, 24885–24892. https://doi.org/10.1073/pnas.2014084117

Kaack, L., Altaner, C.M., Carmesin, C., Diaz, A., Holler, M., Kranz, C., Neusser, G., Odstrcil, M., Jochen Schenk, H., Schmidt, V., Weber, M., Zhang, Y., Jansen, S., 2019. Function and three-dimensional structure of intervessel pit membranes in angiosperms: a review. IAWA J. 40, 673–702. https://doi.org/10.1163/22941932-40190259

Kagawa, A., Sugimoto, A., Maximov, T.C., 2006. Seasonal course of translocation, storage and remobilization of ^{13}C pulse-labeled photoassimilate in naturally growing *Larix gmelinii* saplings. New Phytologist 171, 793–804. https://doi.org/10.1111/j.1469-8137.2006.01780.x

Kannenberg, S.A., Novick, K.A., Alexander, M.R., Maxwell, J.T., Moore, D.J.P., Phillips, R.P., Anderegg, W.R.L., 2019a. Linking drought legacy effects across scales: From leaves to tree rings to ecosystems. Glob Change Biol 25, 2978–2992. https://doi.org/10.1111/gcb.14710

Kannenberg, S.A., Novick, K.A., Phillips, R.P., 2019b. Anisohydric behavior linked to persistent hydraulic damage and delayed drought recovery across seven North American tree species. New Phytol 222, 1862–1872. https://doi.org/10.1111/nph.15699

Keel, S.G., Siegwolf, R.T.W., Jäggi, M., Körner, C., 2007. Rapid mixing between old and new C pools in the canopy of mature forest trees. Plant Cell Environ 30, 963–972. https://doi.org/10.1111/j.1365-3040.2007.01688.x

Klein, D., Schulz, C., 2011. Wälder und Holzprodukte als Kohlenstoffspeicher. LWF Aktuell 85, 40–43.

Klein, T., Cohen, S., Paudel, I., Preisler, Y., Rotenberg, E., Yakir, D., 2016. Diurnal dynamics of water transport, storage and hydraulic conductivity in pine trees under seasonal drought. IForest - Biogeosciences For. 9, 710–719. https://doi.org/10.3832/ifor2046-009

Klein, T., Hemming, D., Lin, T., Grünzweig, J.M., Maseyk, K., Rotenberg, E., Yakir, D., 2005. Association between tree-ring and needle $\delta^{13}C$ and leaf gas exchange in *Pinus halepensis* under semi-arid conditions. Oecologia 144, 45–54. https://doi.org/10.1007/s00442-005-0002-y

Klein, T., Hoch, G., 2015. Tree carbon allocation dynamics determined using a carbon mass balance approach. New Phytol 205, 147–159. https://doi.org/10.1111/nph.12993

Klein, T., Zeppel, M.J.B., Anderegg, W.R.L., Bloemen, J., De Kauwe, M.G., Hudson, P., Ruehr, N.K., Powell, T.L., von Arx, G., Nardini, A., 2018. Xylem embolism refilling and resilience against drought-induced mortality in woody plants: processes and trade-offs. Ecol. Res. https://doi.org/10.1007/s11284-018-1588-y

Körner, C., 2019. No need for pipes when the well is dry—a comment on hydraulic failure in trees. Tree Physiology 39, 695–700. https://doi.org/10.1093/treephys/tpz030

Krakau, U.K., Liesebach, M., Aronen, T., Lelu-Walter, M.A., Schneck, V., 2013. Scots pine (*Pinus sylvestris* L.). In Forest tree breeding in Europe 267-323. Springer, Dordrecht.

Kreuzwieser, J., Gessler, A., 2010. Global climate change and tree nutrition: influence of water availability. Tree Physiology 30, 1221–1234. https://doi.org/10.1093/treephys/tpq055

Kumarathunge, D.P., Drake, J.E., Tjoelker, M.G., López, R., Pfautsch, S., Vårhammar, A., Medlyn, B.E., 2020. The temperature optima for tree seedling photosynthesis and growth depend on water inputs. Glob. Change Biol. gcb.14975. https://doi.org/10.1111/gcb.14975

Kurz, W.A., Stinson, G., Rampley, G.J., Dymond, C.C., Neilson, E.T., 2008. Risk of natural disturbances makes future contribution of Canada's forests to the global carbon cycle highly uncertain. Proceedings of the National Academy of Sciences 105, 1551–1555. https://doi.org/10.1073/pnas.0708133105

Kuznetsova, A., Brockhoff, P.B., Christensen, R.H.B., 2017. lmerTest Package: Tests in Linear Mixed Effects Models. J. Stat. Softw. 82. https://doi.org/10.18637/jss.v082.i13

Kuzyakov, Y., Gavrichkova, O., 2010. Time lag between photosynthesis and carbon dioxide efflux from soil: a review of mechanisms and controls. Global Change Biology 16, 3386–3406. https://doi.org/10.1111/j.1365-2486.2010.02179.x

Lalonde, S., Tegeder, M., Throne-Holst, M., Frommer, W.B., Patrick, J.W., 2003. Phloem loading and unloading of sugars and amino acids. Plant Cell Environ. 26, 37–56. https://doi.org/10.1046/j.1365-3040.2003.00847.x

Landhäusser, S.M., Chow, P.S., Dickman, L.T., Furze, M.E., Kuhlman, I., Schmid, S., Wiesenbauer, J., Wild, B., Gleixner, G., Hartmann, H., Hoch, G., McDowell, N.G., Richardson, A.D., Richter, A., Adams, H.D., 2018. Standardized protocols and procedures can precisely and accurately quantify non-structural carbohydrates. Tree Physiology 38, 1764–1778. https://doi.org/10.1093/treephys/tpy118

Larkindale, J., Knight, M.R., 2002. Protection against heat stress-induced oxidative damage in Arabidopsis involves calcium, abscisic acid, ethylene, and salicylic acid. Plant Physioloy 128, 682–695. https://doi.org/10.1104/pp.010320

Laumer, W., Andreu, L., Helle, G., Schleser, G.H., Wieloch, T., Wissel, H., 2009. A novel approach for the homogenization of cellulose to use micro-amounts for stable isotope analyses. Rapid Commun. Mass Spectrom. 23, 1934–1940. https://doi.org/10.1002/rcm.4105

Laur, J., Hacke, U.G., 2014. Exploring *Picea glauca* aquaporins in the context of needle water uptake and xylem refilling. New Phytologist 203, 388–400. https://doi.org/10.1111/nph.12806

Lehmann, M.M., Rinne, K.T., Blessing, C., Siegwolf, R.T.W., Buchmann, N., Werner, R.A., 2015. Malate as a key carbon source of leaf dark-respired CO_2 across different environmental conditions in potato plants. Journal of Experimental Botany 66, 5769–5781. https://doi.org/10.1093/jxb/erv279

Leng, H., Lu, M., Wan, X., 2012. Variation in embolism occurrence and repair along the stem in drought-stressed and re-watered seedlings of a poplar clone. Physiol. Plant. 147, 329–339. https://doi.org/doi:10.1111/j.1399-3054.2012.01665.x

Lenth, R., Singmann, H., Love, J., Buerkner, P., Herve, M., 2020. emmeans: Estimated Marginal Means, aka Least-Squares Means.

Lenth, R.V., 2017. Using lsmeans. J. Stat. Softw. 69, 1–33.

Le Quéré, C., Andrew, R.M., Friedlingstein, P., Sitch, S., Hauck, J., Pongratz, J., Pickers, P.A., Korsbakken, J.I., Peters, G.P., Canadell, J.G. et al. 2018. Global Carbon Budget 2018. Earth Syst. Sci. Data 10, 2141–2194. https://doi.org/10.5194/essd-10-2141-2018

Lévesque, M., Saurer, M., Siegwolf, R., Eilmann, B., Brang, P., Bugmann, H., Rigling, A., 2013. Drought response of five conifer species under contrasting water availability suggests high vulnerability of Norway spruce and European larch. Glob Change Biol 19, 3184–3199. https://doi.org/10.1111/gcb.12268

Li, S., Feifel, M., Karimi, Z., Schuldt, B., Choat, B., Jansen, S., 2015. Leaf gas exchange performance and the lethal water potential of five European species during drought. Tree Physiology tpv117. https://doi.org/10.1093/treephys/tpv117

Li, Q., Zhao, M., Wang, N., Liu, S., Wang, J., Zhang, W., Yang, N., Fan, P., Wang, R., Wang, H., Du, N., 2020. Water use strategies and drought intensity define the relative contributions of hydraulic failure and carbohydrate depletion during seedling mortality. Plant Physiology and Biochemistry 153, 106–118. https://doi.org/10.1016/j.plaphy.2020.05.023

Lindner, M., Maroschek, M., Netherer, S., Kremer, A., Barbati, A., Garcia-Gonzalo, J., Seidl, R., Delzon, S., Corona, P., Kolström, M., Lexer, M.J., Marchetti, M., 2010. Climate change impacts, adaptive capacity, and vulnerability of European forest ecosystems. Forest Ecology and Management 259, 698–709. https://doi.org/10.1016/j.foreco.2009.09.023

Liu, Y.Y., van Dijk, A.I.J.M., de Jeu, R.A.M., Canadell, J.G., McCabe, M.F., Evans, J.P., Wang, G., 2015. Recent reversal in loss of global terrestrial biomass. Nature Clim Change 5, 470–474. https://doi.org/10.1038/nclimate2581

Löf, M., Welander, N.T., 2000. Carry-over effects on growth and transpiration in *Fagus sylvatica* seedlings after drought at various stages of development. Can. J. For. Res. 30, 468–475. https://doi.org/10.1139/cjfr-30-3-468

Lo Gullo, M.A., Nardini, A., Trifilo, P., Salleo, S., 2005. Diurnal and seasonal variations in leaf hydraulic conductance in evergreen and deciduous trees. Tree Physiology 25, 505–512. https://doi.org/10.1093/treephys/25.4.505

Loreto, F., Schnitzler, J.-P., 2010. Abiotic stresses and induced BVOCs. Trends in Plant Science 15, 154–166. https://doi.org/10.1016/j.tplants.2009.12.006

Lukac, M., Calfapietra, C., Lagomarsino, A., Loreto, F., 2010. Global climate change and tree nutrition: effects of elevated CO_2 and temperature. Tree Physiology 30, 1209–1220. https://doi.org/10.1093/treephys/tpq040

Luyssaert, S., Schulze, E.-D., Börner, A., Knohl, A., Hessenmöller, D., Law, B.E., Ciais, P., Grace, J., 2008. Old-growth forests as global carbon sinks. Nature 455, 213–215. https://doi.org/10.1038/nature07276

Marias, D.E., Meinzer, F.C., Still, C., 2017. Impacts of leaf age and heat stress duration on photosynthetic gas exchange and foliar nonstructural carbohydrates in *Coffea arabica*. Ecol. Evol. 7, 1297–1310. https://doi.org/10.1002/ece3.2681

Martínez-Vilalta, J., Cochard, H., Mencuccini, M., Sterck, F., Herrero, A., Korhonen, J.F.J., Llorens, P., Nikinmaa, E., Nolè, A., Poyatos, R., Ripullone, F., Sass-Klaassen, U., Zweifel, R., 2009. Hydraulic adjustment of Scots pine across Europe. New Phytologist 184, 353–364.

Martínez-Vilalta, J., Garcia-Forner, N., 2017. Water potential regulation, stomatal behaviour and hydraulic transport under drought: deconstructing the iso/anisohydric concept. Plant, Cell & Environment 40, 962–976. https://doi.org/10.1111/pce.12846

Martínez-Vilalta, J., Sala, A., Asensio, D., Galiano, L., Hoch, G., Palacio, S., Piper, F.I., Lloret, F., 2016. Dynamics of non-structural carbohydrates in terrestrial plants: a global synthesis. Ecol. Monogr. 86, 495–516. https://doi.org/10.1002/ecm.1231

Martínez-Vilalta, J., Sala, A., Piñol, J., 2004. The hydraulic architecture of *Pinaceae* – a review. Plant Ecol. Former. Veg. 171, 3–13. https://doi.org/10.1023/B:VEGE.0000029378.87169.b1

Martin-StPaul, N., Delzon, S., Cochard, H., 2017. Plant resistance to drought depends on timely stomatal closure. Ecology Letters 20, 1437–1447. https://doi.org/10.1111/ele.12851

Matías, L., Jump, A.S., 2012. Interactions between growth, demography and biotic interactions in determining species range limits in a warming world: The case of *Pinus sylvestris*. Forest Ecology and Management 282, 10–22. https://doi.org/10.1016/j.foreco.2012.06.053

Mayr, S., Cochard, H., 2003. A new method for vulnerability analysis of small xylem areas reveals that compression wood of Norway spruce has lower hydraulic safety than opposite wood. Plant Cell Environ. 26, 1365–1371. https://doi.org/10.1046/j.0016-8025.2003.01060.x

Mayr, S., Schmid, P., Beikircher, B., Feng, F., Badel, E., 2020. Die hard: timberline conifers survive annual winter embolism. New Phytologist 226, 13–20. https://doi.org/10.1111/nph.16304
Mayr, S., Schmid, P., Laur, J., Rosner, S., Charra-Vaskou, K., Dämon, B., Hacke, U.G., 2014. Uptake of water via branches helps timberline conifers refill embolized xylem in late winter. Plant Physiology 164, 1731–1740. https://doi.org/10.1104/pp.114.236646
McCulloh, K.A., Johnson, D.M., Meinzer, F.C., Lachenbruch, B., 2011. An annual pattern of native embolism in upper branches of four tall conifer species. Am. J. Bot. 98, 1007–1015. https://doi.org/10.3732/ajb.1000503
McCulloh, K.A., Petitmermet, J., Stefanski, A., Rice, K.E., Rich, R.L., Montgomery, R.A., Reich, P.B., 2016. Is it getting hot in here? Adjustment of hydraulic parameters in six boreal and temperate tree species after 5 years of warming. Glob Change Biol 22, 4124–4133. https://doi.org/10.1111/gcb.13323
McDowell, N.G., 2011. Mechanisms linking drought, hydraulics, carbon metabolism, and vegetation mortality. Plant Physiology 155, 1051–1059. https://doi.org/10.1104/pp.110.170704
McDowell, N.G., Allen, C.D., Anderson-Teixeira, K., Aukema, B.H., Bond-Lamberty, B., Chini, L., Clark, J.S., Dietze, M., Grossiord, C., Hanbury-Brown, A. et al. 2020. Pervasive shifts in forest dynamics in a changing world. Science 368, eaaz9463. https://doi.org/10.1126/science.aaz9463
McDowell, N.G., Pockman, W.T., Allen, C.D., Breshears, D.D., Cobb, N., Kolb, T., Plaut, J., Sperry, J., West, A., Williams, D.G., Yepez, E.A., 2008. Mechanisms of plant survival and mortality during drought: why do some plants survive while others succumb to drought? New Phytologist 178, 719–739. https://doi.org/10.1111/j.1469-8137.2008.02436.x
Meehl, G.A., Zwiers, F., Evans, J., Knutson, T., Mearns, L., Whetton, P., 2000. Trends in extreme weather and climate events: issues related to modeling extremes in projections of future climate change. Bulletin of the American Meteorological Society 8, 10.
Meinzer, F.C., 2002. Co-ordination of vapour and liquid phase water transport properties in plants. Plant Cell Environ. 25, 265–274. https://doi.org/10.1046/j.1365-3040.2002.00781.x
Meinzer, F.C., Clearwater, M.J., Goldstein, G., 2001. Water transport in trees: current perspectives, new insights and some controversies. Environmental and Experimental Botany 45, 239–262. https://doi.org/10.1016/S0098-8472(01)00074-0
Meinzer, F.C., McCulloh, K.A., 2013. Xylem recovery from drought-induced embolism: where is the hydraulic point of no return? Tree Physiology 33, 331–334. https://doi.org/10.1093/treephys/tpt022
Mena-Petite, A., Robredo, A., Alcalde, S., Duñabeitia, M., González-Moro, M., Lacuesta, M., Muñoz-Rueda, A., 2003. Gas exchange and chlorophyll fluorescence responses of *Pinus radiata* D. Don seedlings during and after several storage regimes and their effects on post-planting survival. Trees 17, 133–143. https://doi.org/10.1007/s00468-002-0216-0
Merganičová, K., Merganič, J., Lehtonen, A., Vacchiano, G., Sever, M.Z.O., Augustynczik, A.L.D., Grote, R., Kyselová, I., Mäkelä, A., Yousefpour, R., Krejza, J., Collalti, A., Reyer, C.P.O., 2019. Forest carbon allocation modelling under climate change. Tree Physiology tpz105. https://doi.org/10.1093/treephys/tpz105
Millar, C.I., Stephenson, N.L., 2015. Temperate forest health in an era of emerging megadisturbance. Science 349, 823–826. https://doi.org/10.1126/science.aaa9933
Millard, P., Grelet, G.-A., 2010. Nitrogen storage and remobilization by trees: ecophysiological relevance in a changing world. Tree physiology, 30(9), 1083-1095.
Millennium Ecosystem Assessment, 2005. Ecosystems and Human Well-Being: Synthesis. Island Press, Washington, DC.
Mitchell, P.J., O'Grady, A.P., Tissue, D.T., White, D.A., Ottenschlaeger, M.L., Pinkard, E.A., 2013. Drought response strategies define the relative contributions of hydraulic dysfunction and carbohydrate depletion during tree mortality. New Phytologist 197, 862–872.
Morison, J.I.L., Lawlor, D.W., 1999. Interactions between increasing CO 2 concentration and temperature on plant growth. Plant Cell Environment 22, 659–682. https://doi.org/10.1046/j.1365-3040.1999.00443.x
Morris, H., Plavcová, L., Cvecko, P., Fichtler, E., Gillingham, M.A.F., Martínez-Cabrera, H.I., McGlinn, D.J., Wheeler, E., Zheng, J., Ziemińska, K., Jansen, S., 2016. A global analysis of parenchyma tissue fractions in secondary xylem of seed plants. New Phytologist 209, 1553–1565. https://doi.org/10.1111/nph.13737
Mu, M., Kauwe, M.G.D., Ukkola, A.M., Pitman, A.J., Guo, W., Briggs, P.R., 2021. Exploring how groundwater buffers the influence of heatwaves on vegetation function during multi-year droughts. Earth System Dynamics Discussions 1–29.

Muller, B., Pantin, F., Génard, M., Turc, O., Freixes, S., Piques, M., Gibon, Y., 2011. Water deficits uncouple growth from photosynthesis, increase C content, and modify the relationships between C and growth in sink organs. Journal of Experimental Botany 62, 1715–1729. https://doi.org/10.1093/jxb/erq438

Münch, E., 1930. Die Stoffbewegungen in der Pflanze. Gustav Fischer, Jena.

Murchie, E.H., Lawson, T., 2013. Chlorophyll fluorescence analysis: a guide to good practice and understanding some new applications. Journal of Experimental Botany 64, 3983–3998.

Nadal-Sala, D., Medlyn, B.E., Ruehr, N.K., Barton, C.V.M., Ellsworth, D.S., Gracia, C., Tissue, D.T., Tjoelker, M.G., Sabaté, S., 2021. Increasing aridity will not offset CO_2 fertilization in fast-growing eucalypts with access to deep soil water. Global Change Biology 27, 2970–2990.

Nardini, A., Lo Gullo, M.A., Salleo, S., 2011. Refilling embolized xylem conduits: Is it a matter of phloem unloading? Plant Science 180, 604–611. https://doi.org/10.1016/j.plantsci.2010.12.011

Nardini, A., Salleo, S., 2000. Limitation of stomatal conductance by hydraulic traits: sensing or preventing xylem cavitation? Trees 15, 14–24. https://doi.org/10.1007/s004680000071

Nardini, A., Savi, T., Losso, A., Petit, G., Pacilè, S., Tromba, G., Mayr, S., Trifilò, P., Lo Gullo, M.A., Salleo, S., 2017. X-ray microtomography observations of xylem embolism in stems of *Laurus nobilis* are consistent with hydraulic measurements of percentage loss of conductance. New Phytologist 213, 1068–1075. https://doi.org/10.1111/nph.14245

Näsholm, T., Kielland, K., Ganeteg, U., 2009. Uptake of organic nitrogen by plants. New Phytologist 182, 31–48. https://doi.org/10.1111/j.1469-8137.2008.02751.x

Netto, A.T., Campostrini, E., Oliveira, J.G. de, Bressan-Smith, R.E., 2005. Photosynthetic pigments, nitrogen, chlorophyll a fluorescence and SPAD-502 readings in coffee leaves. Sci. Hortic. 104, 199–209. https://doi.org/10.1016/j.scienta.2004.08.013

Nobel, P.S., 2020. Physiochemical and environmental plant physiology. Academic Press, London.

Ogasa, M., Miki, N.H., Murakami, Y., Yoshikawa, K., 2013. Recovery performance in xylem hydraulic conductivity is correlated with cavitation resistance for temperate deciduous tree species. Tree Physiology 33, 335–344. https://doi.org/10.1093/treephys/tpt010

Ogle, K., Barber, J.J., Willson, C., Thompson, B., 2009. Hierarchical statistical modeling of xylem vulnerability to cavitation. New Phytologist 182, 541–554. https://doi.org/10.1111/j.1469-8137.2008.02760.x

Öhlund, J., Näsholm, T., 2004. Regulation of organic and inorganic nitrogen uptake in Scots pine (*Pinus sylvestris*) seedlings. Tree Physiology 24, 1397–1402. https://doi.org/10.1093/treephys/24.12.1397

O'Kane, D., Gill, V., Boyd, P., Burdon, R., 1996. Chilling, oxidative stress and antioxidant responses in *Arabidopsis thaliana callus*. Planta 198, 371–377.

O'Leary, B.M., Asao, S., Millar, A.H., Atkin, O.K., 2019. Core principles which explain variation in respiration across biological scales. New Phytologist 222, 670–686. https://doi.org/10.1111/nph.15576

Olivas-García, J.M., Cregg, B.M., Hennessey, T.C., 2000. Genotypic variation in carbon isotope discrimination and gas exchange of ponderosa pine seedlings under two levels of water stress. Can. J. For. Res. 30, 1581–1590. https://doi.org/10.1139/x00-080

Oren, R., Ellsworth, D.S., Johnsen, K.H., Phillips, N., Ewers, B.E., Maier, C., Schäfer, K.V.R., McCarthy, H., Hendrey, G., McNulty, S.G., Katul, G.G., 2001. Soil fertility limits carbon sequestration by forest ecosystems in a CO_2-enriched atmosphere. Nature 411, 469–472. https://doi.org/10.1038/35078064

Otieno, D.O., Schmidt, M.W.T., Adiku, S., Tenhunen, J., 2005. Physiological and morphological responses to water stress in two *Acacia* species from contrasting habitats. Tree Physiology 25, 361–371. https://doi.org/10.1093/treephys/25.3.361

Palacio, S., Camarero, J.J., Maestro, M., Alla, A.Q., Lahoz, E., Montserrat-Martí, G., 2018. Are storage and tree growth related? Seasonal nutrient and carbohydrate dynamics in evergreen and deciduous Mediterranean oaks. Trees 32, 777-790. https://doi.org/10.1007/s00468-018-1671-6

Pan, Y., Birdsey, R.A., Fang, J., Houghton, R., Kauppi, P.E., Kurz, W.A., Phillips, O.L., Shvidenko, A., Lewis, S.L., Canadell, J.G. et al. 2011. A large and persistent carbon sink in the world's forests. Sci. New Ser. 333, 988–993.

Patra, P.K., Maksyutov, S., Nakazawa, T., 2005. Analysis of atmospheric CO_2 growth rates at Mauna Loa using CO_2 fluxes derived from an inverse model. Tellus B: Chemical and Physical Meteorology 57, 357–365. https://doi.org/10.3402/tellusb.v57i5.16560

Pellicer, V., Guehl, J.-M., Daudet, F.-A., Riviere, L.M., Maillard, P., 2000. Carbon and nitrogen mobilization in *Larix* × *eurolepis* leafy stem cuttings assessed by dual ^{13}C and ^{15}N labeling: relationships with rooting. Tree physiology, 20(12), 807-814.

Petruzzellis, F., Pagliarani, C., Savi, T., Losso, A., Cavalletto, S., Tromba, G., Dullin, C., Bär, A., Ganthaler, A., Miotto, A., Mayr, S., Zwieniecki, M.A., Nardini, A., Secchi, F., 2018. The pitfalls of *in vivo* imaging techniques: evidence for cellular damage caused by synchrotron X-ray computed micro-tomography. New Phytologist 220, 104-110. https://doi.org/10.1111/nph.15368

Petty, J.A., Preston, R.D., 1970. Permeability and structure of the wood of Sitka spruce. Proc. R. Soc. Lond. B Biol. Sci. 175, 149–166.

Pickard, W.F., 2003. The riddle of root pressure. I. Putting Maxwell's demon to rest. Funct. Plant biology 30, 121. https://doi.org/10.1071/FP02035

Pidcock, R., McSweeney, R., 2021. Mapped: How climate change affects extreme weather around the world. Carbon Brief. https://www.carbonbrief.org/mapped-how-climate-change-affects-extreme-weather-around-the-world.

Poyatos, R., Llorens, P., Piñol, J., Rubio, C., 2008. Response of Scots pine (*Pinus sylvestris* L.) and pubescent oak (*Quercus pubescens* Willd.) to soil and atmospheric water deficits under Mediterranean mountain climate. Ann. For. Sci. 65, 306. https://doi.org/10.1051/forest:2008003

Preisler, Y., Tatarinov, F., Grünzweig, J.M., Yakir, D., 2021. Seeking the "point of no return" in the sequence of events leading to mortality of mature trees. Plant, Cell & Environment 44, 1315–1328.

Pumpanen, J.S., Heinonsalo, J., Rasilo, T., Hurme, K.-R., Ilvesniemi, H., 2009. Carbon balance and allocation of assimilated CO_2 in Scots pine, Norway spruce, and Silver birch seedlings determined with gas exchange measurements and ^{14}C pulse labelling. Trees 23, 611–621. https://doi.org/10.1007/s00468-008-0306-8

R Core Team, 2019. R: A language and environment for statistical computing. R Foundation for Statistical Computing, Vienna, Austria.

Rehschuh, R., Cecilia, A., Zuber, M., Faragó, T., Baumbach, T., Hartmann, H., Jansen, S., Mayr, S., Ruehr, N., 2020. Drought-induced xylem embolism limits the recovery of leaf gas exchange in Scots pine. Plant Physiology 184, 852–864. https://doi.org/10.1104/pp.20.00407

Rehschuh, R., Mette, T., Menzel, A., Buras, A., 2017. Soil properties affect the drought susceptibility of Norway spruce. Dendrochronologia 45, 81–89. https://doi.org/10.1016/j.dendro.2017.07.003

Rehschuh, R., Ruehr, N.K., 2021. Unrevealing water and carbon relations during and after heat and hot drought stress in *Pinus sylvestris*. bioRxiv 2021.06.29.450316. https://doi.org/10.1101/2021.06.29.450316

Reichstein, M., Bahn, M., Ciais, P., Frank, D., Mahecha, M.D., Seneviratne, S.I., Zscheischler, J., Beer, C., Buchmann, N., Frank, D.C., Papale, D., Rammig, A., Smith, P., Thonicke, K., van der Velde, M., Vicca, S., Walz, A., Wattenbach, M., 2013. Climate extremes and the carbon cycle. Nature 500, 287–295. https://doi.org/10.1038/nature12350

Rennenberg, H., Dannenmann, M., 2015. Nitrogen nutrition of trees in temperate forests—the significance of nitrogen availability in the pedosphere and atmosphere. Forests 6, 2820–2835. https://doi.org/10.3390/f6082820

Rennenberg, H., Dannenmann, M., Gessler, A., Kreuzwieser, J., Simon, J., Papen, H., 2009. Nitrogen balance in forest soils: nutritional limitation of plants under climate change stresses. Plant Biology 11, 4–23. https://doi.org/10.1111/j.1438-8677.2009.00241.x

Rennenberg, H., Loreto, F., Polle, A., Brilli, F., Fares, S., Beniwal, R.S., Gessler, A., 2006. Physiological responses of forest trees to heat and drought. Plant Biology 8, 556–571. https://doi.org/10.1055/s-2006-924084

Richter, A., Wanek, W., Werner, R.A., Ghashghaie, J., Jäggi, M., Gessler, A., Brugnoli, E., Hettmann, E., Göttlicher, S.G., Salmon, Y. et al. 2009. Preparation of starch and soluble sugars of plant material for the analysis of carbon isotope composition: a comparison of methods. Rapid Commun. Mass Spectrom. 23, 2476–2488. https://doi.org/10.1002/rcm.4088

Riederer, M., Schreiber, L., 2001. Protecting against water loss: analysis of the barrier properties of plant cuticles. Journal of Experimental Botany 52, 2023–2032. https://doi.org/10.1093/jexbot/52.363.2023

Rigling, A., Bigler, C., Eilmann, B., Feldmeyer-Christe, E., Gimmi, U., Ginzler, C., Graf, U., Mayer, P., Vacchiano, G., Weber, P., Wohlgemuth, T., Zweifel, R., Dobbertin, M., 2013. Driving factors of a vegetation shift from Scots pine to pubescent oak in dry Alpine forests. Glob. Change Biol. 19, 229–240. https://doi.org/10.1111/gcb.12038

Riutta, T., Slade, E.M., Bebber, D.P., Taylor, M.E., Malhi, Y., Riordan, P., Macdonald, D.W., Morecroft, M.D., 2012. Experimental evidence for the interacting effects of forest edge, moisture and soil macrofauna on leaf litter decomposition. Soil Biology and Biochemistry 49, 124–131. https://doi.org/10.1016/j.soilbio.2012.02.028

Rockwell, F.E., Wheeler, J.K., Holbrook, N.M., 2014. Cavitation and its discontents: opportunities for resolving current controversies. Plant Physiology 164, 1649–1660. https://doi.org/10.1104/pp.113.233817

Rueden, C.T., Eliceiri, K.W., 2019. ImageJ for the next generation of scientific image data. Microsc. Microanal. 25, 142–143. https://doi.org/10.1017/S1431927619001442

Ruehr, N.K., Gast, A., Weber, C., Daub, B., Arneth, A., 2016. Water availability as dominant control of heat stress responses in two contrasting tree species. Tree Physiology, 36(2), 164-178. https://doi.org/10.1093/treephys/tpv102

Ruehr, N.K., Grote, R., Mayr, S., Arneth, A., 2019. Beyond the extreme: recovery of carbon and water relations in woody plants following heat and drought stress. Tree Physiology 39, 1285–1299. https://doi.org/10.1093/treephys/tpz032

Ruehr, N.K., Offermann, C.A., Gessler, A., Winkler, J.B., Ferrio, J.P., Buchmann, N., Barnard, R.L., 2009. Drought effects on allocation of recent carbon: from beech leaves to soil CO_2 efflux. New Phytol. 184, 950–961. https://doi.org/10.1111/j.1469-8137.2009.03044.x

Sack, L., Buckley, T.N., Scoffoni, C., 2016. Why are leaves hydraulically vulnerable? Journal of Experimental Botany 67, 4917–4919. https://doi.org/10.1093/jxb/erw304

Sack, L., Scoffoni, C., 2012. Measurement of leaf hydraulic conductance and stomatal conductance and their responses to irradiance and dehydration using the Evaporative Flux Method (EFM). J. Vis. Exp. 4179. https://doi.org/10.3791/4179

Saelim, S., Zwiazek, J.J., 2000. Preservation of thermal stability of cell membranes and gas exchange in high temperature acclimated *Xylia xylocarpa* seedlings. Journal of Plant Physiology 156, 380–385. https://doi.org/10.1016/S0176-1617(00)80077-2

Sage, R.F., Way, D.A., Kubien, D.S., 2008. Rubisco, rubisco activase, and global climate change. Journal of Experimental Botany 59, 1581–1595. https://doi.org/10.1093/jxb/ern053

Saijo, Y., Loo, E.P., 2020. Plant immunity in signal integration between biotic and abiotic stress responses. New Phytol 225, 87–104. https://doi.org/10.1111/nph.15989

Sala, A., Woodruff, D.R., Meinzer, F.C., 2012. Carbon dynamics in trees: feast or famine? Tree Physiology 32, 764–775. https://doi.org/10.1093/treephys/tpr143

Salleo, S., Gullo, M.A.L., Paoli, D., Zippo, M., 1996. Xylem recovery from cavitation-induced embolism in young plants of *Laurus nobilis* : a possible mechanism. New Phytologist 132, 47–56. https://doi.org/10.1111/j.1469-8137.1996.tb04507.x

Salleo, S., Trifilò, P., Esposito, S., Nardini, A., Lo Gullo, M.A., 2009. Starch-to-sugar conversion in wood parenchyma of field-growing *Laurus nobilis* plants: a component of the signal pathway for embolism repair? Funct. Plant biology 36, 815. https://doi.org/10.1071/FP09103

Salmon, Y., Torres-Ruiz, J.M., Poyatos, R., Martinez-Vilalta, J., Meir, P., Cochard, H., Mencuccini, M., 2015. Balancing the risks of hydraulic failure and carbon starvation: a twig scale analysis in declining Scots pine. Plant Cell Environ. 38, 2575–2588. https://doi.org/10.1111/pce.12572

Salomón, R.L., De Roo, L., Bodé, S., Boeckx, P., Steppe, K., 2021. Efflux and assimilation of xylem-transported CO_2 in stems and leaves of tree species with different wood anatomy. Plant, Cell & Environment 1–15. https://doi.org/10.1111/pce.14062

Savi, T., Casolo, V., Luglio, J., Bertuzzi, S., Trifilo', P., Lo Gullo, M.A., Nardini, A., 2016. Species-specific reversal of stem xylem embolism after a prolonged drought correlates to endpoint concentration of soluble sugars. Plant Physiology and Biochemistry 106, 198–207. https://doi.org/10.1016/j.plaphy.2016.04.051

Saxe, H., Cannell, M.G.R., Johnsen, Ø., Ryan, M.G., Vourlitis, G., 2001. Tree and forest functioning in response to global warming. New Phytologist 149, 369–399. https://doi.org/10.1046/j.1469-8137.2001.00057.x

Scherrer, D., Bader, M.K.-F., Körner, C., 2011. Drought-sensitivity ranking of deciduous tree species based on thermal imaging of forest canopies. Agric. For. Meteorol. 151, 1632–1640. https://doi.org/10.1016/j.agrformet.2011.06.019

Schindelin, J., Arganda-Carreras, I., Frise, E., Kaynig, V., Longair, M., Pietzsch, T., Preibisch, S., Rueden, C., Saalfeld, S., Schmid, B., Tinevez, J.-Y., White, D.J., Hartenstein, V., Eliceiri, K., Tomancak, P., Cardona, A., 2012. Fiji: an open-source platform for biological-image analysis. Nat. Methods 9, 676–682. https://doi.org/10.1038/nmeth.2019

Schönbeck, L., Li, M.-H., Lehmann, M.M., Rigling, A., Schaub, M., Hoch, G., Kahmen, A., Gessler, A., 2020. Soil nutrient availability alters tree carbon allocation dynamics during drought. Tree Physiology 24.

Schrader, S.M., Wise, R.R., Wacholtz, W.F., Ort, D.R., Sharkey, T.D., 2004. Thylakoid membrane responses to moderately high leaf temperature in Pima cotton. Plant Cell Environ. 27, 725–735. https://doi.org/10.1111/j.1365-3040.2004.01172.x

Schuldt, B., Buras, A., Arend, M., Vitasse, Y., Beierkuhnlein, C., Damm, A., Gharun, M., Grams, T.E.E., Hauck, M., Hajek, P. et al. 2020. A first assessment of the impact of the extreme 2018 summer drought on Central European forests. Basic Appl. Ecol. 45, 86–103. https://doi.org/10.1016/j.baae.2020.04.003

Schwalm, C.R., Anderegg, W.R.L., Michalak, A.M., Fisher, J.B., Biondi, F., Koch, G., Litvak, M., Ogle, K., Shaw, J.D., Wolf, A., Huntzinger, D.N., Schaefer, K., Cook, R., Wei, Y., Fang, Y., Hayes, D., Huang, M., Jain, A., Tian, H., 2017. Global patterns of drought recovery. Nature 548, 202–205. https://doi.org/10.1038/nature23021

Scoffoni, C., Vuong, C., Diep, S., Cochard, H., Sack, L., 2014. Leaf shrinkage with dehydration: coordination with hydraulic vulnerability and drought tolerance. Plant Physiology 164, 1772–1788. https://doi.org/10.1104/pp.113.221424

Seidl, R., Thom, D., Kautz, M., Martin-Benito, D., Peltoniemi, M., Vacchiano, G., Wild, J., Ascoli, D., Petr, M., Honkaniemi, J., Lexer, M.J., Trotsiuk, V., Mairota, P., Svoboda, M., Fabrika, M., Nagel, T.A., Reyer, C.P.O., 2017. Forest disturbances under climate change. Nature Clim Change 7, 395–402. https://doi.org/10.1038/nclimate3303

Sellin, A., Kupper, P., 2007. Temperature, light and leaf hydraulic conductance of little-leaf linden (*Tilia cordata*) in a mixed forest canopy. Tree Physiology 27, 679–688. https://doi.org/10.1093/treephys/27.5.679

Sevanto, S., 2018. Drought impacts on phloem transport. Curr. Opin. Plant biology 43, 76–81. https://doi.org/10.1016/j.pbi.2018.01.002

Sevanto, S., 2014. Phloem transport and drought. Journal of Experimental Botany 65, 1751–1759. https://doi.org/10.1093/jxb/ert467

Sevanto, S., Mcdowell, N.G., Dickman, L.T., Pangle, R., Pockman, W.T., 2014. How do trees die? A test of the hydraulic failure and carbon starvation hypotheses. Plant Cell Environ 37, 153–161. https://doi.org/10.1111/pce.12141

Sheil, D., 2018. Forests, atmospheric water and an uncertain future: the new biology of the global water cycle. For. Ecosyst. 5, 19. https://doi.org/10.1186/s40663-018-0138-y

Simon, J., Dannenmann, M., Gasche, R., Holst, J., Mayer, H., Papen, H., Rennenberg, H., 2011. Competition for nitrogen between adult European beech and its offspring is reduced by avoidance strategy. Forest Ecology and Management 262, 105–114. https://doi.org/10.1016/j.foreco.2011.01.035

Sippel, S., Reichstein, M., Ma, X., Mahecha, M.D., Lange, H., Flach, M., Frank, D., 2018. Drought, heat, and the carbon cycle: a review. Curr Clim Change Rep 4, 266–286. https://doi.org/10.1007/s40641-018-0103-4

Skelton, R.P., Brodribb, T.J., McAdam, S.A.M., Mitchell, P.J., 2017. Gas exchange recovery following natural drought is rapid unless limited by loss of leaf hydraulic conductance: evidence from an evergreen woodland. New Phytologist 215, 1399–1412. https://doi.org/10.1111/nph.14652

Skelton, R.P., West, A.G., Dawson, T.E., 2015. Predicting plant vulnerability to drought in biodiverse regions using functional traits. Proc. Natl. Acad. Sci. 112, 5744–5749. https://doi.org/10.1073/pnas.1503376112

Smith, A.M., Stitt, M., 2007. Coordination of carbon supply and plant growth. Plant Cell Environ. 30, 1126–1149. https://doi.org/10.1111/j.1365-3040.2007.01708.x

Sperry, J.S., 2004. Coordinating stomatal and xylem functioning–an evolutionary perspective. New Phytologist 162, 568–570.

Sperry, J.S., Holbrook, N.M., Zimmermann, M.H., Tyree, M.T., 1987. Spring filling of xylem vessels in wild grapevine. Plant Physiology 83, 414–417. https://doi.org/10.1104/pp.83.2.414

Sperry, J.S., Love, D.M., 2015. What plant hydraulics can tell us about responses to climate-change droughts. New Phytologist 207, 14–27. https://doi.org/10.1111/nph.13354

Sperry, J.S., Tyree, M.T., 1988. Mechanism of water stress-induced xylem embolism. Plant Physiology 88, 581–587. https://doi.org/10.1104/pp.88.3.581

Stéfanon, M., Drobinski, P., D'Andrea, F., Lebeaupin-Brossier, C., Bastin, S., 2014. Soil moisture-temperature feedbacks at meso-scale during summer heat waves over Western Europe. Clim. Dyn. 42, 1309–1324. https://doi.org/10.1007/s00382-013-1794-9

Subke, J.-A., Inglima, I., Francesca Cotrufo, M., 2006. Trends and methodological impacts in soil CO_2 efflux partitioning: A metaanalytical review. Global Change Biology 12, 921–943. https://doi.org/10.1111/j.1365-2486.2006.01117.x

Taiz, L., Zeiger, E., Møller, I.M., Murphy, A.S., 2014. Plant physiology and development. MA: Sinauer Associates, Sunderland.

Teskey, R., Wertin, T., Bauweraerts, I., Ameye, M., Mcguire, M.A., Steppe, K., 2015. Responses of tree species to heat waves and extreme heat events: Tree response to extreme heat. Plant Cell Environ. 38, 1699–1712. https://doi.org/10.1111/pce.12417

Thalmann, M., Santelia, D., 2017. Starch as a determinant of plant fitness under abiotic stress. New Phytologist 214, 943–951. https://doi.org/10.1111/nph.14491

Thorpe, M.R., Minchin, P.E.H., Gould, N., McQueen, J.C., 2005. The stem apoplast: a potential communication channel in plant growth regulation. Elsevier, Burlington, pp. 355–371.

Timofeeva, G., Treydte, K., Bugmann, H., Rigling, A., Schaub, M., Siegwolf, R., Saurer, M., 2017. Long-term effects of drought on tree-ring growth and carbon isotope variability in Scots pine in a dry environment. Tree Physiology 37, 1028–1041. https://doi.org/10.1093/treephys/tpx041

Töchterle, P., Yang, F., Rehschuh, S., Rehschuh, R., Ruehr, N.K., Rennenberg, H., Dannenmann, M., 2020. Hydraulic water redistribution by silver fir (*Abies alba* Mill.) occurring under severe soil drought. Forests 11, 162. https://doi.org/10.3390/f11020162

Tomasella, M., Häberle, K.-H., Nardini, A., Hesse, B., Machlet, A., Matyssek, R., 2017. Post-drought hydraulic recovery is accompanied by non-structural carbohydrate depletion in the stem wood of Norway spruce saplings. Sci. Rep. 7. https://doi.org/10.1038/s41598-017-14645-w

Tomasella, M., Petrussa, E., Petruzzellis, F., Nardini, A., Casolo, V., 2019. The possible role of non-structural carbohydrates in the regulation of tree hydraulics. Int. J. Mol. Sci. 21, 144. https://doi.org/10.3390/ijms21010144

Torres-Ruiz, J.M., Cochard, H., Mencuccini, M., Delzon, S., Badel, E., 2016. Direct observation and modelling of embolism spread between xylem conduits: a case study in Scots pine: Embolism formation and spread in Scots pine. Plant Cell Environ. 39, 2774–2785. https://doi.org/10.1111/pce.12840

Trifiló, P., Raimondo, F., Savi, T., Lo Gullo, M.A., Nardini, A., 2016. The contribution of vascular and extra-vascular water pathways to drought-induced decline of leaf hydraulic conductance. EXBOTJ 67, 5029–5039. https://doi.org/10.1093/jxb/erw268

Trugman, A.T., Detto, M., Bartlett, M.K., Medvigy, D., Anderegg, W.R.L., Schwalm, C., Schaffer, B., Pacala, S.W., 2018. Tree carbon allocation explains forest drought-kill and recovery patterns. Ecol. Lett. 21, 1552–1560. https://doi.org/10.1111/ele.13136

Tyree, M.T., Sperry, J.S., 1989. Vulnerability of xylem to cavitation and embolism. Annu. Rev. Plant biology 40, 19–36.

Tyree, M.T., Sperry, J.S., 1988. Do woody plants operate near the point of catastrophic xylem dysfunction caused by dynamic water stress? Answers from a model. Plant Physiol. 88, 574–580. https://doi.org/10.1104/pp.88.3.574

Umebayashi, T., Morita, T., Utsumi, Y., Kusumoto, D., Yasuda, Y., Haishi, T., Fukuda, K., 2016. Spatial distribution of xylem embolisms in the stems of *Pinus thunbergii* at the threshold of fatal drought stress. Tree Physiology 36, 1210–1218. https://doi.org/10.1093/treephys/tpw050

Urban, J., Ingwers, M., McGuire, M.A., Teskey, R., 2017a. Stomatal conductance increases with rising temperature. Plant Signal. Behav. 12, e1356534.

Urban, J., Ingwers, M.W., McGuire, M.A., Teskey, R.O., 2017b. Increase in leaf temperature opens stomata and decouples net photosynthesis from stomatal conductance in *Pinus taeda* and *Populus deltoides x nigra*. Journal of Experimental Botany 68 (7), 1757–1767.

Usta, I., Hale, M.D., 2006. Comparison of the bordered pits of two species of spruce (*Pinaceae*) in a green and kiln-dried condition and their effects on fluid flow in the stem wood in relation to wood preservation. Forestry 79, 467–475. https://doi.org/10.1093/forestry/cpl011

Utsumi, Y., Sano, Y., Funada, R., Ohtani, J., Fujikawa, S., 2003. Seasonal and perennial changes in the distribution of water in the sapwood of conifers in a sub-frigid zone. Plant Physiology 131, 1826–1833. https://doi.org/10.1104/pp.102.014795

van Bel, A.J.E., 2003. Phloem transport: the collective power of single modules. Springer-Verlag, New York, pp. 151–155.

Vance, E.D., Brookes, P.C., Jenkinson, D.S., 1987. An extraction method for measuring soil microbial biomass C. Soil Biol. Biochem. 19, 703–707. https://doi.org/10.1016/0038-0717(87)90052-6

Vandegehuchte, M.W., Bloemen, J., Vergeynst, L.L., Steppe, K., 2015. Woody tissue photosynthesis in trees: salve on the wounds of drought? New Phytologist 208, 998–1002. https://doi.org/10.1111/nph.13599

Venturas, M.D., Sperry, J.S., Hacke, U.G., 2017. Plant xylem hydraulics: What we understand, current research, and future challenges. Journal of Integrative Plant Biology 59, 356–389. https://doi.org/10.1111/jipb.12534

Vogelgesang, M., Farago, T., Morgeneyer, T.F., Helfen, L., dos Santos Rolo, T., Myagotin, A., Baumbach, T., 2016. Real-time image-content-based beamline control for smart 4D X-ray imaging. J. Synchrotron Radiat. 23, 1254–1263. https://doi.org/10.1107/S1600577516010195

von Caemmerer, S., Evans, J.R., 2015. Temperature responses of mesophyll conductance differ greatly between species: Temperature responses of mesophyll conductance. Plant Cell Environ. 38, 629–637. https://doi.org/10.1111/pce.12449

Wagg, C., Bender, S.F., Widmer, F., van der Heijden, M.G.A., 2014. Soil biodiversity and soil community composition determine ecosystem multifunctionality. Proc. Natl. Acad. Sci. 111, 5266–5270. https://doi.org/10.1073/pnas.1320054111

Walentowski, H., Falk, W., Mette, T., Kunz, J., Bräuning, A., Meinardus, C., Zang, C., Sutcliffe, L.M.E., Leuschner, C., 2017. Assessing future suitability of tree species under climate change by multiple methods: a case study in southern Germany. Ann. For. Res. 60. https://doi.org/10.15287/afr.2016.789

Watson, J.E.M., Evans, T., Venter, O., Williams, B., Tulloch, A., Stewart, C., Thompson, I., Ray, J.C., Murray, K., Salazar, A. et al., 2018. The exceptional value of intact forest ecosystems. Nat. Ecol. Evol. 2, 599–610. https://doi.org/10.1038/s41559-018-0490-x

Way, D.A., Domec, J.-C., Jackson, R.B., 2013. Elevated growth temperatures alter hydraulic characteristics in trembling aspen (*Populus tremuloides*) seedlings: implications for tree drought tolerance. Plant Cell Environ. 36, 103–115.

Weber, P., Bugmann, H., Rigling, A., 2007. Radial growth responses to drought of *Pinus sylvestris* and *Quercus pubescens* in an inner-Alpine dry valley. Journal of Vegetation Science 18, 777–792. https://doi.org/10.1111/j.1654-1103.2007.tb02594.x

Weber, R., Gessler, A., Hoch, G., 2019. High carbon storage in carbon-limited trees. New Phytologist 222, 171–182. https://doi.org/10.1111/nph.15599

Wermelinger, B., Rigling, A., Schneider Mathis, D., Dobbertin, M., 2008. Assessing the role of bark- and wood-boring insects in the decline of Scots pine (*Pinus sylvestris*) in the Swiss Rhone valley. Ecol Entomol 33, 239–249. https://doi.org/10.1111/j.1365-2311.2007.00960.x

Weston, D.J., Bauerle, W.L., 2007. Inhibition and acclimation of C3 photosynthesis to moderate heat: a perspective from thermally contrasting genotypes of *Acer rubrum* (red maple). Tree Physiology 27, 1083–1092. https://doi.org/10.1093/treephys/27.8.1083

Wheeler, J.K., Huggett, B.A., Tofte, A.N., Rockwell, F.E., Holbrook, N.M., 2013. Cutting xylem under tension or supersaturated with gas can generate PLC and the appearance of rapid recovery from embolism. Plant Cell Environ. 36 (11), 1938–1949. https://doi.org/10.1111/pce.12139

Wingler, A., Lea, P.J., Quick, W.P., Leegood, R.C., 2000. Photorespiration: metabolic pathways and their role in stress protection. Philosophical Transactions: Biological Sciences 355, 1517–1529.

Xu, X., Luo, X., 2012. Effect of wetting intensity on soil GHG fluxes and microbial biomass under a temperate forest floor during dry season. Geoderma 170, 118–126. https://doi.org/10.1016/j.geoderma.2011.11.016

Yang, S., Tyree, M.T., 1992. A theoretical model of hydraulic conductivity recovery from embolism with comparison to experimental data on *Acer saccharum*. Plant Cell Environ 15, 633–643. https://doi.org/10.1111/j.1365-3040.1992.tb01005.x

Yin, J., Bauerle, T.L., 2017. A global analysis of plant recovery performance from water stress. Oikos 126, 1377–1388. https://doi.org/10.1111/oik.04534

Yu, G., Zare, A., Sheng, H., Matamala, R., Reyes-Cabrera, J., Fritschi, F.B., Juenger, T.E., 2020. Root identification in minirhizotron imagery with multiple instance learning. Machine Vision and Applications 31, 43. https://doi.org/10.1007/s00138-020-01088-z

Zang, U., Goisser, M., Grams, T.E.E., Haberle, K.-H., Matyssek, R., Matzner, E., Borken, W., 2014. Fate of recently fixed carbon in European beech (*Fagus sylvatica*) saplings during drought and subsequent recovery. Tree Physiology 34, 29–38. https://doi.org/10.1093/treephys/tpt110

Zhao, J., Hartmann, H., Trumbore, S., Ziegler, W., Zhang, Y., 2013. High temperature causes negative whole-plant carbon balance under mild drought. New Phytol. 200, 330–339. https://doi.org/10.1111/nph.12400

Zweifel, R., Häsler, R., 2000. Frost-induced reversible shrinkage of bark of mature subalpine conifers. Agric. For. Meteorol. 102, 213–222. https://doi.org/10.1016/S0168-1923(00)00135-0

Zweifel, R., Item, H., Häsler, R., 2000. Stem radius changes and their relation to stored water in stems of young Norway spruce trees. Trees 15, 50–57. https://doi.org/10.1007/s004680000072

Erklärung:

Eidesstattliche Versicherung

Eidesstattliche Versicherung gemäß § 6 Abs. 1 Ziff. 4 der Promotionsordnung des Karlsruher Instituts für Technologie für die Fakultät für Bauingenieur-, Geo- und Umweltwissenschaften

1. Bei der eingereichten Dissertation zu dem Thema “Stress and recovery dynamics in Scots pine: The impacts of heat and drought on carbon and water cycling” handelt es sich um meine eigenständig erbrachte Leistung.
2. Ich habe nur die angegebenen Quellen und Hilfsmittel benutzt und mich keiner unzulässigen Hilfe Dritter bedient. Insbesondere habe ich wörtlich oder sinngemäß aus anderen Werken übernommene Inhalte als solche kenntlich gemacht.

3. Die Arbeit oder Teile davon habe ich wie folgt/ bislang nicht an einer Hochschule des In- oder Auslands als Bestandteil einer Prüfungs- oder Qualifikationsleistung vorgelegt.

Titel der Arbeit: “Stress and recovery dynamics in Scots pine: The impacts of heat and drought on carbon and water cycling”

Hochschule und Jahr: *Karlsruher Institute für Technologie, 2021*

Art der Prüfungs- oder Qualifikationsleistung: *Dissertation*

4. Die Richtigkeit der vorstehenden Erklärungen bestätige ich.

5. Die Bedeutung der eidesstattlichen Versicherung und die strafrechtlichen Folgen einer unrichtigen oder unvollständigen eidesstattlichen Versicherung sind mir bekannt.

Ich versichere an Eides statt, dass ich nach bestem Wissen die reine Wahrheit erklärt und nichts verschwiegen habe.

Ort und Datum Unterschrift

Eidesstattliche Versicherung

Belehrung

Die Universitäten in Baden-Württemberg verlangen eine Eidesstattliche Versicherung über die Eigenständigkeit der erbrachten wissenschaftlichen Leistungen, um sich glaubhaft zu versichern, dass der Promovend die wissenschaftlichen Leistungen eigenständig erbracht hat.

Weil der Gesetzgeber der Eidesstattlichen Versicherung eine besondere Bedeutung beimisst und sie erhebliche Folgen haben kann, hat der Gesetzgeber die Abgabe einer falschen eidesstattlichen Versicherung unter Strafe gestellt. Bei vorsätzlicher (also wissentlicher) Abgabe einer falschen Erklärung droht eine Freiheitsstrafe bis zu drei Jahren oder eine Geldstrafe.

Eine fahrlässige Abgabe (also Abgabe, obwohl Sie hätten erkennen müssen, dass die Erklärung nicht den Tatsachen entspricht) kann eine Freiheitsstrafe bis zu einem Jahr oder eine Geldstrafe nach sich ziehen. Die entsprechenden Strafvorschriften sind in § 156 StGB (falsche Versicherung an Eides Statt) und in § 161 StGB (fahrlässiger Falscheid, fahrlässige falsche Versicherung an Eides Statt) wiedergegeben.

§ 156 StGB: Falsche Versicherung an Eides Statt

Wer vor einer zur Abnahme einer Versicherung an Eides Statt zuständigen Behörde eine solche Versicherung falsch abgibt oder unter Berufung auf eine solche Versicherung falsch aussagt, wird mit Freiheitsstrafe bis zu drei Jahren oder mit Geldstrafe bestraft.

§ 161 StGB: Fahrlässiger Falscheid, fahrlässige falsche Versicherung an Eides Statt

Abs. 1: Wenn eine der in den § 154 bis 156 bezeichneten Handlungen aus Fahrlässigkeit begangen worden ist, so tritt Freiheitsstrafe bis zu einem Jahr oder Geldstrafe ein. Abs. 2: Straflosigkeit tritt ein, wenn der Täter die falsche Angabe rechtzeitig berichtigt. Die Vorschriften des § 158 Abs. 2 und 3 gelten entsprechend.

Ort und Datum Unterschrift